

REPORT DOCUMENTATION PAGE			Form Approved OMB No. 0704-0188	
Public reporting burden for this collection of information is estimated to average 1 hour per response, including the time for reviewing instructions, searching existing data sources, gathering and maintaining the data needed, and completing and reviewing the collection of information. Send comments regarding this burden estimate or any other aspect of this collection of information, including suggestions for reducing this burden, to Washington Headquarters Services, Directorate for Information Operations and Reports, 1215 Jefferson Davis Highway, Suite 1204, Arlington, VA 22202-4302, and to the Office of Management and Budget, Paperwork Reduction Project (0704-0188), Washington, DC 20503.				
1. AGENCY USE ONLY (Leave blank)	2. REPORT DATE 26.Jul.99	3. REPORT TYPE AND DATES COVERED DISSERTATION		
4. TITLE AND SUBTITLE PREDICTION AND VERIFICATION OF INTERNAL ELECTRIC CURRENT DISTRIBUTION IN MUSCLE FROM SURFACE APPLICATION		5. FUNDING NUMBERS		
6. AUTHOR(S) MAJ WAUGAMAN WILLIAM A				
7. PERFORMING ORGANIZATION NAME(S) AND ADDRESS(ES) UNIVERSITY OF TEXAS SAN ANTONIO		8. PERFORMING ORGANIZATION REPORT NUMBER		
9. SPONSORING/MONITORING AGENCY NAME(S) AND ADDRESS(ES) THE DEPARTMENT OF THE AIR FORCE AFIT/CIA, BLDG 125 2950 P STREET WPAFB OH 45433		10. SPONSORING/MONITORING AGENCY REPORT NUMBER  FY99-155		
11. SUPPLEMENTARY NOTES				
12a. DISTRIBUTION AVAILABILITY STATEMENT Unlimited distribution In Accordance With AFI 35-205/AFIT Sup 1		12b. DISTRIBUTION CODE		
13. ABSTRACT (Maximum 200 words)				
<p style="text-align: center;"><b>DISTRIBUTION STATEMENT A</b> Approved for Public Release Distribution Unlimited</p>				
14. SUBJECT TERMS		15. NUMBER OF PAGES 219		16. PRICE CODE
17. SECURITY CLASSIFICATION OF REPORT	18. SECURITY CLASSIFICATION OF THIS PAGE	19. SECURITY CLASSIFICATION OF ABSTRACT	20. LIMITATION OF ABSTRACT	

**Prediction and Verification of Internal Electric Current  
Distribution in Muscle From Surface Application**

by

William A. Waugaman

BSEE, United States Air Force Academy, 1985

MSEE, University of Texas, San Antonio, 1993

A thesis submitted to the

Faculty of the Graduate School of the

University of Colorado in partial fulfillment

of the requirement for the degree of

Doctor of Philosophy

Department of Electrical and Computer Engineering

DTIC QUALITY INSPECTED 2

1999

19990804 189

This thesis entitled:  
Prediction and Verification of Internal Electric Current  
Distribution in Muscle From Surface Application  
written by William A. Waugaman  
has been approved for the department of Electrical and Computer Engineering



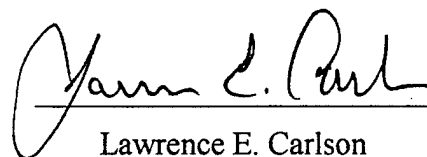
Howard Wachtel



Ewald F. Fuchs



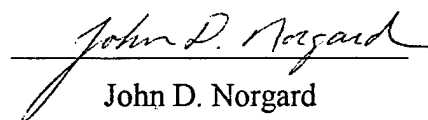
Frank Barnes



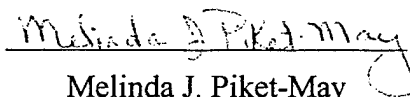
Lawrence E. Carlson



Richard T. Mihran



John D. Norgard



Melinda J. Piket-May

Date July 12, 1999

The final copy of this thesis has been examined by the signators, and we find that both the content and the form meet acceptable presentation standards of scholarly work in the above mentioned discipline.

## **ABSTRACT**

Waugaman, William A. (Ph.D. Electrical Engineering)

Prediction and Verification of Internal Electric Current Distribution in Muscle From Surface Application

Thesis directed by Professor Howard Wachtel

The use of surface electrical stimulation therapy for clinical rehabilitation has created the need for an improved modeling method to predict internal current density. Some stimulation protocols do not produce measurable physiological effects, such as muscle contraction. Therefore, traditional response-based current density modeling cannot be used. Additionally, lumped circuit models do not provide the resolution needed to optimize electrode size, shape, and placement. In this study, a method was developed to model quantitatively the current density delivered to the target muscle and it can also be used to optimize electrical stimulation protocols.

The finite element method (FEM) was used to model the internal electric current density in muscle resulting from surface application because the FEM provides the ability to model complex properties found in living tissue. To test the FEM programming method used in this research, electric current was passed through a cylinder of normal saline. Current density was measured and recorded. A replica of the saline cylinder was then modeled using the FEM. The results of the FEM model matched both the laboratory measurements and a previously published analytical



solution for bipolar stimulation of a saline cylinder. With the verification of the programming methodology complete, two additional FEM cylindrical models were created to test the ability to model the non-linearities, anisotropisms, and inhomogeneities found in biological tissue.

The next step was to move from modeling the simple cylindrical geometry to the geometry found in a hind leg of a lamb. This leg of lamb was modeled because its size and level of tissue complexity is similar to that of a human thigh. Internal muscle voltage gradient measurements were made upon a sacrificed leg of lamb during the application of bipolar stimulation. These measurements allowed for the mapping of muscle current density. The leg of lamb was then sliced and photographed to be able to create the finite element model. The empirical data compared favorably to the results of the FEM model, better than for a lumped element model. The validation of the modeling approach will eventually enable clinicians to accurately predict and optimize therapeutic muscle current densities.

## **DEDICATION**

The author would like to thank his family for their loving support during the time of this research. I would like to thank Dr. Howard Wachtel for his guidance and support. Finally, I would like to thank my daughter Carrie for the motivation to begin research in the first place.

## **ACKNOWLEDGEMENTS**

The author would like to acknowledge the I-DEAS software license and technical support provided by Structural Dynamics Research Corporation, Milford, OH. I would like to thank the Department of Electrical Engineering at the United States Air Force Academy for the use of laboratory space and equipment and for providing feedback.

## TABLE OF CONTENTS

ABSTRACT .....	iii
DEDICATION .....	v
ACKNOWLEDGEMENTS .....	v
TABLE OF CONTENTS .....	vi
LIST OF TABLES .....	ix
LIST OF FIGURES .....	x
INTRODUCTION AND MOTIVATION .....	1
GENERAL OBJECTIVE AND SPECIFIC AIMS .....	3
BACKGROUND .....	8
MUSCLE ATROPHY .....	9
<i>Muscle Types</i> .....	9
<i>Effects of exercise</i> .....	9
<i>Causes of atrophy</i> .....	10
ELECTRICAL CURRENT MUSCLE THERAPY .....	11
<i>Therapeutic Electrical Stimulation</i> .....	11
<i>Electrical Stimulation To Treat Incontinence</i> .....	13
<i>Blood flow</i> .....	15
<i>Muscle strengthening</i> .....	16
<i>Magnetic stimulation</i> .....	17
FINITE ELEMENT MODELING .....	17
<i>Mathematical Formulation of Electric Potentials in the Body</i> .....	20
<i>Boundary Conditions</i> .....	23
<i>Mathematical Formulation of the Finite Element Method</i> .....	23
BIOELECTRIC IMPEDANCE ANALYSIS (BIA) .....	24
<i>Tissue Sample Impedance Measurement</i> .....	29
METHODS .....	31
MATERIALS .....	31
LABORATORY SETUP .....	35
<i>Equipment</i> .....	35
<i>Tissue Impedance Measurement Device</i> .....	38
<i>Leg of Lamb Field Measurements</i> .....	41
BUILDING THE FEM MODEL FROM THE LEG OF LAMB .....	42
VALIDATION OF FEM HEAT TRANSFER ANALYSIS FOR BIOLOGICAL MODELING ..	46
LABORATORY SETUP .....	47
FINITE ELEMENT SALINE MODEL .....	48
SALINE MODELING RESULTS .....	49
DISCUSSION OF THE FEM RESULTS .....	63
RESULTS .....	65
TISSUE MEASUREMENTS .....	65
<i>Resistivity measurements</i> .....	66

<i>Frequency Response of Muscle</i> .....	68
<i>Current density response</i> .....	69
LEG OF LAMB FEM RESULTS .....	71
<i>Boundary Conditions Applied</i> .....	72
<i>FEM Model Attributes</i> .....	73
<i>FEM Model Primary Current Path Results</i> .....	77
<i>Current Density Results</i> .....	80
LABORATORY MEASUREMENTS IN LEG OF LAMB .....	89
<i>Comparison of the measured and modeled voltage gradient patterns</i> .....	90
<i>Comparison of the measured and modeled voltage gradient values</i> .....	95
<b>ADDITIONAL INVESTIGATIONS WITH LEG OF LAMB FEM MODEL</b> .....	<b>101</b>
ATROPHIED LEG OF LAMB MODEL.....	101
THE INVERSE PROBLEM.....	108
<b>DISCUSSION AND CONCLUSION</b> .....	<b>110</b>
DISCUSSION .....	110
ADDITIONAL SIGNIFICANCE OF THIS RESEARCH AND ITS CLINICAL UTILITY .....	113
<i>Atrophied muscle impedance database</i> .....	113
<i>Incontinence and bladder stimulation</i> .....	113
<i>Bone healing</i> .....	114
<i>Prolonged space flight and disuse atrophy</i> .....	114
CONCLUSION.....	115
<b>REFERENCES</b> .....	<b>115</b>
<b>APPENDIX A - LAMB SLICES</b> .....	<b>122</b>
LAMB SLICE AT Z = 1 CM .....	122
LAMB SLICE AT Z = 2 CM .....	123
LAMB SLICE AT Z = 3 CM .....	124
LAMB SLICE AT Z = 4 CM .....	125
LAMB SLICE AT Z = 5 CM .....	126
LAMB SLICE AT Z = 6 CM .....	127
LAMB SLICE AT Z = 7 CM .....	128
LAMB SLICE AT Z = 8 CM .....	129
LAMB SLICE AT Z = 9 CM .....	130
LAMB SLICE AT Z = 10 CM .....	131
LAMB SLICE AT Z = 11 CM .....	132
LAMB SLICE AT Z = 12 CM .....	133
<b>APPENDIX B - SALINE LABORATORY MEASUREMENTS</b> .....	<b>134</b>
<b>APPENDIX C - GRAPHICAL RESULTS OF LEG OF LAMB LABORATORY MEASUREMENTS</b> .....	<b>135</b>
LABORATORY VOLTAGE GRADIENT MEASUREMENTS OF THE X-Y PLANE AT Z = 0 CM.....	135
LABORATORY VOLTAGE GRADIENT MEASUREMENTS OF THE X-Y PLANE AT Z = 2 CM.....	136
LABORATORY VOLTAGE GRADIENT MEASUREMENTS OF THE X-Y PLANE AT Z = 4 CM.....	137
LABORATORY VOLTAGE GRADIENT MEASUREMENTS OF THE X-Y PLANE AT Z = 6 CM.....	138
LABORATORY VOLTAGE GRADIENT MEASUREMENTS OF THE X-Y PLANE AT Z = 8 CM.....	139
LABORATORY VOLTAGE GRADIENT MEASUREMENTS OF THE X-Y PLANE AT Z = 12 CM.....	140
<b>APPENDIX D - LEG OF LAMB LABORATORY MEASUREMENTS</b> .....	<b>141</b>
<b>APPENDIX E - FEM CONVERSION TABLES FOR LEG OF LAMB MODEL</b> .....	<b>143</b>

APPENDIX F - ATROPHY LAMB FEM MODEL TARGET MUSCLE ELEMENT .....215

APPENDIX G - MATLAB CODE USED TO CREATE LABORATORY MEASUREMNT  
RESULTS GRAPHS.....217

## LIST OF TABLES

Table 1 - Summary of the tissue impedance measurements made on the leg of lamb samples. This table lists the average resistivity and standard deviation for the three types of tissues modeled. Also, the corresponding conductivity used in the FEM model is given. ....	67
Table 2 - Summary of leg of lamb FEM model results compared to emperical measurements. ....	91
Table 3 - A comparison of the measure verses predicted voltage gradient values in the leg of lamb. ....	96
Table 4 - Summary Table of Laboratory Measurements Made in Saline Cylinder .....	134
Table 5 - Voltage Gradient Laboratory Measurements in Leg of Lamb .....	141
Table 6 - FEM Conversion Table for Leg of Lamb at $Z = 1$ cm.....	143
Table 7 - FEM Conversion Table for Leg of Lamb at $Z = 2$ cm.....	149
Table 8 - FEM Conversion Table for Leg of Lamb at $Z = 3$ cm.....	155
Table 9 - FEM Conversion Table for Leg of Lamb at $Z = 4$ cm.....	161
Table 10 - FEM Conversion Table for Leg of Lamb at $Z = 5$ cm.....	167
Table 11 - FEM Conversion Table for Leg of Lamb at $Z = 6$ cm.....	173
Table 12 - FEM Conversion Table for Leg of Lamb at $Z = 7$ cm.....	179
Table 13 - FEM Conversion Table for Leg of Lamb at $Z = 8$ cm.....	185
Table 14 - FEM Conversion Table for Leg of Lamb at $Z = 9$ cm.....	191
Table 15 - FEM Conversion Table for Leg of Lamb at $Z = 10$ cm.....	197
Table 16 - FEM Conversion Table for Leg of Lamb at $Z = 11$ cm.....	203
Table 17 - FEM Conversion Table for Leg of Lamb at $Z = 12$ cm.....	209
Table 18 - Leg of Lamb FEM Model Target Muscle Elements .....	215

## LIST OF FIGURES

- Figure 1 - A three layer concentric cylinder FEM model setup for testing layered tissues. It contains an outer layer of skin modeled with two dimensional surface elements, a middle layer of muscle, and an inner layer of bone both modeled with solid elements. ....6
- Figure 2 - Tetrapolar configuration used in BIA. The source electrodes pass a known current through the tissue. The measurement electrodes sense the voltage at a fixed distance. ....28
- Figure 3 - Photo of the leg of lamb prior electric current density and tissue impedance measurements (top view). ....33
- Figure 4 - Photo of the leg of lamb prior electric current density and tissue impedance measurements (bottom view). ....34
- Figure 5 - Distal end of the leg of lamb. Template used to apply markings for probe measurement locations. ....35
- Figure 6 - The instrumentation amplifier circuit setup used for all the laboratory measurements. ....36
- Figure 7 - Saline Voltage Measurement Probe .....37
- Figure 8 - Diagram showing the tissue measurement probe. It consists of two insulated needles with 1 mm Ag-AgCl exposed tips. The probe has 1 cm markings on the needle shaft to determine tissue depth. ....38
- Figure 9 - Diagram showing tissue impedance measuring device. It had two source plate electrodes and four sensing electrodes. 2 cm<sup>2</sup> tissue samples were placed between the plate electrodes and the voltage outputs were measured on an oscilloscope. The four sensing electrodes allowed measurements in two directions by repositioning the switches. ....39
- Figure 10 - Photo of the tissue impedance measurement device with an adipose tissue sample placed in it. The two lower sensing electrodes are exposed for demonstration purposes. ....40
- Figure 11 - Photo of the leg of lamb after the first set 1 cm reference markings are in place. ....41
- Figure 12 - Diagram showing the saline model laboratory setup. One liter of 0.9% saline was placed in the 10 cm diameter glass cylinder. The electrodes were placed on opposite sides of the glass cylinder walls, 1 cm below the surface. The electrodes were Ag-AgCl wires with 2 mm exposed at the ends. The measurement probe was also a Ag-AgCl electrode controlled by a three degrees of freedom manipulator. The signal was passed through a Burr-Brown INA120 instrumentation amplifier. The output signal from the op amp was measured and recorded with an oscilloscope. The callout is a close-up of the measurement probe tip. ....48
- Figure 13 - Graph comparing the voltage gradient measurements and saline FEM model results. The location of these values was on a line directly between the electrodes. ....50
- Figure 14 - Contour plot shows the voltage potential in the X-Y plane, 1 cm below the surface, level with the electrodes. The voltage potential was uniform outside 2 cm of the electrodes. The number on the contour line corresponds to its color bar segment. ....51
- Figure 15 - Plot showing the saline model voltage results midplane between the electrodes in the X-Z plane. The results confirmed a uniform field all the way to the bottom of the solution and match the empirical measurements (Appendix D). Both the

- empirical measurements and the model's results provided uniform values throughout the midplane. This was expected since saline is a good conductor.....52
- Figure 16 - Arrow plots showing the current density in a cylinder of homogeneous saline. The color and length each arrow indicates the current's magnitude. The current density is uniform outside of 2 cm of the electrodes. ....53
- Figure 17 - Arrow plots showing the current density results. The medium was made anisotropic to simulate muscle. The surface application was from top to bottom to represent bipolar stimulation along the length of a muscle.....54
- Figure 18 - Current density plot showing the anisotropic FEM model's midplane results between the electrodes in the X-Y plane. The current density is no longer uniform at midplane. The anisotropic conductivity focuses the current flow directly between the electrodes. ....55
- Figure 19 - Front view of a three dimensional contour line plot showing the surface voltage on the multi-layer FEM model. This plot is of just the thin shell elements representing the skin. The voltage changed rapidly around the source electrode and became more uniform as the distance increased. The number on the contour line corresponds to its color bar segment.....57
- Figure 20 - Plot showing the front view current density results of the multi-layer FEM model. This figure is only the top half of the cylinder. The results are similar to the anisotropic FEM model with the addition of the bone further limiting the current spread. ....59
- Figure 21 - Plot showing the side view current density results of the multi-layer FEM model. This figure is only the top half of the cylinder. The results are similar to the anisotropic FEM model with the addition of the bone further limiting the current spread. ....60
- Figure 22 - Plot showing the top view current density results of the multi-layer FEM model. The results are similar to the anisotropic FEM model with the addition of the bone further limiting the current spread. Also, the current inside the bone was significantly lower due to its poor conductivity.....61
- Figure 23 - Plot showing the midplane current density results of the multi-layer FEM model. This figure is only the top half of the cylinder. The results are similar to the anisotropic FEM model with the addition of the bone further limiting the current spread. Note the direction of the current vector inside the bone. The insulative bone created a voltage gradient laterally causing the current vector to shift away from the electrodes. This effect was more pronounced near the source.62
- Figure 24 - Graph comparing the average resistivity of the measured lamb tissues to published human tissue values.....68
- Figure 25 - Graph showing the measured resistivity of muscle tissue against the source frequency it was measured at using BIA. The muscle tissue resistivity was stable over the low frequency range.....69
- Figure 26 - Plot showing that muscle tissue resistivity is stable in the low current density range. The voltage response to changes in current intensity were indeed linear. The muscle's resistivity was constant and Ohm's Law applied for the voltage/current relationship. The linear regression analysis of the measured data resulted in a near perfect fit with a  $p = 0.0054$ . ....71
- Figure 27 - An end view of the leg of lamb FEM model used including the air padding elements. ....74



Figure 28 - A top view of the leg of lamb FEM model used including the air padding elements.....	75
Figure 29 - A side view of the leg of lamb FEM model used including the air padding elements.....	76
Figure 30 - A three dimensional view of the leg of lamb model used with air padding elements hidden.....	77
Figure 31 - End view plot of the primary current path through the leg of lamb. The path starting locations were programmed at each of the four source electrode points. The resulting paths traced out were the paths with the greatest current density in the model. The current paths remained completely within the target muscle. Each path flowed in through the surface fat layer into the muscle then turned towards the anode. The current path also spread out as it flowed away from the source, reaching a maximum dispersion half way between the electrodes. ....	78
Figure 32 - Top view plot of the primary current path through the leg of lamb. The path starting locations were programmed at each of the four source electrode points. The resulting paths traced out were the paths with the greatest current density in the model. The current paths remained completely within the target muscle. Each path flowed in through the surface fat layer into the muscle then turned towards the anode. The current path also spread out as it flowed away from the source, reaching a maximum dispersion half way between the electrodes. ....	79
Figure 33 - Side view plot of the primary current path through the leg of lamb. The path starting locations were programmed at each of the four source electrode points. The resulting paths traced out were the paths with the greatest current density in the model. The current paths remained completely within the target muscle. Each path flowed in through the surface fat layer into the muscle then turned towards the anode. The current path also spread out as it flowed away from the source, reaching a maximum dispersion half way between the electrodes. ....	80
Figure 34 - End view vector plot showing the current density above the $10 \mu\text{A}/\text{cm}^2$ vasodilatation threshold. The dashed line is the outline of the entire leg of lamb model. The plot shows the main concentration of the stimulation energy remained in the target muscle.....	82
Figure 35 - Top view vector plot showing the current density above the $10 \mu\text{A}/\text{cm}^2$ vasodilatation threshold. The dashed line is the outline of the entire leg of lamb model. The plot shows the main concentration of the stimulation energy remained in the target muscle.....	83
Figure 36 - Side view vector plot showing the current density above the $10 \mu\text{A}/\text{cm}^2$ vasodilatation threshold. The dashed line is the outline of the entire leg of lamb model. The plot shows the main concentration of the stimulation energy remained in the target muscle.....	84
Figure 37 - Contour plot of the leg of lamb FEM model results showing the current density in the X-Y plane at $Z = 2 \text{ cm}$ . The red, yellow, and blue elements represent muscle, fat, and bone, respectively. The number on the contour line corresponds to its color bar segment.....	85
Figure 38 - Contour plot of the leg of lamb FEM model results showing the current density in the X-Y plane at $Z = 4 \text{ cm}$ . The red, yellow, and blue elements represent muscle, fat, and bone, respectively. The number on the contour line corresponds to its color bar segment.....	86

- Figure 39 - Contour plot of the leg of lamb FEM model results showing the current density in the X-Y plane at  $Z = 6$  cm. The red, yellow, and blue elements represent muscle, fat, and bone, respectively. The number on the contour line corresponds to its color bar segment.....87
- Figure 40 - Contour plot of the leg of lamb FEM model results showing the current density in the X-Y plane at  $Z = 8$  cm. The red, yellow, and blue elements represent muscle, fat, and bone, respectively. The number on the contour line corresponds to its color bar segment.....88
- Figure 41 - Contour plot of the leg of lamb FEM model results showing the current density in the X-Y plane at  $Z = 10$  cm. The red, yellow, and blue elements represent muscle, fat, and bone, respectively. The number on the contour line corresponds to its color bar segment.....89
- Figure 42 - Leg of lamb FEM model results compared to empirical measurements made at  $Z = 2$  cm. The square data points are the laboratory measurements. The superimposed contour plot is the leg of lamb FEM model voltage gradient results. The black dot is the origin. The laboratory values which do not match the FEM model generated contours and are off by one color segment are circled. The number on the contour line corresponds to its color bar segment. ....92
- Figure 43 - Leg of lamb FEM model results compared to empirical measurements made at  $Z = 4$  cm. The square data points are the laboratory measurements. The superimposed contour plot is the leg of lamb FEM model voltage gradient results. The black dot is the origin. The laboratory values which do not match the FEM model generated contours and are off by one color segment are circled. The number on the contour line corresponds to its color bar segment. ....93
- Figure 44 - Leg of lamb FEM model results compared to empirical measurements made at  $Z = 6$  cm. The square data points are the laboratory measurements. The superimposed contour plot is the leg of lamb FEM model voltage gradient results. The black dot is the origin. The laboratory values which do not match the FEM model generated contours and are off by one color segment are circled. The number on the contour line corresponds to its color bar segment. ....94
- Figure 45 - Leg of lamb FEM model results compared to empirical measurements made at  $Z = 8$  cm. The square data points are the laboratory measurements. The superimposed contour plot is the leg of lamb FEM model voltage gradient results. The black dot is the origin. The laboratory values which do not match the FEM model generated contours and are off by one color segment are circled. The values which do not agree by two or more color segments are marked by an X. The number on the contour line corresponds to its color bar segment. ....95
- Figure 46 - Lumped circuit model of the leg of lamb.  $R_{tm}$  was the target muscle,  $R_f$  was the adipose tissue, and  $R_b$  was the bone.  $R_a$  represented the anisotropic property of striated muscle. Each resistor with a vertical orientation represented 4 cm of tissue along the Z axis. The horizontal branches provided for the lateral current spread. The resistor values were  $R_{tm} = 468 \Omega$ ,  $R_a = 3.18 \text{ k}\Omega$ ,  $R_f = 2.065 \text{ k}\Omega$ , and  $R_b = 53.2 \text{ k}\Omega$ .....99
- Figure 47 - Three dimensional diagram showing the modified target muscle in the leg of lamb FEM model with atrophied elements added in yellow. .... 102
- Figure 48 - A plot comparing the voltage gradient of all the muscle elements in the normal muscle verses the atrophied muscle. The results of the simulation did show an

increased current density in the muscle elements. All the muscle elements in the target muscle showed this increase. The closer the element was to a converted atrophy element, the greater the effect. ....	103
Figure 49 - A graph comparing the current densities in adipose elements. The adipose tissue reduces the current density (purple line). Using the voltage gradient results of the converted elements and then reapplying the original muscle tissue's conductivity value produces an increased current density (yellow line). The increased current density around the adipose tissue causes the higher voltage gradient across the muscle elements since they are essentially in parallel with each adjacent element. ....	105
Figure 50 - Contour plot showing the current density in X-Y plane at $Z = 6$ cm before atrophy was applied to the target muscle. The dashed line highlights the target muscle elements. The number on the contour line corresponds to its color bar segment. ....	106
Figure 51 - Contour plot showing the current density in X-Y plane at $Z = 6$ cm with atrophy applied to the target muscle. The dashed line highlights the target muscle elements. The current density pattern has little change from Figure 50. The number on the contour line corresponds to its color bar segment. ....	106
Figure 52 - Top view of the atrophied leg of lamb FEM model results showing the current density vectors. ....	107
Figure 53 - Side view of the atrophied leg of lamb FEM model results showing the current density vectors. ....	108
Figure 54 - Photograph of the leg of lamb sliced at $Z = 1$ cm. ....	122
Figure 55 - Photograph of the leg of lamb sliced at $Z = 2$ cm. ....	123
Figure 56 - Photograph of the leg of lamb sliced at $Z = 3$ cm. ....	124
Figure 57 - Photograph of the leg of lamb sliced at $Z = 4$ cm. ....	125
Figure 58 - Photograph of the leg of lamb sliced at $Z = 5$ cm. ....	126
Figure 59 - Photograph of the leg of lamb sliced at $Z = 6$ cm. ....	127
Figure 60 - Photograph of the leg of lamb sliced at $Z = 7$ cm. ....	128
Figure 61 - Photograph of the leg of lamb sliced at $Z = 8$ cm. ....	129
Figure 62 - Photograph of the leg of lamb sliced at $Z = 9$ cm. ....	130
Figure 63 - Photograph of the leg of lamb sliced at $Z = 10$ cm. ....	131
Figure 64 - Photograph of the leg of lamb sliced at $Z = 11$ cm. ....	132
Figure 65 - Photograph of the leg of lamb sliced at $Z = 12$ cm. ....	133
Figure 66 - Three-dimensional view of laboratory voltage gradient measurements of X-Y plane at $z = 0$ cm. ....	135
Figure 67 - Three-dimensional view of laboratory voltage gradient measurements of X-Y plane at $z = 2$ cm. ....	136
Figure 68 - Three-dimensional view of laboratory voltage gradient measurements of X-Y plane at $z = 4$ cm. ....	137
Figure 69 - Three-dimensional view of laboratory voltage gradient measurements of X-Y plane at $z = 6$ cm. ....	138
Figure 70 - Three-dimensional view of laboratory voltage gradient measurements of X-Y plane at $z = 8$ cm. ....	139
Figure 71 - Three-dimensional view of laboratory voltage gradient measurements of X-Y plane at $z = 12$ cm. ....	140

## **CHAPTER 1**

### **INTRODUCTION AND MOTIVATION**

The use of electrical stimulation for rehabilitation has a long history. It typically involves the recruitment of a target muscle or motor neuron resulting in the contraction of a muscle group. Recently, a new electrical stimulation protocol has been developed called Therapeutic Electrical Stimulation (TES). TES is different from other stimulation protocols since its low stimulation current levels do not lead to contraction of the muscle. Its original application in rehabilitation therapy was for mobility enhancement in children and adults with neuromuscular disorders (spina bifida, cerebral palsy, and spinal cord injury). During these treatments, it was also found to be effective for improving bowel and bladder continence for those with a neuropathic bladder (caused by paraplegia, lumbosacral myelomeningocele, or other neurological disorders). It continues to be developed for use in both of these therapies.

The end goal of TES is to gain function typically in the area of improved ambulation. The electrical stimulation is believed to promote muscle growth, neuron sprouting, and increased sensation. This trophic response of the muscle is then strengthened by means of traditional physical therapy. TES uses low frequency (35 Hz), low intensity, constant current, surface stimulation. The signal intensity used is below that which causes active recruitment of the underlying target muscle and is approximately at the sensory perception level. TES is believed to be effective through enhanced blood flow [1], increased protein synthesis [2], and/or increased muscle innervation [3].

To better study the effects of sub contractile electrical currents on muscles and test its therapeutic efficacy, a method to determine the electrical current density passing through the muscle is needed. Currently, there is no exact method for determining the amount of sub contractive electrical current that reaches the target muscle from surface electrodes. Presently used TES stimulator settings were determined empirically by clinical studies. The results of the Balcom *et. al.* study [4] showed that TES was safe and effective for improving bladder and bowel continence in children with myelomeningocele. It also increased bladder capacity and improved pelvic floor fullness sensation. The Pape *et al* studies [5, 6] showed marked improvement in functional neuromuscular control of the extremities for children with cerebral palsy. After 6 months, significant improvement was noted on the Peabody Developmental Motor Scales scores for gross motor, locomotion, and receipt/propulsion skills [5]. Other improvements include reduced spasticity and improved functional gross motor control [6].

Simple lumped circuit models have been developed to predict electrical current densities due to surface stimulation [7]. However, these are limited to simple geometries and normal, healthy tissue. This is not the case for much of the target patient population. Their muscle tissue is typically highly atrophied or neuropathic. Since an atrophied muscle contains a much greater concentration of adipose tissue, its impedance can vary greatly from healthy muscle tissue. Thus, atrophy can be expected to have an effect on the distribution pattern of the electrical current density in the target tissue.

Advancements in computer processing power allows the use of the Finite Element Method (FEM) to model the electrical current density from surface electrodes to the target muscle. Computer modeling provides an efficient method to test various electrical stimulation parameters and electrode geometries. Ultimately, better dosimetry could be achieved in clinical trials using validated results from computer modeling.

### **General Objective And Specific Aims**

The overall objective of this research was to verify that the FEM was an appropriate numerical tool for creating models of complex biological tissue. With this verification established, a procedure was developed to replicate an actual animal thigh in a FEM model. A sacrificed hind leg of a lamb was used for the thigh model because its size, anatomy, and tissue complexity closely resembles a human child's thigh. The use of an animal leg provided an opportunity to validate the FEM model with an empirical comparison. This leg of lamb FEM model may then be used to

determine the effects of atrophy in the target muscle, (the quadriceps femoris in this case). Further extension of this research can lead to a FEM model of the human thigh. This FEM model may be used to determine the optimum TES protocol which provides a uniform electrical current density in the target muscle. The goal would be to have a current density between  $10 \mu\text{A}/\text{cm}^2$  and  $1 \text{mA}/\text{cm}^2$  in the target muscle. This would, supposedly, elicit a vasodilatation response without causing muscle contraction. Additionally, the surface application would maintain the current density in the other thigh muscles below the  $10 \mu\text{A}/\text{cm}^2$  level (which is safely below contracture thresholds).

Four steps are needed to demonstrate that the FEM model is valid for determining electric current densities from surface application. The first step is the verification of the FEM model using a cylinder of saline. This saline model provides a simple homogeneous medium to confirm the method both empirically and analytically. The FEM software uses a heat transfer module to calculate results. This thermal technique needs to be tested to ensure that the thermal programming methodology provides accurate results for the electric current densities in a volume conductor. Using the quasi-static approximation for the low frequency stimulation source, the steady state solution is calculated and compared to both laboratory results and previously published analytical solution [8]. Comparable empirical measurements and a mathematical solution provides verification of the programming methods.

Subsequently, two FEM cylindrical models are created to test the ability to model the complexities found in biological tissue. The first FEM model incorporates the anisotropic property of striated muscle. The second FEM tests the bipolar surface electrical stimulation of a multi-tissue cylinder. It is a cylindrical model containing three concentric layers. These layers represent the skin, muscle, and bone of the thigh. Each of these layers are considered homogeneous in tissue type. The tissue conductivities used are the values published by Geddes [9]. Figure 1 shows the model setup. From this data, the electrical current density throughout the layers is calculated. These three cylindrical models provide verification of the programming method. All of the non-linearities anticipated are tested using these simple models. Now, modeling the more complex leg of lamb can be accomplished.



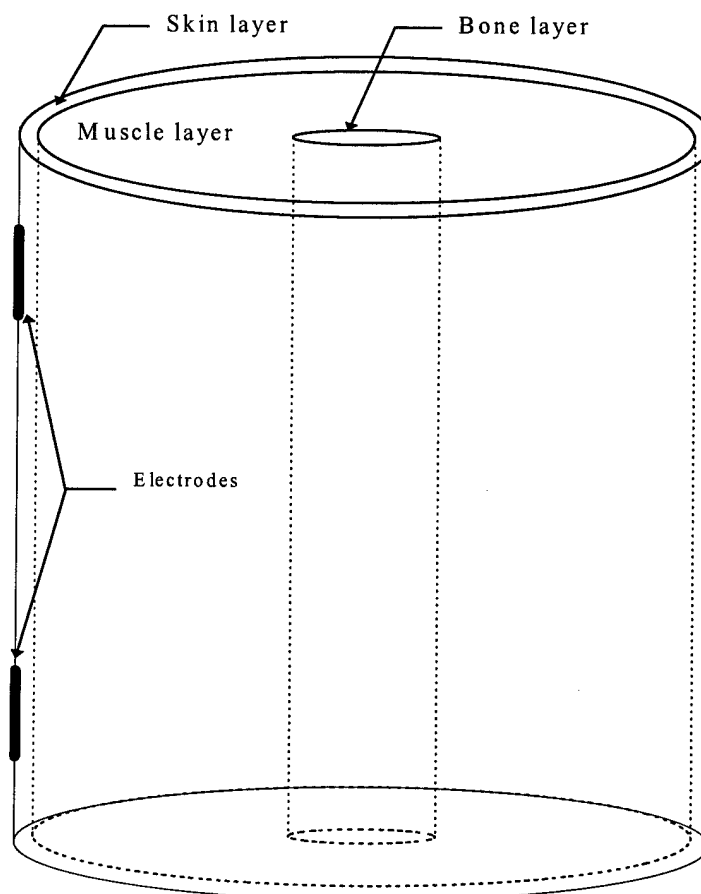


**Figure 1 -A three layer concentric cylinder FEM model setup for testing layered tissues. It contains an outer layer of skin modeled with two dimensional surface elements, a middle layer of muscle, and an inner layer of bone both modeled with solid elements.**

The second step is collecting tissue impedance measurements from leg of lamb samples. This bioimpedance analysis (BIA) is accomplished using a four electrode technique on tissue cubes of striated muscle, adipose tissue, and bone. The tissue conductivity,  $\sigma(x,y,z)$ , is calculated for use in the leg of lamb FEM model.

In the third step, the quadriceps femoris muscle in the leg of lamb is stimulated. Voltage gradient measurements are made at regular intervals in the target

muscle to map out the current density resulting from the surface application. After the measurements are made, the leg of lamb is sliced perpendicular to the bone. Each slice is 1cm thick. This allows visualization of the exact geometry and tissue locations in the leg of lamb.

The fourth and last step is to make a FEM model of the leg of lamb. By applying boundary conditions to create the same stimulation parameters, a direct comparison of the results can be made. This comparison of results provides the support for the FEM model as a valid method for determining electric current density in the human thigh. The model is then modified by adding adipose tissue to simulate mild muscle atrophy. The effects of atrophy on the current density and the resulting current distribution pattern are studied.

The FEM modeling technique developed here provides the first quantification of subthreshold current densities of bipolar surface stimulation. This method can be applied in future work to develop an accurate model of the human thigh using the visible man database. Then, the TES protocol, along with many others, can be optimized more quickly than with clinical methods, saving time and money. Ultimately, the creation of a personalized FEM model using data from imaging sources could determine individual stimulation dosage.

## **CHAPTER 2**

### **BACKGROUND**

Several different disciplines are combined in this research project. To understand the need for computer modeling of electric current densities in biological tissue, a review of three areas is necessary. The first is muscle physiology and the effects of electric current on muscle. Next, the finite element method is explained as an approach to solve for the electric current density. Third, bioimpedance analysis (BIA) is covered as a method for determining the electrical conductivity of the tissues modeled.

One of the most important muscles for walking is the quadriceps femoris. It is often the target muscle in TES therapy for children with neuromuscular disorders. These children commonly have some form of muscle atrophy. The Food and Drug Administration has approved neuromuscular stimulation as a treatment for and prevention of disuse muscle atrophy.

## **Muscle Atrophy**

### *Muscle Types*

There are two main types of striated muscle fibers; slow-twitch fibers and fast-twitch fibers. Slow-twitch fibers are composed of thin red cells which contract slowly using slow-acting myosin ATPases. They have a rich capillary supply, abundant mitochondria, and a highly active aerobic pathway for ATP synthesis. These fibers are extremely fatigue resistant and can contract for prolonged periods. Their primary function is for posture control and repetitive motions that require endurance.

Fast-twitch fibers are generally composed of large pale white cells with a diameter twice that of the slow-twitch fibers. They use fast-acting myosin ATPases and can contract rapidly. They have large glycogen reserves and use the anaerobic pathway to generate ATP for energy. Fast-twitch fibers can produce powerful contractions, but fatigue quickly.

### *Effects of exercise*

Aerobic exercise produces several changes in skeletal muscles. The capillaries surrounding the muscle fibers increase in number, as do the mitochondria inside the cell. The muscle fibers also synthesize more myoglobin. These changes take place in both fiber types, but are the most dramatic in the fast-twitch fibers. The latter become "immediate" fast-twitch fibers. They have the added ability for the aerobic production of ATP. In contrast, isometric exercise results in muscle hypertrophy of primarily the fast twitch fibers. This increased muscle bulk is a result of increased muscle fiber size, rather than an increase in the number of muscle fibers.

Vigorously stressed fibers contain more mitochondria, form more myofilaments and myofibrils, and have increased glycogen reserves for anaerobic ATP production. Together, these result in increased muscle size and strength.

### *Causes of atrophy*

Muscles must remain physically active if they are to be healthy. If a muscle is immobilized completely, for example due to casting, then muscle atrophy (degeneration and loss of mass) begins immediately. This form of atrophy is called disuse atrophy. When a muscle is immobilized, it can lose up to 5% of its strength per day [10]. Muscle atrophy is also observed in all cases of neurologic dysfunction. A muscle which is totally deprived of a neural stimulation is functionally paralyzed and will ultimately atrophy to about one quarter of its original size. Even muscles with partial innervation will atrophy. In the case of cerebral palsy, the muscles tend to be spastic, which leads to generalized muscle fiber atrophy with the predominance of slow-twitch fibers. A spastic muscle tends to be shorter and creates a problem of muscle balance about its joint. The decrease in function of a person with muscle atrophy results in a vicious cycle of disuse and increased atrophy.

The effects of muscle atrophy on the cellular level are many. In addition to the decrease in fiber size and strength, there is a decrease in blood flow, protein synthesis in the cell, and an increase in adipose tissue between the fascicles. The increase in adipose tissue and decrease in muscle size is hypothesized to decrease the muscle's electrical conductivity. The overall muscle length also tends to shorten,

resulting in contractures. Ultimately, if the muscle atrophy continues long enough, muscle tissue is replaced by fibrous connective tissue [11].

### **Electrical Current Muscle Therapy**

Neuromuscular stimulation therapy is finding an increasing number of new applications in rehabilitation medicine. One such application is in the area of enhanced muscle growth and neuron sprouting in children with neurological disorders such as cerebral palsy and spina bifida.

#### *Therapeutic Electrical Stimulation*

TES is a new application of sub contractile electrical stimulation aimed at the treatment of disuse atrophy. It was developed to overcome some of the problems with high intensity (contraction causing) stimulation protocols. Some of the difficulties encountered with high intensity stimulation for children are the treatment time and cost of daily visits, poor toleration, and safety considerations [6]. The safety considerations involved in high intensity electrical stimulation are possible damage to growing muscles, tendons, and bones, and the possibility of overworking a weak atrophied muscle [12]. In TES, a low intensity, constant current, biphasic waveform is applied to targeted major muscle groups, such as the quadriceps femoris. The intensity of the applied current is below the level needed for active contraction of the muscle (approximately 3 mA at a fundamental frequency of 35 Hz).

The TES protocol has the added benefit of falling in the middle of the range used in chronic low-level electrical stimulation animal studies. This allows a more direct comparison of current densities used and the results achieved in these animal

studies. The new TES therapy protocol is applied at night for approximately eight hours per twenty four hours. This is accomplished every night while the patient sleeps. The treatment can last from one to four years. The mechanism believed to be responsible for the success of TES is the localized increase in blood flow during a period of increased trophic hormone levels. A study conducted by Steinbok *et al.*, using children with weakened muscles following a selective posterior rhizotomy, showed statistically significant ( $p=0.001$ ) and clinical improvement in the treated children [13]. The increased muscle growth may then be strengthened using either conventional physical therapy methods or active electrical stimulation of the muscle groups. Improvement in muscle bulk can be seen within six to eight weeks. Functional level changes are expected in the six month to one year time frame. This allows children greater use of and control over their extremities. TES is a powerful adjunct in a total rehabilitation program for children with neuromuscular disorders causing muscle atrophy.

The success of subthreshold TES therapy is excellent [14]. There is reduced spasticity, increased strength, and increased control in both cerebral palsy and spina bifida patients. This results in the child having an improved gait. Also, the need for orthotics may be reduced. A child may go from walking with a walker and long leg braces to using just short leg braces and crutches. Another example would be a child in a wheelchair now becoming a household ambulator. Some children no longer need bracing at all and walk independently [15]. The patient's independence increases with any advancement in muscle function or control. Additionally, this new TES therapy is currently being investigated for other uses and in different patient

populations. For example, it has been found to retard disuse atrophy in bedrest patients and may help maintain fat free muscle mass for astronauts during prolonged space flight.

#### *Electrical Stimulation To Treat Incontinence*

A recent innovation for the patient with a chronic neuropathic bladder is to use electrical stimulation for the treatment of incontinence. The ultimate goal of this treatment is to regain urinary control. Electrical stimulation is used in a variety of ways to achieve this end. Its first use was in a functional stimulation capacity to cause detrusor contraction and voiding. This functional electrical stimulation is typically performed by implanted stimulators targeting the sacral nerve in conjunction with a sacral rhizotomy to reduce urethral resistance caused by the sphincter muscle [16, 17]. The most recent advance in this area uses an implantable computerized electrical stimulation system for controlling micturition and also reducing the urethral resistance. This was accomplished in dogs by first stimulating the sphincter muscle to the point of fatigue with a high frequency waveform. Then, using a low frequency waveform, the detrusor was recruited to cause total voiding of the bladder [18]. If this approach can be implemented in humans, then sacral rhizotomies can be avoided.

Another approach for the use of electrical stimulation for treating incontinence is in the area of rehabilitation. It has been shown that electrical stimulation of the bladder can increase its capacity, improve pelvic floor sensation, and sometimes allow cognitive control of voiding learned with the use of biofeedback. Intravesical transurethral bladder stimulation was performed on 88 children with neuropathic



bladders. Bladder capacity increased significantly over the control group while maintaining low bladder pressures [19]. Increasing urine capacity while maintaining low bladder pressure clearly is beneficial to these children. This will allow an increase in the interval between intermittent catheterization and may also reduce the need for a surgical bladder augmentation. Kaplan also reported success in initiating sensory awareness of bladder filling and in stimulating detrusor contractions. The emergence of sensation is a prerequisite for becoming continent [20].

Next, the use of transcutaneous electrical nerve stimulation (TENS) was studied for the treatment of idiopathic detrusor instability [21]. Seventy-one adults underwent the use of TENS over the S2-S3 dermatomes with the electrical current intensity set at sensory perception. The mean duration of TENS stimulation was 3 weeks. The stimulation parameters used in the TENS stimulation are similar to those used in TES. Urodynamic analysis showed significant improvements in total bladder capacity and voided volume [20]. It also decreased the number and frequency of unstable contractions. In addition, Hasan *et al.* compared the TENS subjects to a control group which underwent S3 neuromodulation using implanted electrodes. No significant difference was noted between the two groups. The surface electrode stimulation method is preferred to the implanted electrodes since there are fewer complications.

Finally, results similar to Kaplan were shown with TES in the same myelomeningocele population [4]. Using the less invasive surface electrodes, 11 children underwent the TES home based therapy to improve continence. This study

was based on the premise that the pelvic floor musculature was weakened because of a type of disuse muscle atrophy. TES was used to improve muscle control and thus enhance functional continence of urine and stool. The TES protocol is easier to administer than intravascular stimulation since it can be done at home while the patient sleeps. This improves patient compliance and motivation. The result of the study was a mean increase in bladder capacity from 133 ml to 196 ml after nine months of stimulation. There was also a subjective improvement in the sensation of pelvic fullness after the 6-month point.

The effectiveness of electrical stimulation in the treatment of incontinence merits increased study of the most effective means of implementation for the neuropathic bladder population. Initial results show that lasting benefits of TES may persist for years after electrical stimulation is discontinued, but further study of long-term benefits is needed [13]. The transition from sacral root stimulation with implanted electrodes to TES using surface electrodes still requires a better characterization of the electrical current flow because of the increased distance between target muscle and electrodes. An improved understanding of electric current flow should lead to an optimized TES stimulation protocol and TES therapy results.

### *Blood flow*

The study of the effects of electrical stimulation on blood flow has a long history. Bayliss in 1901 made the first mention of electrical stimulation of vasodilator nerve fibers for the hind limb of a dog [22]. Stimulation of the posterior roots of the spinal cord is an appropriate therapy for individuals with peripheral vascular disease when

other methods fail. The electrical stimulation of these roots and also stimulation of the sympathetic fibers within the spinal cord produces arterial dilation in the extremities targeted [23]. Brown *et al* and Dodd *et al* both showed that low frequency (10 Hz) stimulation of rabbit muscles produced a twofold increase in capillary density after 28 days of chronic stimulation. The increase in capillary density could be seen as early as four days. These studies also showed the transformations of fast-twitch muscle to slow-twitch muscle [24, 25].

Blood flow increases, as well as increased capillary perfusion, has been demonstrated during direct current stimulation for the regeneration of peripheral nerves. Zanakis, using nerve cuff electrodes in rats, showed a dramatic increase in the vasculature while trying to induce axon repair. While performing dose range studies, he determined a minimum threshold of  $1.4 \mu\text{A}/\text{cm}^2$  at 1.4V [26]. This is the lowest current density known to cause vasodilatation. This effect has also been shown using low frequency stimulation. Increased blood flow and capillary density are thought to be the reason that TES therapy causes muscle growth.

### *Muscle strengthening*

Electrical stimulation can also be used for muscle strengthening. This usually occurs in the paraplegic population or in sports medicine. It is usually called functional neuromuscular stimulation (FNS). This is different from the other forms of electrical stimulation mentioned earlier in that active contraction of the muscle occurs. The goal is to strengthen the muscle through maximal contraction. The effect is supposedly the same as repetitive maximum isometric contractions or weight

lifting. The efficacy of the stimulation is usually determined by measuring the joint torque produced by the target muscle.

### *Magnetic stimulation*

Magnetic stimulation is an alternative way to cause AC electrical current to flow in a target area of the body. Magnetic stimulation has the benefit of not having electrode-skin interface impedance mismatch problems due to the magnetic permeability of the body being the same as air. However, magnetic stimulation requires greater complexity and bulkier coils to perform focused stimulation [27].

The main uses of magnetic stimulation are for bone healing and cerebral-cortical stimulation. Carter *et al* performed a dose response study in rats to determine the induced electrical current density on the surface of the bone needed to reverse osteoporosis. They determined  $100 \mu\text{A}/\text{cm}^2$  at 60 Hz to be the optimum level [28]. This is just below the level of sensory perception of current and well below that required for active recruitment of nerves or muscle tissue.

### **Finite Element Modeling**

The ability to determine the electric fields and the electric current induced by them in the body is a difficult but manageable task. The complex geometries of the human body prevent the direct solving of Maxwell's equations. Maxwell's equations describe the flow of electric and magnetic fields through any medium. The analytical solutions to these equations can be solved only for standard geometries. Previously, electric current predictions were made based on lumped parameter circuit models. Circuit theory for biological tissue is derived from electromagnetic field theory by

assuming that, under certain conditions, the body can be represented by a combination of discrete components such as resistors and capacitors. This method provides a good prediction for simple geometries and tissue properties. However, the complexities of the human body prevent this method from providing an accurate solution.

Several numerical methods are available for solving complex problems: the finite difference method, the method of moments, and the finite element method. The FEM is the most powerful and versatile numerical technique for handling problems which involve complex geometries and inhomogeneous media [29]. The FEM is general enough in structure to solve a wide range of problems. This allows software programs written for one particular discipline to be applied successfully to solve problems in a different discipline with little to no modification [30].

FEM has been used in mechanical engineering for over 40 years. Only in the past decade has it been used in biomedical applications [31, 32]. FEM allows for three dimensional modeling of complex geometries. It also allows for inhomogeneous, nonlinear, and anisotropic tissue properties to be incorporated into the model. Thus, FEM should, in principle, produce a more accurate result than lumped circuit models and one of the objectives of this study was to test that assumption.

Recent changes allow the use of a higher resolution FEM to accurately model electric fields in the human body [32]. Improvement in processing power and the amount of memory in today's computers allow more sophisticated models to be used. The development of interactive computer graphics allows the visualization of electric

current distributions in complex geometries. Development of numerical methods allow Maxwell's equations to be represented in digital form and solved using matrix methods [31].

Finite element analysis involves breaking down the body into hundreds or thousands of standard shapes (elements) and the simultaneous solution for the electric field for each of these elements. To determine the proportion of electric current that passes through the target muscle (quadriceps femoris) due to surface stimulation, the anatomy of the thigh region must be modeled. The I-DEAS Master Series software by SDRC Operations, Inc. (Milford, OH.) meets that demand. It includes a solid modeling package, an FEM simulator and the ability to import data.

To create a FEM using I-DEAS, several pieces of data must be supplied. First, the size and shape of the overall biological tissues to be modeled must be provided. The resolution must be determined. The finer the resolution, the greater the detail of the result, but not without a computational cost. The number of elements determines the resolution. As the number of elements ( $N$ ) required to match the overall geometry increases, the processing time required to solve the electric fields increases at a rate of  $N^3$ . Also, the amount of memory required to store and display the model increases linearly.

Second, the types, locations, and electrical conductivity properties of each element are required. The conductivity (the reciprocal of resistivity) of the tissue is given in siemens/cm. The conductivity is determined by the biological impedance analysis described below. The tissues modeled here are striated muscle, fat, and bone.

Third, the boundary conditions of stimulator input current and location must be supplied. The electrode skin model is a forward bioelectric field analysis problem. This means the source is given or known and the magnitude and direction of the resulting field is determined. Surface stimulation problems, therefore, tend to be solved using the FEM over the moment of methods technique.

Most biological tissues are not homogeneous. However, their conductivities are fairly uniform throughout a tissue type. This results in discrete domains of constant conductivities which are considered piecewise homogeneous for modeling purposes. This inhomogeneity can still easily be model with linear elements so long as the element edges are collocated with the tissue boundaries.

One important advantage that computer modeling has over clinical trials, is the ability to test protocols for difficult and complex problems which are costly and time consuming with human subject trials. With FEM, the subcutaneous electric current density can now be quantified. The optimization of various stimulation protocols can be set up and analyzed quickly, as well as economically.

#### *Mathematical Formulation of Electric Potentials in the Body*

The steady state potential due to current flow in the body is governed by Poisson's equation,

$$\nabla \cdot (\vec{\sigma} \cdot \nabla \Phi) = -I_v \quad (1)$$

where  $\Phi$  is the field strength,  $\sigma$  is the tissue conductivity tensor, and  $I_v$  is the current source density per unit volume of tissue. In the case of excitable tissue (muscle and nerve), the current is typically expressed as a divergence of a current density,

$$I_v = -\nabla \cdot J_i \quad (2)$$

where  $J_i$  is a non-ohmic source current field per unit area created by the combination of electrical, diffusional, and displacement currents through the active cell membrane. The membrane current,  $I_m$ , is obtained by dividing  $I_v$  by a surface to volume ratio,  $\beta$ . The membrane current can also be considered as the sum of the membrane capacitive current and the ionic current,

$$I_m = C_m \frac{\partial V_m}{\partial t} + I_{ionic} \quad (3)$$

where  $C_m$  is the membrane capacitance and  $V_m$  is the transmembrane potential given by

$$V_m = V_{inside} - V_{outside} \quad (4)$$

For the case of passive tissue like skin,  $I_v$  is

$$I_v = \frac{\beta}{R_m} V_m \quad (5)$$

where  $R_m$  is the membrane resistance.

Combining Equations 1 and 2 results in

$$\nabla \cdot (\sigma \cdot \nabla \Phi) = \nabla \cdot J_i \quad (6)$$



If the conductivity is constant in a uniform region, then Equation 6 in integral form is,

$$\Phi = \frac{1}{4\pi\sigma} \int_v \frac{\nabla \cdot J_i}{r} dV \quad (7)$$

where  $r$  is the distance from the source,  $J_i$ , in a volume [33]. Equation 7 is similar to the electrostatic potential due to a charge distribution. In fact, if the area of tissue is passive, like skin, then the potential is the solution of Laplace's equation.

For this research, a heat transfer solver was used. This can be done because of the duality of the underlying mathematics. Thermal conduction is described by Fourier's Law which is [34],

$$q = -kA \frac{\partial T}{\partial n} \quad (8)$$

where  $q$  is the rate of heat flow in the positive direction, through area  $A$  normal to its surface and  $T$  is the temperature. Application of the first law of thermodynamics to a control volume yields the general form of the conduction equation [34],

$$\frac{\partial}{\partial x} \left( k \frac{\partial T}{\partial x} \right) + \frac{\partial}{\partial y} \left( k \frac{\partial T}{\partial y} \right) + \frac{\partial}{\partial z} \left( k \frac{\partial T}{\partial z} \right) + q''' = \rho c \frac{\partial T}{\partial t} \quad (9)$$

for  $T$  as a function of  $x$ ,  $y$ ,  $z$ , and  $t$ , which is time. Additionally,  $\rho$  is the density of the material,  $c$  is the specific heat of the material, and  $q'''$  is the rate of internal heat generation. Equation 9 can be simplified to Laplace's equation when the problem is steady state and there is no internal energy conversion,

$$\frac{\partial^2 T}{\partial x^2} + \frac{\partial^2 T}{\partial y^2} + \frac{\partial^2 T}{\partial z^2} = 0. \quad (10)$$

Therefore, there is a direct analogy between temperature and voltage, thermal conductivity and electrical conductivity, and heat flux and electric current density.

Using this duality allows for the direct implementation of heat transfer FEM software package to solve for electric current densities in biological tissue [33].

### *Boundary Conditions*

To determine a unique solution, the boundary conditions (BC) need to be met. Two types of sources are used to supply electrical currents into the body. The electric stimulator is either a constant voltage source or a constant current source. The specification of a fixed potential,  $V_o$ , requires the Dirichlet BC

$$\Phi = V_o(x, y) \quad (11)$$

at the electrode interface. For a constant current source, the Neumann BC is specified,

$$\mathbf{n} \cdot \vec{\sigma} \cdot \nabla \Phi = J_n(x, y) \quad (12)$$

where  $J_n$  is the electrode current. When trying to stimulate muscle, the electric stimulator is the constant current type and the Neumann BC applies with the current equaling zero at the edges of the surface electrode.

### *Mathematical Formulation of the Finite Element Method*

The numerical technique of the finite element method relies on the ability to show that the energy  $W$  is stationary with respect to the variational  $\delta V$ . For bipolar

With the governing equations understood, the application of these equations to the FEM follows. First, the basis function for the voltage potential ( $\Phi$ ) must be selected. Construction of the approximate solution for  $\Phi$  is

$$\Phi \cong \tilde{\Phi} = \sum_{a=1}^n \phi_a N_a \quad (13)$$

where  $\phi_a$  is the local field in each element. Let  $N_a$  be any piecewise-smooth function spanning the  $n$ -dimensional linear space. This solution will not satisfy Equation 6 exactly. The method of weighted residuals (MWR) is used to minimize the error for a given set of basis functions. The most common MWR technique used is the Galerkin method. The mesh generation on the object being modeled, solution of the resulting matrix equations, and the graphical output to the user is typically performed by one of many commercially available codes. The FEM software used for this research is I-DEAS Master Series 6A by Structural Dynamics Research Corp., Milford, OH.

### **Bioelectric Impedance Analysis (BIA)**

Recent improvements in impedance plethysmography now allow for regional measurements of tissue *in vivo*. Previously, biological impedance analysis (BIA) was used to predict fat-free muscle mass of the whole body [35-37]. It has been shown that BIA is an accurate, economical, and simple method to determine body fat. RJL Systems of Detroit, MI. has developed an impedance plethysmograph which has a better than tenfold increase in resolution over previous impedance systems. Impedance plethysmography can now be used to accurately measure the impedance of a major muscle group such as the quadriceps femoris.

There are a number of traditional techniques available to measure the composition of a limb in terms of fat and muscle. These include anthropometric measurement, computerized tomography (CT), magnetic resonance imaging (MRI), and bioelectric impedance measurements. The anthropometric method uses skinfold thickness and limb circumference to calculate the cross sectional muscle area [38, 39]. This method makes assumptions concerning the average cross-sectional area of bone and vascular tissue. It assumes that the muscle mass is predominantly fat-free. Children with neuromuscular disorders do not fit the normal growth curves and body proportions upon which the anthropometric data is based. The muscles receiving treatment are atrophied and also do not fit the normal published data. Additionally, there is no procedure to apply limb measurements to a child with a neuropathic bladder and atrophied pelvic floor muscles. The CT and MRI techniques would work well to determine muscle condition but they are costly, time consuming, and have limited availability. Additionally, CT scan radiation exposure makes it impractical for multiple serial measurements to follow the changes in muscle atrophy due to subthreshold TES therapy.

Bioelectric impedance measurements have been correlated to provide the conductivity properties of the underlying tissue [37, 40, 41] but do not include the fat that is contained inside the muscle area as a result of atrophy. Bioelectric impedance analysis (BIA) has been shown to be as accurate as CT scans in determining the muscle and fat areas in the upper arm [42]. BIA, which is inexpensive and has no side effects, provides an easy method to determine muscle impedance [39]. With the recent improvements in BIA resolution cited earlier, localized impedance

measurements can now be made. Using impedance plethysmography, exact measurements of the electrical properties of striated muscle, adipose tissue, and bone can be made. The information now available to allow such measurements is described below.

The electrical properties of normal biological tissue are well known [43, 44]. Striated muscle is highly anisotropic while smooth muscle is more uniform [45]. In striated muscle, the longitudinal resistivity (the desired stimulation direction) is about 1/10th the transverse resistivity and is about 1.18 ohm-meters. If the tissue is anisotropic then the current will tend to flow parallel to the muscle fibers. Smooth muscle is considered to be isotropic, thus the current flow is considered even in all directions. Both types of muscle are well separated in terms of impedance from fat tissue which has a resistivity of 16 ohm-meters.

These electrical properties are valid for measurements made at frequencies below 100 kHz. At frequencies below 25 kHz, the current is carried primarily by ionic concentration in the extracellular fluids. Between 25 kHz and 100 kHz, the signal travels in both intracellular and extracellular fluid. BIA uses a 50 kHz signal to provide both intra and extracellular information. Because of the higher resistivity, adipose tissue is seen as insulators around which the current travels. Lean mass contains nearly all the water and conducting ions in the body; therefore, conductivity is much greater in fat free muscle mass than in fatty muscle mass (adipose tissue) [46].

Bioelectrical impedance measurements are based on the principle that the impedance of a geometrical system is related to conductor length, electrode configuration, cross-sectional area, tissue type, and signal frequency [47]. The bioelectrical impedance to current flowing in a volume of conductive tissue is

$$Z = \rho \frac{L}{A} \quad (14)$$

where the impedance,  $Z$ , is measured in ohms,  $\rho$  is the volume resistivity in ohm-meters,  $L$  is the conductor length in meters and  $A$  is the cross-sectional area. Equation (14) can be written in terms of the volume,  $V$ :

$$V = \frac{\rho L^2}{Z}. \quad (15)$$

The impedance of the conductor has two components, a resistance,  $R$ , and a reactance,  $X_c$ ,

$$Z = R + jX_c. \quad (16)$$

The reactance is due mainly to the capacitance of the cell membrane and produces a phase shift in the signal. By measuring only the current in phase with the source, the resistance component of the impedance can be found. Therefore Equation (15) becomes

$$V = \frac{\rho L^2}{R}. \quad (17)$$

Bioelectric impedance analysis is accomplished by using a tetrapolar configuration with the distal electrodes placed beyond the target region. These electrodes inject a

constant current reference signal which is considered to remain uniform in the area of interest. Then the proximal electrodes are positioned to measure the reference signal potential in the region of interest. See Figure 2 for an illustration of the setup for measuring a whole muscle's impedance.

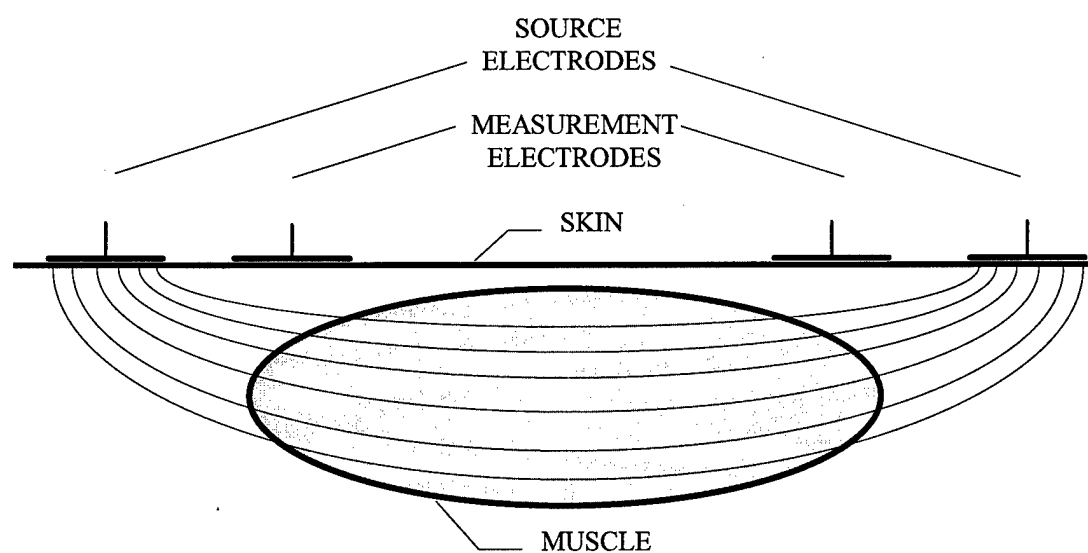


**Figure 2 - Tetrapolar configuration used in BIA. The source electrodes pass a known current through the tissue. The measurement electrodes sense the voltage at a fixed distance.**

Using Ohm's law,  $V = IZ$ , impedance can be calculated. Then a parallel resistance model is used incorporating the four main tissues; muscle, fat, bone, and neurovascular tissue. Since the resistivity of bone is far greater than the others at 100 ohm-meters, it is omitted from the electrical model with an error of less than 1%. Using the resistivities listed earlier; muscle, ( $\rho_m = 1.18$  ohm-meters), fat, ( $\rho_f = 16$

ohm-meters), and neurovascular resistivity equal to that of blood, ( $\rho_n = 1.6$  ohm-meters), the model yields

$$\frac{L}{R} = \frac{A_m}{\rho_m} + \frac{A_f}{\rho_f} + \frac{A_n}{\rho_n} \quad (18)$$

where  $R$  is the parallel resistance of the body segment between the measuring electrodes spaced at length,  $L$ . Also,  $A_m$ ,  $A_f$ , and  $A_n$ , are the respective areas of muscle, fat, and neurovascular tissue. The total cross-sectional area is

$$A = A_m + A_f + A_n + B \quad (19)$$

where  $B$  is the area of bone. To be able to use Equations (18) and (19) to determine the amount of fat in the muscle, the area of the bone and neurovascular tissue must first be computed using anthropometric measurements.

#### *Tissue Sample Impedance Measurement*

The measurement of tissue impedance is performed with a method similar to the *in vivo* method. The four electrode technique is used to determine the resistivity of a tissue sample. At low frequencies, the quasi-static approximation applies since the capacitive effects are negligible. The measurement is more accurate because of the isolation of a single tissue type. Additionally, the resistivity can be measured for each orientation of the tissue sample. This is especially important for anisotropic tissues such as striated muscle. The details of this process will be discussed more thoroughly in the next chapter.



These areas provide the foundation needed to understand the research. With a better understanding of the biology of muscle tissue, the finite element method, and bioimpedance analysis, the methods of how the laboratory experiments were conducted and the computer models were constructed is covered.

## CHAPTER 3

### METHODS

This chapter discusses the materials used in this research, the laboratory setup for both the saline model and leg of lamb measurements, and the methods used to create the finite element model from the leg of lamb.

#### Materials

Normal saline which has 0.9% NaCl in sterile water was used to create the cylindrical phantom model. The saline was placed into a standard one liter Pyrex™ chemistry beaker. The beaker was 10 cm in diameter and had a height of 12 cm. One liter of saline was used creating a depth of 11 cm. The saline has an electrical conductivity of .018 siemens/cm at 25°C [48]. To correct for the saline at room temperature (20°C), a correction factor, developed by Stogryn, was applied [49]. Given  $T = 20^{\circ}\text{C}$  and the concentration of saline,  $S = .009\text{ PPM}$ , then the temperature correction factor,  $\Delta$ , was

$$\Delta = 25 - T \quad (20)$$

and the normality,  $N$ , of saline was calculated by

$$N = S(0.01707 + 1.205 \times 10^{-5} \times S + 4.058 \times 10^{-9} \times S^2). \quad (21)$$

Using the conductivity value of  $\sigma_{25} = 0.018$  siemens/cm from Weast [48] and then applying it to the following equation,

$$\begin{aligned} \sigma_{20} = \sigma_{25} [ & 1 - 1.962 \times 10^{-2} \times \Delta + 8.08 \times 10^{-5} \times \Delta^2 - \\ & \Delta \times N [3.02 \times 10^{-5} + 3.922 \times 10^{-5} \times \Delta + \\ & N(1.721 \times 10^{-5} - 6.584 \times 10^{-6} \times \Delta)] ] \end{aligned} \quad (22)$$

resulted in a conductivity value of 0.0163 siemens/cm. Saline is considered a good conductor since the loss tangent,  $\sigma/2\pi f\epsilon$  is greater than 100 at frequencies below 100 kHz where  $f$  is the frequency and  $\epsilon$  is the permittivity and is found multiplying the relative permittivity ( $\epsilon_r = 80$ ) by the free space permittivity [50].

A leg of lamb was used as the animal thigh tissue. It was chosen because its size, tissue complexity, and muscle anatomy are similar to the human thigh. There are some differences in the hip structure since lambs are quadrupeds. These differences are insignificant since the FEM model developed did not include the pelvic region. A one centimeter resolution replica of the leg of lamb was used for the computer model. The process for generating the computer model will be discussed later in this chapter. Mountain Meadows meat processing plant in Denver, CO. supplied the lamb hind quarter. Figure 3 and Figure 4 are the top and bottom view of the leg after lower leg removal. Special arrangements were made to ensure that the specimen was used as close to sacrifice as possible. The animal tissue was brought

straight to the laboratory and the measurements were made approximately 2 ½ hours postmortem.

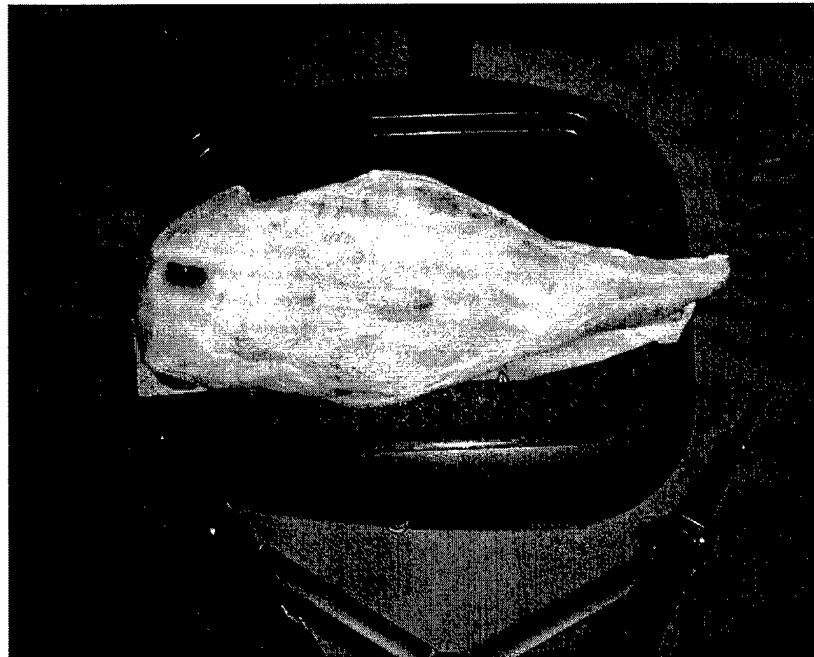


**Figure 3 - Photo of the leg of lamb prior electric current density and tissue impedance measurements (top view).**

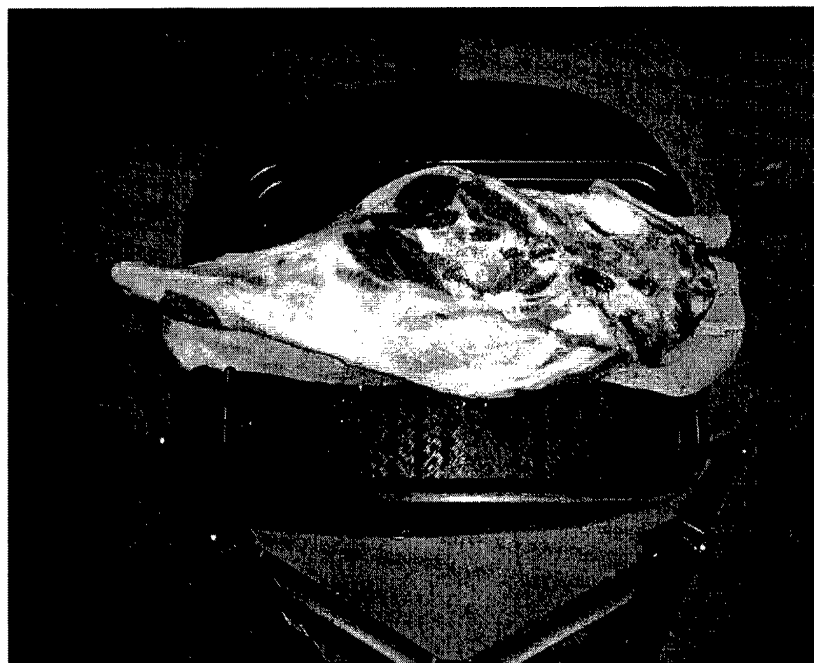


**Figure 4 - Photo of the leg of lamb prior electric current density and tissue impedance measurements (bottom view).**

Preparation of the leg of lamb included the removal of the hoof and insertion of a wooden dowel through the femur. The dowel rod provided the ability to mount the leg in a stand to suspend and isolate the tissue in the air. Placing the dowel rod inside the bone minimized the effect on the overall impedance characteristics of the animal tissue, because the bone, which is also a poor conductor, isolated the rod from affecting the current flow in the leg. Suspending the leg in the stand also prevented any deformation of the soft tissue and prevented any current flow outside of the tissue.

In addition to the electrical considerations, the dowel rod was used to provide a global reference point and was assigned as the Z axis. Figure 5 is an end view of the leg of lamb in the holder. The dimensions of the leg were 28 cm long with

circumferences (from right to left in Figure 3) of approximately 22 cm, 41 cm mid-thigh, and 30 cm on the left end.

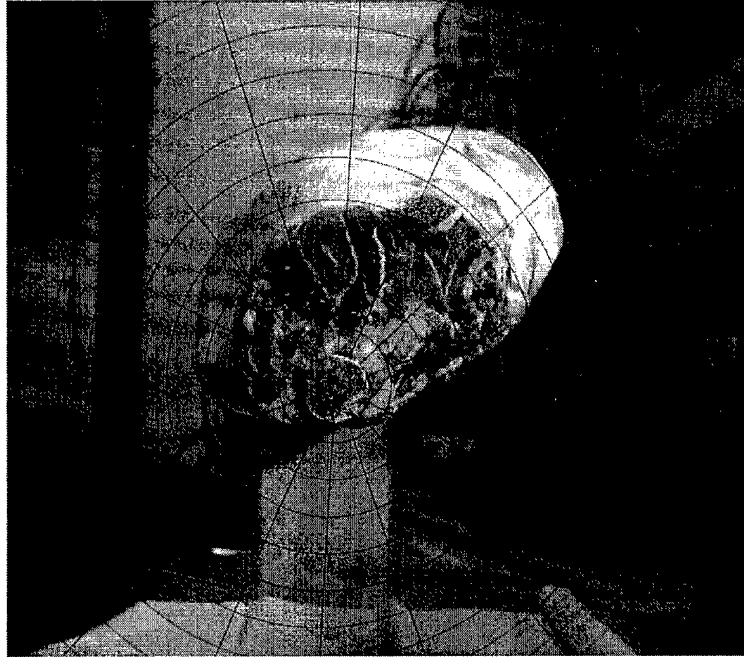


**Figure 5 - Distal end of the leg of lamb. Template used to apply markings for probe measurement locations.**

## **Laboratory Setup**

### *Equipment*

Several pieces of test equipment were used for the various BIA measurements in this research. They were:

- Philips PM 5134 Function Generator
- Tektronix #2246 Oscilloscope
- Hewlett Packard 34401A Digital Multimeter

- Hewlett Packard E3617A DC Power Supplies
- Fluke 77/BN Digital Multimeters

In addition to the test equipment, several other pieces of equipment were developed to aid in the speed, accuracy, and repeatability of the laboratory measurements. The first was an instrumentation amplifier circuit to reduce noise and provide signal gain for the measurements made with the saline and tissue probes. It consisted of the Burr-Brown INA120 precision instrumentation amplifier. It provided the necessary high common-mode rejection, high input impedance, and digitally selectable gain control for improved measurement accuracy. This operational amplifier, in conjunction with the impedance probe's shielded cables, provided the signal to noise ratio required to make low-noise measurements over the signal ranges involved. Figure 6 is a diagram of this circuit.

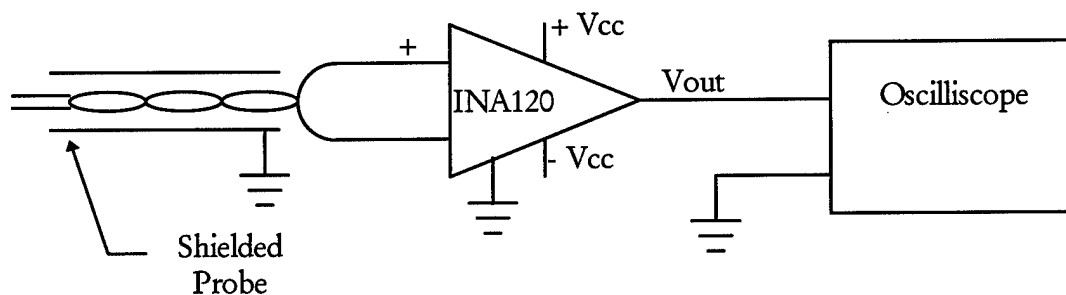


**Figure 6 - The instrumentation amplifier circuit setup used for all the laboratory measurements.**

All the electrodes used in this research were silver-silver chloride (Ag-AgCl) electrodes. This type of electrode reacts the least with biologic tissue in the way of a

DC potential from ionic reaction with the metal. The electrodes were made by coating stainless steel needles with silver then applying a thin chloride layer using electrolysis in hydrogen chloride (HCl). For the saline electrodes, the Ag-AgCl surface was 1 mm in length and 0.5 mm in diameter. The electrodes were spaced 5 mm apart at the end of a nonconductive rod. See Figure 7 for a diagram.

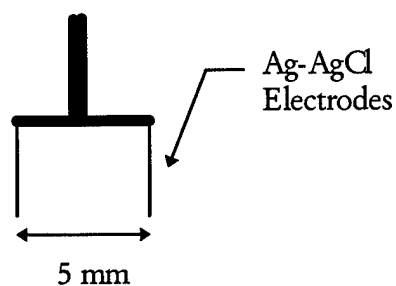


**Figure 7 - Saline Voltage Measurement Probe**

The probe for measurements in the leg of lamb had 1 mm Ag-AgCl surface at the end of stainless steel needles which were 6 cm on length. All but the electrode tips were coated with epoxy to insulate the needles. They were placed in a holder to keep them parallel to each other. The shafts of the needles were indexed with 1 cm markings to determine the measurement depth. The tissue probe is shown in Figure 8.



Two sets of electrodes were used in the tissue impedance measurement device as part of a four electrode impedance measurement. Ag-AgCl plate electrodes were used to supply a uniform field to the tissue samples. They measured  $2\text{ cm}^2$  and were rectangular in shape. The detection electrodes were needle electrodes measuring 2 mm in length. All the electrodes were attached to shielded cables to connect them to the instrumentation amplifier. See the electrodes in Figure 9.

#### *Tissue Impedance Measurement Device*

A special device was designed to allow quick, reliable, and repeatable BIA of the tissue cubes excised from the leg of lamb. The holder was designed to accept tissue cubes from of  $1.5\text{ cm}^3$  up to  $2\text{ cm}^3$  in size. The tissue impedance measurement device had a built in isolation transformer for signal input and measurement circuitry using the four electrode technique. The instrumentation circuit was the same op amp design as in Figure 6. The device actually made simultaneous impedance measurements at two separate parallel locations along the X or Y axis in the tissue sample. These two values were then averaged to produce the final measurement

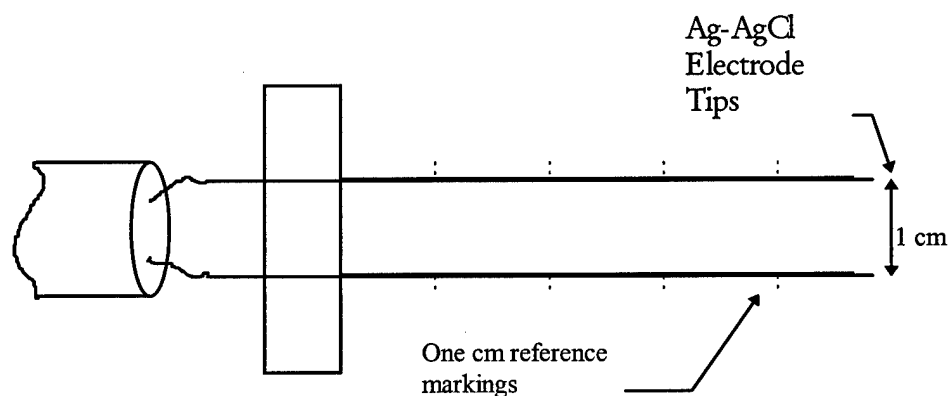


**Figure 8 - Diagram showing the tissue measurement probe. It consists of two insulated needles with 1 mm Ag-AgCl exposed tips. The probe has 1 cm markings on the needle shaft to determine tissue depth.**

value. A manual switch position determined the measurement axis. This allowed two orthogonal impedance measurements to be accomplished without moving the tissue sample. Figure 9 is a diagram of this device.

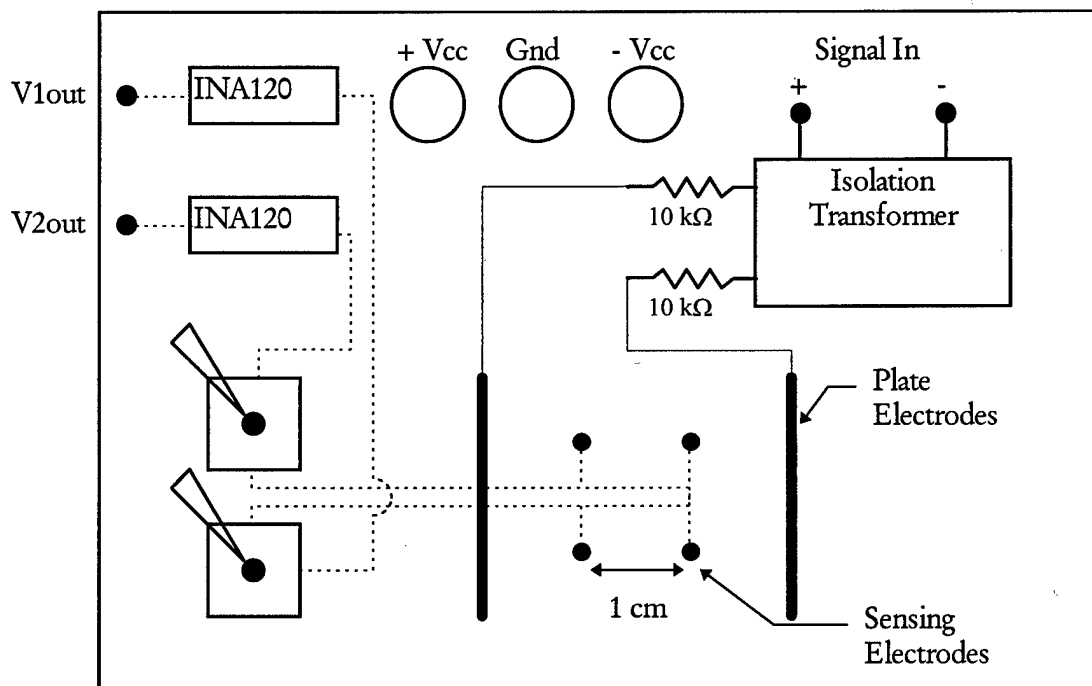


**Figure 9 - Diagram showing tissue impedance measuring device. It had two source plate electrodes and four sensing electrodes.  $2\text{ cm}^2$  tissue samples were placed between the plate electrodes and the voltage outputs were measured on an oscilloscope. The four sensing electrodes allowed measurements in two directions by repositioning the switches.**

The tissue impedance measuring device was connected to the test equipment and power supply. A tissue sample cube from the leg of lamb was placed over the sensing electrodes and the source electrode plates were moved against the sides of the tissue. A constant  $500\text{ }\mu\text{A}$  sinusoidal current at 35 Hz was passed through the cube

creating the tetrapolar setup used for BIA. The output voltages allowed the calculation of the voltage gradient per cm. The voltage across one of the 10 k $\Omega$  resistors was also measured to calculate and control the value of the input current. With these measurements, the tissue impedance was calculated. Measurements were made for all three axes. Since the device could measure two axes without moving the sample, when the cube was turned to measure the Z axis, the X axis measurement was repeated to validate the measurement conditions. Figure 10 is a photo of adipose tissue impedance measurement.

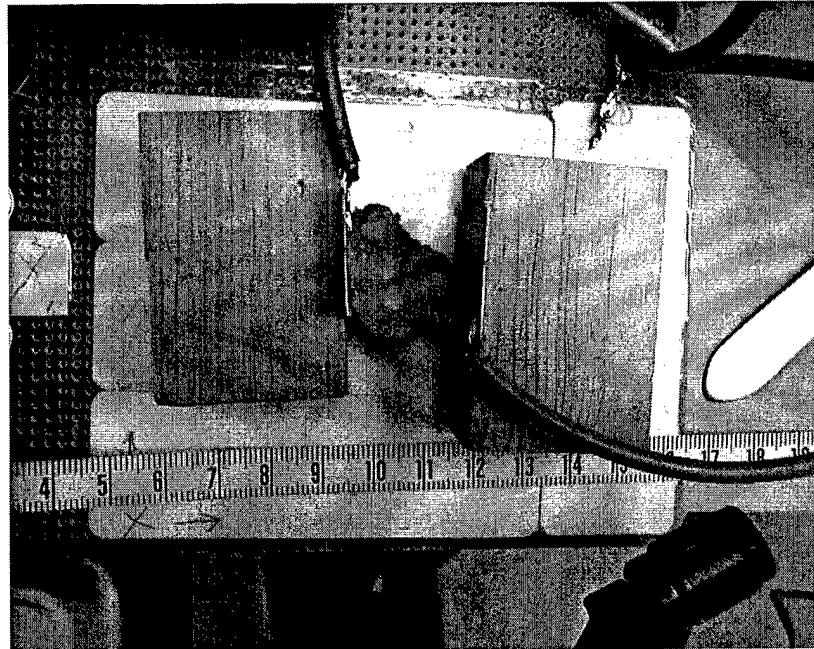


**Figure 10 - Photo of the tissue impedance measurement device with an adipose tissue sample placed in it. The two lower sensing electrodes are exposed for demonstration purposes.**

### *Leg of Lamb Field Measurements*

After preparing the leg of lamb, the quadriceps muscle was located as the target muscle for stimulation. Reference markings were applied to the outside surface fat layer. The electrode site was placed along the longitudinal axis of the target muscle. The Ag-AgCl active electrodes were 10 cm apart. One centimeter divisions were marked on the surface to be the guide markings for probe measurements. These markings also provided the cutting locations to slice the leg of lamb to identify the anatomy and tissue types for the FEM lamb model. Additionally, the radial lines from the holder's origin were marked at  $\pm 22.5^\circ$  and  $45^\circ$ . Figure 11 shows a close-up of the leg of lamb with these markings applied.



**Figure 11 - Photo of the leg of lamb after the first set 1 cm reference markings are in place.**

The stimulation signal for the leg of lamb was a constant current (500  $\mu$ A) 35 Hz sinusoidal wave. Using the tissue probe in Figure 8, voltage gradient measurements were made at 0, 2, 4, 6, 8, and 12 cm along the Z axis. A measurement was taken at the surface and at 1 cm intervals up to a depth of 4 cm at each location. Measurements were also taken at the same points on the Z axis along each radial line. At several locations some of these measurements could not be made as bone was contacted.

### **Building The FEM Model From The Leg of Lamb**

A resolution of 1 cm brick elements was chosen for the FEM model to match the voltage gradient measurements and the thickness of the slices. Linear elements were used and each element was allowed only one tissue type. The tissues modeled were the three dominant tissue found in the leg of lamb. They were striated muscle, fat, and bone. Both the fat and the bone were modeled with homogeneous conductivity while the muscle was modeled as anisotropic. The conductivity of muscle along the Z axis (longitudinally) was approximately ten times greater than in the X - Y plane (laterally). The actual values for the conductivity used in the model were the averages measured in the tissue samples and are listed in Table 1 Chapter 5.

To determine the tissue type for every element, the leg of lamb was sliced orthogonally to the rod placed in the bone (sliced in the X - Y plane) at the 1 cm markings. A total of 12 slices were made. These slices were then imaged with the reference markings labeled. A 1 cm digital grid was then aligned over the slice using the center of the rod as the origin. The radial lines from the origin were also applied

to determine the measurement locations. The grid also provided X - Y coordinates with the center of the dowel rod at  $X = 0$ ,  $Y = 0$ . Since the slices were one cm thick, the slice number corresponded to the Z coordinate. These images are shown in Appendix A.

To convert the images into a FEM model, the one cm grid was used as the element boundaries. One grid cube became an element with eight nodes. The majority tissue identified visually in the grid was made the tissue type for the whole element. Since the slices varied in size according to the circumference at points along the thigh, the smaller slices required padding with air elements to maintain a uniform numbering scheme. Each element was labeled using a four digit number. The element number was assigned according to,

$$\text{Element Number} = Z \times 1000 + (X + 7 + ((Y + 3) \times 18)) \quad (23)$$

where X, Y, and Z were the global coordinate location of the lower left hand corner of the tissue sample. This results in the thousands unit of the element number corresponding to the Z location also referred to as the slice number.

Each node was also given a four digit label. The node in the lower left corner of the front face of the element was assigned the same label value as the element number. The remaining nodes were numbered according to the same numbering scheme. The results of creating the element and node numbers along with the tissue type assigned are shown in Table 6 through Table 17 in Appendix E.

All the tissue characterization and location data from these tables was then converted into an ASCII file to be imported into I-DEAS. This conversion followed the universal file set format used by the software. All the FEM characteristics of each element were imported into the software using the finished universal file set found in Appendix H. The only additional modifications made to the leg of lamb FEM model was grouping the elements into common characteristics for post processing display purposes. These groups included:

- Even slices 0 - 12
- All muscle elements
- All fat elements
- All bone elements
- Entire leg of lamb elements with air padding removed
- Measured elements
- Target muscle elements

With a 1 cm resolution replication of the leg of lamb imported into the I-DEAS software, the only remaining task was to model the application of the bipolar stimulation using the boundary conditions. This finished model provided the ability to duplicate the laboratory setup of the stimulated leg of lamb.

Now with an understanding of the materials used in the laboratory, and the techniques used to make the empirical measurements and create the FEM model to

duplicate the leg of lamb, the validation of the FEM heat transfer analysis application for biological modeling must be confirmed.



## **CHAPTER 4**

### **VALIDATION OF FEM HEAT TRANSFER ANALYSIS FOR BIOLOGICAL MODELING**

The purpose of this chapter is to validate the ability of a heat transfer finite element model to determine the electrical voltage gradient (modeled by temperature gradient) in a phantom saline solution model. The FEM software used the heat transfer equations to determine the model results. Since the saline model was a volume conductor, the heat transfer method and electrical field equations both used the same underlying mathematics: Poisson's equation. The empirical results measured in normal saline compared favorably to the FEM output, validating the assumption that heat transfer finite element software packages can be used to model bioelectric phenomena at low frequencies.

In addition, this chapter confirms the FEM's ability to handle the effects of an anisotropic medium and layered tissues encountered in biological medium. Several modifications were made to the saline phantom model to create new models. The results were investigated to ensure that skeletal muscle and multiple tissue types could be accurately modeled in the next phase of this research.

### Laboratory setup

The laboratory setup used to measure the voltage gradient in normal saline solution is shown in Figure 12. One liter of 0.9% saline was placed in the 10 cm diameter glass cylinder. The saline had a conductivity of 0.0016 S/cm as calculated in Chapter 3. The input signal was a 35 Hz, 500  $\mu$ A peak, constant current sinusoidal wave. The electrodes were placed on opposite sides of the glass cylinder walls, 1 cm below the surface. This allowed the signal to be measured up to 10 cm away from the source and provided asymmetry to the problem to more thoroughly test the FEM.

The electrodes were Ag-AgCl wires with 2 mm exposed at the ends. The measurement probe was also a Ag-AgCl electrode controlled by a three degrees of freedom manipulator. The signal was passed through a Burr-Brown INA120 instrumentation amplifier to reduce noise and provide a high input impedance. The gain was set at unity. The output signal from the op amp was measured and recorded with an oscilloscope, reference Figure 12.

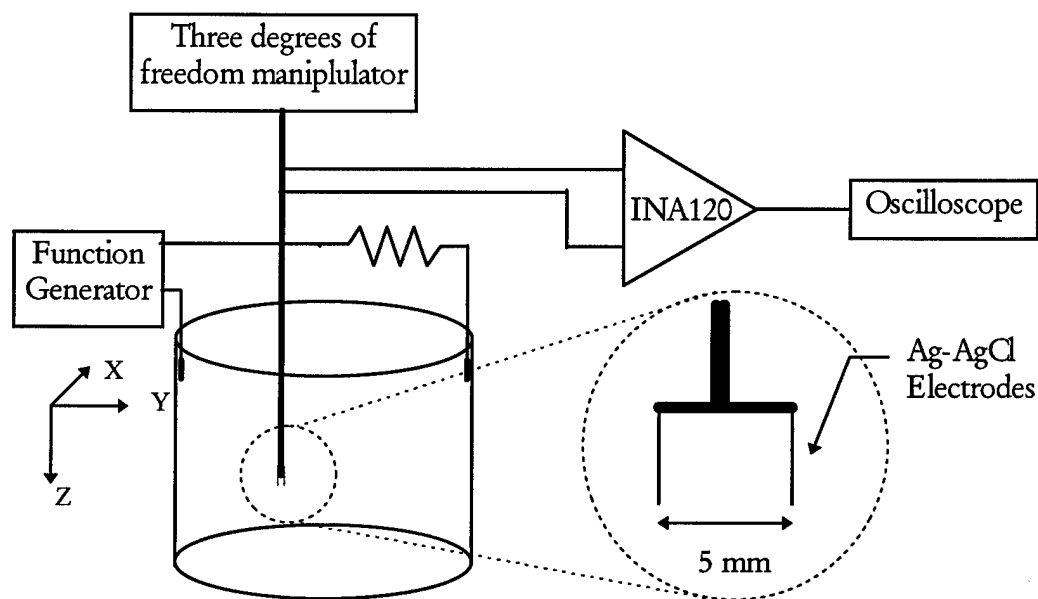


**Figure 12 - Diagram showing the saline model laboratory setup. One liter of 0.9% saline was placed in the 10 cm diameter glass cylinder. The electrodes were placed on opposite sides of the glass cylinder walls, 1 cm below the surface. The electrodes were Ag-AgCl wires with 2 mm exposed at the ends. The measurement probe was also a Ag-AgCl electrode controlled by a three degrees of freedom manipulator. The signal was passed through a Burr-Brown INA120 instrumentation amplifier. The output signal from the op amp was measured and recorded with an oscilloscope. The callout is a close-up of the measurement probe tip.**

### Finite Element Saline Model

Three FEM models were programmed. The first replicated the saline laboratory setup. The second FEM model was designed to more closely duplicate stimulation along the quadriceps muscle using the same size cylinder. The stimulation electrodes were aligned with the vertical axis and were placed on the same side of the cylinder wall 10 cm apart. The medium's conductivity was modeled as if it were anisotropic. The conductivity along the Z axis was then programmed as ten times greater than in the lateral direction (X-Y plane). This is similar to the

properties of striated muscle. This was done to simulate the bipolar stimulation pattern of the human thigh muscle found in many stimulation protocols. The model was automatically meshed by I-DEAS using linear tetrahedron elements with lengths averaging 5 mm per side.

The final model was designed to replicate the same cylinder with the bipolar stimulation pattern but with three different concentric layers. This configuration tested different material interfaces similar to a skin, muscle, and bone arrangement found in a thigh. This model was also automeshed by I-DEAS. The only difference was that 2D surface elements were used to simulate the skin layer.

### **Saline Modeling Results**

The results of the saline FEM model compared favorably with laboratory measurements made in the saline solution. Since saline is a good conductor, the current spread out quickly and evenly throughout the cylinder. The field strength was evenly distributed outside 2 cm of the electrodes. Table 4 in Appendix B is a summary of the measurements at the main points in the cylinder and the corresponding saline FEM model values for the same location. Figure 13 is a graph of the voltages between the bipolar electrodes. The difference in the two values can be attributed to the measurement probe having a 5 mm spacing. This causes an averaging of values over that distance. This difference has the greatest affect near the electrodes where the potential changes rapidly. The difference results in a smoothing of the measurement curves. Conversely, the values listed for the FEM are at discrete points which correspond to nodes in the FEM. When comparing the model results

with the empirical measurements away from the electrodes the results were the same, reference Figure 14 through Figure 16. Both the model and empirical data showed the uniform current density at all points greater then 2 cm from either electrode.

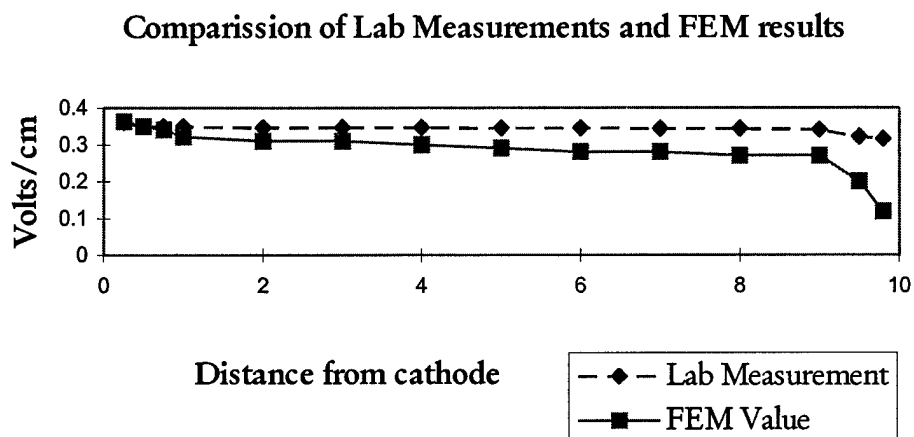


**Figure 13 - Graph comparing the voltage gradient measurements and saline FEM model results. The location of these values was on a line directly between the electrodes.**

Figure 14 shows a plot of the voltage potential in the X-Y plane, 1 cm below the surface, level with the electrodes. Notice the rapid dispersion of the electric field which is expected in a good conductor.

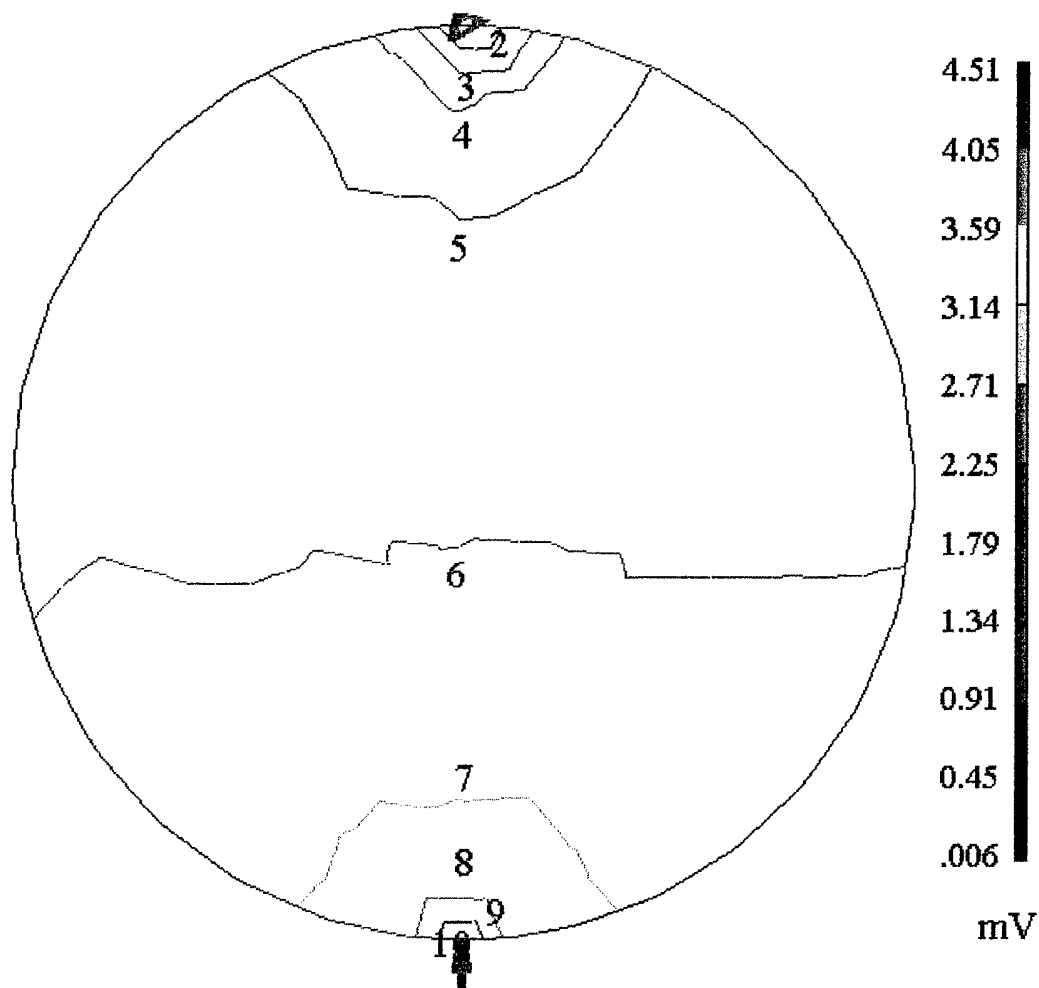


**Figure 14 - Contour plot shows the voltage potential in the X-Y plane, 1 cm below the surface, level with the electrodes. The voltage potential was uniform outside 2 cm of the electrodes. The number on the contour line corresponds to its color bar segment.**

Figure 15 shows the voltage midplane between the electrodes in the X-Z plane. The results confirmed a uniform field all the way to the bottom of the solution and match the empirical measurements (Appendix D). Both the empirical measurements and the model's results provided uniform values throughout the midplane. This was expected since saline is a good conductor. The favorable

comparison also verifies the FEM model's ability to handle the asymmetry created by the location of the electrodes near the top surface.

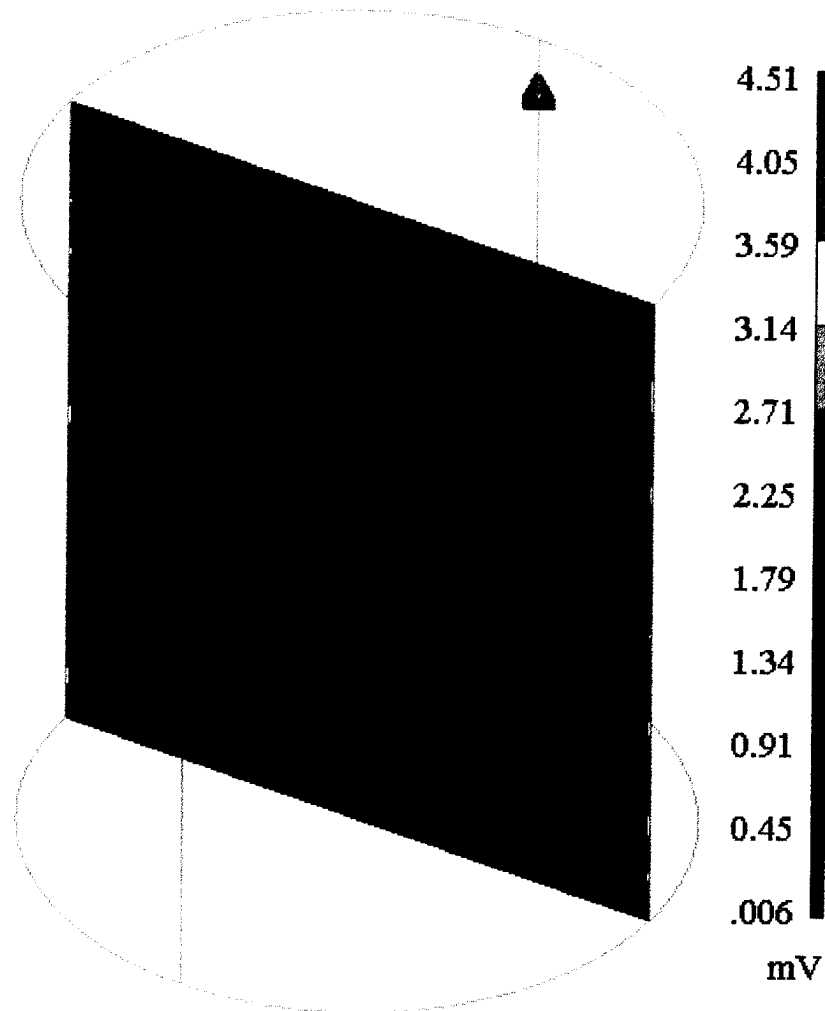


**Figure 15 - Plot showing the saline model voltage results midplane between the electrodes in the X-Z plane. The results confirmed a uniform field all the way to the bottom of the solution and match the empirical measurements (Appendix D). Both the empirical measurements and the model's results provided uniform values throughout the midplane. This was expected since saline is a good conductor.**

Additionally, the FEM provided the ability to plot the current flow (modeled by heat flux) throughout the cylinder. This is shown in Figure 16. The color and length each arrow indicates the current's magnitude.

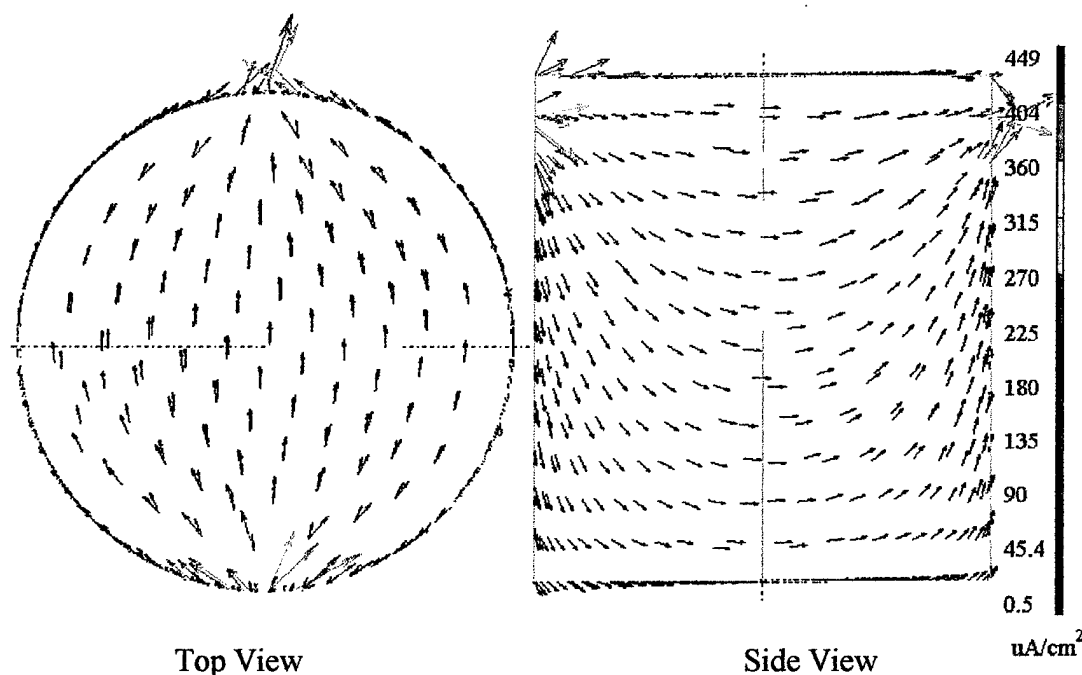


**Figure 16 - Arrow plots showing the current density in a cylinder of homogeneous saline. The color and length each arrow indicates the current's magnitude. The current density is uniform outside of 2 cm of the electrodes.**

The second FEM modeling effort tested the ability of the heat transfer software to model anisotropic medium. The saline properties were changed to be similar to that of skeletal muscle setting the preferred direction for current flow longitudinally along the Z axis. This was along the length of the cylinder. The stimulation mode was also changed to represent bipolar surface stimulation using patch electrodes. The simulated anisotropic saline affected the current spread in the transverse direction as can be seen in Figure 17. The current distribution was no



longer uniform through out the cylinder but was concentrated along the path between the electrodes, favoring the preferred direction of conductivity. Thus, it appears that anisotropic property of muscle helps to minimize the lateral current spread during bipolar stimulation.

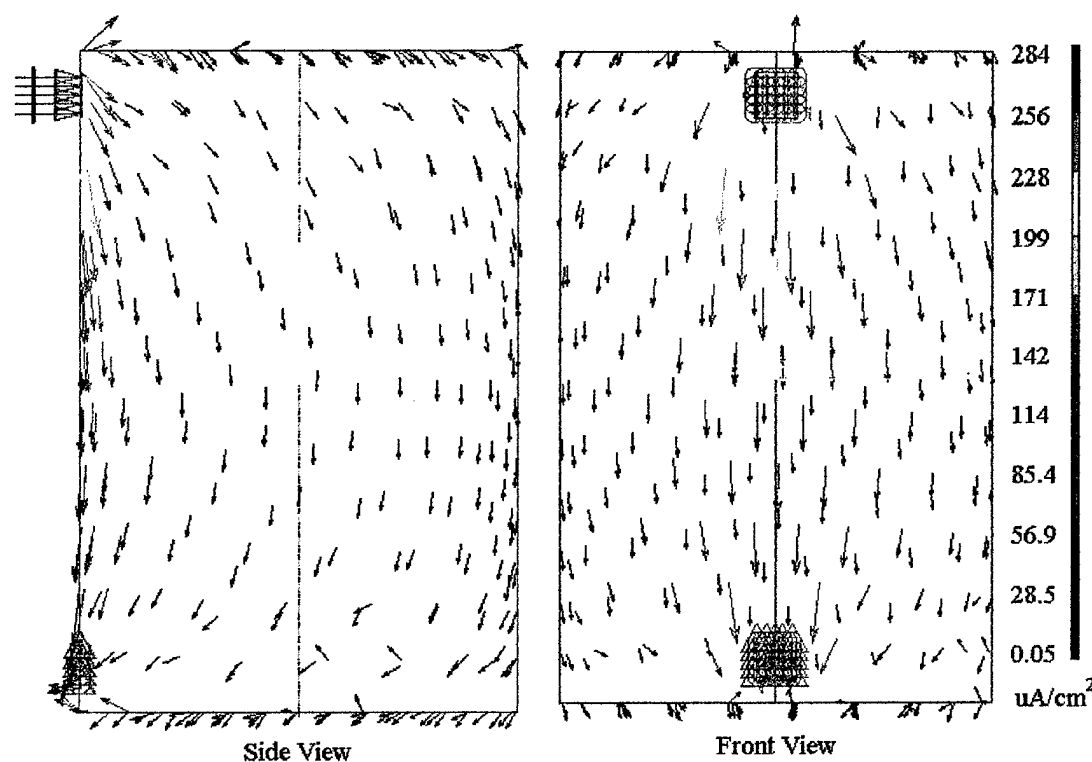


**Figure 17 - Arrow plots showing the current density results. The medium was made anisotropic to simulate muscle. The surface application was from top to bottom to represent bipolar stimulation along the length of a muscle.**

Figure 18 further shows this focusing of the current because of the anisotropic property in the midplane slice between the bipolar stimulation electrodes. This pattern was similar to the current flux in the isotropic, homogeneous midplane slice in the laboratory saline model (Figure 15). The change caused by the anisotropic property was clear and can be seen in the comparison of these figures.

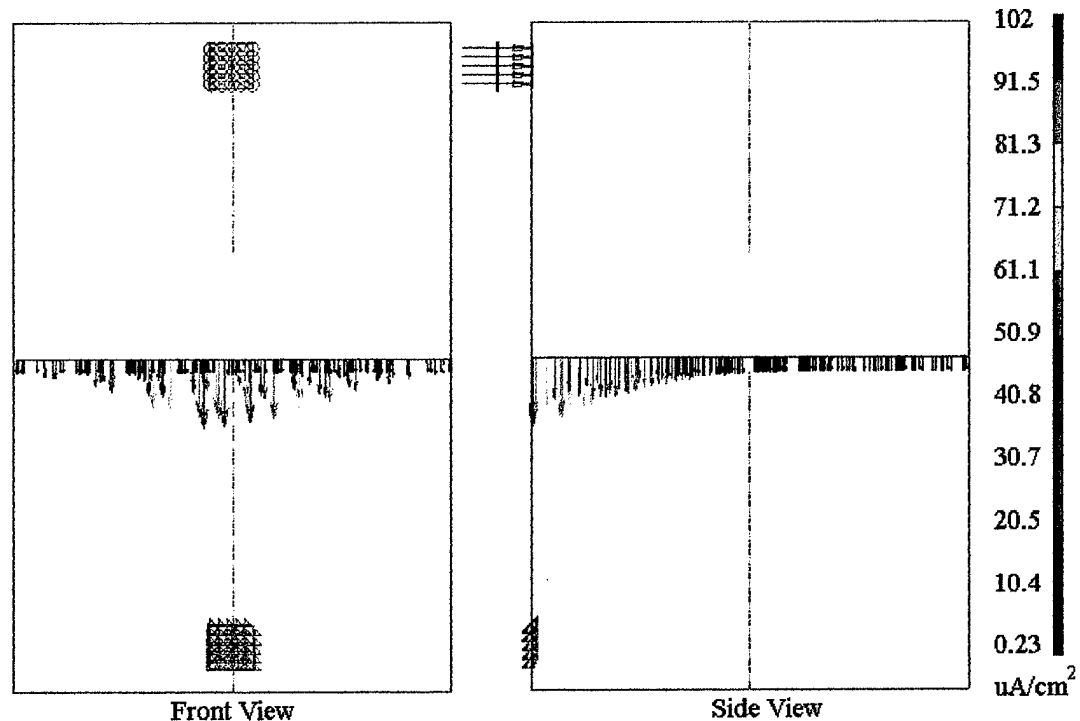


**Figure 18 - Current density plot showing the anisotropic FEM model's midplane results between the electrodes in the X-Y plane. The current density is no longer uniform at midplane. The anisotropic conductivity focuses the current flow directly between the electrodes.**

The final FEM modeling effort investigated the ability of the FEM to handle changes in material properties such as those found at tissue boundaries. The model was the same as the top half of the anisotropic saline model with the addition of three different concentric layers. Only half of the cylinder was needed due to the symmetry of the model. The model had an outer layer of skin followed by a cylinder representing striated muscle, and finally, an inner cylinder representing bone. In addition to testing the different tissue properties, the skin was also meshed with thin shell elements. The thin shell elements were two dimensional elements. This tested the ability to create a model with both solid and thin shell elements. These additions

brought the model one step closer to the ultimate long term goal of modeling a human thigh model.

Figure 19 shows the voltage contour line plot of just the thin shell elements representing the skin. The voltage changed rapidly around the source electrode and became more uniform as the distance increased. This FEM model results showed the ability of the thermal software to handle the complexity required to accurately model the various inhomogeneities encountered when modeling the electrical impedance of biological tissues.

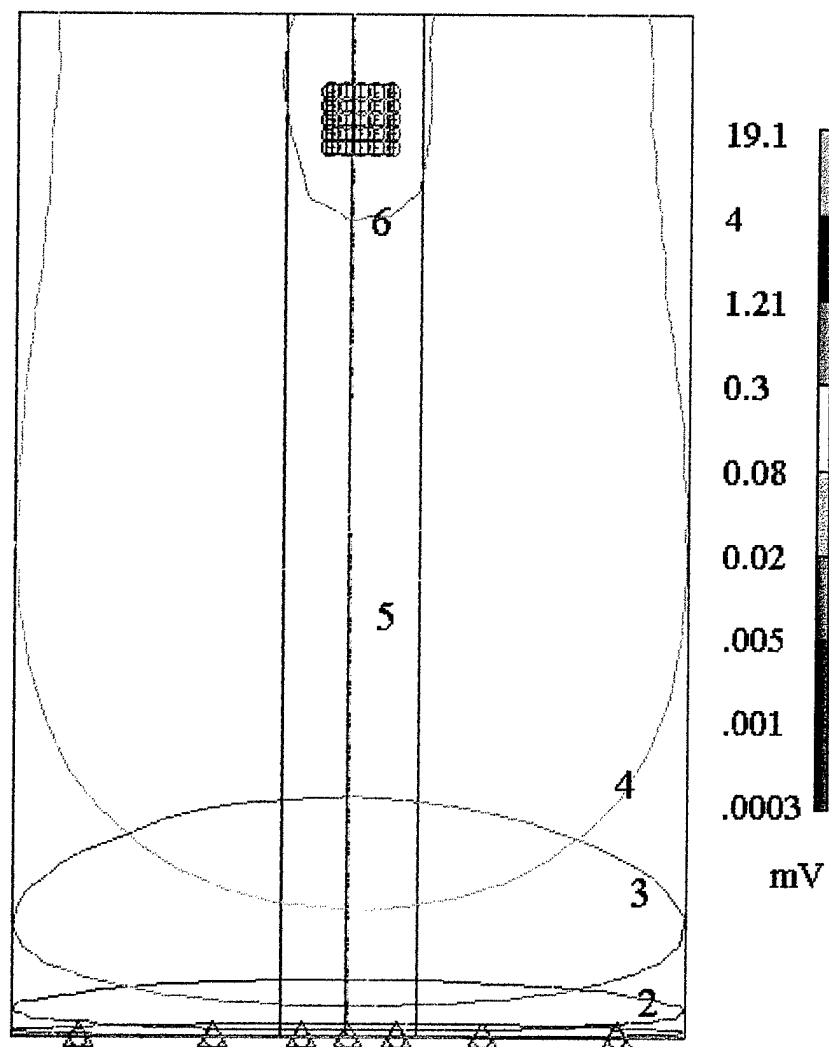


**Figure 19 - Front view of a three dimensional contour line plot showing the surface voltage on the multi-layer FEM model. This plot is of just the thin shell elements representing the skin. The voltage changed rapidly around the source electrode and became more uniform as the distance increased. The number on the contour line corresponds to its color bar segment.**

The modeling results using solid elements representing muscle and bone showed a similar concentration of current along the longitudinal axis as the 2nd model. However, bone further limited the current spread by inserting an insulator in

the middle of the muscle conductor. This insulator created a voltage gradient laterally across the bone causing the current vector to shift away from the electrodes. The effect was more pronounced near the cathode. The current inside the bone was significantly lower due to its poor conductivity. Figure 20 -Figure 23 show the different views of the current density plots of the multi-layered FEM model.

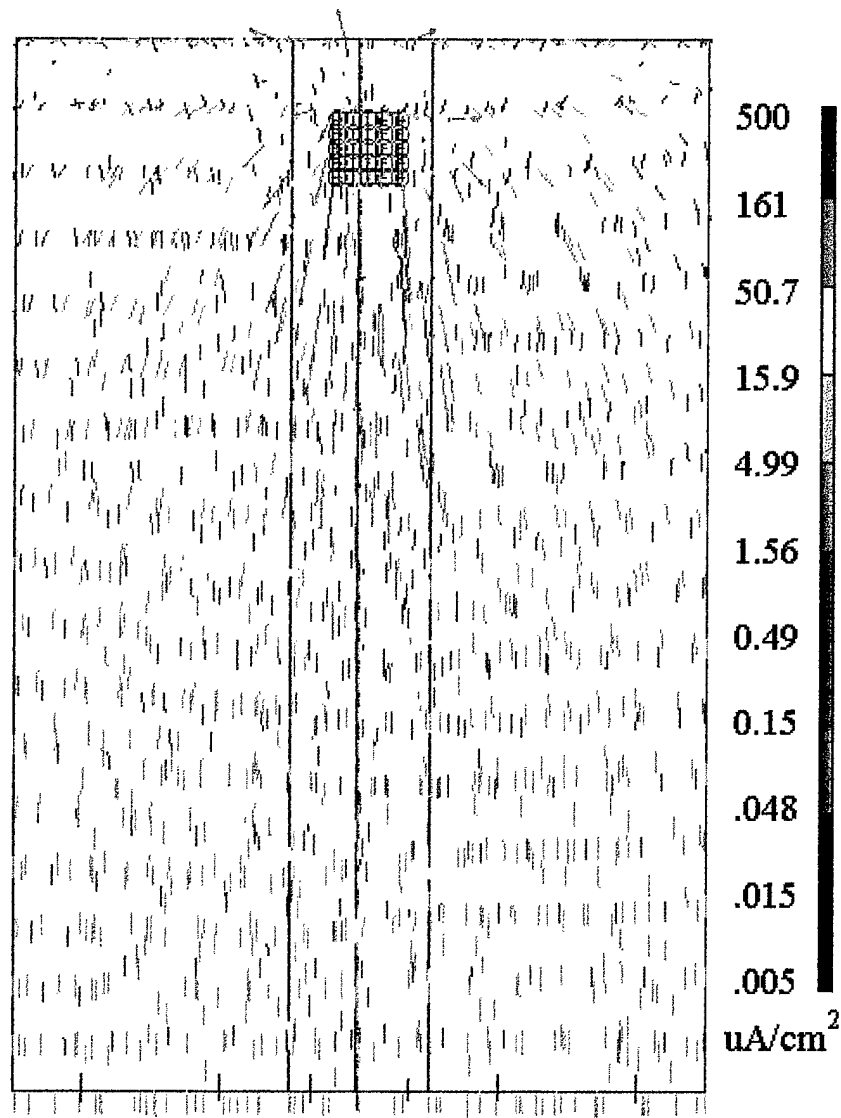


**Figure 20 - Plot showing the front view current density results of the multi-layer FEM model. This figure is only the top half of the cylinder. The results are similar to the anisotropic FEM model with the addition of the bone further limiting the current spread.**

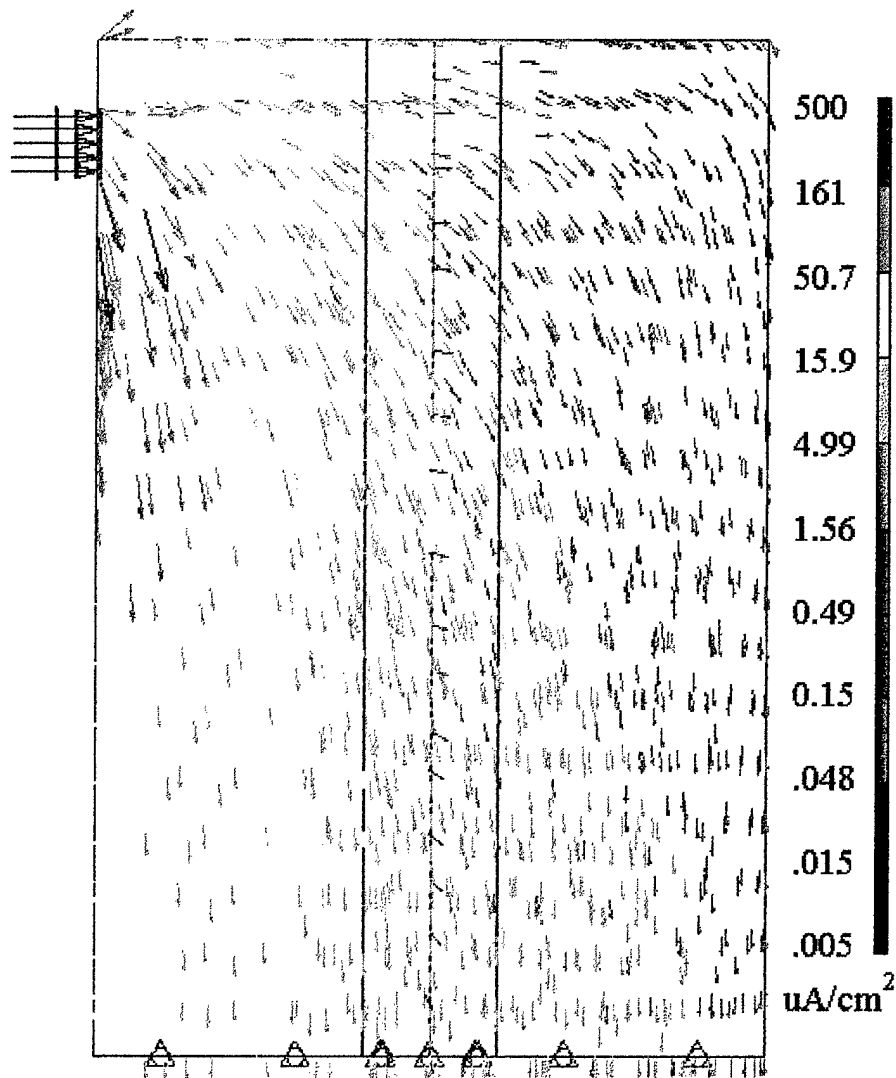


**Figure 21 - Plot showing the side view current density results of the multi-layer FEM model. This figure is only the top half of the cylinder. The results are similar to the anisotropic FEM model with the addition of the bone further limiting the current spread.**

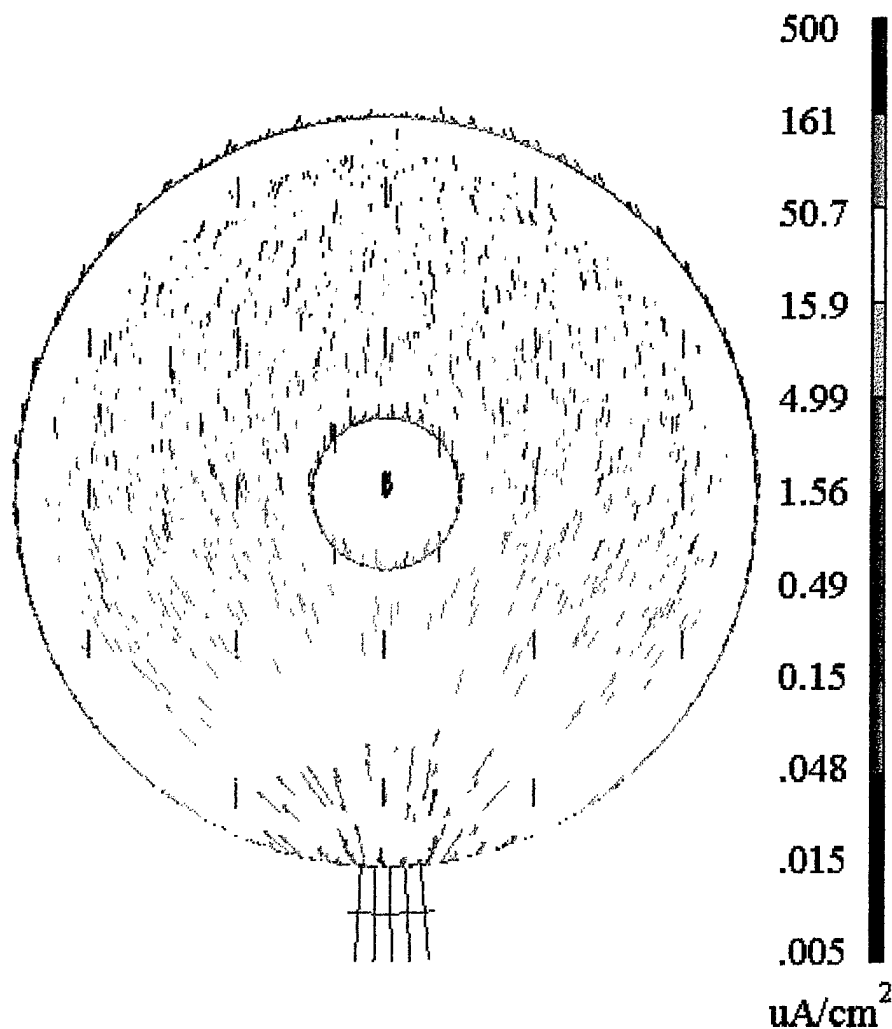


**Figure 22 - Plot showing the top view current density results of the multi-layer FEM model. The results are similar to the anisotropic FEM model with the addition of the bone further limiting the current spread. Also, the current inside the bone was significantly lower due to its poor conductivity.**

Once again, the midplane view of the Y-Z plane is provided in Figure 23. This figure shows a clearer picture of the current in the muscle layer vs. the bone layer. The concentration of the current resulting from the anisotropic property of striated muscle can still be seen.



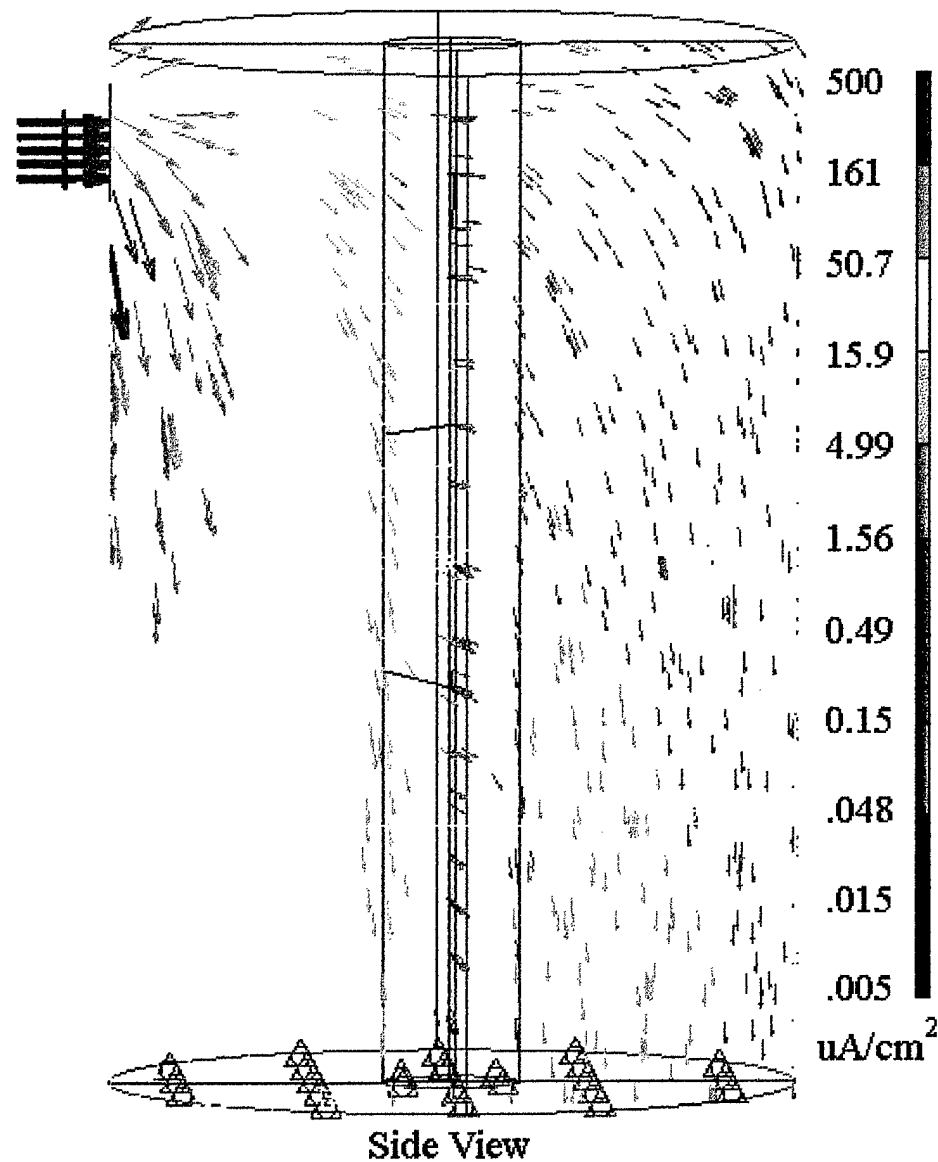


**Figure 23 - Plot showing the midplane current density results of the multi-layer FEM model. This figure is only the top half of the cylinder. The results are similar to the anisotropic FEM model with the addition of the bone further limiting the current spread. Note the direction of the current vector inside the bone. The insulative bone created a voltage gradient laterally causing the current vector to shift away from the electrodes. This effect was more pronounced near the source.**

## Discussion of the FEM Results

The heat transfer solver in the FEM software provided an effective way to model electric fields in biological tissue. The FEM software had the added benefit of many graphical outputs to help visualize complex field patterns. Attention to the boundary conditions and meshing detail were required to ensure accurate results. The good correlation between the laboratory measurements and the FEM model results also validate the quasi-static assumption made for the low frequency steady state solution. FEM software also provide the ability to model complex geometries, inhomogeneities, and non-linearities. These properties allow accurate modeling of complex geometries and tissues found in various portions of the human body.

In addition to the direct comparison between the empirical results and model results to verify the accuracy of the isotropic tissue computer modeling method, the geometry of the saline model setup provided the comparison of the model results to an analytical solution. By modeling bipolar stimulation in a cylindrical phantom of saline, the model set up was similar to previously published analytical solutions for magnetic stimulation in a cylinder by Esselle *et.al*. The results for the first homogeneous saline model matched their magnetic stimulation field pattern for a cylinder [8].

The two other FEM models provided confidence that the FEM technique can accurately solve the complexities present in modeling biological tissue. The models of the anisotropic medium and different tissue boundaries were easily incorporated into the FEM software. The results produced by these inhomogeneities and

anisotropisms were as expected. With adequate support for the programing method of the FEM modeling complete, the next step was to build a FEM model not based on a cylindrical geometry but one that closely matched the actual geometry found *in vivo*.

## **CHAPTER 5**

### **RESULTS**

The results of this research are divided into three parts. The first results described are for the BIA of the three modeled tissues; striated muscle, bone and adipose tissue. The measured values for these tissues were compared to published resistivities for human tissues excited below 100 Hz since no published lamb tissue values were available. Next, these measured conductivities were used in the computer model to solve for the electric current density in the animal test leg. Finally, the results of the FEM model were compared to the laboratory measurements.

#### **Tissue Measurements**

Tissue measurements were made in three areas: first, BIA to determine the resistivity on tissue samples of muscle, bone, and fat from the leg of lamb; second, a low frequency response measurement of muscle tissue to validate the quasi-static assumption, and finally, a measurement of the resistivity stability to varying current density.

### *Resistivity measurements*

Tissue measurements were made on samples taken from the leg of lamb for use in the bioimpedance analysis. Approximately fifty measurements were made on each of the three tissue types. The sample locations along with the tissue type were recorded. The tissue samples were dissected to provide a single tissue type and to be as uniform as possible. For the muscle tissue, measurements were made in all three axes. Initially, this was performed in all the tissue types, but the values were the same for each direction in the adipose tissue as expected. Therefore, only one value is listed for fat and bone. There was some difficulty in obtaining accurate measurements for bone. Because of the BIA tissue measurement device's construction and the rigidity of bone, only the resistivity for the Z direction for bone was made. It was necessary for the bone to have a flat surface for the source electrodes, which occurred only on the cut ends. This has only a minor effect since bone impedance varies slightly with orientation with the Z direction having the lowest resistivity. The bone still contained the bone marrow. When the marrow was removed, the impedance measurements were in the mega-ohms range. These values were disregarded since the marrow is present *in vivo*. Table 1 lists the average measured values for muscle, fat, and bone.

**Table 1 - Summary of the tissue impedance measurements made on the leg of lamb samples. This table lists the average resistivity and standard deviation for the three types of tissues modeled. Also, the corresponding conductivity used in the FEM model is given.**

Tissue Type	Measurement Direction	Average Resistivity ( $\Omega \bullet \text{cm}$ )	Standard Deviation ( $\Omega \bullet \text{cm}$ )	Conductivity (mS/cm)
Muscle	X	860	32	1.16
	Y	1161	35	.86
	Z	117	36	8.55
Fat	All	2065	95	.48
Bone	Z	13305	1051	.075

Additionally, various muscle samples were taken which were not uniform to observe the effects of connective tissue and fat in striated muscle. If the embedded adipose tissue was parallel to the field, there was little affect on the measurement. However, if it was perpendicular to the current path, it increased the impedance 20 - 40%. Connective tissue had a similar yet smaller affect, approximately a 10% increase. This varied with thickness and orientation. No quantitative measurement method to provide an exact relationship could be developed. There were too many confounding factors, such as random orientation and varying thickness.

The tissue resistivity values were consistent with published values for the same kinds of human tissues. The small differences can probably be attributed to lamb being a different mammalian tissue and the lamb measurements not being made

*in vivo*. Figure 24 is a visual comparison of the measured averages of lamb tissue to an average of the published human values reported by Geddes [9], Duck [51], Rush [52], and Gabriel [53].

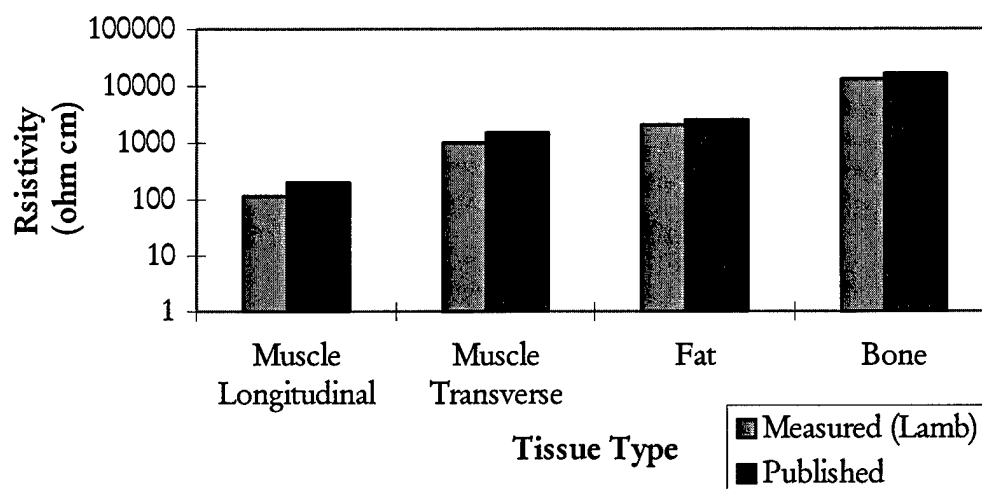


**Figure 24 - Graph comparing the average resistivity of the measured lamb tissues to published human tissue values.**

The good correlation between the lamb and human data provides confidence in the resistivity results. The value for each lamb tissue type in Figure 24 was used subsequently as the material property in the leg of lamb FEM model.

#### *Frequency Response of Muscle*

The low frequency response was investigated using a sample of striated muscle measured along its longitudinal axis. The resistivity change over a frequency from 20 Hz to 20 kHz was measured. The result was a flat response in the low frequency range shown in Figure 25. This showed that only the resistive component of tissue impedance was necessary in low frequency stimulation models.

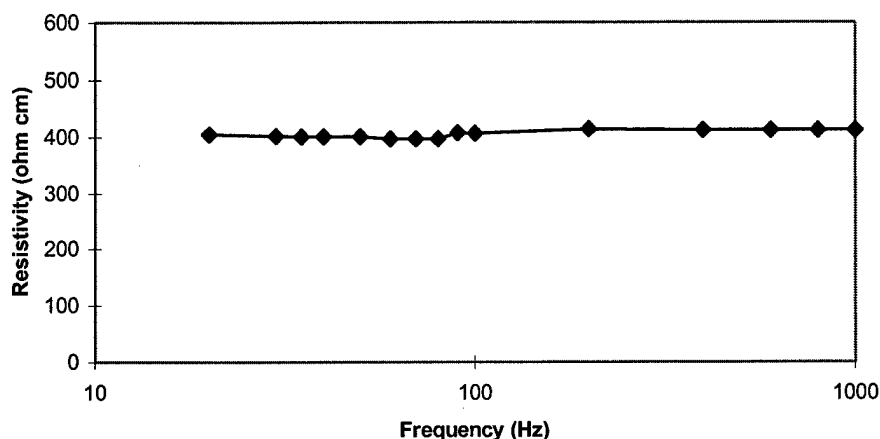


**Figure 25 - Graph showing the measured resistivity of muscle tissue against the source frequency it was measured at using BIA. The muscle tissue resistivity was stable over the low frequency range.**

The lack of resistivity change in this frequency range allows BIA measurements to use a sinusoid as the signal source. Various waveforms are used for stimulation patterns in functional electrical stimulation, TENS, and TES. These waveforms include pulses and ramps. The higher harmonic frequency components of these waveforms appeared to have little effect on tissue resistivity properties. Even the higher frequency components of these signals still lie well within the examined frequency range.

#### *Current density response*

Since the dosage intensity in stimulation protocols varies among treatments as well as from the current density used for BIA, measurements were made over the current density range of interest to ensure a linear resistivity response. The BIA tissue measurements were accomplished at 500  $\mu\text{A}$ . The leg of lamb laboratory setup used a



constant current source of 500  $\mu\text{A}$ . TES therapy uses an approximately 1 mA current source. The difference in current intensities from the model to the clinical level should not affect the results measured in the model since they are in a linear region for biological tissue. Figure 26 is a plot of the linear regression fit to the measurements.

This was confirmed by testing the changes in striated muscle resistivity over the entire current range. The voltage response to changes in current intensity were indeed linear. The muscle's resistivity was constant and Ohm's Law applied for the voltage/current relationship. The linear regression analysis of the measured data resulted in a near perfect fit with a  $p = 0.0054$  and multiple  $R = 0.9997$ . By being in the linear region shows that the impedance of muscle tissue does not vary with changes in current density. The impedance values obtained by BIA are valid for both the FEM and therapeutic stimulation intensities.

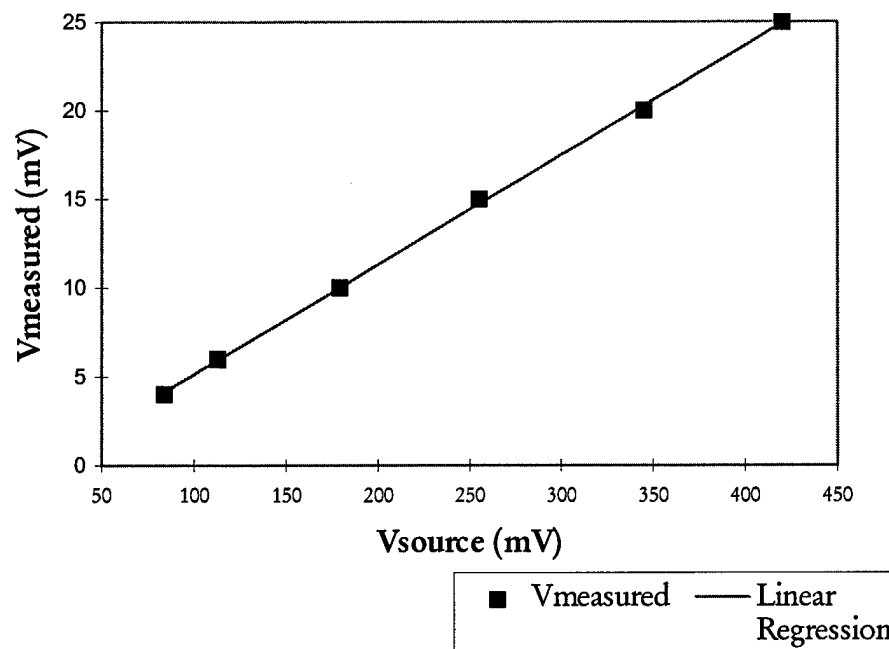


**Figure 26 - Plot showing that muscle tissue resistivity is stable in the low current density range. The voltage response to changes in current intensity were indeed linear. The muscle's resistivity was constant and Ohm's Law applied for the voltage/current relationship. The linear regression analysis of the measured data resulted in a near perfect fit with a  $p = 0.0054$ .**

### **Leg of Lamb FEM Results**

The finite element model of the leg of lamb had a one centimeter resolution in all directions. The results of the BIA conductivity measurements of the three tissue types modeled (striated muscle, adipose tissue, and bone) from the previous section were used to define each element's thermal conductivity property. The portion of the leg modeled contained the quadriceps muscle. The lamb was chosen to closely match the physical size and anatomy of a human thigh. The leg of lamb was divided into 12 one cm thick transverse slices. The slice number represented the location in the Z

axis. For example, slice 1 was the first slice and its thickness extended from  $z = 1$  to  $z = 2$  centimeters.

### *Boundary Conditions Applied*

Several boundary conditions were applied to the assembled brick elements to duplicate the laboratory setup. Bipolar stimulation was modeled by representing the cathode as a constant heat flux of  $125 \text{ W/m}^2\text{C}$  at each of the four nodes of the external surface of the element at which the electrode was attached. This was element number 1132 face 5 which was in slice 1 at  $x = 0$ ,  $y = 5$ , and  $z = 1$ . Figure 54 in Appendix A shows this location. It was centered directly over the quadriceps, the target muscle. This heat flux intensity matched the  $500 \mu\text{A}$  constant current source used for laboratory measurements. Distributing the load evenly over the surface of the source element provided more accurate results close to the electrodes even with the 1 cm resolution. If a point source were used (heat flux applied only to a single node) the model results would require several element lengths or a finer mesh to be accurate near the source.

The boundary condition required to model the anode was a constant temperature restraint at  $0^\circ \text{C}$ . This was the thermal correlate of electrical ground and completes the path for the bipolar stimulation. It, too, was distributed over the four external surface nodes representing the second electrode. The element was number 10205 located in slice 10 at  $x = 0$ ,  $y = 7$ ,  $z = 10$ . See Figure 63 in Appendix A shows its location.

The leg of lamb model's final boundary condition was no radiation from the external surfaces. In this model, all the current flowed in the animal leg. The conductivity of the air padding elements could not be set to zero due to software limitations but was made extremely small, 0.0001 mS/cm, effectively zero.

#### *FEM Model Attributes*

The conversion methods mentioned earlier to digitize the leg of lamb produced a finite element model containing 2873 3-dimensional brick elements. Approximately 25% of those elements were air surrounding the animal leg. These air elements were used to make the importing and element number system consistent. The air elements were color-coded sky blue, muscle elements were red, fat elements were yellow, and bone elements were dark blue. The FEM model was also arranged to correspond to the measurement slices. The elements were grouped by tissue type and measurement slice to enhance displays of the results. Figure 27 through Figure 29 show the different views of the overall finished model with the boundary conditions.

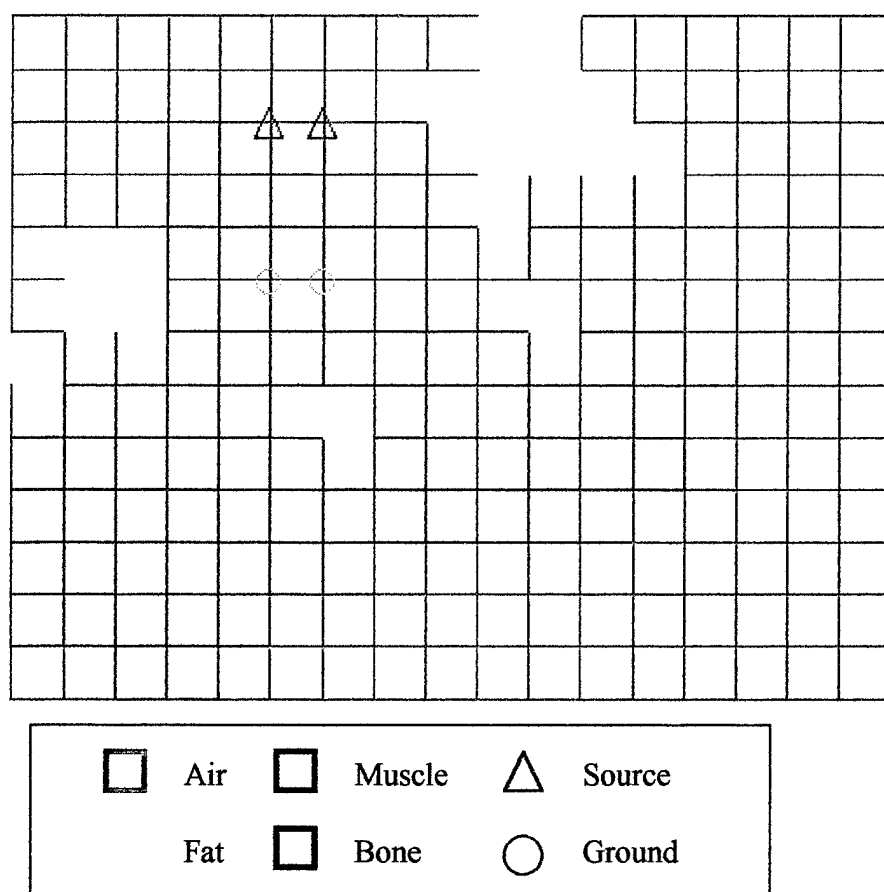


**Figure 27 - An end view of the leg of lamb FEM model used including the air padding elements.**

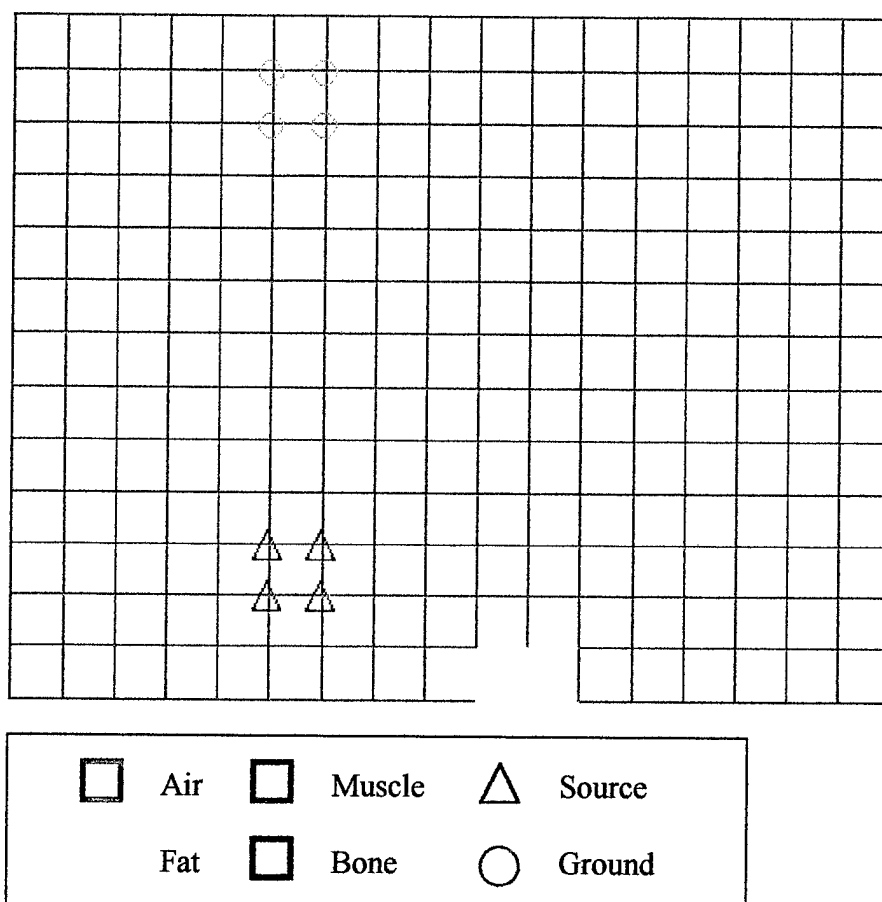


**Figure 28 - A top view of the leg of lamb FEM model used including the air padding elements.**

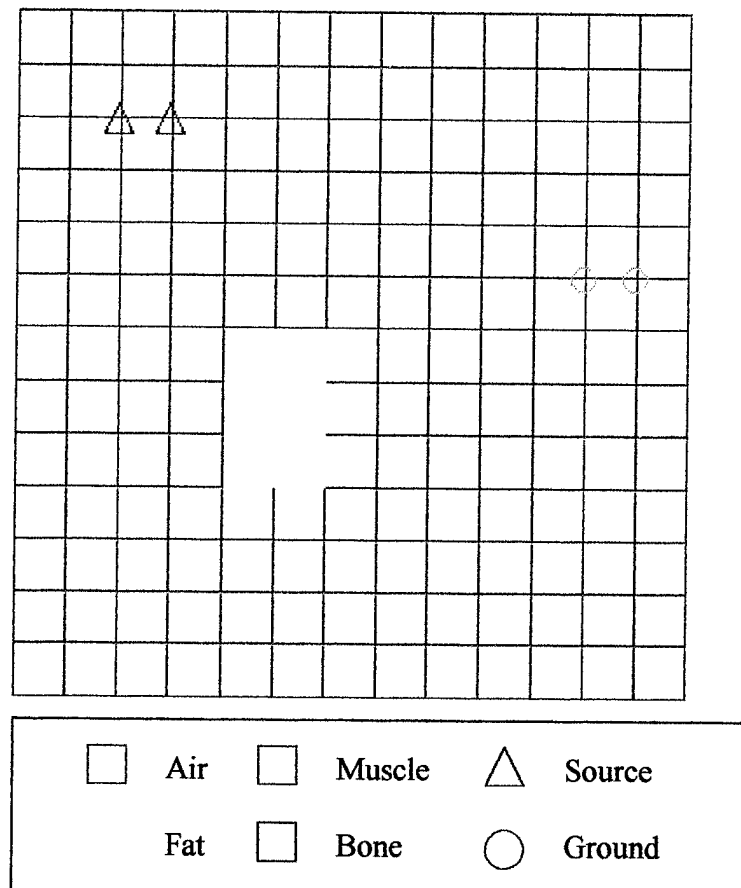


**Figure 29 - A side view of the leg of lamb FEM model used including the air padding elements.**

Figure 30 is a 3-dimensional view of the leg of lamb group of elements with the air padding elements removed. It matches the overall dimensions of the actual leg of lamb used for laboratory measurements.

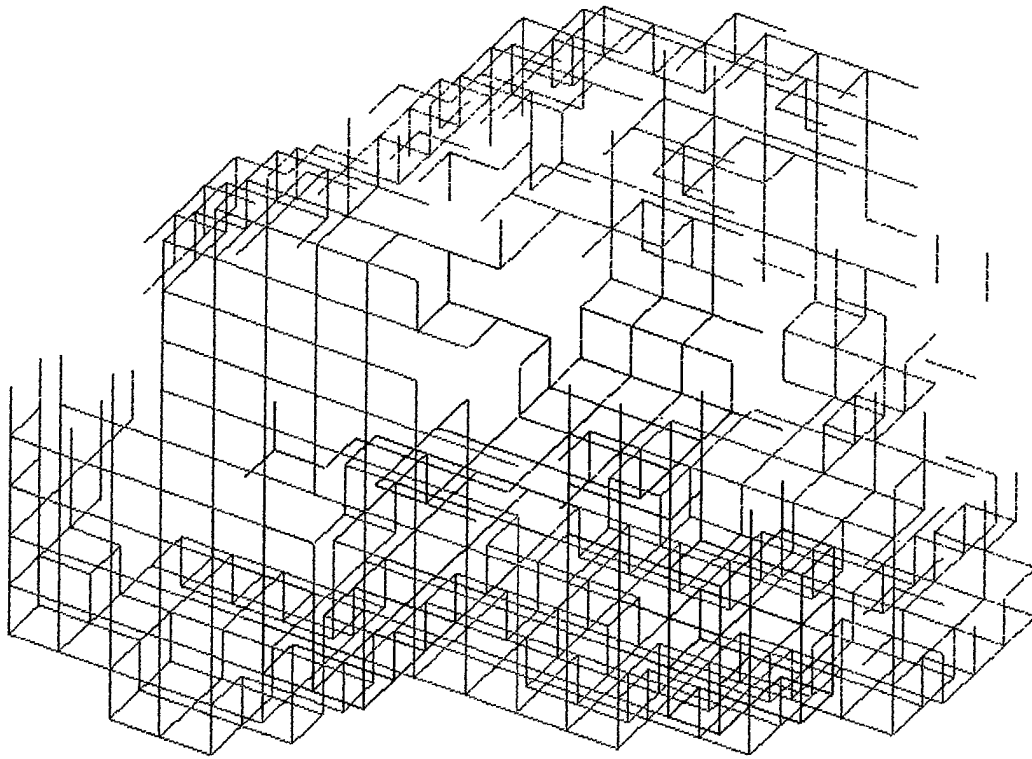


**Figure 30 - A three dimensional view of the leg of lamb model used with air padding elements hidden.**

#### *FEM Model Primary Current Path Results*

I-DEAS software provides a function to plot the path along the maximum heat flux. The path starting locations were programmed at each of the four source electrode points. The resulting paths traced out were the paths with the greatest current density in the model. The current paths remained completely within the target muscle. Each path flowed in through the surface fat layer into the muscle then turned towards the anode. The current path also spread out as it flowed away from the source, reaching a maximum dispersion half way between the electrodes. After the midpoint it began to reconverge towards the anode. Figure 31 through Figure 33



show the end, top, and side views, respectively. The air elements have been removed and only the leg of lamb group is shown for ease of interpretation.

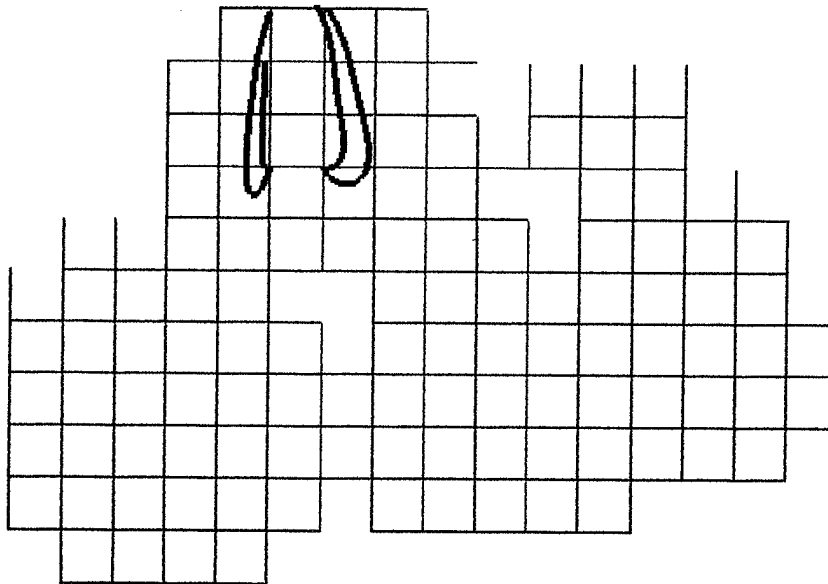


**Figure 31 - End view plot of the primary current path through the leg of lamb. The path starting locations were programmed at each of the four source electrode points. The resulting paths traced out were the paths with the greatest current density in the model. The current paths remained completely within the target muscle. Each path flowed in through the surface fat layer into the muscle then turned towards the anode. The current path also spread out as it flowed away from the source, reaching a maximum dispersion half way between the electrodes.**

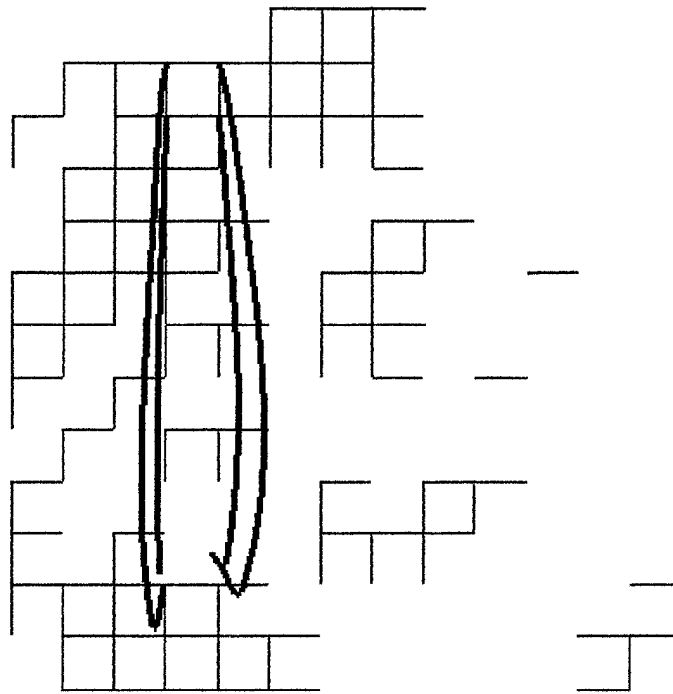


**Figure 32 - Top view plot of the primary current path through the leg of lamb. The path starting locations were programmed at each of the four source electrode points. The resulting paths traced out were the paths with the greatest current density in the model. The current paths remained completely within the target muscle. Each path flowed in through the surface fat layer into the muscle then turned towards the anode. The current path also spread out as it flowed away from the source, reaching a maximum dispersion half way between the electrodes.**

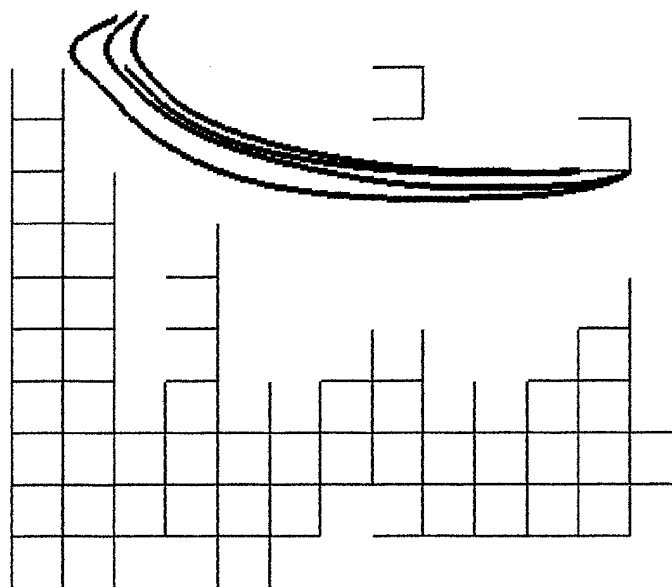


**Figure 33 - Side view plot of the primary current path through the leg of lamb. The path starting locations were programmed at each of the four source electrode points. The resulting paths traced out were the paths with the greatest current density in the model. The current paths remained completely within the target muscle. Each path flowed in through the surface fat layer into the muscle then turned towards the anode. The current path also spread out as it flowed away from the source, reaching a maximum dispersion half way between the electrodes.**

### *Current Density Results*

In addition to the paths of maximum current density, current density vector plots provided an additional visual image of the bipolar stimulation pattern. In the vector plots, the arrow's length and color represent the magnitude while the arrow points in the direction of current flow. The following figures (Figure 34 - Figure 36) reveal several important characteristics. First, the majority of the current remained in

the target muscle. With a constant current input of 500  $\mu\text{A}$  at the source electrode, the lower limit of plotted current density of 10  $\mu\text{A}$  was only 2% of the maximum. The plots show the main concentration of the stimulation energy remained in the target muscle. Explanations for this current pattern include the effects of the anisotropic property of striated muscle, the adipose tissue and connective tissue between muscle groups, and the spacing between electrodes.

The primary effect appears to be the anisotropic property of muscle. As shown previously in the saline model, the preferential impedance path limits the current spread. Second, as mentioned in the tissue results section, the connective tissue provides a small insulative barrier, as does adipose tissue, to the current spread. Since the primary bipolar stimulation modality is longitudinally over the target muscle, the physiology of the muscle groups helps direct the current flow down the length of the muscle and limits its spread.

Finally, the closer the electrode spacing, the less distance the current has to spread out. This effect can be seen in the elliptical shape of the current density vectors. Figure 34 through Figure 36 show the end, top, and side views of the current density vector plots, respectively. The element outlines have been removed to prevent obscuring the arrow detail and only a dashed line outlining the target muscle was added.

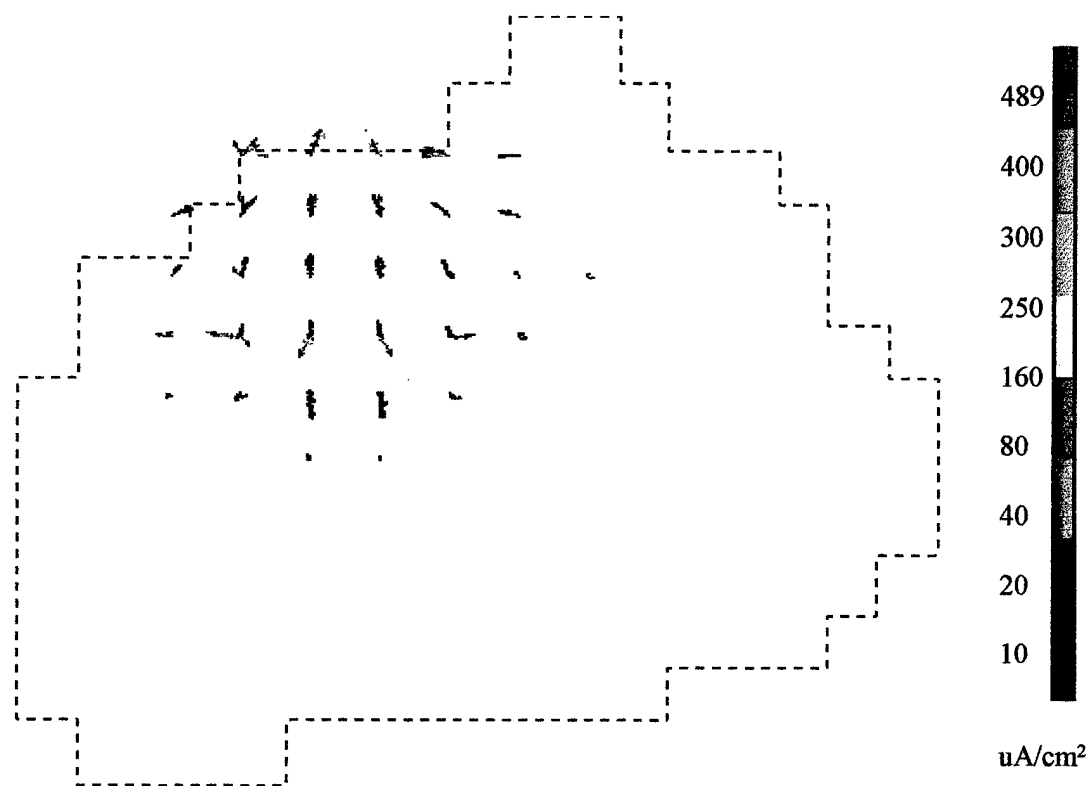


**Figure 34 - End view vector plot showing the current density above the  $10 \mu\text{A}/\text{cm}^2$  vasodilatation threshold. The dashed line is the outline of the entire leg of lamb model. The plot shows the main concentration of the stimulation energy remained in the target muscle.**

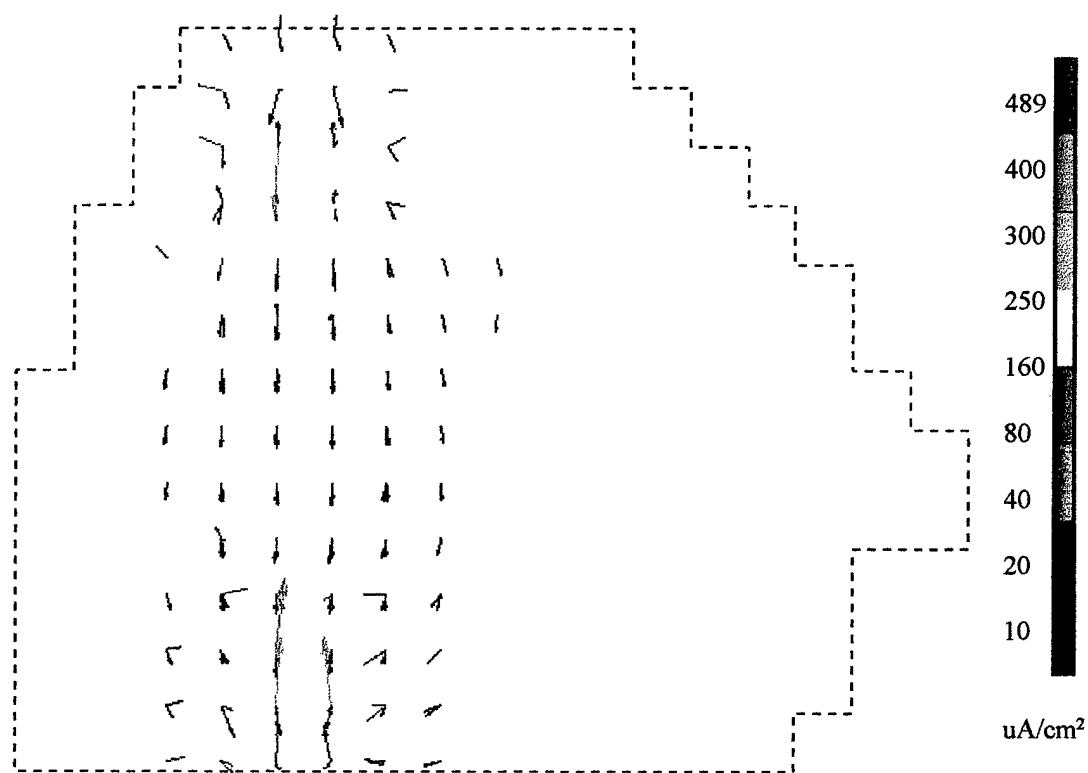


**Figure 35 - Top view vector plot showing the current density above the  $10 \mu\text{A}/\text{cm}^2$  vasodilatation threshold. The dashed line is the outline of the entire leg of lamb model. The plot shows the main concentration of the stimulation energy remained in the target muscle.**

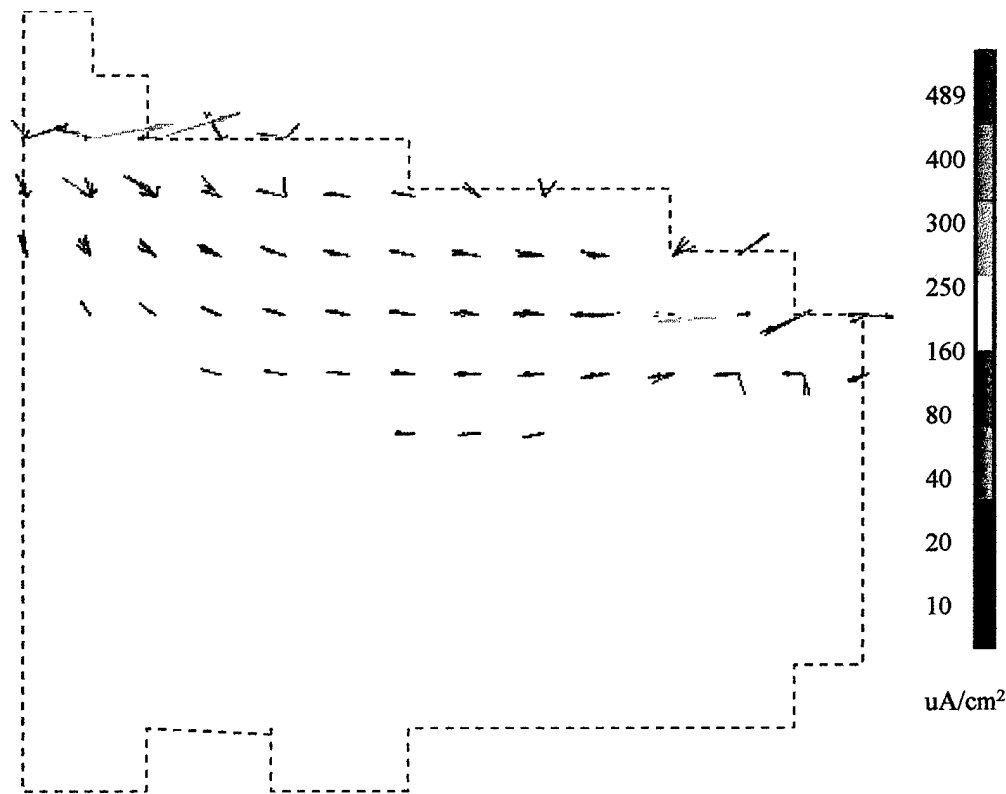


**Figure 36 - Side view vector plot showing the current density above the  $10 \mu\text{A}/\text{cm}^2$  vasodilatation threshold. The dashed line is the outline of the entire leg of lamb model. The plot shows the main concentration of the stimulation energy remained in the target muscle.**

To get a more detailed idea of the current density in between the electrodes, contour plots of the leg of lamb FEM results in the X-Y plane at  $Z = 2, 4, 6, 8$ , and  $10$  are shown. These plots also show the concentration of the current in the target muscle. Furthermore, they provide information on the current density throughout the entire slice. Note that the current density was much less in the fat elements and significantly less in bone as you would expect. There was a  $10^5$  order of magnitude difference between the average current density between muscle and bone. This was

because of two factors, the higher impedance in the bone and the greater distance from the electrodes. Figure 37 through Figure 41 are of the even numbered slices. As a reminder, the source electrodes were attached at the surface of slice 1 and 10.

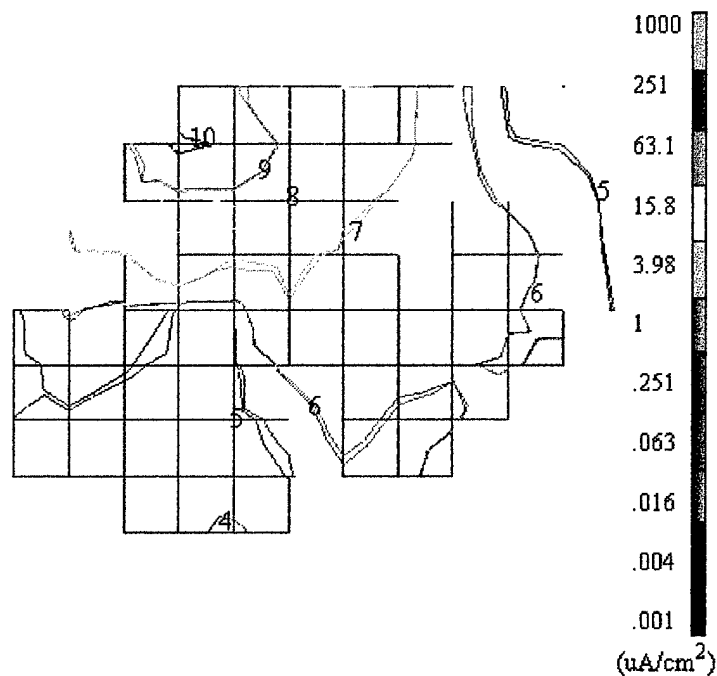


**Figure 37 - Contour plot of the leg of lamb FEM model results showing the current density in the X-Y plane at  $Z = 2$  cm. The red, yellow, and blue elements represent muscle, fat, and bone, respectively. The number on the contour line corresponds to its color bar segment.**



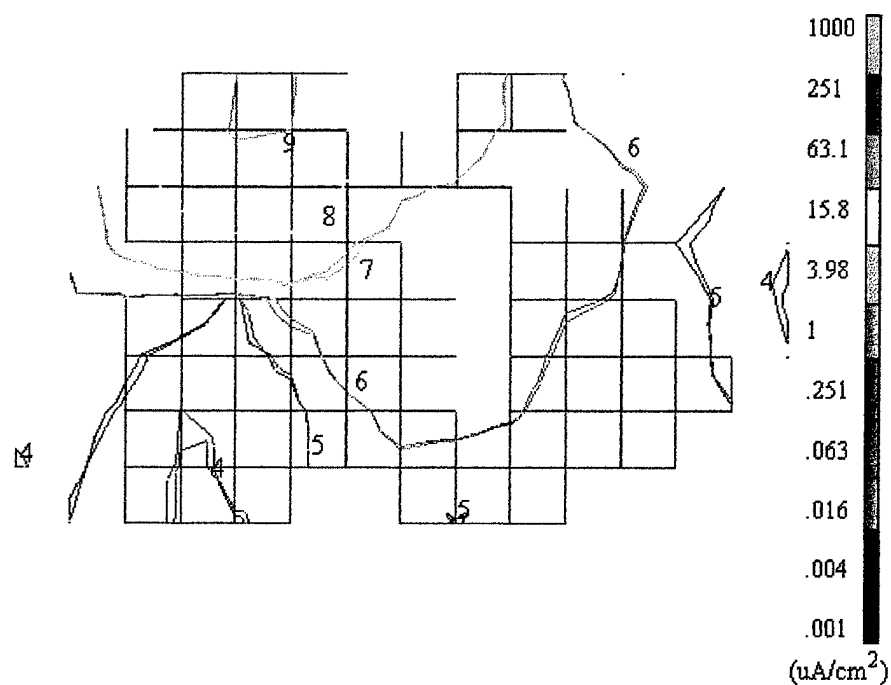


**Figure 38 - Contour plot of the leg of lamb FEM model results showing the current density in the X-Y plane at  $Z = 4$  cm. The red, yellow, and blue elements represent muscle, fat, and bone, respectively. The number on the contour line corresponds to its color bar segment.**

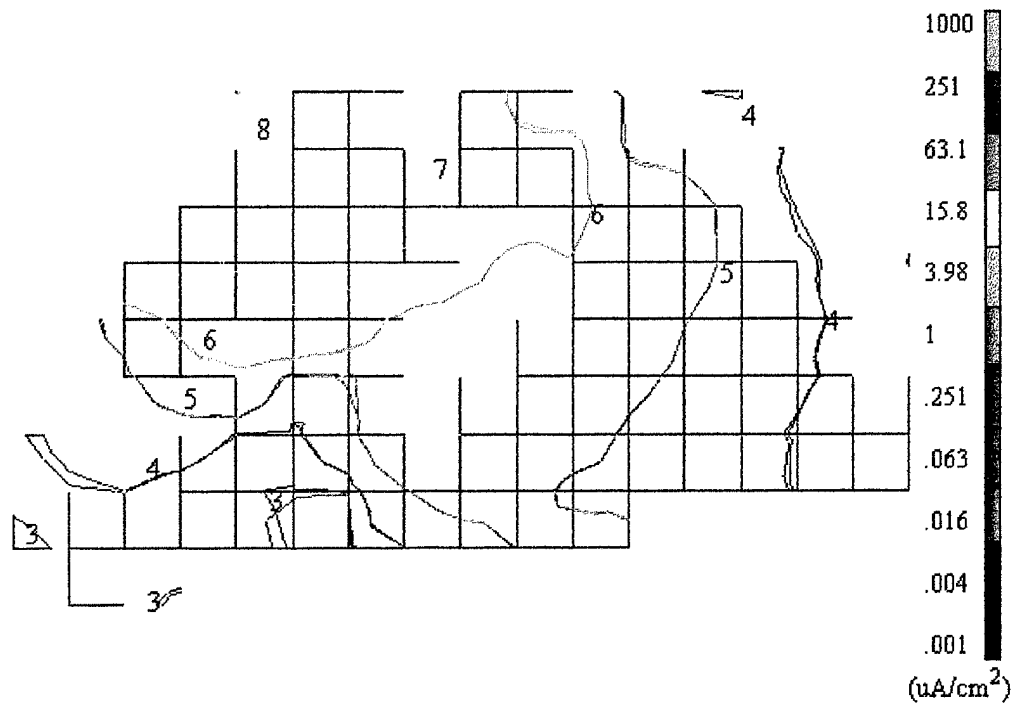


**Figure 39 - Contour plot of the leg of lamb FEM model results showing the current density in the X-Y plane at  $Z = 6$  cm. The red, yellow, and blue elements represent muscle, fat, and bone, respectively. The number on the contour line corresponds to its color bar segment.**

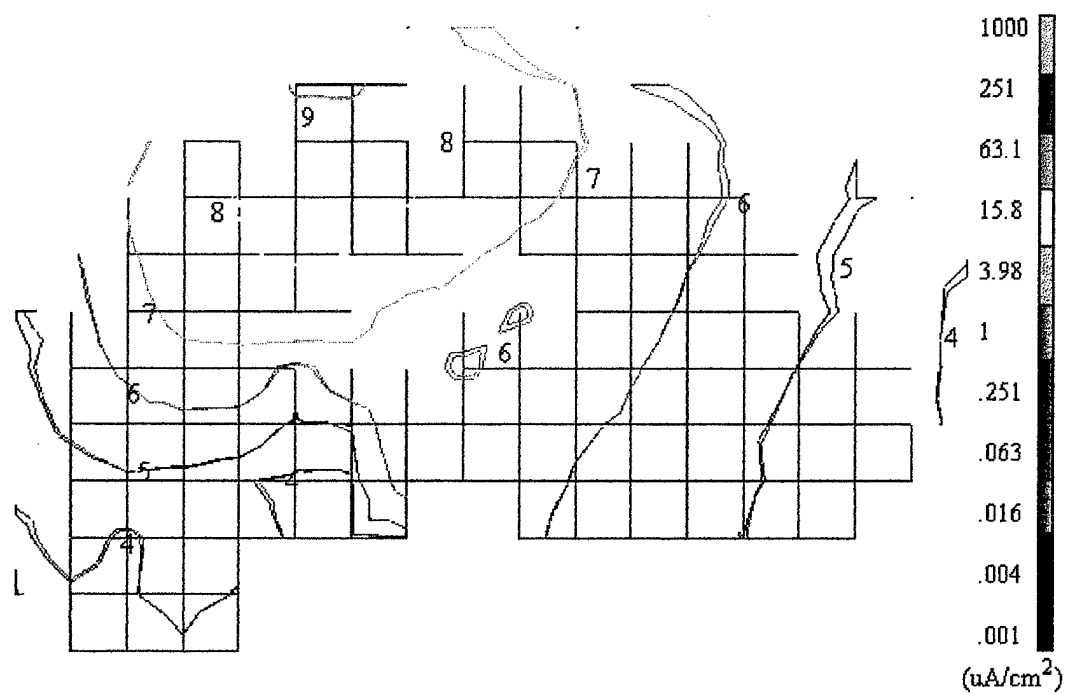


**Figure 40 - Contour plot of the leg of lamb FEM model results showing the current density in the X-Y plane at  $Z = 8$  cm. The red, yellow, and blue elements represent muscle, fat, and bone, respectively. The number on the contour line corresponds to its color bar segment.**

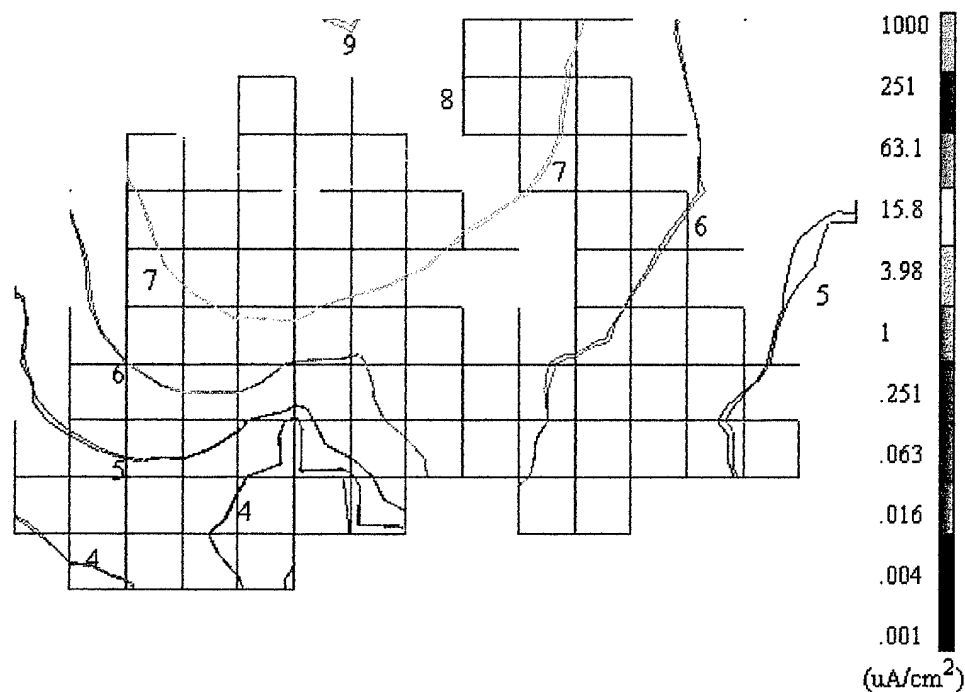


**Figure 41 - Contour plot of the leg of lamb FEM model results showing the current density in the X-Y plane at  $Z = 10$  cm. The red, yellow, and blue elements represent muscle, fat, and bone, respectively. The number on the contour line corresponds to its color bar segment.**

The voltage gradient FEM model results will be shown in the next section, compared to the laboratory measurements.

### **Laboratory Measurements in Leg of Lamb**

The laboratory voltage gradient measurements made on the leg of lamb were compared to the output of the leg of lamb FEM model in this section. This comparison provided the necessary validation of the FEM for modeling complex biological structures and ultimately the human thigh. Measurements were made at 2 cm intervals along the Z axis in the target muscle between the stimulation electrodes.

concentration of current in the target muscle. These plots are provided in Appendix C (the MatLab code that generated these plots is in Appendix G).

Additionally, I-DEAS voltage gradient contour plots with the lab measurement values were superimposed on the contours using the same false color scale. The superimposed plots verify the FEM model's ability to predict the electrical stimulation pattern in three dimensions. The FEM model generated contours which do not match the laboratory measurements by one color segment are circled. The values which do not agree by two or more color segments are marked by an X. Table 2 summarizes the results of the comparison.

**Table 2 - Summary of leg of lamb FEM model results compared to emperical measurements.**

Location	Number of Measurements in slice	Measurements differing by 1 segment	Measurements differing by 2 segments	Percent corresponding
Slice 2	13	2	0	85 %
Slice 4	15	1	0	93 %
Slice 6	17	3	0	82 %
Slice 8	18	4	1	72 %
<b>Total</b>	63	10	1	83 %

The increase in the number of disagreements in slice locations at  $z = 6$  cm and  $z = 8$  cm were caused by poor resolution of the FEM model around the bone. Many of these elements had all three tissue types but were constrained by the model limitation that only allowed an element to represent one tissue type. This limitation provided the differences between the two methods. Increasing the resolution of the model would correct this problem. Overall, the voltage gradient pattern matches for

model would correct this problem. Overall, the voltage gradient pattern matches for each slice provided a good current density pattern correlation with the FEM model.

Figure 42 - Figure 45 are these comparison plots.

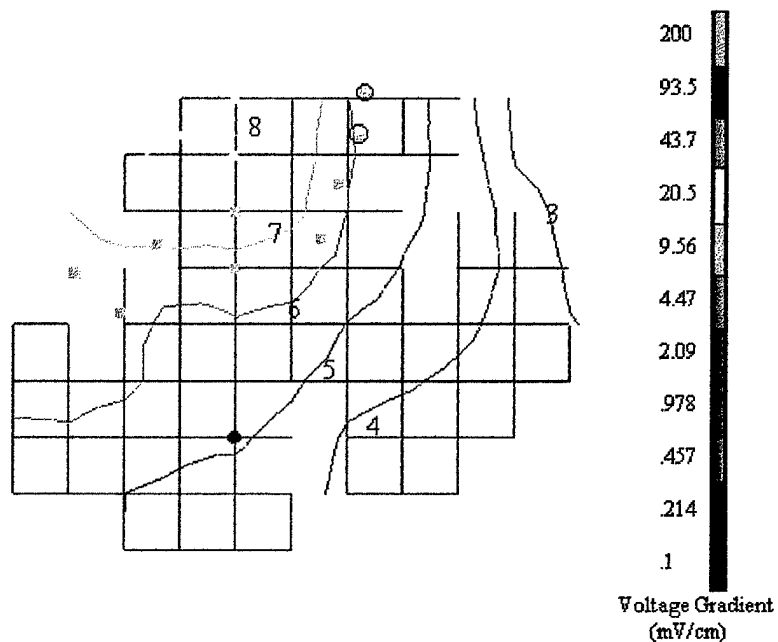


**Figure 42 - Leg of lamb FEM model results compared to emperical measurements made at  $Z = 2$  cm. The square data points are the laboratory measurements. The superimposed contour plot is the leg of lamb FEM model voltage gradient results. The black dot is the origin. The laboratory values which do not match the FEM model generated contours and are off by one color segment are circled. The number on the contour line corresponds to its color bar segment.**

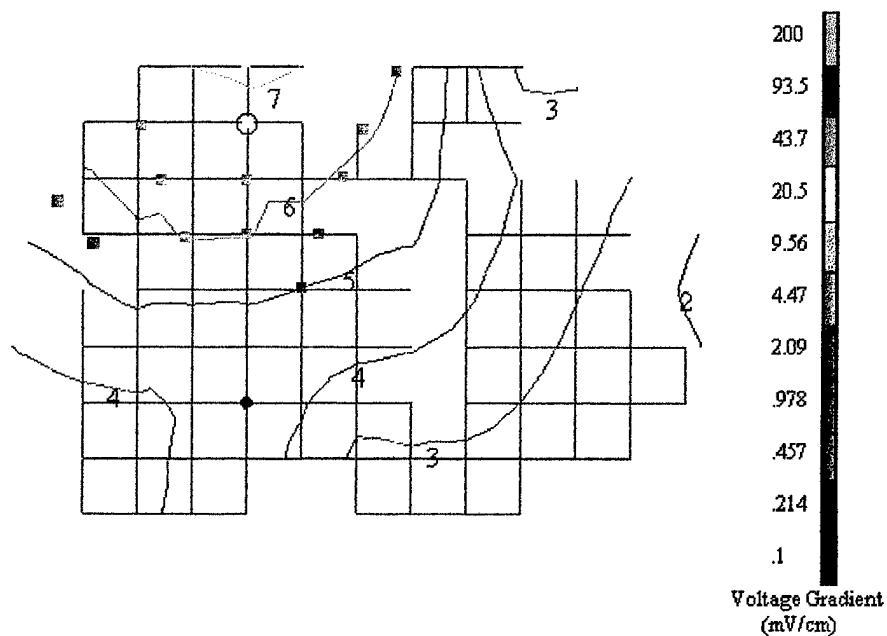


**Figure 43 - Leg of lamb FEM model results compared to empirical measurements made at  $Z = 4$  cm. The square data points are the laboratory measurements. The superimposed contour plot is the leg of lamb FEM model voltage gradient results. The black dot is the origin. The laboratory values which do not match the FEM model generated contours and are off by one color segment are circled. The number on the contour line corresponds to its color bar segment.**

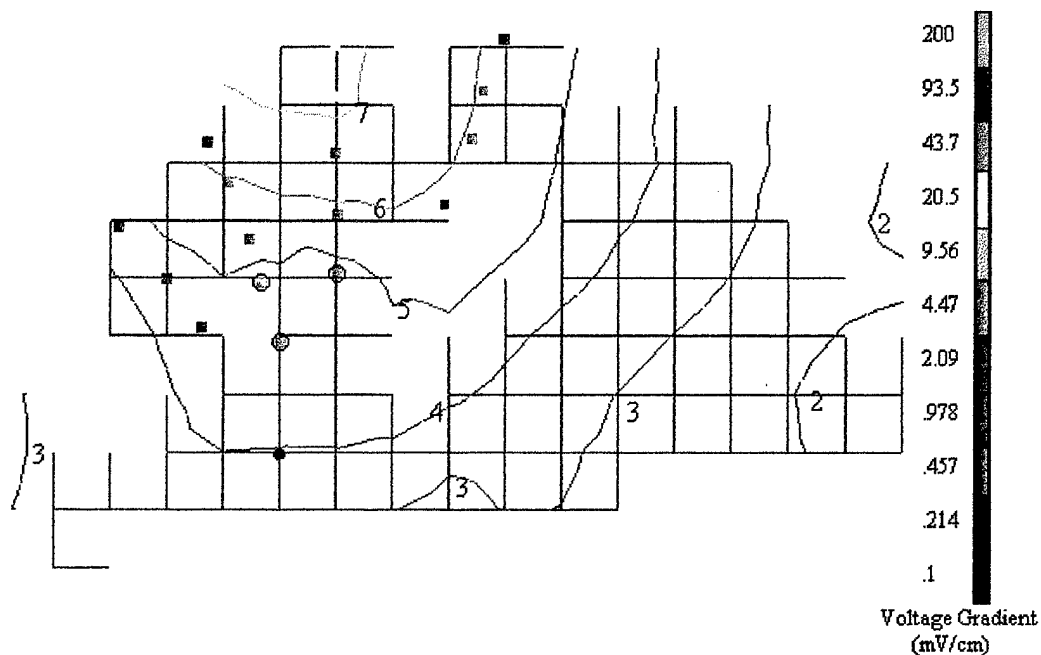


**Figure 44 - Leg of lamb FEM model results compared to empirical measurements made at  $Z = 6$  cm. The square data points are the laboratory measurements. The superimposed contour plot is the leg of lamb FEM model voltage gradient results. The black dot is the origin. The laboratory values which do not match the FEM model generated contours and are off by one color segment are circled. The number on the contour line corresponds to its color bar segment.**



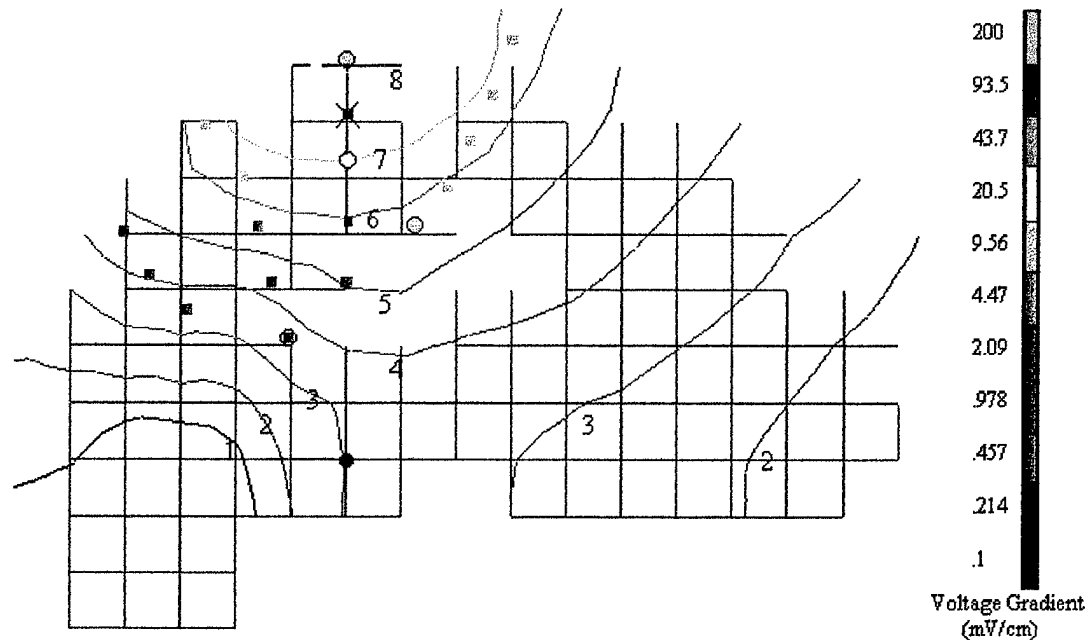


**Figure 45 - Leg of lamb FEM model results compared to empirical measurements made at  $Z = 8$  cm. The square data points are the laboratory measurements. The superimposed contour plot is the leg of lamb FEM model voltage gradient results. The black dot is the origin. The laboratory values which do not match the FEM model generated contours and are off by one color segment are circled. The values which do not agree by two or more color segments are marked by an X. The number on the contour line corresponds to its color bar segment.**

#### *Comparison of the measured and modeled voltage gradient values*

The second method for validation of the leg of lamb FEM model was numerical. A comparison was made of the measured voltage gradients along the Z axis to the FEM model predictions. A total of sixty-three measurements were made in the target muscle. The average voltage gradient measurement,  $V_z$ , was 10 mV with a maximum and minimum value of 22 mV and 1.4 mV, respectively. The FEM model predicted for the same locations as the measurements were made, an average of 10.7 mV with a maximum and minimum of 37.5 mV and 1.1 mV, respectively. A

direct comparison of each measurement location was also made. The average error between each measured and predicted value was 5.3 mV with standard deviation of 4.9 mV. This may seem high but when looking at the percent error for each location, the FEM model prediction was good. This also agrees with the overall current density pattern correlation discussed earlier. The average percent error was 57.8% with a standard deviation of 53.5%. However, eight of the locations were model as air padding elements due to the 1 cm resolution cubes and curved nature of the outside surface. These poor matches skewed the statistical results higher. With these eight element's percent error not included, the average percent error lowered to 43% with a standard deviation of only 25.6%. The median percent error value was even lower at 36.7%. This shows that the majority of the predictions were good. The individual measurement comparison is listed in Table 3. This was a significant increase in accuracy over the lumped circuit prediction method.

**Table 3 - A comparison of the measure verses predicted voltage gradient values in the leg of lamb.**

I-DEAS Element Label	X	Y	Z	Measured Voltage Gradient	Model Voltage Gradient	Difference between voltage gradients	Percent error	Percent error with 8 elements removed
2169	0	6	2	0.022	0.0118	0.0102	46.36	46.36
2151	0	5	2	0.02	0.0174	0.0026	13.00	13.00
2133	0	4	2	0.013	0.0138	0.0008	6.15	6.15
2115	0	3	2	0.011	0.0099	0.0011	10.00	10.00
2097	0	2	2	0.011	0.007	0.004	36.36	36.36
2171	2.6	6.3	2	0.011	0.016625	0.005625	51.14	51.14
2153	2.3	5.5	2	0.0104	0.016625	0.006225	59.86	59.86
2134	1.8	4.5	2	0.00945	0.0028	0.00665	70.37	70.37
2116	1.5	3.6	2	0.0085	0.003675	0.004825	56.76	56.76
2131	-1.9	4.6	2	0.012	0.0371	0.0251	209.17	
2113	-1.5	3.6	2	0.01	0.0182	0.0082	82.00	82.00
2111	-3.2	3.3	2	0.0097	0.0231	0.0134	138.14	
2094	-2.5	2.5	2	0.01	0.0189	0.0089	89.00	89.00
4169	0	6	4	0.0182	0.0245	0.0063	34.62	34.62

I-DEAS Element Label	X	Y	Z	Measured Voltage Gradient	Model Voltage Gradient	Difference between voltage gradients	Percent error	Percent error with 8 elements removed
4151	0	5	4	0.018	0.0245	0.0065	36.11	36.11
4133	0	4	4	0.016	0.02065	0.00465	29.06	29.06
4115	0	3	4	0.015	0.0112	0.0038	25.33	25.33
4097	0	2	4	0.011	0.0049	0.0061	55.45	55.45
4171	2.5	6	4	0.0101	0.028	0.0179	177.23	
4153	2.1	5.1	4	0.0106	0.01785	0.00725	68.40	68.40
4134	1.8	4.2	4	0.0102	0.00665	0.00355	34.80	34.80
4116	1.3	3.3	4	0.0089	0.002275	0.006625	74.44	74.44
4097	1	2.3	4	0.0096	0.001855	0.007745	80.68	80.68
4130	-2.1	5	4	0.0108	0.0182	0.0074	68.52	
4131	-1.7	4.1	4	0.009	0.01645	0.00745	82.78	82.78
4113	-1.3	3.2	4	0.0095	0.0091	0.0004	4.21	4.21
4111	-3.7	3.6	4	0.0097	0.01225	0.00255	26.29	26.29
4094	-2.9	2.9	4	0.0092	0.01015	0.00095	10.33	10.33
6187	0	7.2	6	0.0198	0.0154	0.0044	22.22	22.22
6169	0	6.3	6	0.018	0.014	0.004	22.22	22.22
6151	0	5.3	6	0.016	0.0147	0.0013	8.13	8.13
6133	0	4.3	6	0.013	0.008225	0.004775	36.73	36.73
6115	0	3.3	6	0.011	0.00105	0.00995	90.45	90.45
6190	3	7.3	6	0.00985	0.0049	0.00495	50.25	
6171	2.7	6.4	6	0.01065	0.0049	0.00575	53.99	53.99
6153	2.3	5.5	6	0.00965	0.006475	0.003175	32.90	32.90
6134	1.8	4.5	6	0.0085	0.009345	0.000845	9.94	9.94
6148	-2.3	5.6	6	0.008	0.0154	0.0074	92.50	92.50
6131	-1.9	4.7	6	0.0104	0.012075	0.001675	16.11	16.11
6113	-1.5	3.7	6	0.0104	0.006825	0.003575	34.38	34.38
6095	-1.2	2.7	6	0.0104	0.004375	0.006025	57.93	57.93
6078	-0.8	1.8	6	0.0103	0.002013	0.008288	80.46	80.46
6111	-3.7	3.8	6	0.008	0.003675	0.004325	54.06	54.06
6111	-3.1	3.1	6	0.007	0.00735	0.00035	5.00	5.00
6094	-2.4	2.4	6	0.007	0.004375	0.002625	37.50	37.50
8187	0	7.4	8	0.0063	0.0132	0.0069	109.52	
8169	0	6.4	8	0.0034	0.0132	0.0098	288.24	
8151	0	5.4	8	0.0026	0.00315	0.00055	21.15	21.15
8133	0	4.4	8	0.0019	0.0035	0.0016	84.21	84.21
8115	0	3.4	8	0.0014	0.0022	0.0008	57.14	57.14
8190	3.2	7.6	8	0.0085	0.007	0.0015	17.65	17.65
8171	2.8	6.7	8	0.0093	0.006563	0.002738	29.44	29.44
8153	2.4	5.8	8	0.0095	0.0042	0.0053	55.79	55.79
8134	2.1	4.9	8	0.013	0.007875	0.005125	39.42	39.42
8116	1.7	3.9	8	0.01	0.00833	0.00167	16.70	16.70
8166	-2.6	6.2	8	0.0105	0.035	0.0245	233.33	
8148	-2.2	5.3	8	0.0097	0.007	0.0027	27.84	27.84
8131	-1.8	4.3	8	0.0095	0.007525	0.001975	20.79	20.79
8113	-1.4	3.4	8	0.003	0.004725	0.001725	57.50	57.50
8095	-1	2.5	8	0.002	0.0035	0.0015	75.00	75.00

I-DEAS Element Label	X	Y	Z	Measured Voltage Gradient	Model Voltage Gradient	Difference between voltage gradients	Percent error	Percent error with 8 elements removed
8128	-4.3	4.3	8	0.004	0.002975	0.001025	25.63	25.63
8111	-3.6	3.5	8	0.0035	0.001663	0.001838	52.50	52.50
8094	-2.8	2.8	8	0.0035	0.001663	0.001838	52.50	52.50
<b>Average</b>				<b>0.010054</b>	<b>0.010695</b>	<b>0.00529</b>	<b>57.87</b>	<b>43.11</b>
				Standard Deviation		0.0049	53.52	25.58
Minimum value				0.0014	0.00105	Median		36.73
Maximum value				0.022	0.0371			

A lumped circuit model was developed to show the improvement of this FEM model. The lumped circuit model contained 28 resistors and a 500  $\mu\text{A}$  current source arranged to simulate the muscle bone and adipose tissue of the leg of lamb. The circuit accounted for the anisotropic property of striated muscle and had separate branches for the target muscle and other muscles in the leg of lamb. Figure 46 shows the circuit for the lumped circuit model.  $R_{tm}$  was the target muscle,  $R_f$  was the adipose tissue, and  $R_b$  was the bone.  $R_a$  represented the anisotropic property of striated muscle. The resistor values were  $R_{tm} = 468 \Omega$ ,  $R_a = 3.18 \text{ k}\Omega$ ,  $R_f = 2.065 \text{ k}\Omega$ , and  $R_b = 53.2 \text{ k}\Omega$ . Each resistor with a vertical orientation in the diagram represented 4 cm of tissue along the Z axis. The horizontal branches modeled the lateral current spread. The lumped circuit model results had much higher average values.

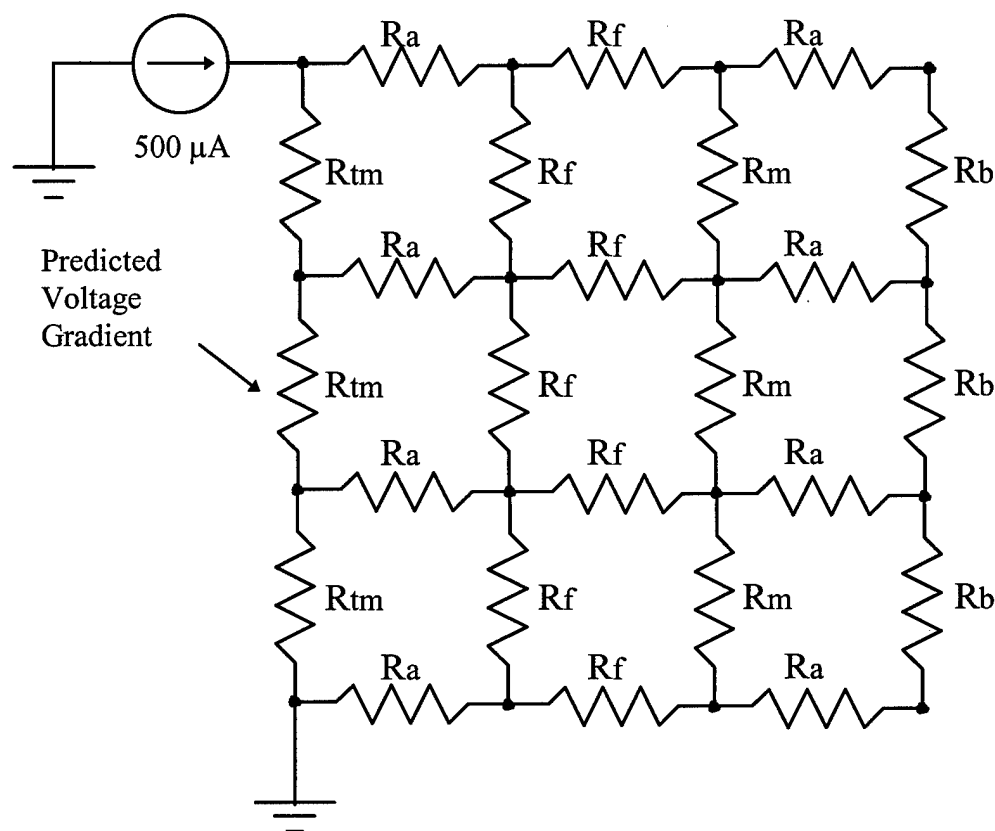


**Figure 46 - Lumped circuit model of the leg of lamb.  $R_{tm}$  was the target muscle,  $R_f$  was the adipose tissue, and  $R_b$  was the bone.  $R_a$  represented the anisotropic property of striated muscle. Each resistor with a vertical orientation represented 4 cm of tissue along the Z axis. The horizontal branches provided for the lateral current spread. The resistor values were  $R_{tm} = 468 \Omega$ ,  $R_a = 3.18 \text{ k}\Omega$ ,  $R_f = 2.065 \text{ k}\Omega$ , and  $R_b = 53.2 \text{ k}\Omega$ .**

The voltage gradient value for the target muscle at  $z = 6 \text{ cm}$  (midplane) was 50 mV and a current density of  $34 \mu\text{A}/\text{cm}^2$  as compared to approximately 10 mV and a current density ranging from 12 - 25  $\mu\text{A}$  depending on location. This midplane between the surface application was where the current density was the most uniform. This was where the lumped circuit method was the closest to the actual values. Even

so, the lumped circuit model had a percent error of approximately 300% compared to the FEM model's percent error of 36.7%. Additionally, the lumped circuit model was unable to predict the high current densities near the source where the FEM model predicted a maximum current density of  $251 \mu\text{A}/\text{cm}^2$ .

A lumped circuit model is unable to make localized predictions. It provides only an average. Use of a lumped circuit model may result in developing stimulation protocols in which localized areas exceed the current density desired. Also, it overestimated the lower end of the current density. While the lumped circuit model predicted  $34 \mu\text{A}/\text{cm}^2$ , over half of the elements in the target muscle were in the 10 - 15  $\mu\text{A}$  range. If one relied on a value close to the desired limit from a lumped circuit model, then up to half of the target muscle may not receive the desired current density level. With the FEM model, one can predict what current level all regions of the desired target muscle would receive.

Overall, the FEM model was able to reproduce the laboratory measurements accurately. It also provided a quantitative, non-invasive method for determining the electrical current densities from bipolar stimulation. Increasing the resolution and number of tissues modeled would enhance the accuracy of the model further.

## **CHAPTER 6**

### **ADDITIONAL INVESTIGATIONS WITH LEG OF LAMB FEM MODEL**

Having shown the leg of lamb FEM model to be accurate for modeling the current densities in muscle from surface application, the model may also be used to investigate effects of atrophy in the target muscle. Additionally, the model can be used to solve the inverse problem: determine the stimulation protocol that achieves a predetermined current density pattern. We look first at an atrophied model of the leg of lamb.

#### **Atrophied Leg of Lamb Model**

The leg of lamb FEM model was modified to reflect the anatomical changes of a mildly atrophied muscle as discussed in Chapter 2. All the elements representing the target quadriceps femoris muscle were identified and grouped together for display purposes. This consisted of 198 elements from the twelve slices along the Z axis. Table 18 in Appendix F is a list of these elements. Then 15 % of them (30 elements) were chosen randomly to be converted to adipose tissue. The net effect of this

conversion was to impregnate the target muscle with single adipose tissue elements. This is similar to the idea of a well marbled steak.

The converted atrophy elements were inspected to determine their anatomical position. The converted elements were well dispersed throughout the target muscle. The majority of them were surrounded by muscle elements and no more than two adipose elements were adjacent in any direction. Figure 47 is a three dimensional view of the atrophied quadriceps muscle with the yellow elements representing the adipose tissue.

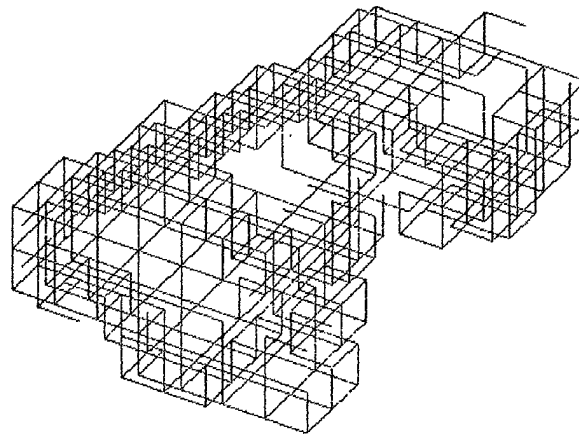


**Figure 47 - Three dimensional diagram showing the modified target muscle in the leg of lamb FEM model with atrophied elements added in yellow.**

The atrophied leg of lamb model used the same 500  $\mu$ A bipolar stimulation boundary conditions as the normal model in Chapter 5. The adipose tissue had a greater resistivity than the muscle (see Table 1), so the expectation was an increase in the current density in the muscle elements surrounding adipose tissue. Since the



converted atrophy elements did not cluster to form an occlusion to the current path in the target muscle, the general path of the current flow was expected to remain the same.

The results of the simulation did show an increased current density in the muscle elements. All the muscle elements in the target muscle showed this increase. The closer the element was to a converted atrophy element, the greater the effect. Figure 48 is a comparison graph of each muscle element in the target muscle with and without the atrophy.

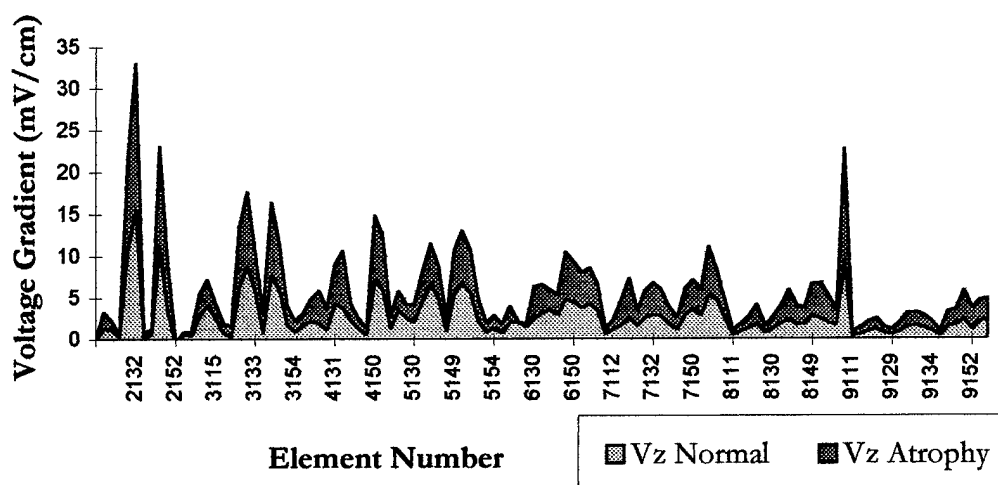


**Figure 48 - A plot comparing the voltage gradient of all the muscle elements in the normal muscle versus the atrophied muscle. The results of the simulation did show an increased current density in the muscle elements. All the muscle elements in the target muscle showed this increase. The closer the element was to a converted atrophy element, the greater the effect.**

Other evidence of the increased current density in the elements adjacent to the adipose tissue was the increased voltage gradient across these elements. The  $V_z/\text{cm}$  was higher for every element that was changed to adipose tissue. If the current

density had not been affected by atrophy, then there would not have been a voltage gradient change. Figure 49 is a plot of the current density in the normal model verses the atrophy model for the changed atrophy elements. Also, the current density in the changed atrophied element's voltage gradient may be used to investigate this effect. Using the voltage gradient results of the converted elements and then reapplying the original muscle tissue's conductivity value produces an increased current density. The increased current density around the adipose tissue causes the higher voltage gradient across the muscle elements since they are essentially in parallel with each adjacent element.

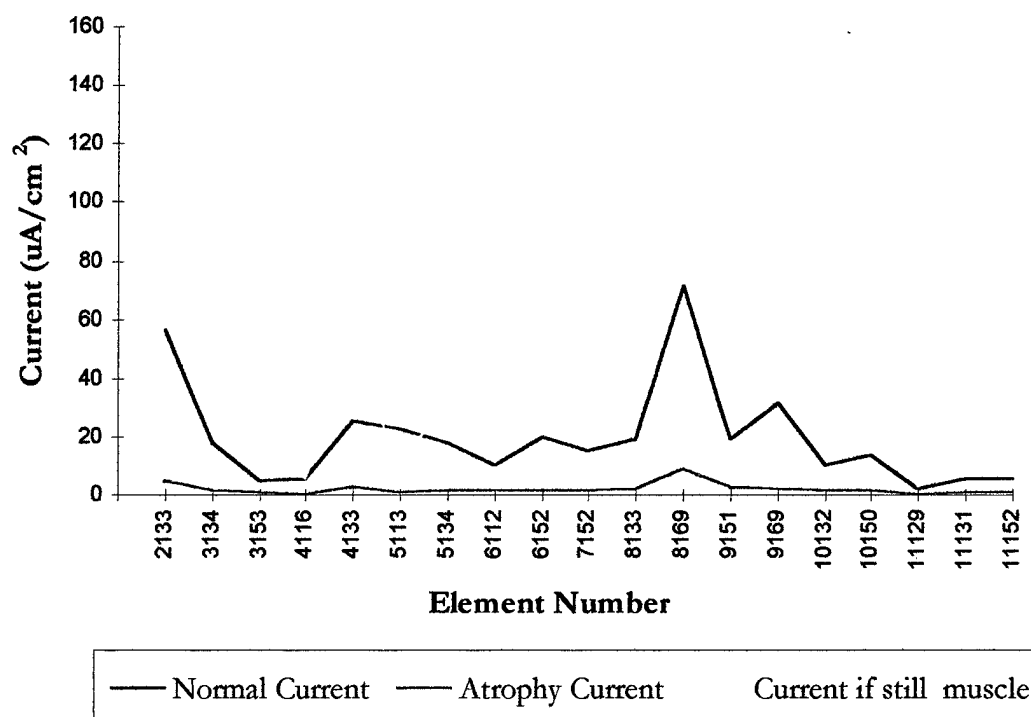


**Figure 49 - A graph comparing the current densities in adipose elements. The adipose tissue reduces the current density (purple line). Using the voltage gradient results of the converted elements and then reapplying the original muscle tissue's conductivity value produces an increased current density (yellow line). The increased current density around the adipose tissue causes the higher voltage gradient across the muscle elements since they are essentially in parallel with each adjacent element.**

Overall, the current density pattern in the target muscle did not change. The energy still remained focused in the target muscle as mentioned in Chapter 5. Figure 50 and Figure 51 is the current density contour plot at the mid-point cross section ( $Z = 6$ ) of both the normal and atrophied models, respectively.

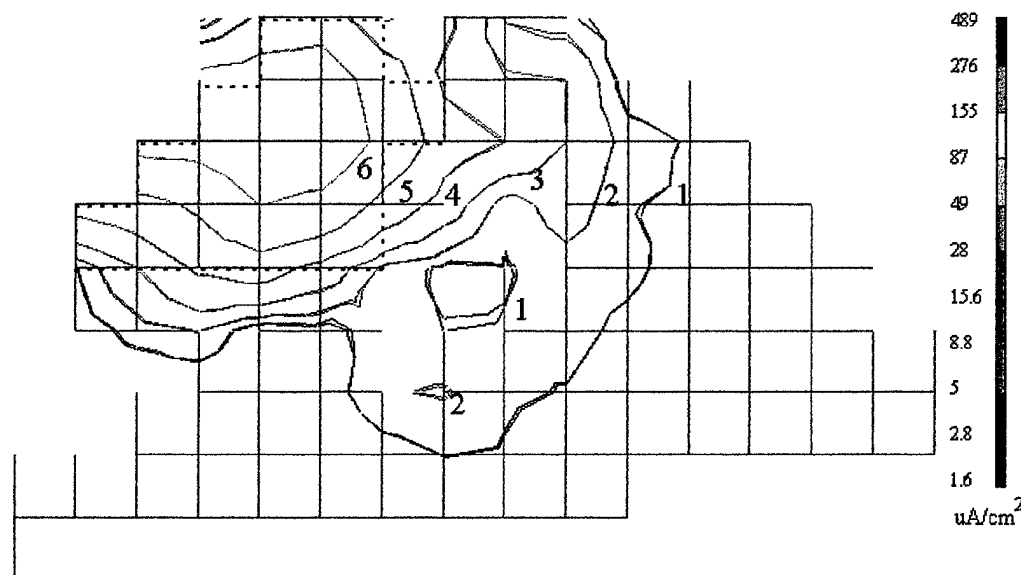


**Figure 50 - Contour plot showing the current density in X-Y plane at Z = 6 cm before atrophy was applied to the target muscle. The dashed line highlights the target muscle elements. The number on the contour line corresponds to its color bar segment.**

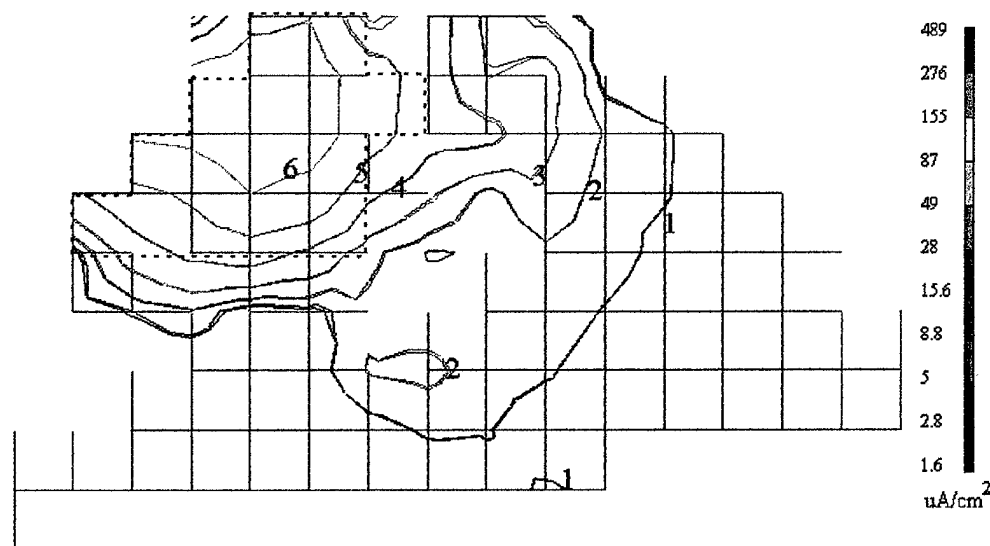


**Figure 51 - Contour plot showing the current density in X-Y plane at Z = 6 cm with atrophy applied to the target muscle. The dashed line highlights the target muscle elements. The current density pattern has little change from Figure 50. The number on the contour line corresponds to its color bar segment.**

The contour plots are nearly identical when superimposed over one another. The primary difference was a 5% increase in the size of the largest current density contour ( $I_z > 27.7 \mu\text{A}$ ) in the atrophied plot. The current pattern outside the target muscle remained the same. Figure 52 and Figure 53 are the current density plots for the atrophied target muscle.

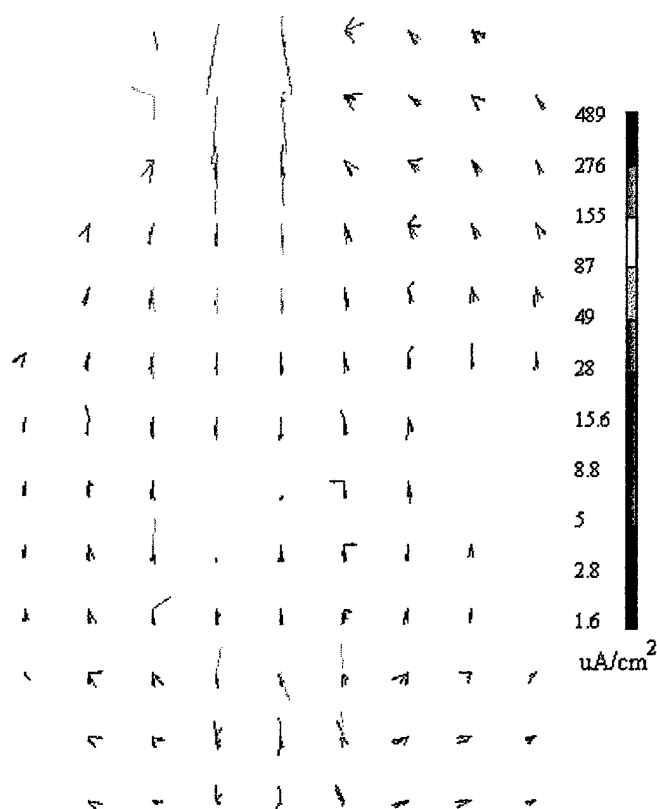


**Figure 52 - Top view of the atrophied leg of lamb FEM model results showing the current density vectors.**

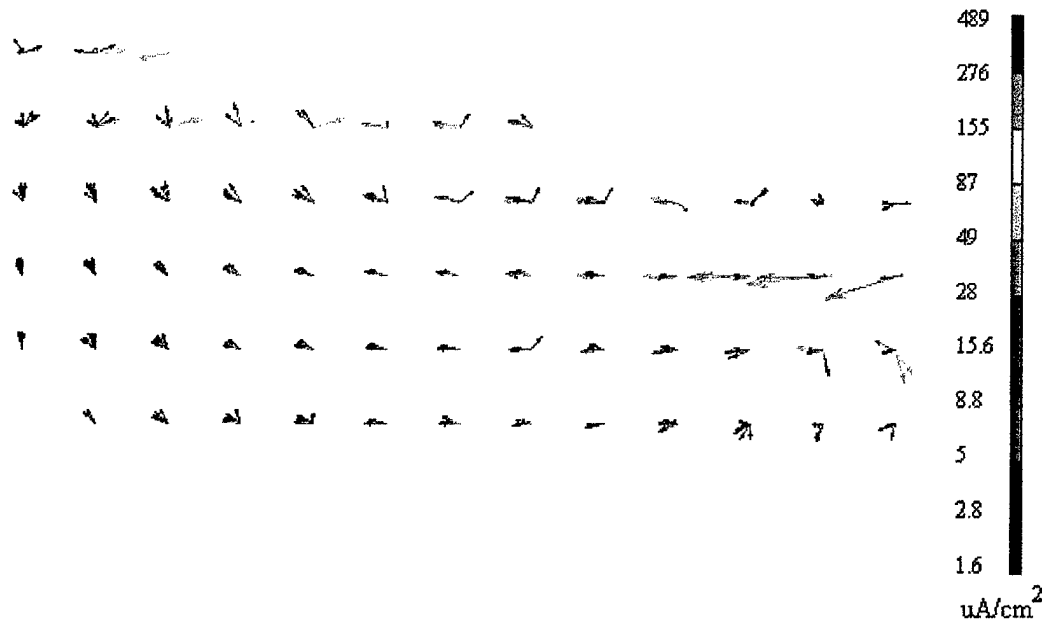


**Figure 53 - Side view of the atrophied leg of lamb FEM model results showing the current density vectors.**

### **The Inverse Problem**

The FEM can be used to optimize the stimulation protocol quickly. Instead of the trial and error subjective method of clinical trials to determine the best stimulation protocol, the computer model can be used to solve for the desired current density pattern. This can save clinician's time while providing optimal treatment. The overall result is enhanced patient care at a lower cost.

Starting with the desired current density in the target muscle as determined by other research, the I-DEAS software optimizer module can work from the element requirements by varying the boundary conditions iteratively to solve for the best fit. This is a geometry based operation. To accomplish this, the desired current density range for the target muscle would be specified. Then the limitations on the variations

permitted for electrode current, electrode size, and electrode location would be supplied. The result is the best fit within the given parameters. This saves the clinician from the trial and error process.

This optimization was not accomplished as part of this research since the leg of lamb was not geometry based. Instead, the leg of lamb FEM model was imported directly into the computer as a wire mesh. The only optimization that can be performed without geometry applied to the model was the variation of the source current to meet current density specifications. Since the goal of this research was not stimulation of a leg of lamb, but verification of the FEM as an accurate modeling method for complex human-like tissue, this would be an unnecessary exercise. The next planned phase of this research, a FEM model of the visible man project, will be able to accomplish the automated optimization of stimulation parameters.

## **CHAPTER 7**

### **DISCUSSION AND CONCLUSION**

#### **Discussion**

The FEM model has been shown to be a valid modeling method for determining the intramuscular electric current density in biological tissue. The progression from the saline phantom models to the complex tissue in the leg of lamb demonstrated that a FEM model will provide an accurate model of the human thigh. The heat transfer module in commercial FEM software packages provides the necessary tool in the low frequency range used by surface stimulation protocols. The same underlying mathematical equations allow the direct conversion of temperature to voltage, heat flux to current density, and thermal conductivity to electrical conductivity. This ability to use readily available FEM software owned by most universities for biological modeling of electric currents saves on the overhead costs of these software programs.

Computer modeling is a time and cost effective means to optimize the stimulation protocol for many different therapies. The conventional trial and error



method of testing on subjects and measuring the physiologic response can be slow, costly, and error prone. Also, for stimulation protocols, such as TES, where there is no direct measurable response, FEM modeling provides a direct, quantifiable means of determining the current densities in the underlying tissue due to the surface stimulation. Additionally, the ability to perform the reverse calculation to determine the optimum stimulation protocol is more cost effective and safer than iterative subject tests. Using the computer model as a tool to determine the best electrode size, shape, and placement is the future for research in stimulation therapy. This limits clinical trials to only a few pre-determined, optimum model results.

The FEM model of the leg of lamb also allows visualization of the resulting stimulation pattern. The focusing effects of the anisotropic conductivity property of striated muscle and adipose layers between major muscle groups may be observed. This capability has practical applications in trying to stimulate one muscle group while avoiding the antagonistic muscles. This is the case with TES for children with cerebral palsy. It also may be useful in functional stimulation research.

The final area of investigation in this research was the effect of atrophy on current density. The computer model was modified to reflect a target muscle with a 15% increase of embedded adipose tissue. This is one of the effects of atrophy which occurs in muscles with incomplete innervation. Muscle atrophy causes a localized current density increase in the muscle adjacent to the adipose tissue in the target muscle. This increase must be taken into account when determining the stimulation intensity for rehabilitation protocols for children with neuromuscular disorders where

atrophy is present in the target muscle. Further investigation is needed for the different levels of atrophy typically found clinically. The 15% value is at the low end of the clinical range. Additionally, a reduction in muscle size which accompanies disuse atrophy needs to be investigated. This approach may also be applied to the disuse atrophy research conducted on astronauts.

### **Additional Significance of this Research and its Clinical Utility**

The application of this research is not limited to just the human thigh and TES therapy. It has several other potential applications.

#### *Atrophied muscle impedance database*

Currently, no impedance data are available for the electrical properties of neuropathic muscle. With recent improvements in biomedical equipment, it is now possible to measure the impedance of major muscle groups *in vivo*. Using BIA, the distributed effects of muscle atrophy on electrical impedance can be measured. The data taken on the test population of children with neuromuscular disorders may then be correlated and statistically analyzed to provide researchers an additional tissue parameter to include in their models. Modeling improvements may be made using actual tissue properties instead of relying on data from healthy tissue properties for individuals with neuromuscular disorders. This capability is especially relevant for the area of functional neuromuscular stimulation.

#### *Incontinence and bladder stimulation*

Electrical stimulation has also been shown to be effective for increasing bladder size and control. However, most stimulation protocols, do not use surface electrodes. They require either implanted electrodes or intravascular electrodes. If the same results can be achieved with surface electrodes that have been achieved with the more invasive implantable or intravesical electrodes, the benefits will be great. The risk of infection will be reduced, patient compliance will be improved, and costs will be reduced since a medical professional will no longer be required to administer

the stimulation therapy daily. Children's self-esteem will also be enhanced by their involvement in helping themselves to improve.

### *Bone healing*

The FEM method may be used to optimize electric current magnetic field application for bone repair and growth. Some work has already been done in this area using FEM to model the vertebrae of the spine [54]. Other bones can also be modeled to optimize current orthopedic practices.

### *Prolonged space flight and disuse atrophy*

Finally, FEM may provide the ability to combine stimulation modalities to prevent disuse atrophy which occurs in microgravity situations. The stimulation may be optimized to provide efficacy for both the muscle atrophy and bone loss. The model would need to include greater portions of the body, encompassing all the load bearing bones. Magnetic stimulation would most likely provide the ability to uniformly induce the required electrical current throughout the body. FEM could be used to determine the minimum pulse duration required to create the necessary current density. It would be necessary to determine the optimum tradeoff between power consumption and obtaining the minimum thresholds for the different stimulation benefits.

## Conclusion

The application of FEM techniques to bioelectric problems in the human body along with recent improvements in computer processing power, provide the ability to accurately calculate the electric current densities in a 3-D model. Computer modeling is an inexpensive means to optimize electrical stimulation therapy protocols. The goal of this research was to verify the FEM model as a valid quantitative method to quantify the current densities resulting from bipolar stimulation. This was accomplished successfully in two steps. First, using a saline phantom, the FEM was compared against both empirical measurements and a published analytical solution. The saline model was also used to test the ability of the FEM to handle the complexities encountered in biological tissue. The second test of the FEM was the direct comparison of the FEM model of a leg of lamb against laboratory measurements made on a leg of lamb. The FEM was shown to provide an accurate means to quantify the current density in the target muscle. This technique can be used to determine the optimum electrical current density for stimulation protocols.

The successful completion of this research provides a stepping stone to a more comprehensive research project. The methods used in this research provide the means to create a FEM model of the visible human database. The verification of this human model would be (1) to predict the point at which active recruitment of the muscle first occurs based on the model's current density results, and (2) test this stimulation level on human subjects to confirm its accuracy. Finally, the human model could be used to solve the inverse problem and optimize many different stimulation protocols.

Ultimately, the goal is to take this research to the clinical application stage. Clinical measurements of children with neuromuscular disorders will need to be used to determine the correlation between atrophy level, functional level, and bioelectric impedance of the muscle. Then the model may be modified to incorporate these individual variations to determine the individualized stimulation protocol for TES therapy. Clinical trials using several promising stimulation protocols may then be made. FEM can be used to save time and money and also help optimize rehabilitation therapies resulting in better treatment and functional improvement for children with neuromuscular disorders.

## REFERENCES

- [1] R. Myrhage and O. Hudlicka, "Capillary growth in chronically stimulated adult skeletal muscle as studied by intravital microscopy and histological methods in rabbits and rats," *Microvasc Res*, vol. 16, pp. 73-90, 1978.
- [2] J. N. A. Gibson, K. Smith, and M. J. Rennie, "Prevention of Disuse Muscle Atrophy by Means of Electrical Stimulation: Maintenance of Protein Synthesis," *The Lancet*, vol. 1-Oct, pp. 767-770, 1988.
- [3] R. B. Borgens, "Stimulation of Neuronal Regeneration and Development by Steady Electrical Fields," in *Functional Recovery in Neurology*, S. G. Waxman, Ed. New York: Raven Press, 1988, pp. 547-564.
- [4] A. H. Balcom, M. Wiatrak, T. Biefeld, K. Rauen, and P. Langenstroer, "Initial experience with home therapeutic electrical stimulation for continence in the myelomeningocele population," *J Urol*, vol. 158, pp. 1272-6, 1997.
- [5] K. E. Pape, S. E. Kirsch, A. Galil, J. E. Boulton, M. A. White, and M. Chipman, "Neuromuscular approach to the motor deficits of cerebral palsy: a pilot study," *J Pediatr Orthop*, vol. 13, pp. 628-33, 1993.
- [6] K. E. Pape, "Therapeutic electrical stimulation (TES) for the treatment of disuse muscle atrophy in cerebral palsy," *Pediatric Physical Therapy*, vol. 9, pp. 110 -112, 1997.
- [7] R. Aaron, M. Huang, and C. A. Shiffman, "Anisotropy of human muscle via non-invasive impedance measurements," *Phys Med Biol*, vol. 42, pp. 1245-62, 1997.
- [8] K. P. Esselle and M. A. Stuchly, "Quasi-static electric field in a cylindrical volume conductor induced by external coils," *IEEE Trans Biomed Eng*, vol. 41, pp. 151-8, 1994.
- [9] L. A. Geddes and L. E. Baker, "The Specific Resistance of Biological Material - Compendium of Data for the Biomedical Engineer and Physiologist," *Biolo. Engng*, vol. .5., pp. 271-293, 1967.
- [10] E. N. Marieb, *Human anatomy and physiology*. Redwood City, CA: The Benjamin Cummings Publishing Company, 1992.
- [11] R. L. Lieber, "Skeletal muscle adaptability. I. Review of basic properties," *Dev Med Child Neurol*, vol. 28, pp. 390-97, 1986.
- [12] K. E. Pape, "Caution urged for NMS use," *Physical Therapy*, vol. 74, pp. 265-267, 1994.

- [13] P. Steinbok, A. M. Reiner, and J. R. W. Kestle, "Therapeutic electrical stimulation (TES) following selective posterior rhizotomy in children with spastic diplegia due to cerebral palsy: a randomized clinical trial," *Dev Med Child Neurol*, vol. 38, pp. 32-33, 1996.
- [14] K. E. Pape, S. E. Kirsch, and J. M. Bugaresti, "New therapies in spastic cerebral palsy," *Contemporary Pediatrics*, vol. 1, pp. 6-13, 1990.
- [15] K. E. Pape and S. E. Kirsch, "Technology-assisted self-care in the treatment of spastic diplegia," in *The Diplegic Child*, M. D. Sussman, Ed. Rosemount, IL: American Academy of Orthopedic Surgeons, 1992, pp. 241-255.
- [16] J. G. Susset and Z. N. Boctor, "Electrical stimulation of the bladder: an experimental study," *Investigative Urology*, vol. 5, pp. 20-29, 1967.
- [17] R. A. Schmidt, "Applications of Neuro-stimulation in Urology," *interferometryNeuro. & Urology*, vol. 7, pp. 585-592, 1988.
- [18] M. Sawan, M. M. Hassouna, J. S. Li, F. Duval, and M. M. Elhilali, "Stimulator design and subsequent stimulation parameter optimization for controlling micturition and reducing urethral resistance," *IEEE Trans Rehabil Eng*, vol. 4, pp. 39-46, 1996.
- [19] W. E. Kaplan, T. W. Richards, and I. Richards, "Intravesical transurethral bladder stimulation to increase bladder capacity," *J Urol*, vol. 142, pp. 600-2; discussion 603-5, 1989.
- [20] D. Motzkin, "The significance of deficient bladder sensation," *J Urol*, vol. 100, pp. 445-50, 1968.
- [21] S. T. Hasan, W. A. Robson, A. K. Pridie, and D. E. Neal, "Transcutaneous electrical nerve stimulation and temporary S3 neuromodulation in idiopathic detrusor instability [see comments]," *J Urol*, vol. 155, pp. 2005-11, 1996.
- [22] W. Bayliss, "On the origin from the spinal cord of the vasodilator fibers of the hind limb and the origin of these fibers," *J. Physiology*, vol. 26, pp. 173-209, 1901.
- [23] D. M. Dooley and M. Kasprak, "Modification of blood flow to the extremities by electrical stimulation of the nervous system," *South Med. J.*, vol. 6910, pp. 1309-1311, 1976.
- [24] M. D. Brown, M. A. Cotter, and O. Hudlická, "The Effects of Different Patterns of Muscle Activity on Capillary Density, Mechanical Properties and Structure of Slow and Fast Rabbit Muscles," *Pflügers Archiv*, vol. 361, pp. 241-250, 1976.



- [25] L. Dodd, S. D. Gray, and O. Hudlická, "Evaluation of capillary density in relation to fiber types in electrically stimulated rabbit fast muscles," *Journal of Physiology-London*, vol. 301, pp. 353-81, 1980.
- [26] M. F. Zanakos, "Differential effects of various electrical parameters on peripheral and central nerve regeneration," *Acupunct Electrother Res (2GR)*, vol. 15, pp. 185-91, 1990.
- [27] R. K. Olney, Y. T. So, and D. S. Goodin, "A Comparison of Magnetic and Electrical Stimulation of Peripheral Nerves," *Muscle & Nerve*, vol. 13, pp. 957-963, 1990.
- [28] E. L. Carter, Jr., E. J. Vresilovic, S. R. Pollack, and C. T. Brighton, "Field distributions in vertebral bodies of the rat during electrical stimulation: a parametric study," *IEEE Trans Biomed Eng*, vol. 36, pp. 333-45, 1989.
- [29] M. N. O. Sadiku, *Numerical Techniques in Electromagnetics*. Boca Raton: CRC Press, 1992.
- [30] C. S. Desai and J. F. Abel, *Introduction to the Finite Element Method: A Numerical Approach for Engineering Analysis*. New York: Van Nostrand Reinhold, 1972.
- [31] Z. Cendes, "Unlocking the magic of Maxwell's equations," in *IEEE Spectrum*, 1989, pp. 29-33.
- [32] D. Dietrich, "FE Analysis for the Body," in *Mechanical Engineering*, 1987, pp. 48-52.
- [33] C. E. Miller and C. S. Henriquez, "Finite element analysis of bioelectric phenomena," *Crit Rev Biomed Eng*, vol. 18, pp. 207-33, 1990.
- [34] D. R. Pitts and L. E. Sissom, *Theory and Problems of Heat Transfer*. New York: McGraw-Hill, 1977.
- [35] L. B. Houtkooper, T. G. Lohman, and S. B. Going, "Validity of Bioelectric Impedance for Body Composition Assessment in Children," *J. Appl. Physiol.*, vol. 66, pp. 814-821, 1989.
- [36] K. Iwata, Y. Satou, and F. Iwata, "Assesment of Body Composition Measured by Bioelectrical Impedance in Children," *Acta Paediatrica Japonica*, vol. 35, pp. 369-372, 1993.
- [37] L. B. Houtkooper, S. B. Going, and T. G. Lohman, "Bioelectrical Impedance Estimation of Fat-Free Body Mass in Children and Youth: A Cross-Validation Study," *J. Appl. Physiol.*, vol. 72, pp. 366-373, 1992.

- [38] S. B. Heymsfield, C. McManus, J. Smith, V. Stevens, and D. W. Nixon, "Anthropometric measurement of muscle mass: Revised equations for calculating bone-free arm muscle area," *AM J. Clin. Nutr.*, vol. 36, pp. 680-90, 1982.
- [39] J. Nyboer, *Electrical Impedance Plethysmography*, 2 ed. Springfield, Illinois: Charles C. Thomas, 1970.
- [40] S. P. Walker, S. Grantham-McGregor, and C. Powell, "Bioelectric Impedance, Anthropometry, and Body Composition in Stunted and Non-Stunted Children," *European Journal of Clinical Nutrition*, vol. 44, pp. 763-768, 1990.
- [41] F. Schaefer, M. Georgi, and A. Zieger, "Usefulness of Bioelectric Impedance and Skinfold Measurements in Predicting Fat-Free Mass Derived from Total Body Potassium in Children," *Pediatric Research*, vol. 35, pp. 617-624, 1994.
- [42] B. H. Brown, T. Karatzas, R. Nakielnny, and R. G. Clark, "Determination of upper arm muscle and fat areas using electrical impedance measurements," *Clin. Phys. Physiol. Meas.*, vol. 91, pp. 47-55, 1988.
- [43] E. Zheng, S. Shao, and J. G. Webster, "Impedance of skeletal muscle from 1 Hz to 1 MHz," *IEEE Trans. Biomed Eng.*, vol. 31, pp. 477-81, 1984.
- [44] D. C. Barber and B. H. Brown, "Applied potential tomography," *J. Phys. E.: Sci. Instrum.*, vol. 17, pp. 723-33, 1984.
- [45] B. R. Epstein and K. R. Foster, "Anisotropy in the dielectric properties of skeletal muscle," *Med Biol Eng Comput*, vol. 21, pp. 51-5, 1983.
- [46] R. Pethig and D. B. Kell, "The Passive Electrical Properties of Biological Systems: Their Significance in Physiology, Biophysics, and Biotechnology," *Phys. Med. Biol.*, vol. 32, pp. 933-970, 1987.
- [47] H. C. Lukaski, P. E. Johnson, and W. W. Olonchuk, "Assesment of Fat-Free Mass Using Bioelectrical Impedance Measurements Of the Human Body," *American Journal of Clinical Nutrition*, vol. 41, pp. 810-817, 1985.
- [48] R. C. Weast, "CRC Handbook of Chemistry and Physics," , 66 ed. Boca Raton: CRC Press, 1986.
- [49] A. Stogryn, "Equations for Calculating the Dielectric Constant of Saline Water," *IEEE Trans Microwave Theory and Techniques*, vol. 19, pp. 733-73, 1971.
- [50] J. D. Kraus and K. R. Carver, *Electromagnetics*, 2 ed. New York: McGraw-Hill, 1973.

- [51] F. Duck, *Physical Properties of Tissue: A Comprehensive Reference Book*. San Diego: Academic Press, 1990.
- [52] S. Rush, J. A. Abildskov, and R. McFee, "Resistivity of Body Tissues at Low Frequencies," *Circulation Research*, vol. 12, pp. 40-50, 1963.
- [53] C. Gabriel and S. Gabriel, "Compilation of the Dielectric Properties of Body Tissues at RF and Microwave Frequencies," Armstrong Lab (AFMC), Brooks AFB, San Antonio, Texas, Final Report AL/OE-TR-1996-0037, June 1996.
- [54] E. L. Carter, Jr., S. R. Pollack, and C. T. Brighton, "Theoretical determination of the current density distributions in human vertebral bodies during electrical stimulation," *IEEE Trans Biomed Eng*, vol. 37, pp. 606-14, 1990.

## APPENDIX A - LAMB SLICES

Lamb Slice at  $Z = 1$  cm

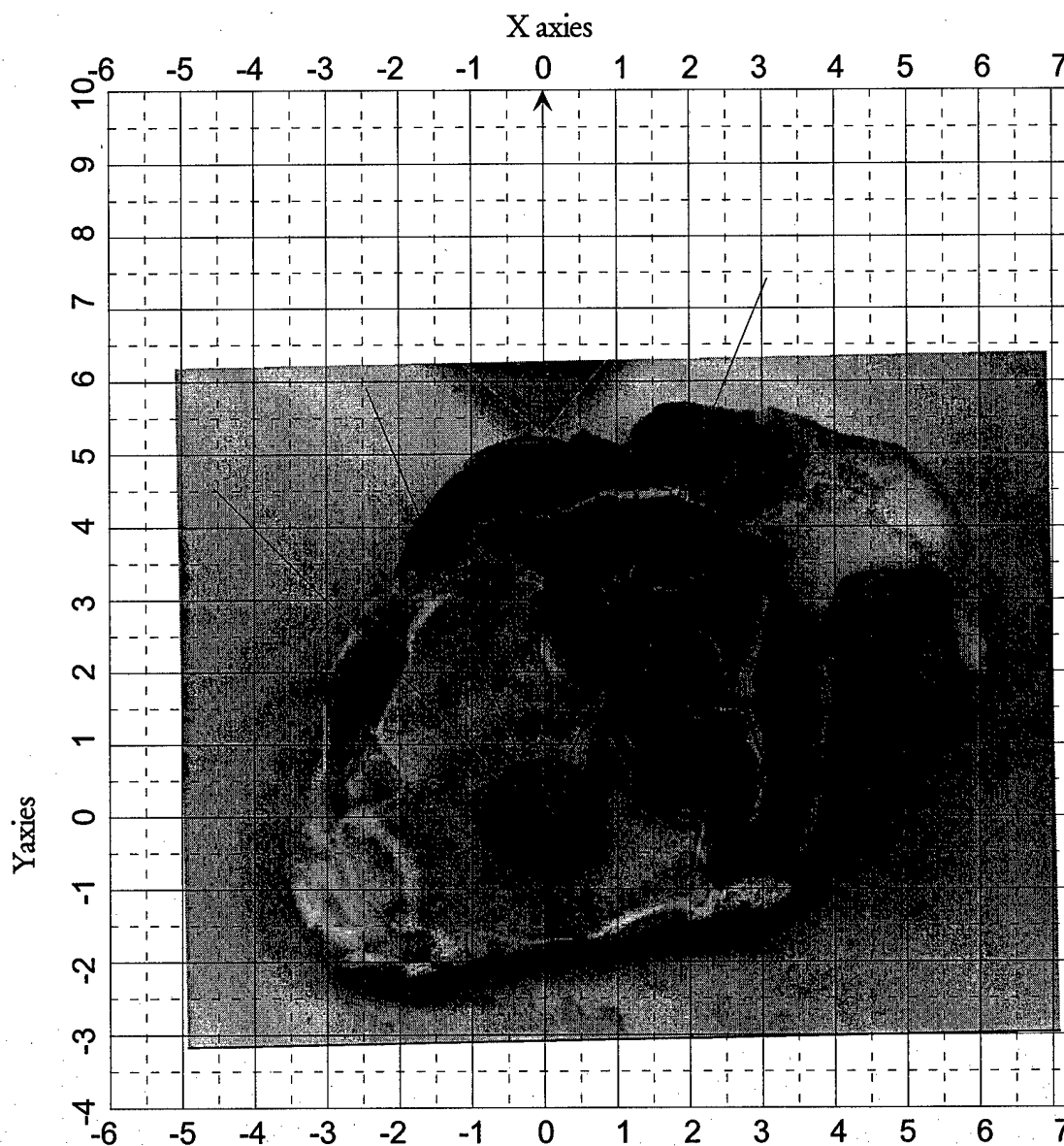


Figure 54 - Photograph of the leg of lamb sliced at  $Z = 1$  cm.

Lamb Slice at  $Z = 2$  cm

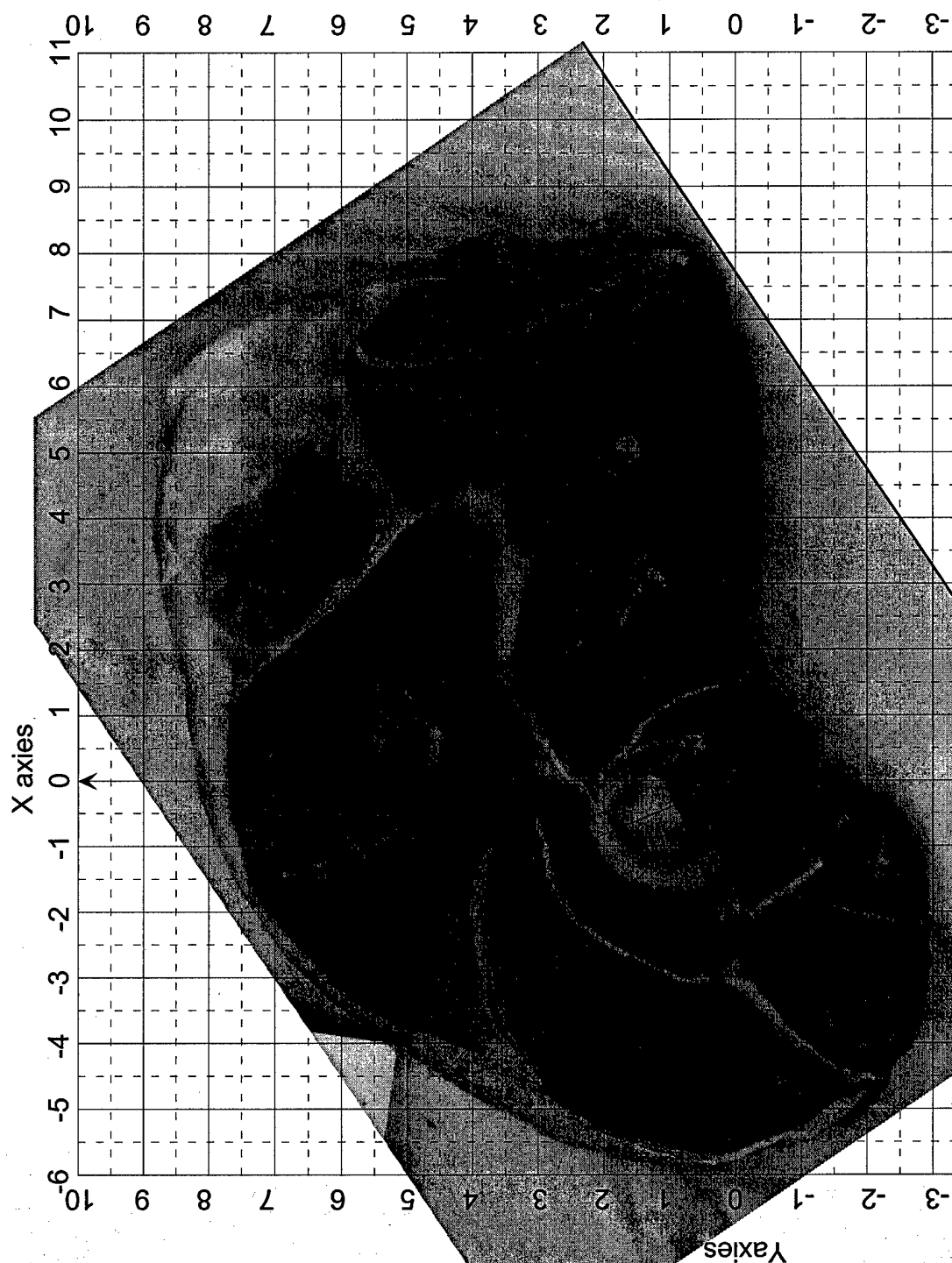
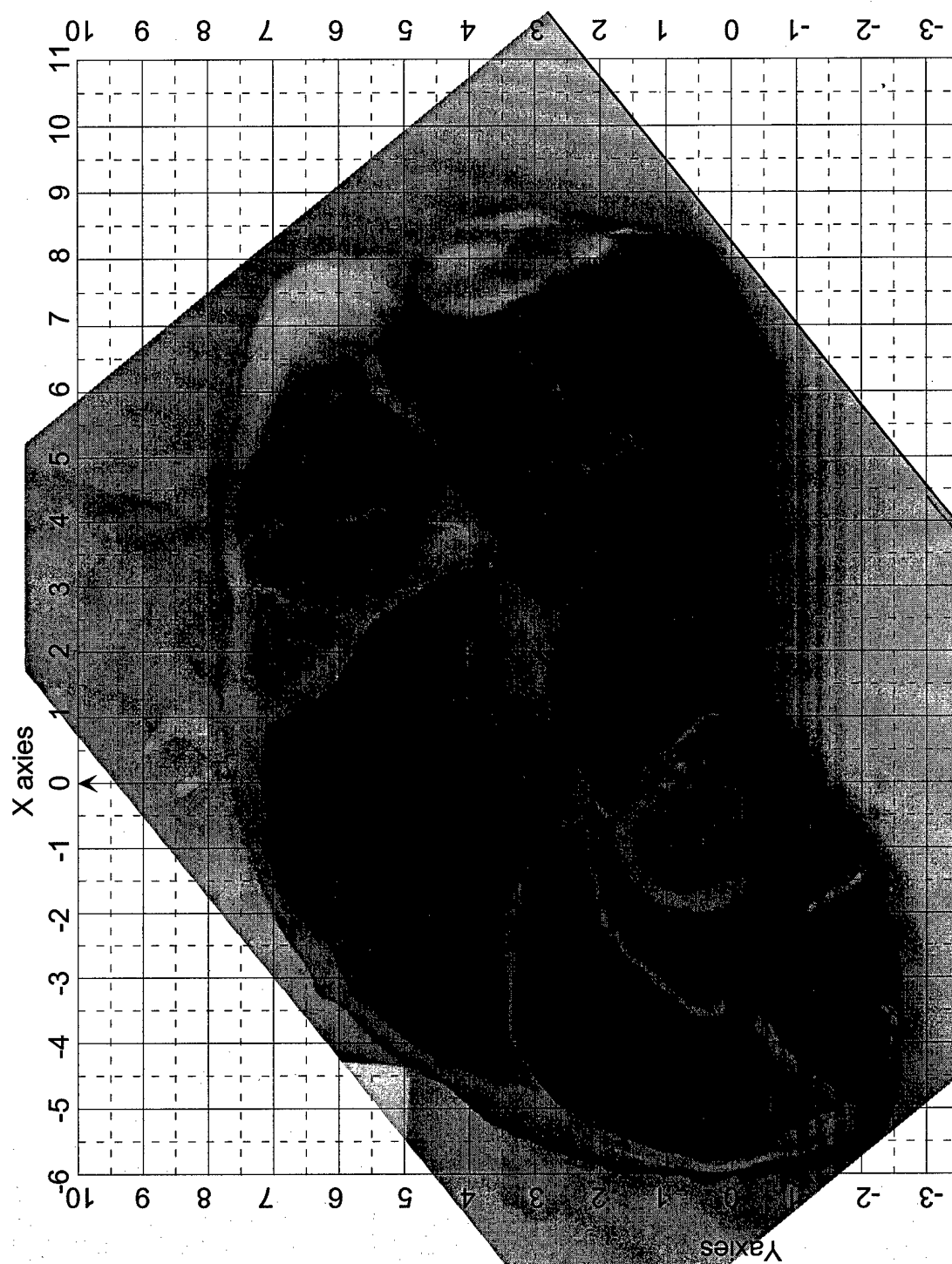


Figure 55 - Photograph of the leg of lamb sliced at  $Z = 2$  cm.

**Lamb Slice at  $Z = 3$  cm****Figure 56 - Photograph of the leg of lamb sliced at  $Z = 3$  cm.**

Lamb Slice at  $Z = 4$  cm

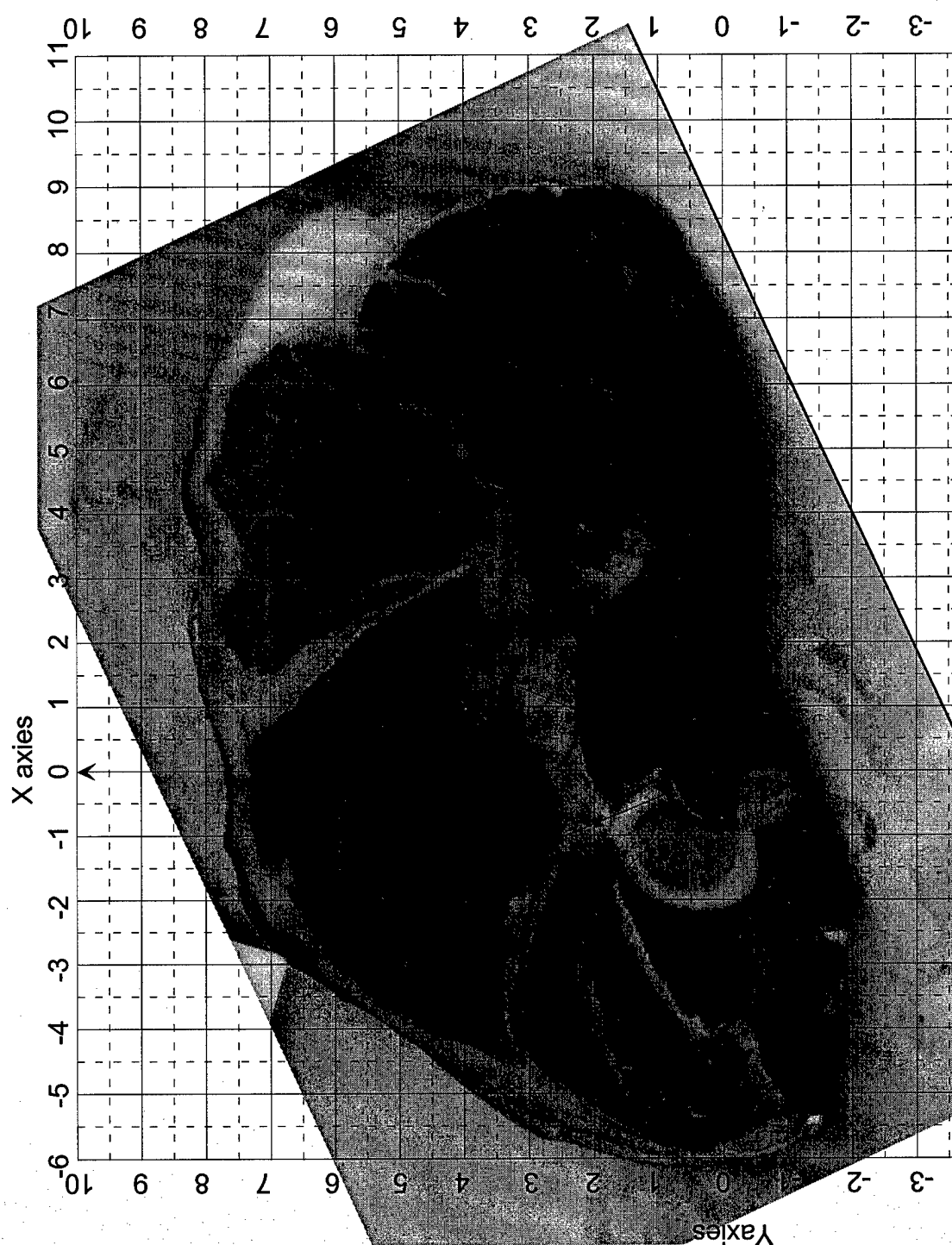


Figure 57 - Photograph of the leg of lamb sliced at  $Z = 4$  cm.

Lamb Slice at  $Z = 5$  cm

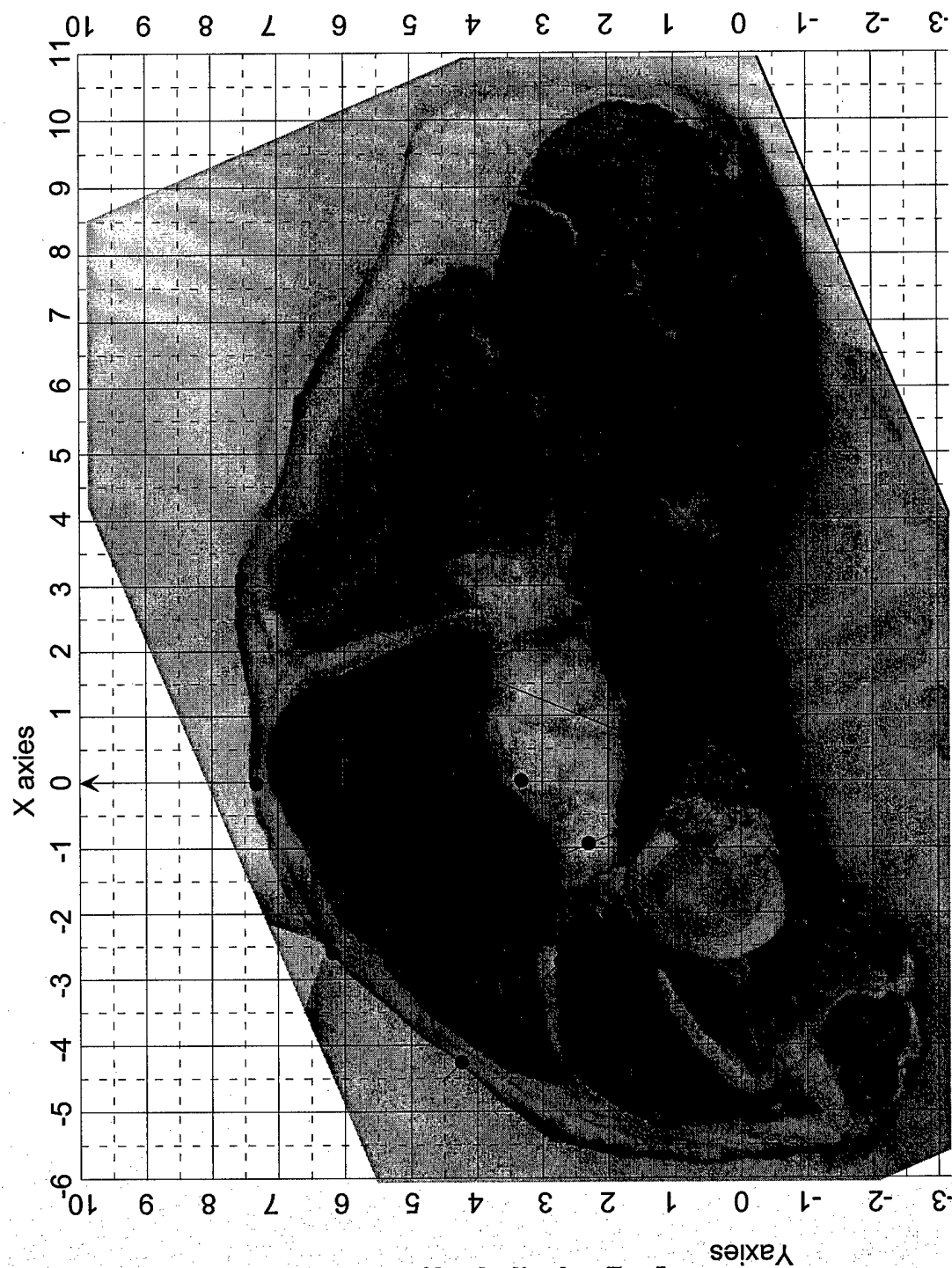


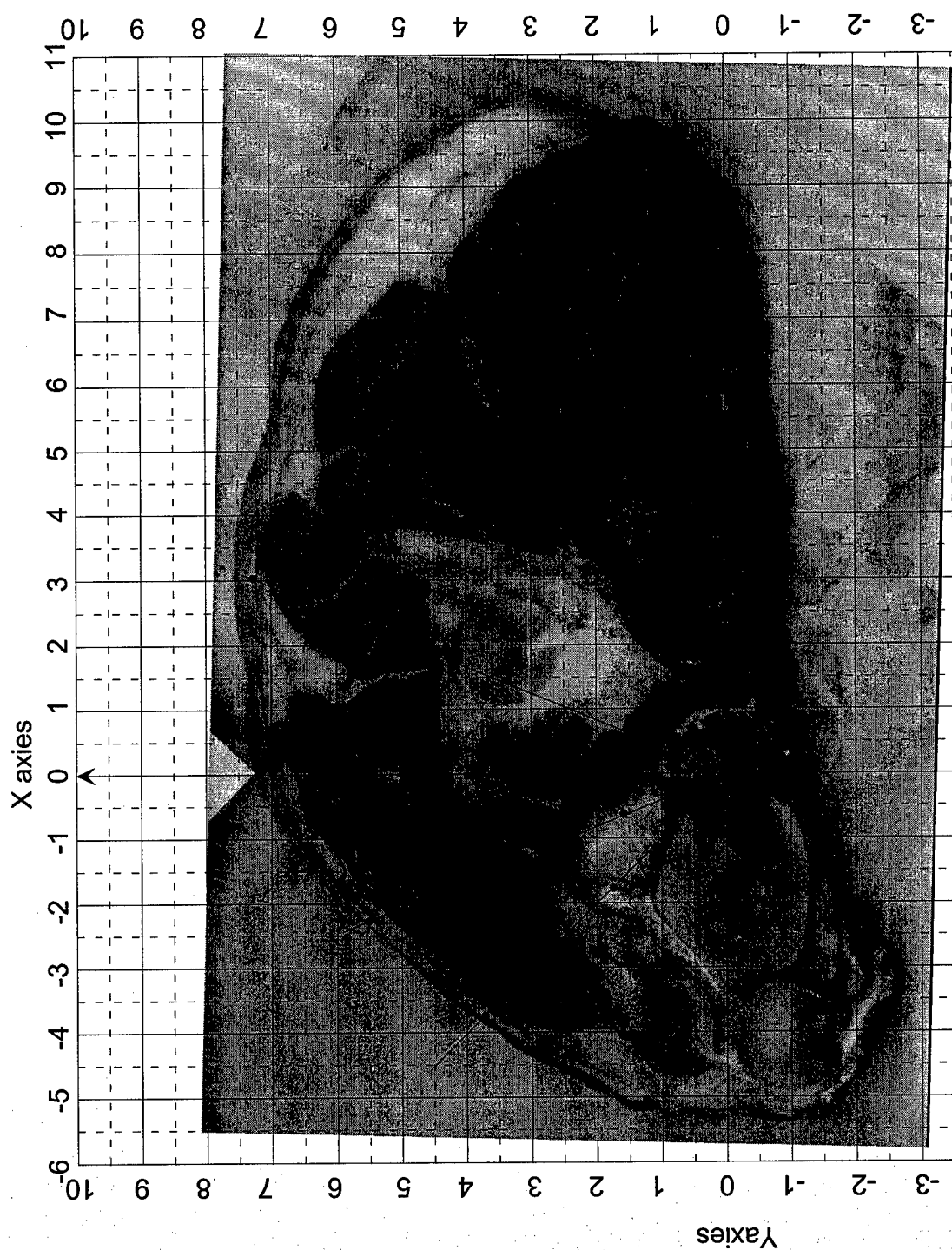
Figure 58 - Photograph of the leg of lamb sliced at  $Z = 5$  cm.



Lamb Slice at  $Z = 6$  cm



Figure 59 - Photograph of the leg of lamb sliced at  $Z = 6$  cm.

Lamb Slice at  $Z = 7$  cmFigure 60 - Photograph of the leg of lamb sliced at  $Z = 7$  cm.

Lamb Slice at  $Z = 8$  cm

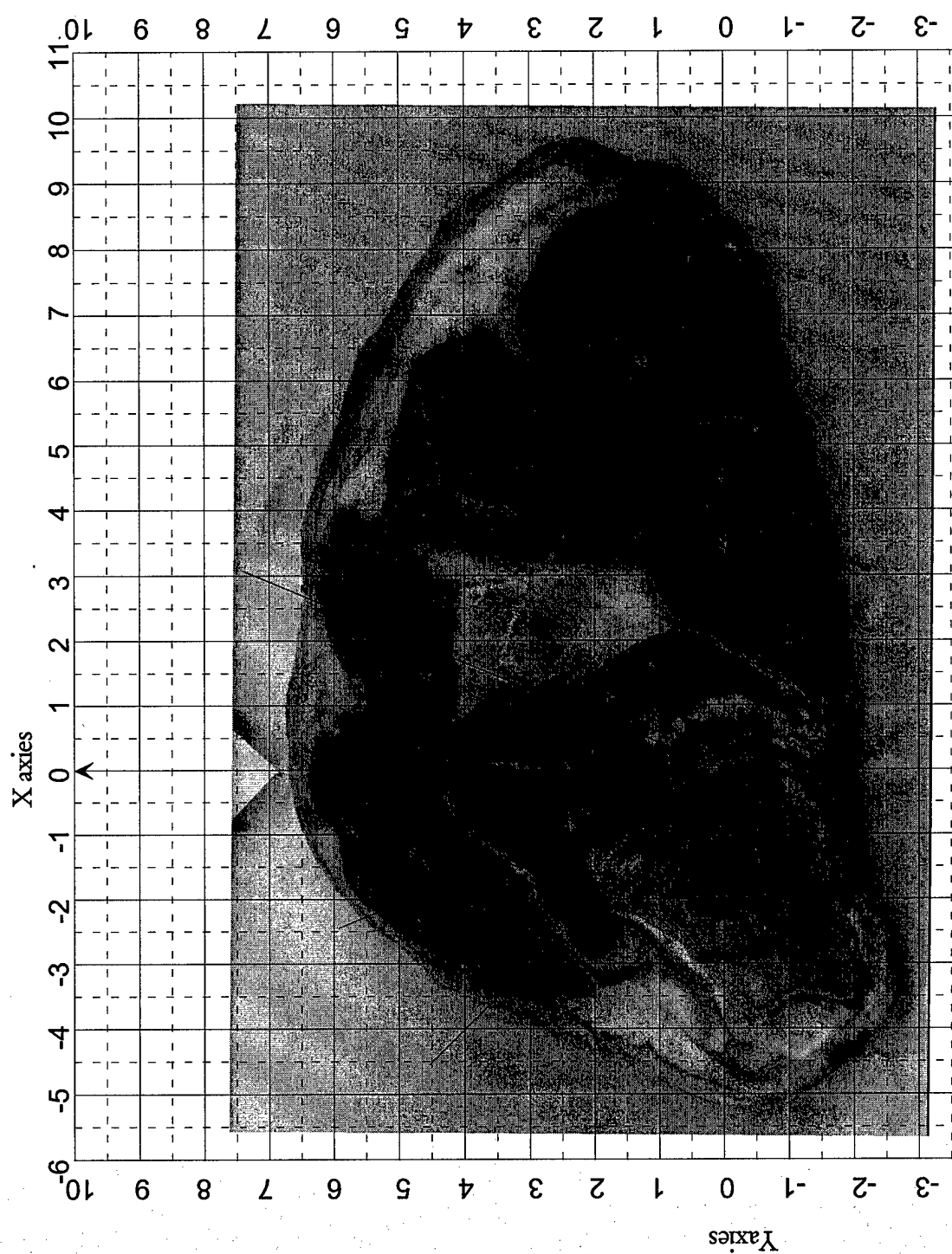


Figure 61 - Photograph of the leg of lamb sliced at  $Z = 8$  cm.

Lamb Slice at  $Z = 9$  cm

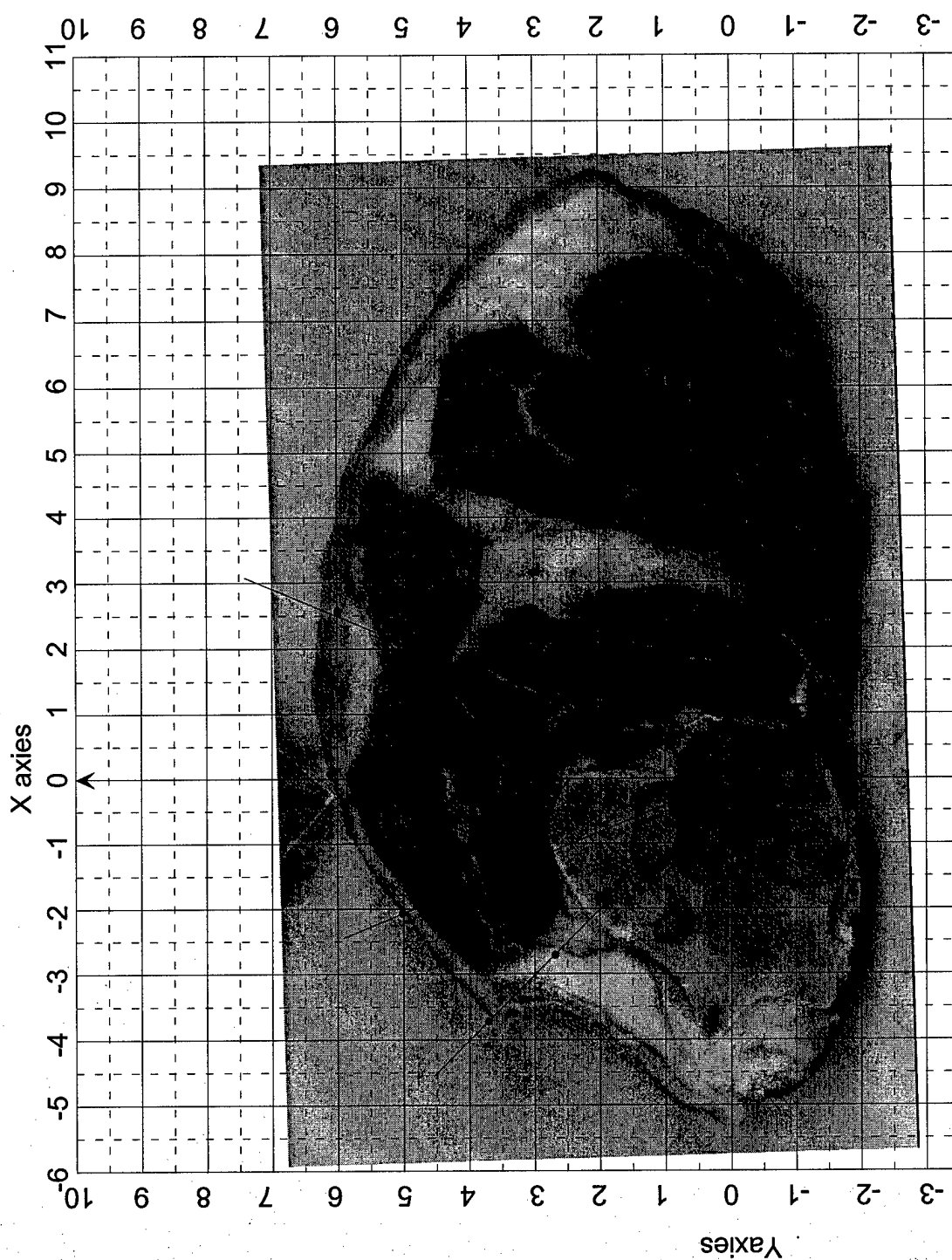
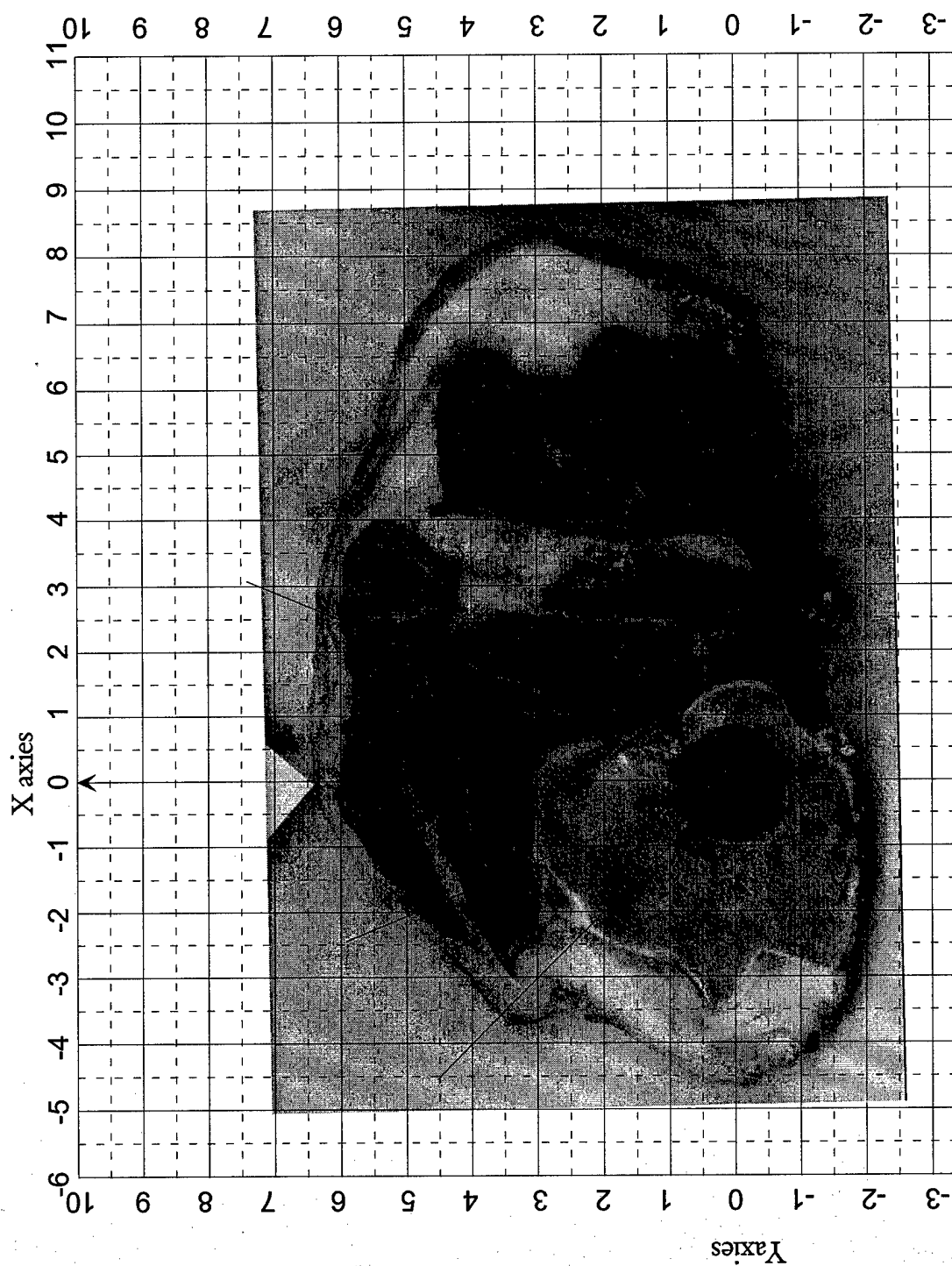
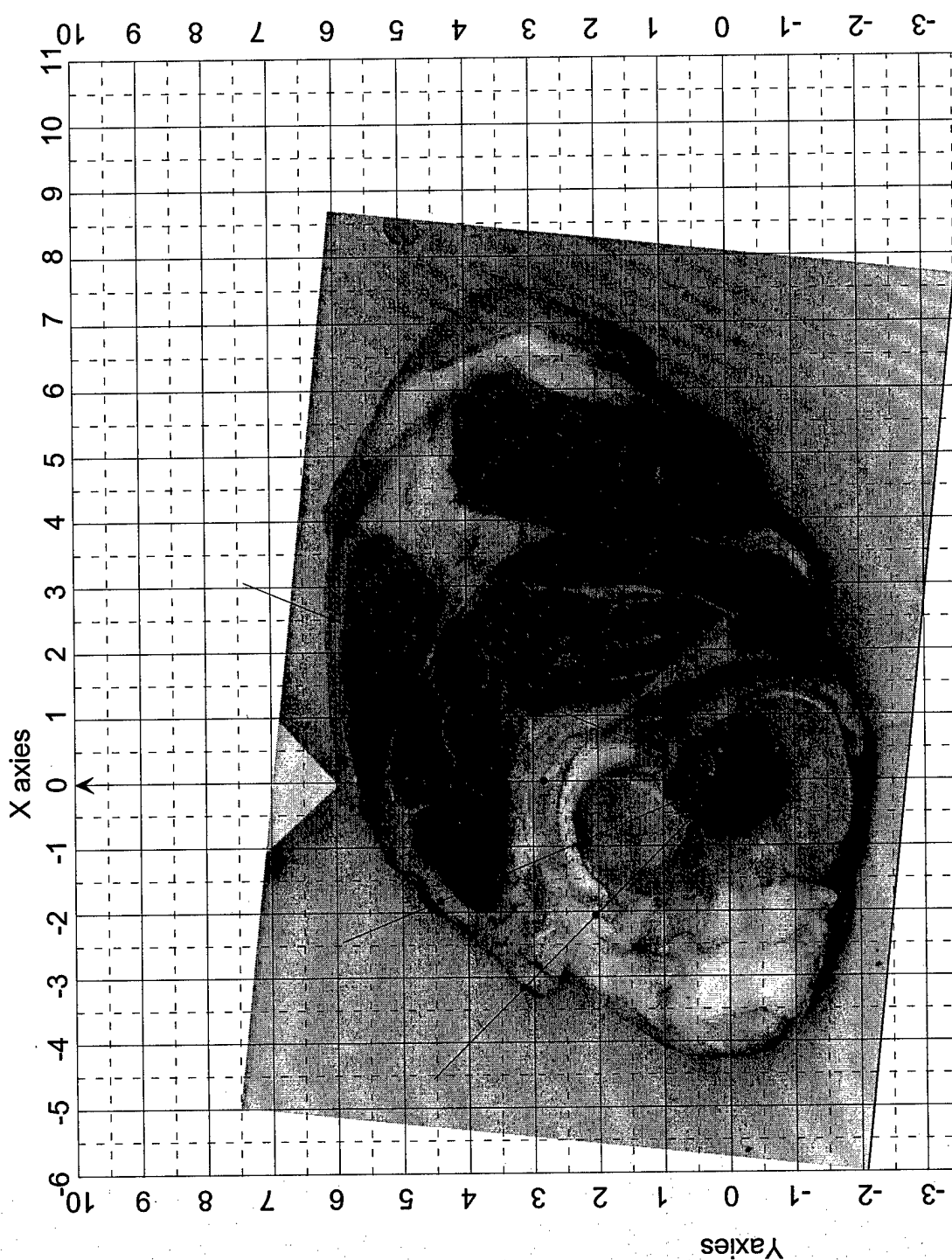
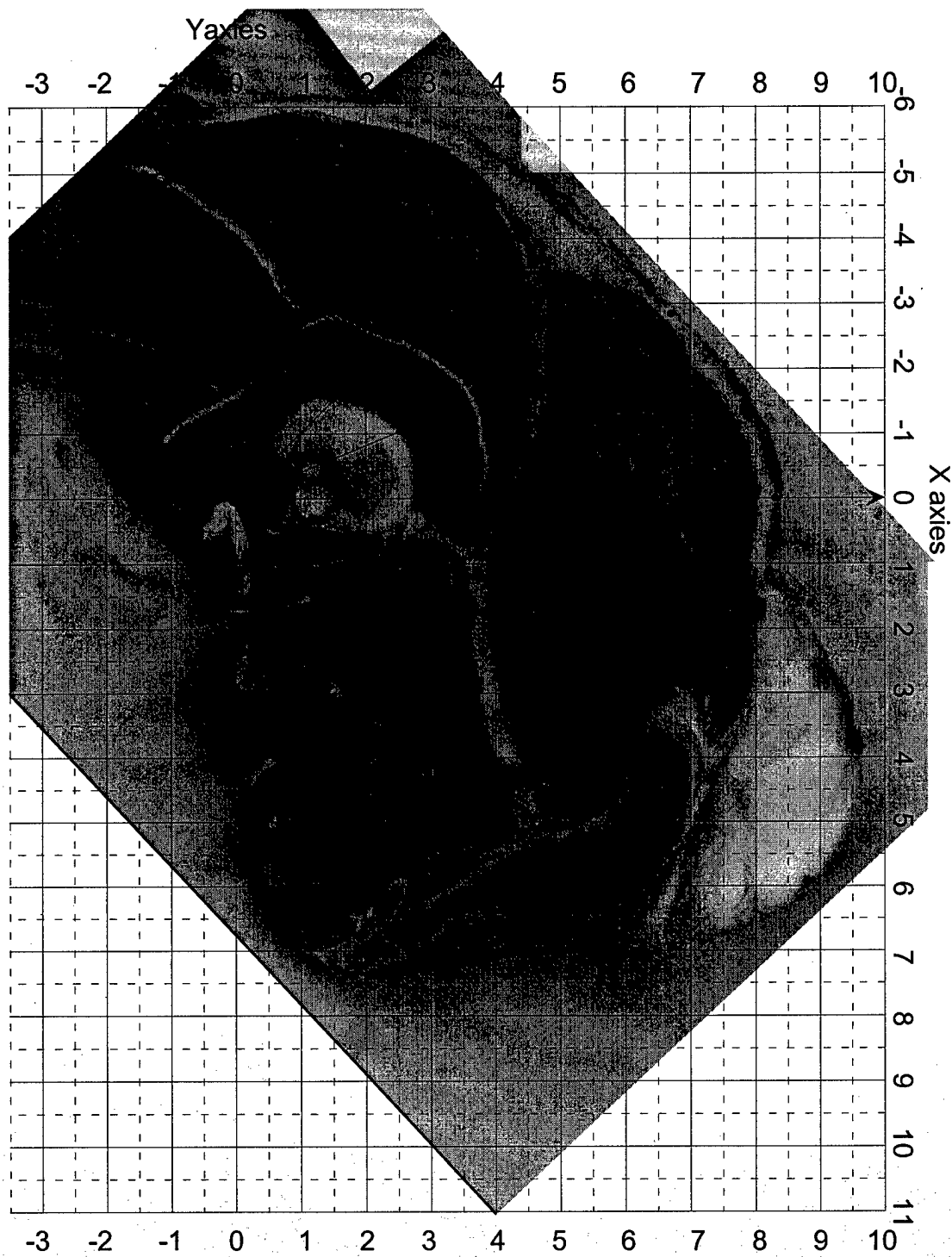


Figure 62 - Photograph of the leg of lamb sliced at  $Z = 9$  cm.

Lamb Slice at  $Z = 10$  cmFigure 63 - Photograph of the leg of lamb sliced at  $Z = 10$  cm.

Lamb Slice at  $Z = 11$  cmFigure 64 - Photograph of the leg of lamb sliced at  $Z = 11$  cm.

**Lamb Slice at  $Z = 12$  cm****Figure 65 - Photograph of the leg of lamb sliced at  $Z = 12$  cm.**

## APPENDIX B - SALINE LABORATORY MEASUREMENTS

<b>Table 4 - Summary Table of Laboratory Measurements Made in Saline Cylinder</b>				
Measurement #	Depth (Z)	X	Y	Volts (peak) above ground
1	0	0	0	0.352
2	1	0.5	0	0.36
3	1	-0.5	0	0.361
4	1	0	0.25	0.362
5	1	0	0.5	0.35
6	1	0	0.75	0.35
7	1	0	1	0.35
8	1	1	0.5	0.35
9	1	-1	0.5	0.35
10	2	0	0	0.35
11	2	0.5	0	0.346
12	2	-0.5	0	0.346
13	2	0	0.5	0.344
14	3	0	0	0.344
15	3	0	1	0.346
16	3	0	2	0.346
17	4	0	0	0.338
18	1	0	9.5	0.322
19	1	0.5	9.8	0.322
20	1	-0.5	9.8	0.322
21	1	0	9.8	0.316
22	All other locations			.344 - .346



## APPENDIX C - GRAPHICAL RESULTS OF LEG OF LAMB LABORATORY MEASUREMENTS

Laboratory Voltage Gradient Measurements of the X-Y Plane at  $Z = 0$  cm.

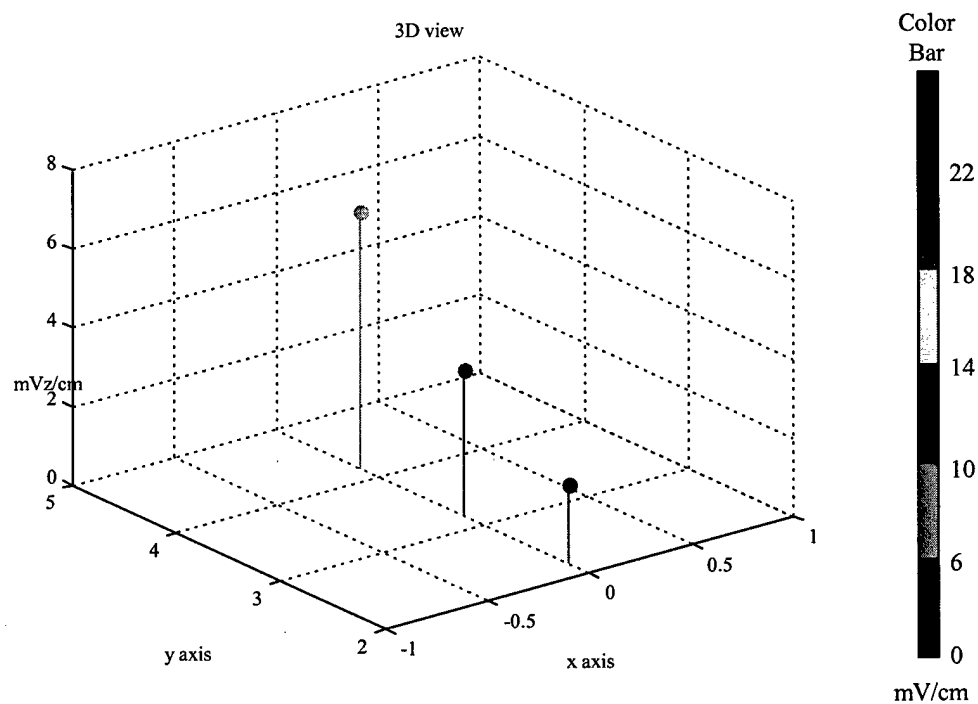
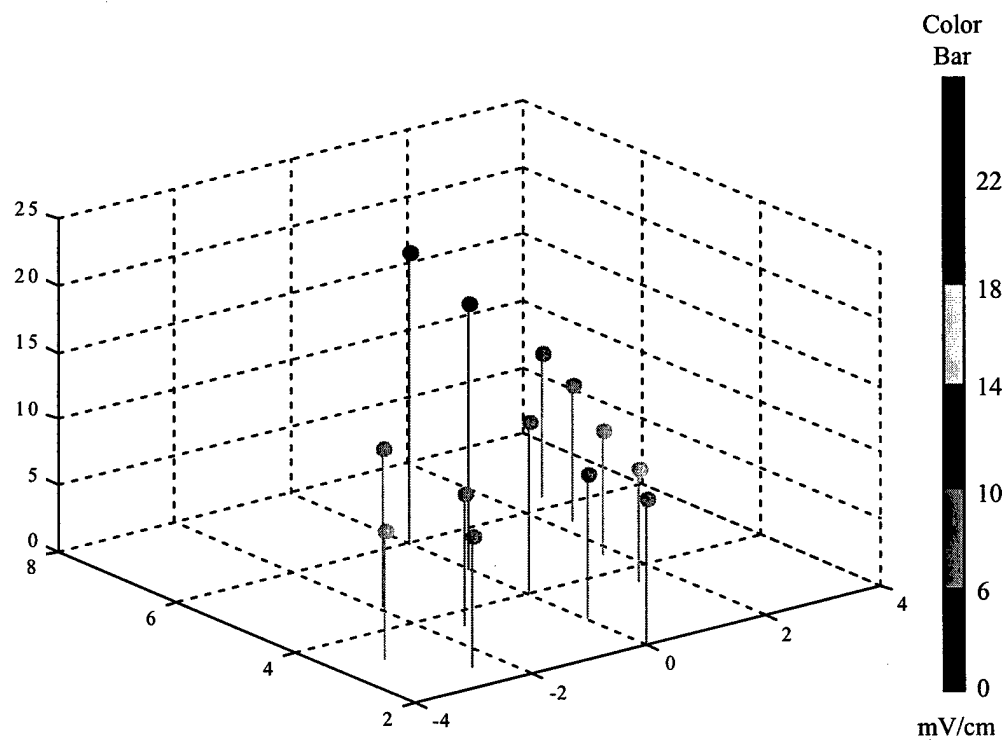
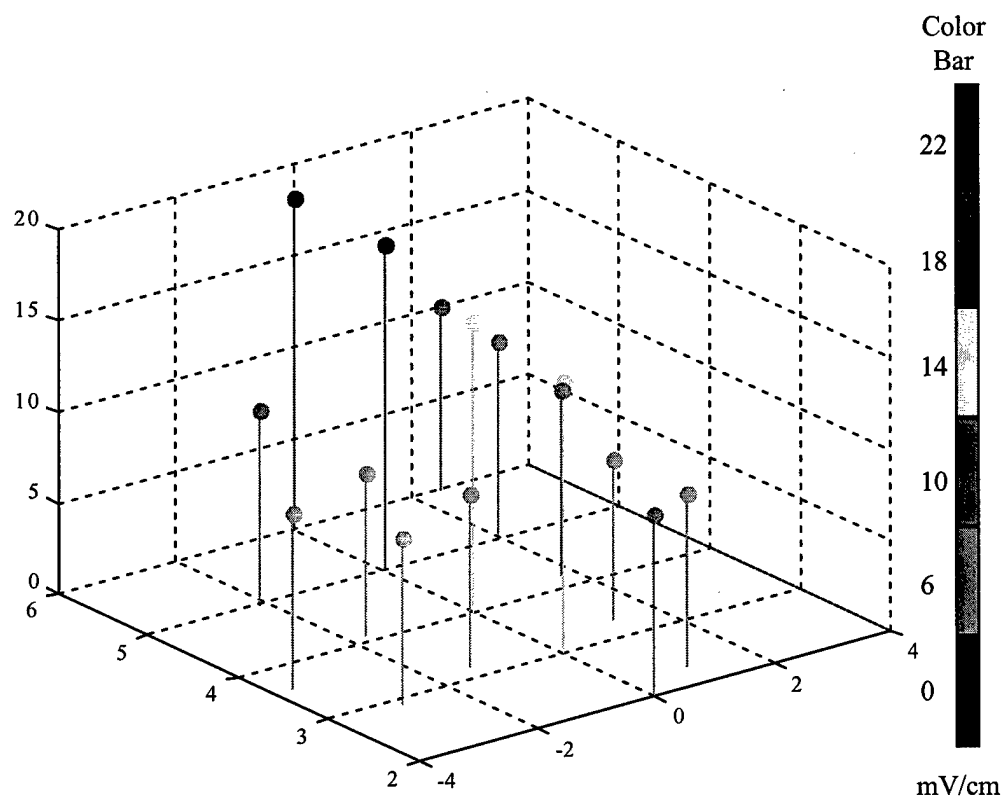


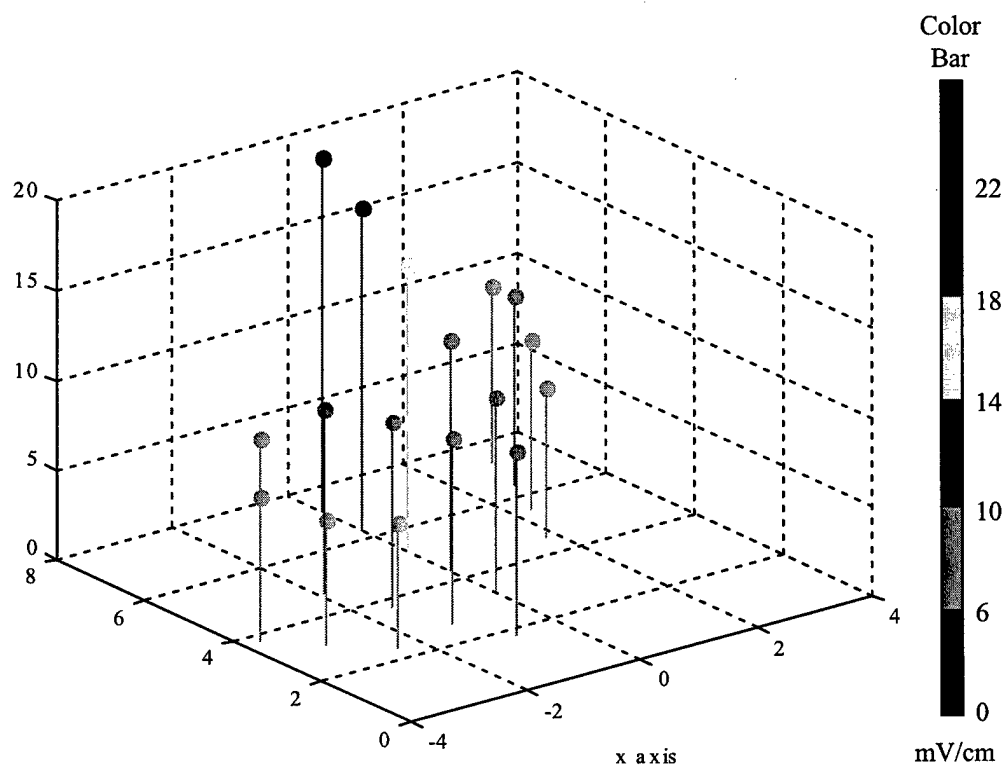
Figure 66 - Three-dimensional view of laboratory voltage gradient measurements of X-Y plane at  $z = 0$  cm.

**Laboratory Voltage Gradient Measurements of the X-Y Plane at  $Z = 2$  cm.**

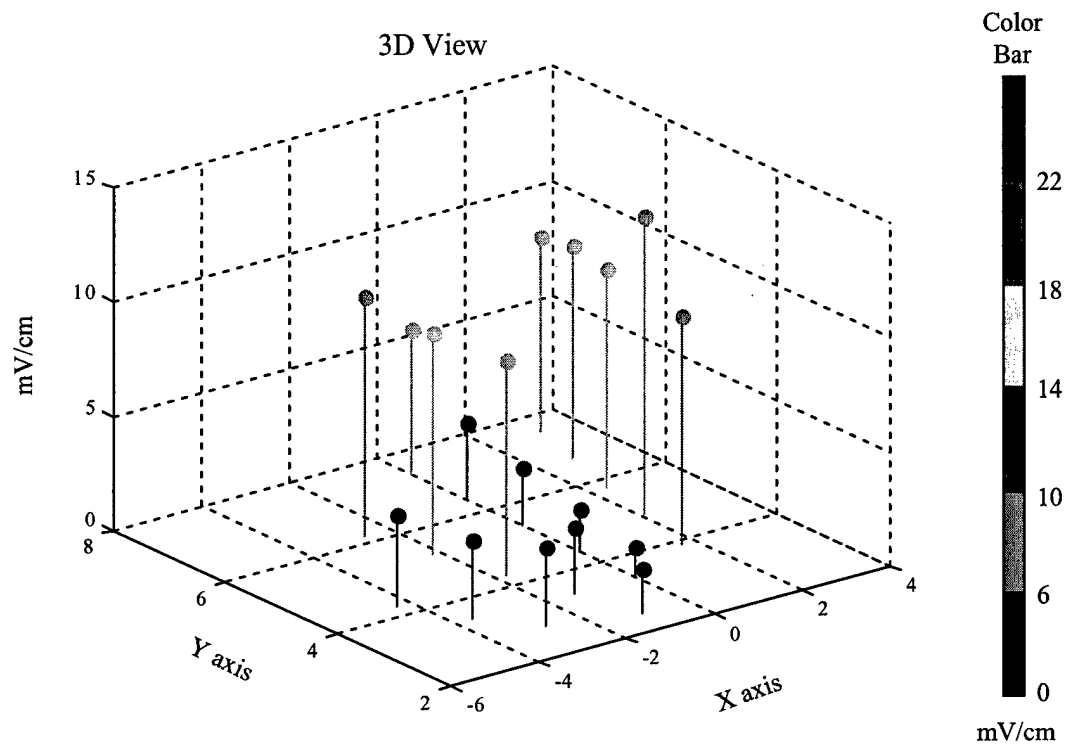
**Figure 67 - Three-dimensional view of laboratory voltage gradient measurements of X-Y plane at  $z = 2$  cm.**

**Laboratory Voltage Gradient Measurements of the X-Y Plane at  $Z = 4$  cm.**

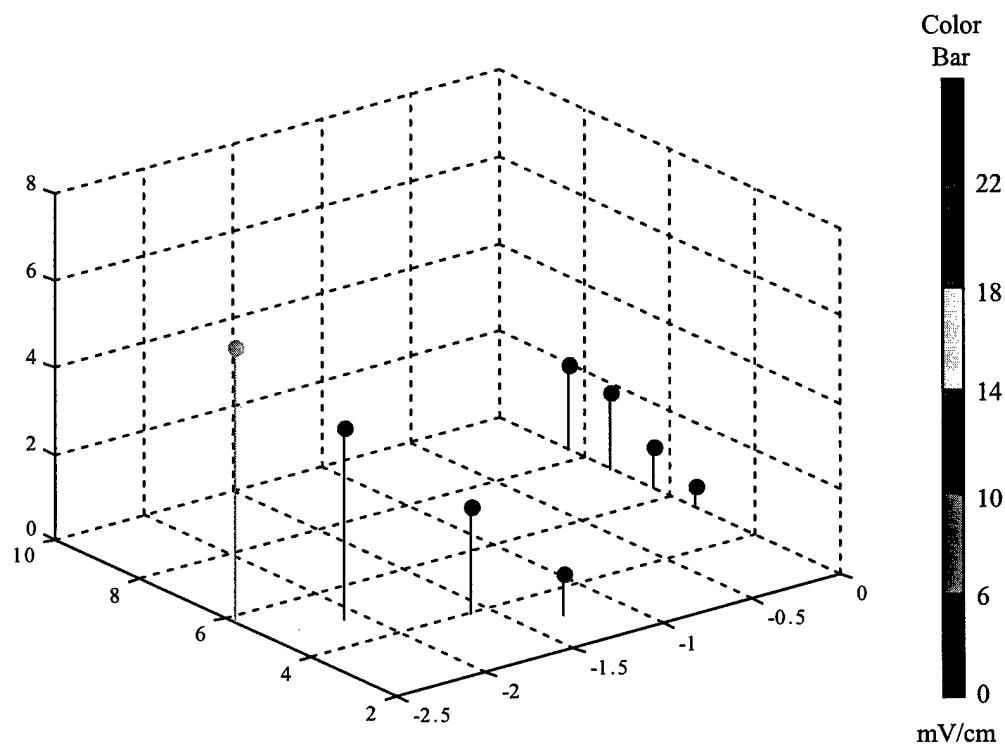
**Figure 68 - Three-dimensional view of laboratory voltage gradient measurements of X-Y plane at  $z = 4$  cm.**

**Laboratory Voltage Gradient Measurements of the X-Y Plane at  $Z = 6$  cm.**

**Figure 69 - Three-dimensional view of laboratory voltage gradient measurements of X-Y plane at  $z = 6$  cm.**

**Laboratory Voltage Gradient Measurements of the X-Y Plane at  $Z = 8$  cm.**

**Figure 70 - Three-dimensional view of laboratory voltage gradient measurements of X-Y plane at  $z = 8$  cm.**

**Laboratory Voltage Gradient Measurements of the X-Y Plane at  $Z = 12$  cm.**

**Figure 71 - Three-dimensional view of laboratory voltage gradient measurements of X-Y plane at  $z = 12$  cm.**

## APPENDIX D - LEG OF LAMB LABORATORY MEASUREMENTS

**Table 5 - Voltage Gradient Laboratory Measurements in Leg of Lamb**

Measure- ment #	Slice #	X	Y	Z	Element Tissue Type	Voltage recorded (Peak)	Voltage corrected for gain	I-DEAS Element Label
1	2	0.0	6.0	2.0	air	0.22	0.022	2169
2	2	0.0	5.0	2.0	muscle	0.2	0.02	2151
3	2	0.0	4.0	2.0	muscle	0.13	0.013	2133
4	2	0.0	3.0	2.0	muscle	0.11	0.011	2115
5	2	0.0	2.0	2.0	bone	0.11	0.011	2097
6	2	2.6	6.3	2.0	air	0.11	0.011	2171
7	2	2.3	5.5	2.0	muscle	0.104	0.0104	2153
8	2	1.8	4.5	2.0	muscle	0.0945	0.00945	2134
9	2	1.5	3.6	2.0	muscle	0.085	0.0085	2116
10	2	-1.9	4.6	2.0	muscle	0.12	0.012	2131
11	2	-1.5	3.6	2.0	muscle	0.1	0.01	2113
12	2	-3.2	3.3	2.0	fat	0.097	0.0097	2111
13	2	-2.5	2.5	2.0	fat	0.1	0.01	2094
14	4	0.0	6.0	4.0	air	0.182	0.0182	4169
15	4	0.0	5.0	4.0	muscle	0.18	0.018	4151
16	4	0.0	4.0	4.0	muscle	0.16	0.016	4133
17	4	0.0	3.0	4.0	muscle	0.15	0.015	4115
18	4	0.0	2.0	4.0	muscle	0.11	0.011	4097
19	4	2.5	6.0	4.0	air	0.101	0.0101	4171
20	4	2.1	5.1	4.0	fat	0.106	0.0106	4153
21	4	1.8	4.2	4.0	muscle	0.102	0.0102	4134
22	4	1.3	3.3	4.0	muscle	0.089	0.0089	4116
23	4	1.0	2.3	4.0	muscle	0.096	0.0096	4097
24	4	-2.1	5.0	4.0	muscle	0.108	0.0108	4130
25	4	-1.7	4.1	4.0	muscle	0.09	0.009	4131
26	4	-1.3	3.2	4.0	muscle	0.095	0.0095	4113
27	4	-3.7	3.6	4.0	fat	0.097	0.0097	4111
28	4	-2.9	2.9	4.0	fat	0.092	0.0092	4094
29	6	0.0	7.2	6.0	fat	0.198	0.0198	6187
30	6	0.0	6.3	6.0	muscle	0.18	0.018	6169
31	6	0.0	5.3	6.0	muscle	0.16	0.016	6151
32	6	0.0	4.3	6.0	muscle	0.13	0.013	6133
33	6	0.0	3.3	6.0	muscle	0.11	0.011	6115
34	6	3.0	7.3	6.0	air	0.0985	0.00985	6190
35	6	2.7	6.4	6.0	muscle	0.1065	0.01065	6171
36	6	2.3	5.5	6.0	muscle	0.0965	0.00965	6153
37	6	1.8	4.5	6.0	muscle	0.085	0.0085	6134
38	6	-2.3	5.6	6.0	fat	0.08	0.008	6148
39	6	-1.9	4.7	6.0	muscle	0.104	0.0104	6131
40	6	-1.5	3.7	6.0	muscle	0.104	0.0104	6113
41	6	-1.2	2.7	6.0	muscle	0.104	0.0104	6095

Measure- ment #	Slice #	X	Y	Z	Element Tissue Type	Voltage recorded (Peak)	Voltage corrected for gain	I-DEAS Element Label
42	6	-0.8	1.8	6.0	muscle	0.103	0.0103	6078
43	6	-3.7	3.8	6.0	muscle	0.08	0.008	6111
44	6	-3.1	3.1	6.0	muscle	0.07	0.007	6111
45	6	-2.4	2.4	6.0	muscle	0.07	0.007	6094
46	8	0.0	7.4	8.0	air	0.063	0.0063	8187
47	8	0.0	6.4	8.0	muscle	0.034	0.0034	8169
48	8	0.0	5.4	8.0	muscle	0.026	0.0026	8151
49	8	0.0	4.4	8.0	muscle	0.019	0.0019	8133
50	8	0.0	3.4	8.0	fat	0.014	0.0014	8115
51	8	3.2	7.6	8.0	fat	0.085	0.0085	8190
52	8	2.8	6.7	8.0	muscle	0.093	0.0093	8171
53	8	2.4	5.8	8.0	muscle	0.095	0.0095	8153
54	8	2.1	4.9	8.0	muscle	0.13	0.013	8134
55	8	1.7	3.9	8.0	fat	0.1	0.01	8116
56	8	-2.6	6.2	8.0	air	0.105	0.0105	8166
57	8	-2.2	5.3	8.0	muscle	0.097	0.0097	8148
58	8	-1.8	4.3	8.0	muscle	0.095	0.0095	8131
59	8	-1.4	3.4	8.0	muscle	0.03	0.003	8113
60	8	-1.0	2.5	8.0	muscle	0.02	0.002	8095
61	8	-4.3	4.3	8.0	muscle	0.04	0.004	8128
62	8	-3.6	3.5	8.0	muscle	0.035	0.0035	8111
63	8	-2.8	2.8	8.0	muscle	0.035	0.0035	8094
64	8	-2.2	2.2	8.0	muscle	hit bone	#VALUE!	8094
65	12	0.0	8.4	12.0	air	0.02	0.002	12205
66	12	0.0	7.4	12.0	muscle	0.018	0.0018	12187
67	12	0.0	6.4	12.0	muscle	0.01	0.001	12169
68	12	0.0	5.4	12.0	muscle	0.005	0.0005	12151
69	12	-2.8	6.8	12.0	muscle	noise	#VALUE!	12166
70	12	-2.5	5.8	12.0	muscle	0.064	0.0064	12148
71	12	-2.1	4.9	12.0	muscle	0.045	0.0045	12130
72	12	-1.6	4.0	12.0	muscle	0.025	0.0025	12131
73	12	-1.3	3.1	12.0	muscle	0.01	0.001	12113
74	0	0.0	4.2	0.0	fat	0.065	0.0065	133
75	0	0.0	3.2	0	muscle	0.037	0.0037	115
76	0	0.0	2.2	0	muscle	0.02	0.002	97



## APPENDIX E - FEM CONVERSION TABLES FOR LEG OF LAMB MODEL

**Table 6 - FEM Conversion Table for Leg of Lamb at Z = 1 cm**

Element Number	Tissue type	Location			Nodes on this slice				Nodes on slice above				Mesh Color
		X	Y	Z	LL	LR	UR	UL	LL	LR	UR	UL	
1001	air	-6	-3	1	1001	1002	1020	1019	2001	2002	2020	2019	3
1002	air	-5	-3	1	1002	1003	1021	1020	2002	2003	2021	2020	3
1003	air	-4	-3	1	1003	1004	1022	1021	2003	2004	2022	2021	3
1004	air	-3	-3	1	1004	1005	1023	1022	2004	2005	2023	2022	3
1005	air	-2	-3	1	1005	1006	1024	1023	2005	2006	2024	2023	3
1006	air	-1	-3	1	1006	1007	1025	1024	2006	2007	2025	2024	3
1007	air	0	-3	1	1007	1008	1026	1025	2007	2008	2026	2025	3
1008	air	1	-3	1	1008	1009	1027	1026	2008	2009	2027	2026	3
1009	air	2	-3	1	1009	1010	1028	1027	2009	2010	2028	2027	3
1010	air	3	-3	1	1010	1011	1029	1028	2010	2011	2029	2028	3
1011	air	4	-3	1	1011	1012	1030	1029	2011	2012	2030	2029	3
1012	air	5	-3	1	1012	1013	1031	1030	2012	2013	2031	2030	3
1013	air	6	-3	1	1013	1014	1032	1031	2013	2014	2032	2031	3
1014	air	7	-3	1	1014	1015	1033	1032	2014	2015	2033	2032	3
1015	air	8	-3	1	1015	1016	1034	1033	2015	2016	2034	2033	3
1016	air	9	-3	1	1016	1017	1035	1034	2016	2017	2035	2034	3
1017	air	10	-3	1	1017	1018	1036	1035	2017	2018	2036	2035	3
1019	air	-6	-2	1	1019	1020	1038	1037	2019	2020	2038	2037	3
1020	air	-5	-2	1	1020	1021	1039	1038	2020	2021	2039	2038	3
1021	fat	-4	-2	1	1021	1022	1040	1039	2021	2022	2040	2039	8
1022	fat	-3	-2	1	1022	1023	1041	1040	2022	2023	2041	2040	8
1023	bone	-2	-2	1	1023	1024	1042	1041	2023	2024	2042	2041	15
1024	bone	-1	-2	1	1024	1025	1043	1042	2024	2025	2043	2042	15
1025	bone	0	-2	1	1025	1026	1044	1043	2025	2026	2044	2043	15
1026	bone	1	-2	1	1026	1027	1045	1044	2026	2027	2045	2044	15
1027	air	2	-2	1	1027	1028	1046	1045	2027	2028	2046	2045	3
1028	air	3	-2	1	1028	1029	1047	1046	2028	2029	2047	2046	3
1029	air	4	-2	1	1029	1030	1048	1047	2029	2030	2048	2047	3
1030	air	5	-2	1	1030	1031	1049	1048	2030	2031	2049	2048	3
1031	air	6	-2	1	1031	1032	1050	1049	2031	2032	2050	2049	3
1032	air	7	-2	1	1032	1033	1051	1050	2032	2033	2051	2050	3
1033	air	8	-2	1	1033	1034	1052	1051	2033	2034	2052	2051	3
1034	air	9	-2	1	1034	1035	1053	1052	2034	2035	2053	2052	3

Element Number	Tissue type	Location			Nodes on this slice				Nodes on slice above				Mesh Color
		X	Y	Z	LL	LR	UR	UL	LL	LR	UR	UL	
1035	air	10	-2	1	1035	1036	1054	1053	2035	2036	2054	2053	3
1037	air	-6	-1	1	1037	1038	1056	1055	2037	2038	2056	2055	3
1038	air	-5	-1	1	1038	1039	1057	1056	2038	2039	2057	2056	3
1039	fat	-4	-1	1	1039	1040	1058	1057	2039	2040	2058	2057	8
1040	bone	-3	-1	1	1040	1041	1059	1058	2040	2041	2059	2058	15
1041	bone	-2	-1	1	1041	1042	1060	1059	2041	2042	2060	2059	15
1042	bone	-1	-1	1	1042	1043	1061	1060	2042	2043	2061	2060	15
1043	bone	0	-1	1	1043	1044	1062	1061	2043	2044	2062	2061	15
1044	bone	1	-1	1	1044	1045	1063	1062	2044	2045	2063	2062	15
1045	muscle	2	-1	1	1045	1046	1064	1063	2045	2046	2064	2063	11
1046	muscle	3	-1	1	1046	1047	1065	1064	2046	2047	2065	2064	11
1047	air	4	-1	1	1047	1048	1066	1065	2047	2048	2066	2065	3
1048	air	5	-1	1	1048	1049	1067	1066	2048	2049	2067	2066	3
1049	air	6	-1	1	1049	1050	1068	1067	2049	2050	2068	2067	3
1050	air	7	-1	1	1050	1051	1069	1068	2050	2051	2069	2068	3
1051	air	8	-1	1	1051	1052	1070	1069	2051	2052	2070	2069	3
1052	air	9	-1	1	1052	1053	1071	1070	2052	2053	2071	2070	3
1053	air	10	-1	1	1053	1054	1072	1071	2053	2054	2072	2071	3
1055	air	-6	0	1	1055	1056	1074	1073	2055	2056	2074	2073	3
1056	air	-5	0	1	1056	1057	1075	1074	2056	2057	2075	2074	3
1057	air	-4	0	1	1057	1058	1076	1075	2057	2058	2076	2075	3
1058	bone	-3	0	1	1058	1059	1077	1076	2058	2059	2077	2076	15
1059	bone	-2	0	1	1059	1060	1078	1077	2059	2060	2078	2077	15
1060	bone	-1	0	1	1060	1061	1079	1078	2060	2061	2079	2078	15
1061	bone	0	0	1	1061	1062	1080	1079	2061	2062	2080	2079	15
1062	muscle	1	0	1	1062	1063	1081	1080	2062	2063	2081	2080	11
1063	muscle	2	0	1	1063	1064	1082	1081	2063	2064	2082	2081	11
1064	muscle	3	0	1	1064	1065	1083	1082	2064	2065	2083	2082	11
1065	muscle	4	0	1	1065	1066	1084	1083	2065	2066	2084	2083	11
1066	air	5	0	1	1066	1067	1085	1084	2066	2067	2085	2084	3
1067	air	6	0	1	1067	1068	1086	1085	2067	2068	2086	2085	3
1068	air	7	0	1	1068	1069	1087	1086	2068	2069	2087	2086	3
1069	air	8	0	1	1069	1070	1088	1087	2069	2070	2088	2087	3
1070	air	9	0	1	1070	1071	1089	1088	2070	2071	2089	2088	3
1071	air	10	0	1	1071	1072	1090	1089	2071	2072	2090	2089	3
1073	air	-6	1	1	1073	1074	1092	1091	2073	2074	2092	2091	3
1074	air	-5	1	1	1074	1075	1093	1092	2074	2075	2093	2092	3
1075	air	-4	1	1	1075	1076	1094	1093	2075	2076	2094	2093	3

Element Number	Tissue type	Location			Nodes on this slice				Nodes on slice above				Mesh Color
		X	Y	Z	LL	LR	UR	UL	LL	LR	UR	UL	
1076	muscle	-3	1	1	1076	1077	1095	1094	2076	2077	2095	2094	11
1077	bone	-2	1	1	1077	1078	1096	1095	2077	2078	2096	2095	15
1078	bone	-1	1	1	1078	1079	1097	1096	2078	2079	2097	2096	15
1079	bone	0	1	1	1079	1080	1098	1097	2079	2080	2098	2097	15
1080	muscle	1	1	1	1080	1081	1099	1098	2080	2081	2099	2098	11
1081	muscle	2	1	1	1081	1082	1100	1099	2081	2082	2100	2099	11
1082	muscle	3	1	1	1082	1083	1101	1100	2082	2083	2101	2100	11
1083	muscle	4	1	1	1083	1084	1102	1101	2083	2084	2102	2101	11
1084	muscle	5	1	1	1084	1085	1103	1102	2084	2085	2103	2102	11
1085	air	6	1	1	1085	1086	1104	1103	2085	2086	2104	2103	3
1086	air	7	1	1	1086	1087	1105	1104	2086	2087	2105	2104	3
1087	air	8	1	1	1087	1088	1106	1105	2087	2088	2106	2105	3
1088	air	9	1	1	1088	1089	1107	1106	2088	2089	2107	2106	3
1089	air	10	1	1	1089	1090	1108	1107	2089	2090	2108	2107	3
1091	air	-6	2	1	1091	1092	1110	1109	2091	2092	2110	2109	3
1092	air	-5	2	1	1092	1093	1111	1110	2092	2093	2111	2110	3
1093	air	-4	2	1	1093	1094	1112	1111	2093	2094	2112	2111	3
1094	muscle	-3	2	1	1094	1095	1113	1112	2094	2095	2113	2112	11
1095	bone	-2	2	1	1095	1096	1114	1113	2095	2096	2114	2113	15
1096	bone	-1	2	1	1096	1097	1115	1114	2096	2097	2115	2114	15
1097	muscle	0	2	1	1097	1098	1116	1115	2097	2098	2116	2115	11
1098	muscle	1	2	1	1098	1099	1117	1116	2098	2099	2117	2116	11
1099	muscle	2	2	1	1099	1100	1118	1117	2099	2100	2118	2117	11
1100	muscle	3	2	1	1100	1101	1119	1118	2100	2101	2119	2118	11
1101	muscle	4	2	1	1101	1102	1120	1119	2101	2102	2120	2119	11
1102	muscle	5	2	1	1102	1103	1121	1120	2102	2103	2121	2120	11
1103	air	6	2	1	1103	1104	1122	1121	2103	2104	2122	2121	3
1104	air	7	2	1	1104	1105	1123	1122	2104	2105	2123	2122	3
1105	air	8	2	1	1105	1106	1124	1123	2105	2106	2124	2123	3
1106	air	9	2	1	1106	1107	1125	1124	2106	2107	2125	2124	3
1107	air	10	2	1	1107	1108	1126	1125	2107	2108	2126	2125	3
1109	air	-6	3	1	1109	1110	1128	1127	2109	2110	2128	2127	3
1110	air	-5	3	1	1110	1111	1129	1128	2110	2111	2129	2128	3
1111	air	-4	3	1	1111	1112	1130	1129	2111	2112	2130	2129	3
1112	air	-3	3	1	1112	1113	1131	1130	2112	2113	2131	2130	3
1113	muscle	-2	3	1	1113	1114	1132	1131	2113	2114	2132	2131	11
1114	bone	-1	3	1	1114	1115	1133	1132	2114	2115	2133	2132	15
1115	muscle	0	3	1	1115	1116	1134	1133	2115	2116	2134	2133	11

Element Number	Tissue type	Location			Nodes on this slice				Nodes on slice above				Mesh Color
		X	Y	Z	LL	LR	UR	UL	LL	LR	UR	UL	
1116	muscle	1	3	1	1116	1117	1135	1134	2116	2117	2135	2134	11
1117	muscle	2	3	1	1117	1118	1136	1135	2117	2118	2136	2135	11
1118	fat	3	3	1	1118	1119	1137	1136	2118	2119	2137	2136	8
1119	fat	4	3	1	1119	1120	1138	1137	2119	2120	2138	2137	8
1120	fat	5	3	1	1120	1121	1139	1138	2120	2121	2139	2138	8
1121	air	6	3	1	1121	1122	1140	1139	2121	2122	2140	2139	3
1122	air	7	3	1	1122	1123	1141	1140	2122	2123	2141	2140	3
1123	air	8	3	1	1123	1124	1142	1141	2123	2124	2142	2141	3
1124	air	9	3	1	1124	1125	1143	1142	2124	2125	2143	2142	3
1125	air	10	3	1	1125	1126	1144	1143	2125	2126	2144	2143	3
1127	air	-6	4	1	1127	1128	1146	1145	2127	2128	2146	2145	3
1128	air	-5	4	1	1128	1129	1147	1146	2128	2129	2147	2146	3
1129	air	-4	4	1	1129	1130	1148	1147	2129	2130	2148	2147	3
1130	air	-3	4	1	1130	1131	1149	1148	2130	2131	2149	2148	3
1131	muscle	-2	4	1	1131	1132	1150	1149	2131	2132	2150	2149	11
1132	muscle	-1	4	1	1132	1133	1151	1150	2132	2133	2151	2150	11
1133	muscle	0	4	1	1133	1134	1152	1151	2133	2134	2152	2151	11
1134	muscle	1	4	1	1134	1135	1153	1152	2134	2135	2153	2152	11
1135	muscle	2	4	1	1135	1136	1154	1153	2135	2136	2154	2153	11
1136	fat	3	4	1	1136	1137	1155	1154	2136	2137	2155	2154	8
1137	fat	4	4	1	1137	1138	1156	1155	2137	2138	2156	2155	8
1138	fat	5	4	1	1138	1139	1157	1156	2138	2139	2157	2156	8
1139	air	6	4	1	1139	1140	1158	1157	2139	2140	2158	2157	3
1140	air	7	4	1	1140	1141	1159	1158	2140	2141	2159	2158	3
1141	air	8	4	1	1141	1142	1160	1159	2141	2142	2160	2159	3
1142	air	9	4	1	1142	1143	1161	1160	2142	2143	2161	2160	3
1143	air	10	4	1	1143	1144	1162	1161	2143	2144	2162	2161	3
1145	air	-6	5	1	1145	1146	1164	1163	2145	2146	2164	2163	3
1146	air	-5	5	1	1146	1147	1165	1164	2146	2147	2165	2164	3
1147	air	-4	5	1	1147	1148	1166	1165	2147	2148	2166	2165	3
1148	air	-3	5	1	1148	1149	1167	1166	2148	2149	2167	2166	3
1149	air	-2	5	1	1149	1150	1168	1167	2149	2150	2168	2167	3
1150	air	-1	5	1	1150	1151	1169	1168	2150	2151	2169	2168	3
1151	air	0	5	1	1151	1152	1170	1169	2151	2152	2170	2169	3
1152	muscle	1	5	1	1152	1153	1171	1170	2152	2153	2171	2170	11
1153	muscle	2	5	1	1153	1154	1172	1171	2153	2154	2172	2171	11
1154	air	3	5	1	1154	1155	1173	1172	2154	2155	2173	2172	3
1155	air	4	5	1	1155	1156	1174	1173	2155	2156	2174	2173	3

Element Number	Tissue type	Location			Nodes on this slice				Nodes on slice above				Mesh Color
		X	Y	Z	LL	LR	UR	UL	LL	LR	UR	UL	
1156	air	5	5	1	1156	1157	1175	1174	2156	2157	2175	2174	3
1157	air	6	5	1	1157	1158	1176	1175	2157	2158	2176	2175	3
1158	air	7	5	1	1158	1159	1177	1176	2158	2159	2177	2176	3
1159	air	8	5	1	1159	1160	1178	1177	2159	2160	2178	2177	3
1160	air	9	5	1	1160	1161	1179	1178	2160	2161	2179	2178	3
1161	air	10	5	1	1161	1162	1180	1179	2161	2162	2180	2179	3
1163	air	-6	6	1	1163	1164	1182	1181	2163	2164	2182	2181	3
1164	air	-5	6	1	1164	1165	1183	1182	2164	2165	2183	2182	3
1165	air	-4	6	1	1165	1166	1184	1183	2165	2166	2184	2183	3
1166	air	-3	6	1	1166	1167	1185	1184	2166	2167	2185	2184	3
1167	air	-2	6	1	1167	1168	1186	1185	2167	2168	2186	2185	3
1168	air	-1	6	1	1168	1169	1187	1186	2168	2169	2187	2186	3
1169	air	0	6	1	1169	1170	1188	1187	2169	2170	2188	2187	3
1170	air	1	6	1	1170	1171	1189	1188	2170	2171	2189	2188	3
1171	air	2	6	1	1171	1172	1190	1189	2171	2172	2190	2189	3
1172	air	3	6	1	1172	1173	1191	1190	2172	2173	2191	2190	3
1173	air	4	6	1	1173	1174	1192	1191	2173	2174	2192	2191	3
1174	air	5	6	1	1174	1175	1193	1192	2174	2175	2193	2192	3
1175	air	6	6	1	1175	1176	1194	1193	2175	2176	2194	2193	3
1176	air	7	6	1	1176	1177	1195	1194	2176	2177	2195	2194	3
1177	air	8	6	1	1177	1178	1196	1195	2177	2178	2196	2195	3
1178	air	9	6	1	1178	1179	1197	1196	2178	2179	2197	2196	3
1179	air	10	6	1	1179	1180	1198	1197	2179	2180	2198	2197	3
1181	air	-6	7	1	1181	1182	1200	1199	2181	2182	2200	2199	3
1182	air	-5	7	1	1182	1183	1201	1200	2182	2183	2201	2200	3
1183	air	-4	7	1	1183	1184	1202	1201	2183	2184	2202	2201	3
1184	air	-3	7	1	1184	1185	1203	1202	2184	2185	2203	2202	3
1185	air	-2	7	1	1185	1186	1204	1203	2185	2186	2204	2203	3
1186	air	-1	7	1	1186	1187	1205	1204	2186	2187	2205	2204	3
1187	air	0	7	1	1187	1188	1206	1205	2187	2188	2206	2205	3
1188	air	1	7	1	1188	1189	1207	1206	2188	2189	2207	2206	3
1189	air	2	7	1	1189	1190	1208	1207	2189	2190	2208	2207	3
1190	air	3	7	1	1190	1191	1209	1208	2190	2191	2209	2208	3
1191	air	4	7	1	1191	1192	1210	1209	2191	2192	2210	2209	3
1192	air	5	7	1	1192	1193	1211	1210	2192	2193	2211	2210	3
1193	air	6	7	1	1193	1194	1212	1211	2193	2194	2212	2211	3
1194	air	7	7	1	1194	1195	1213	1212	2194	2195	2213	2212	3
1195	air	8	7	1	1195	1196	1214	1213	2195	2196	2214	2213	3

Element Number	Tissue type	Location			Nodes on this slice				Nodes on slice above				Mesh Color
		X	Y	Z	LL	LR	UR	UL	LL	LR	UR	UL	
1196	air	9	7	1	1196	1197	1215	1214	2196	2197	2215	2214	3
1197	air	10	7	1	1197	1198	1216	1215	2197	2198	2216	2215	3
1199	air	-6	8	1	1199	1200	1218	1217	2199	2200	2218	2217	3
1200	air	-5	8	1	1200	1201	1219	1218	2200	2201	2219	2218	3
1201	air	-4	8	1	1201	1202	1220	1219	2201	2202	2220	2219	3
1202	air	-3	8	1	1202	1203	1221	1220	2202	2203	2221	2220	3
1203	air	-2	8	1	1203	1204	1222	1221	2203	2204	2222	2221	3
1204	air	-1	8	1	1204	1205	1223	1222	2204	2205	2223	2222	3
1205	air	0	8	1	1205	1206	1224	1223	2205	2206	2224	2223	3
1206	air	1	8	1	1206	1207	1225	1224	2206	2207	2225	2224	3
1207	air	2	8	1	1207	1208	1226	1225	2207	2208	2226	2225	3
1208	air	3	8	1	1208	1209	1227	1226	2208	2209	2227	2226	3
1209	air	4	8	1	1209	1210	1228	1227	2209	2210	2228	2227	3
1210	air	5	8	1	1210	1211	1229	1228	2210	2211	2229	2228	3
1211	air	6	8	1	1211	1212	1230	1229	2211	2212	2230	2229	3
1212	air	7	8	1	1212	1213	1231	1230	2212	2213	2231	2230	3
1213	air	8	8	1	1213	1214	1232	1231	2213	2214	2232	2231	3
1214	air	9	8	1	1214	1215	1233	1232	2214	2215	2233	2232	3
1215	air	10	8	1	1215	1216	1234	1233	2215	2216	2234	2233	3
1217	air	-6	9	1	1217	1218	1236	1235	2217	2218	2236	2235	3
1218	air	-5	9	1	1218	1219	1237	1236	2218	2219	2237	2236	3
1219	air	-4	9	1	1219	1220	1238	1237	2219	2220	2238	2237	3
1220	air	-3	9	1	1220	1221	1239	1238	2220	2221	2239	2238	3
1221	air	-2	9	1	1221	1222	1240	1239	2221	2222	2240	2239	3
1222	air	-1	9	1	1222	1223	1241	1240	2222	2223	2241	2240	3
1223	air	0	9	1	1223	1224	1242	1241	2223	2224	2242	2241	3
1224	air	1	9	1	1224	1225	1243	1242	2224	2225	2243	2242	3
1225	air	2	9	1	1225	1226	1244	1243	2225	2226	2244	2243	3
1226	air	3	9	1	1226	1227	1245	1244	2226	2227	2245	2244	3
1227	air	4	9	1	1227	1228	1246	1245	2227	2228	2246	2245	3
1228	air	5	9	1	1228	1229	1247	1246	2228	2229	2247	2246	3
1229	air	6	9	1	1229	1230	1248	1247	2229	2230	2248	2247	3
1230	air	7	9	1	1230	1231	1249	1248	2230	2231	2249	2248	3
1231	air	8	9	1	1231	1232	1250	1249	2231	2232	2250	2249	3
1232	air	9	9	1	1232	1233	1251	1250	2232	2233	2251	2250	3
1233	air	10	9	1	1233	1234	1252	1251	2233	2234	2252	2251	3

**Table 7 - FEM Conversion Table for Leg of Lamb at Z = 2 cm**

Element Number	Tissue type	Location			Nodes on this slice				Nodes on slice above				Mesh Color
		X	Y	Z	LL	LR	UR	UL	LL	LR	UR	UL	
2001	air	-6	-3	2	2001	2002	2020	2019	3001	3002	3020	3019	3
2002	air	-5	-3	2	2002	2003	2021	2020	3002	3003	3021	3020	3
2003	air	-4	-3	2	2003	2004	2022	2021	3003	3004	3022	3021	3
2004	air	-3	-3	2	2004	2005	2023	2022	3004	3005	3023	3022	3
2005	air	-2	-3	2	2005	2006	2024	2023	3005	3006	3024	3023	3
2006	air	-1	-3	2	2006	2007	2025	2024	3006	3007	3025	3024	3
2007	air	0	-3	2	2007	2008	2026	2025	3007	3008	3026	3025	3
2008	air	1	-3	2	2008	2009	2027	2026	3008	3009	3027	3026	3
2009	air	2	-3	2	2009	2010	2028	2027	3009	3010	3028	3027	3
2010	air	3	-3	2	2010	2011	2029	2028	3010	3011	3029	3028	3
2011	air	4	-3	2	2011	2012	2030	2029	3011	3012	3030	3029	3
2012	air	5	-3	2	2012	2013	2031	2030	3012	3013	3031	3030	3
2013	air	6	-3	2	2013	2014	2032	2031	3013	3014	3032	3031	3
2014	air	7	-3	2	2014	2015	2033	2032	3014	3015	3033	3032	3
2015	air	8	-3	2	2015	2016	2034	2033	3015	3016	3034	3033	3
2016	air	9	-3	2	2016	2017	2035	2034	3016	3017	3035	3034	3
2017	air	10	-3	2	2017	2018	2036	2035	3017	3018	3036	3035	3
2019	air	-6	-2	2	2019	2020	2038	2037	3019	3020	3038	3037	3
2020	air	-5	-2	2	2020	2021	2039	2038	3020	3021	3039	3038	3
2021	air	-4	-2	2	2021	2022	2040	2039	3021	3022	3040	3039	3
2022	air	-3	-2	2	2022	2023	2041	2040	3022	3023	3041	3040	3
2023	bone	-2	-2	2	2023	2024	2042	2041	3023	3024	3042	3041	15
2024	bone	-1	-2	2	2024	2025	2043	2042	3024	3025	3043	3042	15
2025	bone	0	-2	2	2025	2026	2044	2043	3025	3026	3044	3043	15
2026	air	1	-2	2	2026	2027	2045	2044	3026	3027	3045	3044	3
2027	air	2	-2	2	2027	2028	2046	2045	3027	3028	3046	3045	3
2028	air	3	-2	2	2028	2029	2047	2046	3028	3029	3047	3046	3
2029	air	4	-2	2	2029	2030	2048	2047	3029	3030	3048	3047	3
2030	air	5	-2	2	2030	2031	2049	2048	3030	3031	3049	3048	3
2031	air	6	-2	2	2031	2032	2050	2049	3031	3032	3050	3049	3
2032	air	7	-2	2	2032	2033	2051	2050	3032	3033	3051	3050	3
2033	air	8	-2	2	2033	2034	2052	2051	3033	3034	3052	3051	3
2034	air	9	-2	2	2034	2035	2053	2052	3034	3035	3053	3052	3
2035	air	10	-2	2	2035	2036	2054	2053	3035	3036	3054	3053	3
2037	air	-6	-1	2	2037	2038	2056	2055	3037	3038	3056	3055	3
2038	air	-5	-1	2	2038	2039	2057	2056	3038	3039	3057	3056	3
2039	bone	-4	-1	2	2039	2040	2058	2057	3039	3040	3058	3057	15

Element Number	Tissue type	Location X Y Z	Nodes on this slice				Nodes on slice above				Mesh Color
			LL	LR	UR	UL	LL	LR	UR	UL	
2040	bone	-3 -1 2	2040	2041	2059	2058	3040	3041	3059	3058	15
2041	bone	-2 -1 2	2041	2042	2060	2059	3041	3042	3060	3059	15
2042	bone	-1 -1 2	2042	2043	2061	2060	3042	3043	3061	3060	15
2043	bone	0 -1 2	2043	2044	2062	2061	3043	3044	3062	3061	15
2044	fat	1 -1 2	2044	2045	2063	2062	3044	3045	3063	3062	8
2045	muscle	2 -1 2	2045	2046	2064	2063	3045	3046	3064	3063	11
2046	muscle	3 -1 2	2046	2047	2065	2064	3046	3047	3065	3064	11
2047	air	4 -1 2	2047	2048	2066	2065	3047	3048	3066	3065	3
2048	air	5 -1 2	2048	2049	2067	2066	3048	3049	3067	3066	3
2049	air	6 -1 2	2049	2050	2068	2067	3049	3050	3068	3067	3
2050	air	7 -1 2	2050	2051	2069	2068	3050	3051	3069	3068	3
2051	air	8 -1 2	2051	2052	2070	2069	3051	3052	3070	3069	3
2052	air	9 -1 2	2052	2053	2071	2070	3052	3053	3071	3070	3
2053	air	10 -1 2	2053	2054	2072	2071	3053	3054	3072	3071	3
2055	air	-6 0 2	2055	2056	2074	2073	3055	3056	3074	3073	3
2056	air	-5 0 2	2056	2057	2075	2074	3056	3057	3075	3074	3
2057	bone	-4 0 2	2057	2058	2076	2075	3057	3058	3076	3075	15
2058	bone	-3 0 2	2058	2059	2077	2076	3058	3059	3077	3076	15
2059	bone	-2 0 2	2059	2060	2078	2077	3059	3060	3078	3077	15
2060	bone	-1 0 2	2060	2061	2079	2078	3060	3061	3079	3078	15
2061	bone	0 0 2	2061	2062	2080	2079	3061	3062	3080	3079	15
2062	fat	1 0 2	2062	2063	2081	2080	3062	3063	3081	3080	8
2063	muscle	2 0 2	2063	2064	2082	2081	3063	3064	3082	3081	11
2064	muscle	3 0 2	2064	2065	2083	2082	3064	3065	3083	3082	11
2065	muscle	4 0 2	2065	2066	2084	2083	3065	3066	3084	3083	11
2066	air	5 0 2	2066	2067	2085	2084	3066	3067	3085	3084	3
2067	air	6 0 2	2067	2068	2086	2085	3067	3068	3086	3085	3
2068	air	7 0 2	2068	2069	2087	2086	3068	3069	3087	3086	3
2069	air	8 0 2	2069	2070	2088	2087	3069	3070	3088	3087	3
2070	air	9 0 2	2070	2071	2089	2088	3070	3071	3089	3088	3
2071	air	10 0 2	2071	2072	2090	2089	3071	3072	3090	3089	3
2073	air	-6 1 2	2073	2074	2092	2091	3073	3074	3092	3091	3
2074	air	-5 1 2	2074	2075	2093	2092	3074	3075	3093	3092	3
2075	bone	-4 1 2	2075	2076	2094	2093	3075	3076	3094	3093	15
2076	bone	-3 1 2	2076	2077	2095	2094	3076	3077	3095	3094	15
2077	bone	-2 1 2	2077	2078	2096	2095	3077	3078	3096	3095	15
2078	bone	-1 1 2	2078	2079	2097	2096	3078	3079	3097	3096	15
2079	bone	0 1 2	2079	2080	2098	2097	3079	3080	3098	3097	15



Element Number	Tissue type	Location			Nodes on this slice				Nodes on slice above				Mesh Color
		X	Y	Z	LL	LR	UR	UL	LL	LR	UR	UL	
2080	muscle	1	1	2	2080	2081	2099	2098	3080	3081	3099	3098	11
2081	muscle	2	1	2	2081	2082	2100	2099	3081	3082	3100	3099	11
2082	muscle	3	1	2	2082	2083	2101	2100	3082	3083	3101	3100	11
2083	muscle	4	1	2	2083	2084	2102	2101	3083	3084	3102	3101	11
2084	muscle	5	1	2	2084	2085	2103	2102	3084	3085	3103	3102	11
2085	air	6	1	2	2085	2086	2104	2103	3085	3086	3104	3103	3
2086	air	7	1	2	2086	2087	2105	2104	3086	3087	3105	3104	3
2087	air	8	1	2	2087	2088	2106	2105	3087	3088	3106	3105	3
2088	air	9	1	2	2088	2089	2107	2106	3088	3089	3107	3106	3
2089	air	10	1	2	2089	2090	2108	2107	3089	3090	3108	3107	3
2091	air	-6	2	2	2091	2092	2110	2109	3091	3092	3110	3109	3
2092	air	-5	2	2	2092	2093	2111	2110	3092	3093	3111	3110	3
2093	air	-4	2	2	2093	2094	2112	2111	3093	3094	3112	3111	3
2094	fat	-3	2	2	2094	2095	2113	2112	3094	3095	3113	3112	8
2095	bone	-2	2	2	2095	2096	2114	2113	3095	3096	3114	3113	15
2096	bone	-1	2	2	2096	2097	2115	2114	3096	3097	3115	3114	15
2097	bone	0	2	2	2097	2098	2116	2115	3097	3098	3116	3115	15
2098	muscle	1	2	2	2098	2099	2117	2116	3098	3099	3117	3116	11
2099	muscle	2	2	2	2099	2100	2118	2117	3099	3100	3118	3117	11
2100	muscle	3	2	2	2100	2101	2119	2118	3100	3101	3119	3118	11
2101	muscle	4	2	2	2101	2102	2120	2119	3101	3102	3120	3119	11
2102	muscle	5	2	2	2102	2103	2121	2120	3102	3103	3121	3120	11
2103	fat	6	2	2	2103	2104	2122	2121	3103	3104	3122	3121	8
2104	air	7	2	2	2104	2105	2123	2122	3104	3105	3123	3122	3
2105	air	8	2	2	2105	2106	2124	2123	3105	3106	3124	3123	3
2106	air	9	2	2	2106	2107	2125	2124	3106	3107	3125	3124	3
2107	air	10	2	2	2107	2108	2126	2125	3107	3108	3126	3125	3
2109	air	-6	3	2	2109	2110	2128	2127	3109	3110	3128	3127	3
2110	air	-5	3	2	2110	2111	2129	2128	3110	3111	3129	3128	3
2111	air	-4	3	2	2111	2112	2130	2129	3111	3112	3130	3129	3
2112	fat	-3	3	2	2112	2113	2131	2130	3112	3113	3131	3130	8
2113	fat	-2	3	2	2113	2114	2132	2131	3113	3114	3132	3131	8
2114	muscle	-1	3	2	2114	2115	2133	2132	3114	3115	3133	3132	11
2115	muscle	0	3	2	2115	2116	2134	2133	3115	3116	3134	3133	11
2116	muscle	1	3	2	2116	2117	2135	2134	3116	3117	3135	3134	11
2117	muscle	2	3	2	2117	2118	2136	2135	3117	3118	3136	3135	11
2118	fat	3	3	2	2118	2119	2137	2136	3118	3119	3137	3136	8
2119	muscle	4	3	2	2119	2120	2138	2137	3119	3120	3138	3137	11

Element Number	Tissue type	Location			Nodes on this slice				Nodes on slice above				Mesh Color
		X	Y	Z	LL	LR	UR	UL	LL	LR	UR	UL	
2120	muscle	5	3	2	2120	2121	2139	2138	3120	3121	3139	3138	11
2121	fat	6	3	2	2121	2122	2140	2139	3121	3122	3140	3139	8
2122	air	7	3	2	2122	2123	2141	2140	3122	3123	3141	3140	3
2123	air	8	3	2	2123	2124	2142	2141	3123	3124	3142	3141	3
2124	air	9	3	2	2124	2125	2143	2142	3124	3125	3143	3142	3
2125	air	10	3	2	2125	2126	2144	2143	3125	3126	3144	3143	3
2127	air	-6	4	2	2127	2128	2146	2145	3127	3128	3146	3145	3
2128	air	-5	4	2	2128	2129	2147	2146	3128	3129	3147	3146	3
2129	air	-4	4	2	2129	2130	2148	2147	3129	3130	3148	3147	3
2130	air	-3	4	2	2130	2131	2149	2148	3130	3131	3149	3148	3
2131	muscle	-2	4	2	2131	2132	2150	2149	3131	3132	3150	3149	11
2132	muscle	-1	4	2	2132	2133	2151	2150	3132	3133	3151	3150	11
2133	muscle	0	4	2	2133	2134	2152	2151	3133	3134	3152	3151	11
2134	muscle	1	4	2	2134	2135	2153	2152	3134	3135	3153	3152	11
2135	muscle	2	4	2	2135	2136	2154	2153	3135	3136	3154	3153	11
2136	fat	3	4	2	2136	2137	2155	2154	3136	3137	3155	3154	8
2137	fat	4	4	2	2137	2138	2156	2155	3137	3138	3156	3155	8
2138	fat	5	4	2	2138	2139	2157	2156	3138	3139	3157	3156	8
2139	fat	6	4	2	2139	2140	2158	2157	3139	3140	3158	3157	8
2140	air	7	4	2	2140	2141	2159	2158	3140	3141	3159	3158	3
2141	air	8	4	2	2141	2142	2160	2159	3141	3142	3160	3159	3
2142	air	9	4	2	2142	2143	2161	2160	3142	3143	3161	3160	3
2143	air	10	4	2	2143	2144	2162	2161	3143	3144	3162	3161	3
2145	air	-6	5	2	2145	2146	2164	2163	3145	3146	3164	3163	3
2146	air	-5	5	2	2146	2147	2165	2164	3146	3147	3165	3164	3
2147	air	-4	5	2	2147	2148	2166	2165	3147	3148	3166	3165	3
2148	air	-3	5	2	2148	2149	2167	2166	3148	3149	3167	3166	3
2149	air	-2	5	2	2149	2150	2168	2167	3149	3150	3168	3167	3
2150	muscle	-1	5	2	2150	2151	2169	2168	3150	3151	3169	3168	11
2151	muscle	0	5	2	2151	2152	2170	2169	3151	3152	3170	3169	11
2152	muscle	1	5	2	2152	2153	2171	2170	3152	3153	3171	3170	11
2153	muscle	2	5	2	2153	2154	2172	2171	3153	3154	3172	3171	11
2154	muscle	3	5	2	2154	2155	2173	2172	3154	3155	3173	3172	11
2155	fat	4	5	2	2155	2156	2174	2173	3155	3156	3174	3173	8
2156	fat	5	5	2	2156	2157	2175	2174	3156	3157	3175	3174	8
2157	air	6	5	2	2157	2158	2176	2175	3157	3158	3176	3175	3
2158	air	7	5	2	2158	2159	2177	2176	3158	3159	3177	3176	3
2159	air	8	5	2	2159	2160	2178	2177	3159	3160	3178	3177	3

Element Number	Tissue type	Location			Nodes on this slice				Nodes on slice above				Mesh Color
		X	Y	Z	LL	LR	UR	UL	LL	LR	UR	UL	
2160	air	9	5	2	2160	2161	2179	2178	3160	3161	3179	3178	3
2161	air	10	5	2	2161	2162	2180	2179	3161	3162	3180	3179	3
2163	air	-6	6	2	2163	2164	2182	2181	3163	3164	3182	3181	3
2164	air	-5	6	2	2164	2165	2183	2182	3164	3165	3183	3182	3
2165	air	-4	6	2	2165	2166	2184	2183	3165	3166	3184	3183	3
2166	air	-3	6	2	2166	2167	2185	2184	3166	3167	3185	3184	3
2167	air	-2	6	2	2167	2168	2186	2185	3167	3168	3186	3185	3
2168	air	-1	6	2	2168	2169	2187	2186	3168	3169	3187	3186	3
2169	air	0	6	2	2169	2170	2188	2187	3169	3170	3188	3187	3
2170	air	1	6	2	2170	2171	2189	2188	3170	3171	3189	3188	3
2171	air	2	6	2	2171	2172	2190	2189	3171	3172	3190	3189	3
2172	air	3	6	2	2172	2173	2191	2190	3172	3173	3191	3190	3
2173	air	4	6	2	2173	2174	2192	2191	3173	3174	3192	3191	3
2174	air	5	6	2	2174	2175	2193	2192	3174	3175	3193	3192	3
2175	air	6	6	2	2175	2176	2194	2193	3175	3176	3194	3193	3
2176	air	7	6	2	2176	2177	2195	2194	3176	3177	3195	3194	3
2177	air	8	6	2	2177	2178	2196	2195	3177	3178	3196	3195	3
2178	air	9	6	2	2178	2179	2197	2196	3178	3179	3197	3196	3
2179	air	10	6	2	2179	2180	2198	2197	3179	3180	3198	3197	3
2181	air	-6	7	2	2181	2182	2200	2199	3181	3182	3200	3199	3
2182	air	-5	7	2	2182	2183	2201	2200	3182	3183	3201	3200	3
2183	air	-4	7	2	2183	2184	2202	2201	3183	3184	3202	3201	3
2184	air	-3	7	2	2184	2185	2203	2202	3184	3185	3203	3202	3
2185	air	-2	7	2	2185	2186	2204	2203	3185	3186	3204	3203	3
2186	air	-1	7	2	2186	2187	2205	2204	3186	3187	3205	3204	3
2187	air	0	7	2	2187	2188	2206	2205	3187	3188	3206	3205	3
2188	air	1	7	2	2188	2189	2207	2206	3188	3189	3207	3206	3
2189	air	2	7	2	2189	2190	2208	2207	3189	3190	3208	3207	3
2190	air	3	7	2	2190	2191	2209	2208	3190	3191	3209	3208	3
2191	air	4	7	2	2191	2192	2210	2209	3191	3192	3210	3209	3
2192	air	5	7	2	2192	2193	2211	2210	3192	3193	3211	3210	3
2193	air	6	7	2	2193	2194	2212	2211	3193	3194	3212	3211	3
2194	air	7	7	2	2194	2195	2213	2212	3194	3195	3213	3212	3
2195	air	8	7	2	2195	2196	2214	2213	3195	3196	3214	3213	3
2196	air	9	7	2	2196	2197	2215	2214	3196	3197	3215	3214	3
2197	air	10	7	2	2197	2198	2216	2215	3197	3198	3216	3215	3
2199	air	-6	8	2	2199	2200	2218	2217	3199	3200	3218	3217	3
2200	air	-5	8	2	2200	2201	2219	2218	3200	3201	3219	3218	3

Element Number	Tissue type	Location			Nodes on this slice				Nodes on slice above				Mesh Color
		X	Y	Z	LL	LR	UR	UL	LL	LR	UR	UL	
2201	air	-4	8	2	2201	2202	2220	2219	3201	3202	3220	3219	3
2202	air	-3	8	2	2202	2203	2221	2220	3202	3203	3221	3220	3
2203	air	-2	8	2	2203	2204	2222	2221	3203	3204	3222	3221	3
2204	air	-1	8	2	2204	2205	2223	2222	3204	3205	3223	3222	3
2205	air	0	8	2	2205	2206	2224	2223	3205	3206	3224	3223	3
2206	air	1	8	2	2206	2207	2225	2224	3206	3207	3225	3224	3
2207	air	2	8	2	2207	2208	2226	2225	3207	3208	3226	3225	3
2208	air	3	8	2	2208	2209	2227	2226	3208	3209	3227	3226	3
2209	air	4	8	2	2209	2210	2228	2227	3209	3210	3228	3227	3
2210	air	5	8	2	2210	2211	2229	2228	3210	3211	3229	3228	3
2211	air	6	8	2	2211	2212	2230	2229	3211	3212	3230	3229	3
2212	air	7	8	2	2212	2213	2231	2230	3212	3213	3231	3230	3
2213	air	8	8	2	2213	2214	2232	2231	3213	3214	3232	3231	3
2214	air	9	8	2	2214	2215	2233	2232	3214	3215	3233	3232	3
2215	air	10	8	2	2215	2216	2234	2233	3215	3216	3234	3233	3
2217	air	-6	9	2	2217	2218	2236	2235	3217	3218	3236	3235	3
2218	air	-5	9	2	2218	2219	2237	2236	3218	3219	3237	3236	3
2219	air	-4	9	2	2219	2220	2238	2237	3219	3220	3238	3237	3
2220	air	-3	9	2	2220	2221	2239	2238	3220	3221	3239	3238	3
2221	air	-2	9	2	2221	2222	2240	2239	3221	3222	3240	3239	3
2222	air	-1	9	2	2222	2223	2241	2240	3222	3223	3241	3240	3
2223	air	0	9	2	2223	2224	2242	2241	3223	3224	3242	3241	3
2224	air	1	9	2	2224	2225	2243	2242	3224	3225	3243	3242	3
2225	air	2	9	2	2225	2226	2244	2243	3225	3226	3244	3243	3
2226	air	3	9	2	2226	2227	2245	2244	3226	3227	3245	3244	3
2227	air	4	9	2	2227	2228	2246	2245	3227	3228	3246	3245	3
2228	air	5	9	2	2228	2229	2247	2246	3228	3229	3247	3246	3
2229	air	6	9	2	2229	2230	2248	2247	3229	3230	3248	3247	3
2230	air	7	9	2	2230	2231	2249	2248	3230	3231	3249	3248	3
2231	air	8	9	2	2231	2232	2250	2249	3231	3232	3250	3249	3
2232	air	9	9	2	2232	2233	2251	2250	3232	3233	3251	3250	3
2233	air	10	9	2	2233	2234	2252	2251	3233	3234	3252	3251	3

**Table 8 - FEM Conversion Table for Leg of Lamb at Z = 3 cm**

Element Number	Tissue type	Location X Y Z	Nodes on this slice				Nodes on slice above				Mesh Color
			LL	LR	UR	UL	LL	LR	UR	UL	
3001	air	-6 -3 3	3001	3002	3020	3019	4001	4002	4020	4019	3
3002	air	-5 -3 3	3002	3003	3021	3020	4002	4003	4021	4020	3
3003	air	-4 -3 3	3003	3004	3022	3021	4003	4004	4022	4021	3
3004	air	-3 -3 3	3004	3005	3023	3022	4004	4005	4023	4022	3
3005	air	-2 -3 3	3005	3006	3024	3023	4005	4006	4024	4023	3
3006	air	-1 -3 3	3006	3007	3025	3024	4006	4007	4025	4024	3
3007	air	0 -3 3	3007	3008	3026	3025	4007	4008	4026	4025	3
3008	air	1 -3 3	3008	3009	3027	3026	4008	4009	4027	4026	3
3009	air	2 -3 3	3009	3010	3028	3027	4009	4010	4028	4027	3
3010	air	3 -3 3	3010	3011	3029	3028	4010	4011	4029	4028	3
3011	air	4 -3 3	3011	3012	3030	3029	4011	4012	4030	4029	3
3012	air	5 -3 3	3012	3013	3031	3030	4012	4013	4031	4030	3
3013	air	6 -3 3	3013	3014	3032	3031	4013	4014	4032	4031	3
3014	air	7 -3 3	3014	3015	3033	3032	4014	4015	4033	4032	3
3015	air	8 -3 3	3015	3016	3034	3033	4015	4016	4034	4033	3
3016	air	9 -3 3	3016	3017	3035	3034	4016	4017	4035	4034	3
3017	air	10 -3 3	3017	3018	3036	3035	4017	4018	4036	4035	3
3019	air	-6 -2 3	3019	3020	3038	3037	4019	4020	4038	4037	3
3020	air	-5 -2 3	3020	3021	3039	3038	4020	4021	4039	4038	3
3021	air	-4 -2 3	3021	3022	3040	3039	4021	4022	4040	4039	3
3022	bone	-3 -2 3	3022	3023	3041	3040	4022	4023	4041	4040	15
3023	bone	-2 -2 3	3023	3024	3042	3041	4023	4024	4042	4041	15
3024	bone	-1 -2 3	3024	3025	3043	3042	4024	4025	4043	4042	15
3025	bone	0 -2 3	3025	3026	3044	3043	4025	4026	4044	4043	15
3026	air	1 -2 3	3026	3027	3045	3044	4026	4027	4045	4044	3
3027	air	2 -2 3	3027	3028	3046	3045	4027	4028	4046	4045	3
3028	air	3 -2 3	3028	3029	3047	3046	4028	4029	4047	4046	3
3029	air	4 -2 3	3029	3030	3048	3047	4029	4030	4048	4047	3
3030	air	5 -2 3	3030	3031	3049	3048	4030	4031	4049	4048	3
3031	air	6 -2 3	3031	3032	3050	3049	4031	4032	4050	4049	3
3032	air	7 -2 3	3032	3033	3051	3050	4032	4033	4051	4050	3
3033	air	8 -2 3	3033	3034	3052	3051	4033	4034	4052	4051	3
3034	air	9 -2 3	3034	3035	3053	3052	4034	4035	4053	4052	3
3035	air	10 -2 3	3035	3036	3054	3053	4035	4036	4054	4053	3
3037	air	-6 -1 3	3037	3038	3056	3055	4037	4038	4056	4055	3
3038	air	-5 -1 3	3038	3039	3057	3056	4038	4039	4057	4056	3
3039	fat	-4 -1 3	3039	3040	3058	3057	4039	4040	4058	4057	8

Element Number	Tissue type	Location			Nodes on this slice				Nodes on slice above				Mesh Color
		X	Y	Z	LL	LR	UR	UL	LL	LR	UR	UL	
3040	bone	-3	-1	3	3040	3041	3059	3058	4040	4041	4059	4058	15
3041	bone	-2	-1	3	3041	3042	3060	3059	4041	4042	4060	4059	15
3042	bone	-1	-1	3	3042	3043	3061	3060	4042	4043	4061	4060	15
3043	bone	0	-1	3	3043	3044	3062	3061	4043	4044	4062	4061	15
3044	muscle	1	-1	3	3044	3045	3063	3062	4044	4045	4063	4062	11
3045	muscle	2	-1	3	3045	3046	3064	3063	4045	4046	4064	4063	11
3046	muscle	3	-1	3	3046	3047	3065	3064	4046	4047	4065	4064	11
3047	muscle	4	-1	3	3047	3048	3066	3065	4047	4048	4066	4065	11
3048	muscle	5	-1	3	3048	3049	3067	3066	4048	4049	4067	4066	11
3049	air	6	-1	3	3049	3050	3068	3067	4049	4050	4068	4067	3
3050	air	7	-1	3	3050	3051	3069	3068	4050	4051	4069	4068	3
3051	air	8	-1	3	3051	3052	3070	3069	4051	4052	4070	4069	3
3052	air	9	-1	3	3052	3053	3071	3070	4052	4053	4071	4070	3
3053	air	10	-1	3	3053	3054	3072	3071	4053	4054	4072	4071	3
3055	air	-6	0	3	3055	3056	3074	3073	4055	4056	4074	4073	3
3056	fat	-5	0	3	3056	3057	3075	3074	4056	4057	4075	4074	8
3057	fat	-4	0	3	3057	3058	3076	3075	4057	4058	4076	4075	8
3058	bone	-3	0	3	3058	3059	3077	3076	4058	4059	4077	4076	15
3059	bone	-2	0	3	3059	3060	3078	3077	4059	4060	4078	4077	15
3060	bone	-1	0	3	3060	3061	3079	3078	4060	4061	4079	4078	15
3061	bone	0	0	3	3061	3062	3080	3079	4061	4062	4080	4079	15
3062	muscle	1	0	3	3062	3063	3081	3080	4062	4063	4081	4080	11
3063	muscle	2	0	3	3063	3064	3082	3081	4063	4064	4082	4081	11
3064	muscle	3	0	3	3064	3065	3083	3082	4064	4065	4083	4082	11
3065	muscle	4	0	3	3065	3066	3084	3083	4065	4066	4084	4083	11
3066	muscle	5	0	3	3066	3067	3085	3084	4066	4067	4085	4084	11
3067	muscle	6	0	3	3067	3068	3086	3085	4067	4068	4086	4085	11
3068	air	7	0	3	3068	3069	3087	3086	4068	4069	4087	4086	3
3069	air	8	0	3	3069	3070	3088	3087	4069	4070	4088	4087	3
3070	air	9	0	3	3070	3071	3089	3088	4070	4071	4089	4088	3
3071	air	10	0	3	3071	3072	3090	3089	4071	4072	4090	4089	3
3073	air	-6	1	3	3073	3074	3092	3091	4073	4074	4092	4091	3
3074	air	-5	1	3	3074	3075	3093	3092	4074	4075	4093	4092	3
3075	fat	-4	1	3	3075	3076	3094	3093	4075	4076	4094	4093	8
3076	bone	-3	1	3	3076	3077	3095	3094	4076	4077	4095	4094	15
3077	bone	-2	1	3	3077	3078	3096	3095	4077	4078	4096	4095	15
3078	bone	-1	1	3	3078	3079	3097	3096	4078	4079	4097	4096	15
3079	bone	0	1	3	3079	3080	3098	3097	4079	4080	4098	4097	15

Element Number	Tissue type	Location			Nodes on this slice				Nodes on slice above				Mesh Color
		X	Y	Z	LL	LR	UR	UL	LL	LR	UR	UL	
3080	muscle	1	1	3	3080	3081	3099	3098	4080	4081	4099	4098	11
3081	muscle	2	1	3	3081	3082	3100	3099	4081	4082	4100	4099	11
3082	muscle	3	1	3	3082	3083	3101	3100	4082	4083	4101	4100	11
3083	muscle	4	1	3	3083	3084	3102	3101	4083	4084	4102	4101	11
3084	muscle	5	1	3	3084	3085	3103	3102	4084	4085	4103	4102	11
3085	muscle	6	1	3	3085	3086	3104	3103	4085	4086	4104	4103	11
3086	fat	7	1	3	3086	3087	3105	3104	4086	4087	4105	4104	8
3087	air	8	1	3	3087	3088	3106	3105	4087	4088	4106	4105	3
3088	air	9	1	3	3088	3089	3107	3106	4088	4089	4107	4106	3
3089	air	10	1	3	3089	3090	3108	3107	4089	4090	4108	4107	3
3091	air	-6	2	3	3091	3092	3110	3109	4091	4092	4110	4109	3
3092	air	-5	2	3	3092	3093	3111	3110	4092	4093	4111	4110	3
3093	fat	-4	2	3	3093	3094	3112	3111	4093	4094	4112	4111	8
3094	fat	-3	2	3	3094	3095	3113	3112	4094	4095	4113	4112	8
3095	bone	-2	2	3	3095	3096	3114	3113	4095	4096	4114	4113	15
3096	bone	-1	2	3	3096	3097	3115	3114	4096	4097	4115	4114	15
3097	bone	0	2	3	3097	3098	3116	3115	4097	4098	4116	4115	15
3098	muscle	1	2	3	3098	3099	3117	3116	4098	4099	4117	4116	11
3099	muscle	2	2	3	3099	3100	3118	3117	4099	4100	4118	4117	11
3100	fat	3	2	3	3100	3101	3119	3118	4100	4101	4119	4118	8
3101	muscle	4	2	3	3101	3102	3120	3119	4101	4102	4120	4119	11
3102	muscle	5	2	3	3102	3103	3121	3120	4102	4103	4121	4120	11
3103	fat	6	2	3	3103	3104	3122	3121	4103	4104	4122	4121	8
3104	fat	7	2	3	3104	3105	3123	3122	4104	4105	4123	4122	8
3105	air	8	2	3	3105	3106	3124	3123	4105	4106	4124	4123	3
3106	air	9	2	3	3106	3107	3125	3124	4106	4107	4125	4124	3
3107	air	10	2	3	3107	3108	3126	3125	4107	4108	4126	4125	3
3109	air	-6	3	3	3109	3110	3128	3127	4109	4110	4128	4127	3
3110	air	-5	3	3	3110	3111	3129	3128	4110	4111	4129	4128	3
3111	fat	-4	3	3	3111	3112	3130	3129	4111	4112	4130	4129	8
3112	muscle	-3	3	3	3112	3113	3131	3130	4112	4113	4131	4130	11
3113	muscle	-2	3	3	3113	3114	3132	3131	4113	4114	4132	4131	11
3114	muscle	-1	3	3	3114	3115	3133	3132	4114	4115	4133	4132	11
3115	muscle	0	3	3	3115	3116	3134	3133	4115	4116	4134	4133	11
3116	muscle	1	3	3	3116	3117	3135	3134	4116	4117	4135	4134	11
3117	muscle	2	3	3	3117	3118	3136	3135	4117	4118	4136	4135	11
3118	fat	3	3	3	3118	3119	3137	3136	4118	4119	4137	4136	8
3119	muscle	4	3	3	3119	3120	3138	3137	4119	4120	4138	4137	11

Element Number	Tissue type	Location			Nodes on this slice				Nodes on slice above				Mesh Color
		X	Y	Z	LL	LR	UR	UL	LL	LR	UR	UL	
3120	muscle	5	3	3	3120	3121	3139	3138	4120	4121	4139	4138	11
3121	fat	6	3	3	3121	3122	3140	3139	4121	4122	4140	4139	8
3122	fat	7	3	3	3122	3123	3141	3140	4122	4123	4141	4140	8
3123	air	8	3	3	3123	3124	3142	3141	4123	4124	4142	4141	3
3124	air	9	3	3	3124	3125	3143	3142	4124	4125	4143	4142	3
3125	air	10	3	3	3125	3126	3144	3143	4125	4126	4144	4143	3
3127	air	-6	4	3	3127	3128	3146	3145	4127	4128	4146	4145	3
3128	air	-5	4	3	3128	3129	3147	3146	4128	4129	4147	4146	3
3129	air	-4	4	3	3129	3130	3148	3147	4129	4130	4148	4147	3
3130	air	-3	4	3	3130	3131	3149	3148	4130	4131	4149	4148	3
3131	muscle	-2	4	3	3131	3132	3150	3149	4131	4132	4150	4149	11
3132	muscle	-1	4	3	3132	3133	3151	3150	4132	4133	4151	4150	11
3133	muscle	0	4	3	3133	3134	3152	3151	4133	4134	4152	4151	11
3134	muscle	1	4	3	3134	3135	3153	3152	4134	4135	4153	4152	11
3135	muscle	2	4	3	3135	3136	3154	3153	4135	4136	4154	4153	11
3136	fat	3	4	3	3136	3137	3155	3154	4136	4137	4155	4154	8
3137	fat	4	4	3	3137	3138	3156	3155	4137	4138	4156	4155	8
3138	fat	5	4	3	3138	3139	3157	3156	4138	4139	4157	4156	8
3139	fat	6	4	3	3139	3140	3158	3157	4139	4140	4158	4157	8
3140	air	7	4	3	3140	3141	3159	3158	4140	4141	4159	4158	3
3141	air	8	4	3	3141	3142	3160	3159	4141	4142	4160	4159	3
3142	air	9	4	3	3142	3143	3161	3160	4142	4143	4161	4160	3
3143	air	10	4	3	3143	3144	3162	3161	4143	4144	4162	4161	3
3145	air	-6	5	3	3145	3146	3164	3163	4145	4146	4164	4163	3
3146	air	-5	5	3	3146	3147	3165	3164	4146	4147	4165	4164	3
3147	air	-4	5	3	3147	3148	3166	3165	4147	4148	4166	4165	3
3148	air	-3	5	3	3148	3149	3167	3166	4148	4149	4167	4166	3
3149	muscle	-2	5	3	3149	3150	3168	3167	4149	4150	4168	4167	11
3150	muscle	-1	5	3	3150	3151	3169	3168	4150	4151	4169	4168	11
3151	muscle	0	5	3	3151	3152	3170	3169	4151	4152	4170	4169	11
3152	muscle	1	5	3	3152	3153	3171	3170	4152	4153	4171	4170	11
3153	muscle	2	5	3	3153	3154	3172	3171	4153	4154	4172	4171	11
3154	muscle	3	5	3	3154	3155	3173	3172	4154	4155	4173	4172	11
3155	fat	4	5	3	3155	3156	3174	3173	4155	4156	4174	4173	8
3156	air	5	5	3	3156	3157	3175	3174	4156	4157	4175	4174	3
3157	air	6	5	3	3157	3158	3176	3175	4157	4158	4176	4175	3
3158	air	7	5	3	3158	3159	3177	3176	4158	4159	4177	4176	3
3159	air	8	5	3	3159	3160	3178	3177	4159	4160	4178	4177	3



Element Number	Tissue type	Location			Nodes on this slice				Nodes on slice above				Mesh Color
		X	Y	Z	LL	LR	UR	UL	LL	LR	UR	UL	
3160	air	9	5	3	3160	3161	3179	3178	4160	4161	4179	4178	3
3161	air	10	5	3	3161	3162	3180	3179	4161	4162	4180	4179	3
3163	air	-6	6	3	3163	3164	3182	3181	4163	4164	4182	4181	3
3164	air	-5	6	3	3164	3165	3183	3182	4164	4165	4183	4182	3
3165	air	-4	6	3	3165	3166	3184	3183	4165	4166	4184	4183	3
3166	air	-3	6	3	3166	3167	3185	3184	4166	4167	4185	4184	3
3167	air	-2	6	3	3167	3168	3186	3185	4167	4168	4186	4185	3
3168	air	-1	6	3	3168	3169	3187	3186	4168	4169	4187	4186	3
3169	fat	0	6	3	3169	3170	3188	3187	4169	4170	4188	4187	8
3170	fat	1	6	3	3170	3171	3189	3188	4170	4171	4189	4188	8
3171	fat	2	6	3	3171	3172	3190	3189	4171	4172	4190	4189	8
3172	air	3	6	3	3172	3173	3191	3190	4172	4173	4191	4190	3
3173	air	4	6	3	3173	3174	3192	3191	4173	4174	4192	4191	3
3174	air	5	6	3	3174	3175	3193	3192	4174	4175	4193	4192	3
3175	air	6	6	3	3175	3176	3194	3193	4175	4176	4194	4193	3
3176	air	7	6	3	3176	3177	3195	3194	4176	4177	4195	4194	3
3177	air	8	6	3	3177	3178	3196	3195	4177	4178	4196	4195	3
3178	air	9	6	3	3178	3179	3197	3196	4178	4179	4197	4196	3
3179	air	10	6	3	3179	3180	3198	3197	4179	4180	4198	4197	3
3181	air	-6	7	3	3181	3182	3200	3199	4181	4182	4200	4199	3
3182	air	-5	7	3	3182	3183	3201	3200	4182	4183	4201	4200	3
3183	air	-4	7	3	3183	3184	3202	3201	4183	4184	4202	4201	3
3184	air	-3	7	3	3184	3185	3203	3202	4184	4185	4203	4202	3
3185	air	-2	7	3	3185	3186	3204	3203	4185	4186	4204	4203	3
3186	air	-1	7	3	3186	3187	3205	3204	4186	4187	4205	4204	3
3187	air	0	7	3	3187	3188	3206	3205	4187	4188	4206	4205	3
3188	air	1	7	3	3188	3189	3207	3206	4188	4189	4207	4206	3
3189	air	2	7	3	3189	3190	3208	3207	4189	4190	4208	4207	3
3190	air	3	7	3	3190	3191	3209	3208	4190	4191	4209	4208	3
3191	air	4	7	3	3191	3192	3210	3209	4191	4192	4210	4209	3
3192	air	5	7	3	3192	3193	3211	3210	4192	4193	4211	4210	3
3193	air	6	7	3	3193	3194	3212	3211	4193	4194	4212	4211	3
3194	air	7	7	3	3194	3195	3213	3212	4194	4195	4213	4212	3
3195	air	8	7	3	3195	3196	3214	3213	4195	4196	4214	4213	3
3196	air	9	7	3	3196	3197	3215	3214	4196	4197	4215	4214	3
3197	air	10	7	3	3197	3198	3216	3215	4197	4198	4216	4215	3
3199	air	-6	8	3	3199	3200	3218	3217	4199	4200	4218	4217	3
3200	air	-5	8	3	3200	3201	3219	3218	4200	4201	4219	4218	3

Element Number	Tissue type	Location			Nodes on this slice				Nodes on slice above				Mesh Color
		X	Y	Z	LL	LR	UR	UL	LL	LR	UR	UL	
3201	air	-4	8	3	3201	3202	3220	3219	4201	4202	4220	4219	3
3202	air	-3	8	3	3202	3203	3221	3220	4202	4203	4221	4220	3
3203	air	-2	8	3	3203	3204	3222	3221	4203	4204	4222	4221	3
3204	air	-1	8	3	3204	3205	3223	3222	4204	4205	4223	4222	3
3205	air	0	8	3	3205	3206	3224	3223	4205	4206	4224	4223	3
3206	air	1	8	3	3206	3207	3225	3224	4206	4207	4225	4224	3
3207	air	2	8	3	3207	3208	3226	3225	4207	4208	4226	4225	3
3208	air	3	8	3	3208	3209	3227	3226	4208	4209	4227	4226	3
3209	air	4	8	3	3209	3210	3228	3227	4209	4210	4228	4227	3
3210	air	5	8	3	3210	3211	3229	3228	4210	4211	4229	4228	3
3211	air	6	8	3	3211	3212	3230	3229	4211	4212	4230	4229	3
3212	air	7	8	3	3212	3213	3231	3230	4212	4213	4231	4230	3
3213	air	8	8	3	3213	3214	3232	3231	4213	4214	4232	4231	3
3214	air	9	8	3	3214	3215	3233	3232	4214	4215	4233	4232	3
3215	air	10	8	3	3215	3216	3234	3233	4215	4216	4234	4233	3
3217	air	-6	9	3	3217	3218	3236	3235	4217	4218	4236	4235	3
3218	air	-5	9	3	3218	3219	3237	3236	4218	4219	4237	4236	3
3219	air	-4	9	3	3219	3220	3238	3237	4219	4220	4238	4237	3
3220	air	-3	9	3	3220	3221	3239	3238	4220	4221	4239	4238	3
3221	air	-2	9	3	3221	3222	3240	3239	4221	4222	4240	4239	3
3222	air	-1	9	3	3222	3223	3241	3240	4222	4223	4241	4240	3
3223	air	0	9	3	3223	3224	3242	3241	4223	4224	4242	4241	3
3224	air	1	9	3	3224	3225	3243	3242	4224	4225	4243	4242	3
3225	air	2	9	3	3225	3226	3244	3243	4225	4226	4244	4243	3
3226	air	3	9	3	3226	3227	3245	3244	4226	4227	4245	4244	3
3227	air	4	9	3	3227	3228	3246	3245	4227	4228	4246	4245	3
3228	air	5	9	3	3228	3229	3247	3246	4228	4229	4247	4246	3
3229	air	6	9	3	3229	3230	3248	3247	4229	4230	4248	4247	3
3230	air	7	9	3	3230	3231	3249	3248	4230	4231	4249	4248	3
3231	air	8	9	3	3231	3232	3250	3249	4231	4232	4250	4249	3
3232	air	9	9	3	3232	3233	3251	3250	4232	4233	4251	4250	3
3233	air	10	9	3	3233	3234	3252	3251	4233	4234	4252	4251	3

**Table 9 - FEM Conversion Table for Leg of Lamb at Z = 4 cm**

Element Number	Tissue type	Location X Y Z	Nodes on this slice				Nodes on slice above				Mesh Color
			LL	LR	UR	UL	LL	LR	UR	UL	
4001	air	-6 -3 4	4001	4002	4020	4019	5001	5002	5020	5019	3
4002	air	-5 -3 4	4002	4003	4021	4020	5002	5003	5021	5020	3
4003	air	-4 -3 4	4003	4004	4022	4021	5003	5004	5022	5021	3
4004	air	-3 -3 4	4004	4005	4023	4022	5004	5005	5023	5022	3
4005	air	-2 -3 4	4005	4006	4024	4023	5005	5006	5024	5023	3
4006	air	-1 -3 4	4006	4007	4025	4024	5006	5007	5025	5024	3
4007	air	0 -3 4	4007	4008	4026	4025	5007	5008	5026	5025	3
4008	air	1 -3 4	4008	4009	4027	4026	5008	5009	5027	5026	3
4009	air	2 -3 4	4009	4010	4028	4027	5009	5010	5028	5027	3
4010	air	3 -3 4	4010	4011	4029	4028	5010	5011	5029	5028	3
4011	air	4 -3 4	4011	4012	4030	4029	5011	5012	5030	5029	3
4012	air	5 -3 4	4012	4013	4031	4030	5012	5013	5031	5030	3
4013	air	6 -3 4	4013	4014	4032	4031	5013	5014	5032	5031	3
4014	air	7 -3 4	4014	4015	4033	4032	5014	5015	5033	5032	3
4015	air	8 -3 4	4015	4016	4034	4033	5015	5016	5034	5033	3
4016	air	9 -3 4	4016	4017	4035	4034	5016	5017	5035	5034	3
4017	air	10 -3 4	4017	4018	4036	4035	5017	5018	5036	5035	3
4019	air	-6 -2 4	4019	4020	4038	4037	5019	5020	5038	5037	3
4020	air	-5 -2 4	4020	4021	4039	4038	5020	5021	5039	5038	3
4021	fat	-4 -2 4	4021	4022	4040	4039	5021	5022	5040	5039	8
4022	bone	-3 -2 4	4022	4023	4041	4040	5022	5023	5041	5040	15
4023	bone	-2 -2 4	4023	4024	4042	4041	5023	5024	5042	5041	15
4024	bone	-1 -2 4	4024	4025	4043	4042	5024	5025	5043	5042	15
4025	air	0 -2 4	4025	4026	4044	4043	5025	5026	5044	5043	3
4026	air	1 -2 4	4026	4027	4045	4044	5026	5027	5045	5044	3
4027	muscle	2 -2 4	4027	4028	4046	4045	5027	5028	5046	5045	11
4028	muscle	3 -2 4	4028	4029	4047	4046	5028	5029	5047	5046	11
4029	muscle	4 -2 4	4029	4030	4048	4047	5029	5030	5048	5047	11
4030	air	5 -2 4	4030	4031	4049	4048	5030	5031	5049	5048	3
4031	air	6 -2 4	4031	4032	4050	4049	5031	5032	5050	5049	3
4032	air	7 -2 4	4032	4033	4051	4050	5032	5033	5051	5050	3
4033	air	8 -2 4	4033	4034	4052	4051	5033	5034	5052	5051	3
4034	air	9 -2 4	4034	4035	4053	4052	5034	5035	5053	5052	3
4035	air	10 -2 4	4035	4036	4054	4053	5035	5036	5054	5053	3
4037	air	-6 -1 4	4037	4038	4056	4055	5037	5038	5056	5055	3
4038	fat	-5 -1 4	4038	4039	4057	4056	5038	5039	5057	5056	8
4039	fat	-4 -1 4	4039	4040	4058	4057	5039	5040	5058	5057	8

Element Number	Tissue type	Location			Nodes on this slice				Nodes on slice above				Mesh Color
		X	Y	Z	LL	LR	UR	UL	LL	LR	UR	UL	
4040	bone	-3	-1	4	4040	4041	4059	4058	5040	5041	5059	5058	15
4041	bone	-2	-1	4	4041	4042	4060	4059	5041	5042	5060	5059	15
4042	bone	-1	-1	4	4042	4043	4061	4060	5042	5043	5061	5060	15
4043	bone	0	-1	4	4043	4044	4062	4061	5043	5044	5062	5061	15
4044	muscle	1	-1	4	4044	4045	4063	4062	5044	5045	5063	5062	11
4045	muscle	2	-1	4	4045	4046	4064	4063	5045	5046	5064	5063	11
4046	muscle	3	-1	4	4046	4047	4065	4064	5046	5047	5065	5064	11
4047	muscle	4	-1	4	4047	4048	4066	4065	5047	5048	5066	5065	11
4048	muscle	5	-1	4	4048	4049	4067	4066	5048	5049	5067	5066	11
4049	muscle	6	-1	4	4049	4050	4068	4067	5049	5050	5068	5067	11
4050	air	7	-1	4	4050	4051	4069	4068	5050	5051	5069	5068	3
4051	air	8	-1	4	4051	4052	4070	4069	5051	5052	5070	5069	3
4052	air	9	-1	4	4052	4053	4071	4070	5052	5053	5071	5070	3
4053	air	10	-1	4	4053	4054	4072	4071	5053	5054	5072	5071	3
4055	air	-6	0	4	4055	4056	4074	4073	5055	5056	5074	5073	3
4056	fat	-5	0	4	4056	4057	4075	4074	5056	5057	5075	5074	8
4057	fat	-4	0	4	4057	4058	4076	4075	5057	5058	5076	5075	8
4058	bone	-3	0	4	4058	4059	4077	4076	5058	5059	5077	5076	15
4059	bone	-2	0	4	4059	4060	4078	4077	5059	5060	5078	5077	15
4060	bone	-1	0	4	4060	4061	4079	4078	5060	5061	5079	5078	15
4061	bone	0	0	4	4061	4062	4080	4079	5061	5062	5080	5079	15
4062	muscle	1	0	4	4062	4063	4081	4080	5062	5063	5081	5080	11
4063	muscle	2	0	4	4063	4064	4082	4081	5063	5064	5082	5081	11
4064	fat	3	0	4	4064	4065	4083	4082	5064	5065	5083	5082	8
4065	muscle	4	0	4	4065	4066	4084	4083	5065	5066	5084	5083	11
4066	muscle	5	0	4	4066	4067	4085	4084	5066	5067	5085	5084	11
4067	muscle	6	0	4	4067	4068	4086	4085	5067	5068	5086	5085	11
4068	muscle	7	0	4	4068	4069	4087	4086	5068	5069	5087	5086	11
4069	air	8	0	4	4069	4070	4088	4087	5069	5070	5088	5087	3
4070	air	9	0	4	4070	4071	4089	4088	5070	5071	5089	5088	3
4071	air	10	0	4	4071	4072	4090	4089	5071	5072	5090	5089	3
4073	air	-6	1	4	4073	4074	4092	4091	5073	5074	5092	5091	3
4074	air	-5	1	4	4074	4075	4093	4092	5074	5075	5093	5092	3
4075	fat	-4	1	4	4075	4076	4094	4093	5075	5076	5094	5093	8
4076	bone	-3	1	4	4076	4077	4095	4094	5076	5077	5095	5094	15
4077	bone	-2	1	4	4077	4078	4096	4095	5077	5078	5096	5095	15
4078	bone	-1	1	4	4078	4079	4097	4096	5078	5079	5097	5096	15
4079	muscle	0	1	4	4079	4080	4098	4097	5079	5080	5098	5097	11

Element Number	Tissue type	Location			Nodes on this slice				Nodes on slice above				Mesh Color
		X	Y	Z	LL	LR	UR	UL	LL	LR	UR	UL	
4080	muscle	1	1	4	4080	4081	4099	4098	5080	5081	5099	5098	11
4081	muscle	2	1	4	4081	4082	4100	4099	5081	5082	5100	5099	11
4082	fat	3	1	4	4082	4083	4101	4100	5082	5083	5101	5100	8
4083	muscle	4	1	4	4083	4084	4102	4101	5083	5084	5102	5101	11
4084	muscle	5	1	4	4084	4085	4103	4102	5084	5085	5103	5102	11
4085	muscle	6	1	4	4085	4086	4104	4103	5085	5086	5104	5103	11
4086	muscle	7	1	4	4086	4087	4105	4104	5086	5087	5105	5104	11
4087	fat	8	1	4	4087	4088	4106	4105	5087	5088	5106	5105	8
4088	air	9	1	4	4088	4089	4107	4106	5088	5089	5107	5106	3
4089	air	10	1	4	4089	4090	4108	4107	5089	5090	5108	5107	3
4091	air	-6	2	4	4091	4092	4110	4109	5091	5092	5110	5109	3
4092	air	-5	2	4	4092	4093	4111	4110	5092	5093	5111	5110	3
4093	fat	-4	2	4	4093	4094	4112	4111	5093	5094	5112	5111	8
4094	fat	-3	2	4	4094	4095	4113	4112	5094	5095	5113	5112	8
4095	bone	-2	2	4	4095	4096	4114	4113	5095	5096	5114	5113	15
4096	bone	-1	2	4	4096	4097	4115	4114	5096	5097	5115	5114	15
4097	muscle	0	2	4	4097	4098	4116	4115	5097	5098	5116	5115	11
4098	muscle	1	2	4	4098	4099	4117	4116	5098	5099	5117	5116	11
4099	muscle	2	2	4	4099	4100	4118	4117	5099	5100	5118	5117	11
4100	fat	3	2	4	4100	4101	4119	4118	5100	5101	5119	5118	8
4101	muscle	4	2	4	4101	4102	4120	4119	5101	5102	5120	5119	11
4102	muscle	5	2	4	4102	4103	4121	4120	5102	5103	5121	5120	11
4103	muscle	6	2	4	4103	4104	4122	4121	5103	5104	5122	5121	11
4104	fat	7	2	4	4104	4105	4123	4122	5104	5105	5123	5122	8
4105	fat	8	2	4	4105	4106	4124	4123	5105	5106	5124	5123	8
4106	air	9	2	4	4106	4107	4125	4124	5106	5107	5125	5124	3
4107	air	10	2	4	4107	4108	4126	4125	5107	5108	5126	5125	3
4109	air	-6	3	4	4109	4110	4128	4127	5109	5110	5128	5127	3
4110	air	-5	3	4	4110	4111	4129	4128	5110	5111	5129	5128	3
4111	fat	-4	3	4	4111	4112	4130	4129	5111	5112	5130	5129	8
4112	muscle	-3	3	4	4112	4113	4131	4130	5112	5113	5131	5130	11
4113	muscle	-2	3	4	4113	4114	4132	4131	5113	5114	5132	5131	11
4114	muscle	-1	3	4	4114	4115	4133	4132	5114	5115	5133	5132	11
4115	muscle	0	3	4	4115	4116	4134	4133	5115	5116	5134	5133	11
4116	muscle	1	3	4	4116	4117	4135	4134	5116	5117	5135	5134	11
4117	fat	2	3	4	4117	4118	4136	4135	5117	5118	5136	5135	8
4118	fat	3	3	4	4118	4119	4137	4136	5118	5119	5137	5136	8
4119	muscle	4	3	4	4119	4120	4138	4137	5119	5120	5138	5137	11

Element Number	Tissue type	Location			Nodes on this slice				Nodes on slice above				Mesh Color
		X	Y	Z	LL	LR	UR	UL	LL	LR	UR	UL	
4120	muscle	5	3	4	4120	4121	4139	4138	5120	5121	5139	5138	11
4121	muscle	6	3	4	4121	4122	4140	4139	5121	5122	5140	5139	11
4122	fat	7	3	4	4122	4123	4141	4140	5122	5123	5141	5140	8
4123	air	8	3	4	4123	4124	4142	4141	5123	5124	5142	5141	3
4124	air	9	3	4	4124	4125	4143	4142	5124	5125	5143	5142	3
4125	air	10	3	4	4125	4126	4144	4143	5125	5126	5144	5143	3
4127	air	-6	4	4	4127	4128	4146	4145	5127	5128	5146	5145	3
4128	air	-5	4	4	4128	4129	4147	4146	5128	5129	5147	5146	3
4129	air	-4	4	4	4129	4130	4148	4147	5129	5130	5148	5147	3
4130	muscle	-3	4	4	4130	4131	4149	4148	5130	5131	5149	5148	11
4131	muscle	-2	4	4	4131	4132	4150	4149	5131	5132	5150	5149	11
4132	muscle	-1	4	4	4132	4133	4151	4150	5132	5133	5151	5150	11
4133	muscle	0	4	4	4133	4134	4152	4151	5133	5134	5152	5151	11
4134	muscle	1	4	4	4134	4135	4153	4152	5134	5135	5153	5152	11
4135	muscle	2	4	4	4135	4136	4154	4153	5135	5136	5154	5153	11
4136	muscle	3	4	4	4136	4137	4155	4154	5136	5137	5155	5154	11
4137	fat	4	4	4	4137	4138	4156	4155	5137	5138	5156	5155	8
4138	fat	5	4	4	4138	4139	4157	4156	5138	5139	5157	5156	8
4139	fat	6	4	4	4139	4140	4158	4157	5139	5140	5158	5157	8
4140	air	7	4	4	4140	4141	4159	4158	5140	5141	5159	5158	3
4141	air	8	4	4	4141	4142	4160	4159	5141	5142	5160	5159	3
4142	air	9	4	4	4142	4143	4161	4160	5142	5143	5161	5160	3
4143	air	10	4	4	4143	4144	4162	4161	5143	5144	5162	5161	3
4145	air	-6	5	4	4145	4146	4164	4163	5145	5146	5164	5163	3
4146	air	-5	5	4	4146	4147	4165	4164	5146	5147	5165	5164	3
4147	air	-4	5	4	4147	4148	4166	4165	5147	5148	5166	5165	3
4148	air	-3	5	4	4148	4149	4167	4166	5148	5149	5167	5166	3
4149	muscle	-2	5	4	4149	4150	4168	4167	5149	5150	5168	5167	11
4150	muscle	-1	5	4	4150	4151	4169	4168	5150	5151	5169	5168	11
4151	muscle	0	5	4	4151	4152	4170	4169	5151	5152	5170	5169	11
4152	fat	1	5	4	4152	4153	4171	4170	5152	5153	5171	5170	8
4153	fat	2	5	4	4153	4154	4172	4171	5153	5154	5172	5171	8
4154	muscle	3	5	4	4154	4155	4173	4172	5154	5155	5173	5172	11
4155	muscle	4	5	4	4155	4156	4174	4173	5155	5156	5174	5173	11
4156	fat	5	5	4	4156	4157	4175	4174	5156	5157	5175	5174	8
4157	air	6	5	4	4157	4158	4176	4175	5157	5158	5176	5175	3
4158	air	7	5	4	4158	4159	4177	4176	5158	5159	5177	5176	3
4159	air	8	5	4	4159	4160	4178	4177	5159	5160	5178	5177	3

Element Number	Tissue type	Location			Nodes on this slice				Nodes on slice above				Mesh Color
		X	Y	Z	LL	LR	UR	UL	LL	LR	UR	UL	
4160	air	9	5	4	4160	4161	4179	4178	5160	5161	5179	5178	3
4161	air	10	5	4	4161	4162	4180	4179	5161	5162	5180	5179	3
4163	air	-6	6	4	4163	4164	4182	4181	5163	5164	5182	5181	3
4164	air	-5	6	4	4164	4165	4183	4182	5164	5165	5183	5182	3
4165	air	-4	6	4	4165	4166	4184	4183	5165	5166	5184	5183	3
4166	air	-3	6	4	4166	4167	4185	4184	5166	5167	5185	5184	3
4167	air	-2	6	4	4167	4168	4186	4185	5167	5168	5186	5185	3
4168	air	-1	6	4	4168	4169	4187	4186	5168	5169	5187	5186	3
4169	air	0	6	4	4169	4170	4188	4187	5169	5170	5188	5187	3
4170	air	1	6	4	4170	4171	4189	4188	5170	5171	5189	5188	3
4171	air	2	6	4	4171	4172	4190	4189	5171	5172	5190	5189	3
4172	air	3	6	4	4172	4173	4191	4190	5172	5173	5191	5190	3
4173	air	4	6	4	4173	4174	4192	4191	5173	5174	5192	5191	3
4174	air	5	6	4	4174	4175	4193	4192	5174	5175	5193	5192	3
4175	air	6	6	4	4175	4176	4194	4193	5175	5176	5194	5193	3
4176	air	7	6	4	4176	4177	4195	4194	5176	5177	5195	5194	3
4177	air	8	6	4	4177	4178	4196	4195	5177	5178	5196	5195	3
4178	air	9	6	4	4178	4179	4197	4196	5178	5179	5197	5196	3
4179	air	10	6	4	4179	4180	4198	4197	5179	5180	5198	5197	3
4181	air	-6	7	4	4181	4182	4200	4199	5181	5182	5200	5199	3
4182	air	-5	7	4	4182	4183	4201	4200	5182	5183	5201	5200	3
4183	air	-4	7	4	4183	4184	4202	4201	5183	5184	5202	5201	3
4184	air	-3	7	4	4184	4185	4203	4202	5184	5185	5203	5202	3
4185	air	-2	7	4	4185	4186	4204	4203	5185	5186	5204	5203	3
4186	air	-1	7	4	4186	4187	4205	4204	5186	5187	5205	5204	3
4187	air	0	7	4	4187	4188	4206	4205	5187	5188	5206	5205	3
4188	air	1	7	4	4188	4189	4207	4206	5188	5189	5207	5206	3
4189	air	2	7	4	4189	4190	4208	4207	5189	5190	5208	5207	3
4190	air	3	7	4	4190	4191	4209	4208	5190	5191	5209	5208	3
4191	air	4	7	4	4191	4192	4210	4209	5191	5192	5210	5209	3
4192	air	5	7	4	4192	4193	4211	4210	5192	5193	5211	5210	3
4193	air	6	7	4	4193	4194	4212	4211	5193	5194	5212	5211	3
4194	air	7	7	4	4194	4195	4213	4212	5194	5195	5213	5212	3
4195	air	8	7	4	4195	4196	4214	4213	5195	5196	5214	5213	3
4196	air	9	7	4	4196	4197	4215	4214	5196	5197	5215	5214	3
4197	air	10	7	4	4197	4198	4216	4215	5197	5198	5216	5215	3
4199	air	-6	8	4	4199	4200	4218	4217	5199	5200	5218	5217	3
4200	air	-5	8	4	4200	4201	4219	4218	5200	5201	5219	5218	3

Element Number	Tissue type	Location			Nodes on this slice				Nodes on slice above				Mesh Color
		X	Y	Z	LL	LR	UR	UL	LL	LR	UR	UL	
4201	air	-4	8	4	4201	4202	4220	4219	5201	5202	5220	5219	3
4202	air	-3	8	4	4202	4203	4221	4220	5202	5203	5221	5220	3
4203	air	-2	8	4	4203	4204	4222	4221	5203	5204	5222	5221	3
4204	air	-1	8	4	4204	4205	4223	4222	5204	5205	5223	5222	3
4205	air	0	8	4	4205	4206	4224	4223	5205	5206	5224	5223	3
4206	air	1	8	4	4206	4207	4225	4224	5206	5207	5225	5224	3
4207	air	2	8	4	4207	4208	4226	4225	5207	5208	5226	5225	3
4208	air	3	8	4	4208	4209	4227	4226	5208	5209	5227	5226	3
4209	air	4	8	4	4209	4210	4228	4227	5209	5210	5228	5227	3
4210	air	5	8	4	4210	4211	4229	4228	5210	5211	5229	5228	3
4211	air	6	8	4	4211	4212	4230	4229	5211	5212	5230	5229	3
4212	air	7	8	4	4212	4213	4231	4230	5212	5213	5231	5230	3
4213	air	8	8	4	4213	4214	4232	4231	5213	5214	5232	5231	3
4214	air	9	8	4	4214	4215	4233	4232	5214	5215	5233	5232	3
4215	air	10	8	4	4215	4216	4234	4233	5215	5216	5234	5233	3
4217	air	-6	9	4	4217	4218	4236	4235	5217	5218	5236	5235	3
4218	air	-5	9	4	4218	4219	4237	4236	5218	5219	5237	5236	3
4219	air	-4	9	4	4219	4220	4238	4237	5219	5220	5238	5237	3
4220	air	-3	9	4	4220	4221	4239	4238	5220	5221	5239	5238	3
4221	air	-2	9	4	4221	4222	4240	4239	5221	5222	5240	5239	3
4222	air	-1	9	4	4222	4223	4241	4240	5222	5223	5241	5240	3
4223	air	0	9	4	4223	4224	4242	4241	5223	5224	5242	5241	3
4224	air	1	9	4	4224	4225	4243	4242	5224	5225	5243	5242	3
4225	air	2	9	4	4225	4226	4244	4243	5225	5226	5244	5243	3
4226	air	3	9	4	4226	4227	4245	4244	5226	5227	5245	5244	3
4227	air	4	9	4	4227	4228	4246	4245	5227	5228	5246	5245	3
4228	air	5	9	4	4228	4229	4247	4246	5228	5229	5247	5246	3
4229	air	6	9	4	4229	4230	4248	4247	5229	5230	5248	5247	3
4230	air	7	9	4	4230	4231	4249	4248	5230	5231	5249	5248	3
4231	air	8	9	4	4231	4232	4250	4249	5231	5232	5250	5249	3
4232	air	9	9	4	4232	4233	4251	4250	5232	5233	5251	5250	3
4233	air	10	9	4	4233	4234	4252	4251	5233	5234	5252	5251	3



**Table 10 - FEM Conversion Table for Leg of Lamb at Z = 5 cm**

Element Number	Tissue type	Location			Nodes on this slice				Nodes on slice above				Mesh Color
		X	Y	Z	LL	LR	UR	UL	LL	LR	UR	UL	
5001	air	-6	-3	5	5001	5002	5020	5019	6001	6002	6020	6019	3
5002	air	-5	-3	5	5002	5003	5021	5020	6002	6003	6021	6020	3
5003	air	-4	-3	5	5003	5004	5022	5021	6003	6004	6022	6021	3
5004	air	-3	-3	5	5004	5005	5023	5022	6004	6005	6023	6022	3
5005	air	-2	-3	5	5005	5006	5024	5023	6005	6006	6024	6023	3
5006	air	-1	-3	5	5006	5007	5025	5024	6006	6007	6025	6024	3
5007	air	0	-3	5	5007	5008	5026	5025	6007	6008	6026	6025	3
5008	air	1	-3	5	5008	5009	5027	5026	6008	6009	6027	6026	3
5009	air	2	-3	5	5009	5010	5028	5027	6009	6010	6028	6027	3
5010	air	3	-3	5	5010	5011	5029	5028	6010	6011	6029	6028	3
5011	air	4	-3	5	5011	5012	5030	5029	6011	6012	6030	6029	3
5012	air	5	-3	5	5012	5013	5031	5030	6012	6013	6031	6030	3
5013	air	6	-3	5	5013	5014	5032	5031	6013	6014	6032	6031	3
5014	air	7	-3	5	5014	5015	5033	5032	6014	6015	6033	6032	3
5015	air	8	-3	5	5015	5016	5034	5033	6015	6016	6034	6033	3
5016	air	9	-3	5	5016	5017	5035	5034	6016	6017	6035	6034	3
5017	air	10	-3	5	5017	5018	5036	5035	6017	6018	6036	6035	3
5019	air	-6	-2	5	5019	5020	5038	5037	6019	6020	6038	6037	3
5020	fat	-5	-2	5	5020	5021	5039	5038	6020	6021	6039	6038	8
5021	bone	-4	-2	5	5021	5022	5040	5039	6021	6022	6040	6039	15
5022	bone	-3	-2	5	5022	5023	5041	5040	6022	6023	6041	6040	15
5023	bone	-2	-2	5	5023	5024	5042	5041	6023	6024	6042	6041	15
5024	fat	-1	-2	5	5024	5025	5043	5042	6024	6025	6043	6042	8
5025	fat	0	-2	5	5025	5026	5044	5043	6025	6026	6044	6043	8
5026	muscle	1	-2	5	5026	5027	5045	5044	6026	6027	6045	6044	11
5027	muscle	2	-2	5	5027	5028	5046	5045	6027	6028	6046	6045	11
5028	muscle	3	-2	5	5028	5029	5047	5046	6028	6029	6047	6046	11
5029	air	4	-2	5	5029	5030	5048	5047	6029	6030	6048	6047	3
5030	air	5	-2	5	5030	5031	5049	5048	6030	6031	6049	6048	3
5031	air	6	-2	5	5031	5032	5050	5049	6031	6032	6050	6049	3
5032	air	7	-2	5	5032	5033	5051	5050	6032	6033	6051	6050	3
5033	air	8	-2	5	5033	5034	5052	5051	6033	6034	6052	6051	3
5034	air	9	-2	5	5034	5035	5053	5052	6034	6035	6053	6052	3
5035	air	10	-2	5	5035	5036	5054	5053	6035	6036	6054	6053	3
5037	air	-6	-1	5	5037	5038	5056	5055	6037	6038	6056	6055	3
5038	fat	-5	-1	5	5038	5039	5057	5056	6038	6039	6057	6056	8
5039	bone	-4	-1	5	5039	5040	5058	5057	6039	6040	6058	6057	15

Element Number	Tissue type	Location			Nodes on this slice				Nodes on slice above				Mesh Color
		X	Y	Z	LL	LR	UR	UL	LL	LR	UR	UL	
5040	bone	-3	-1	5	5040	5041	5059	5058	6040	6041	6059	6058	15
5041	bone	-2	-1	5	5041	5042	5060	5059	6041	6042	6060	6059	15
5042	bone	-1	-1	5	5042	5043	5061	5060	6042	6043	6061	6060	15
5043	bone	0	-1	5	5043	5044	5062	5061	6043	6044	6062	6061	15
5044	muscle	1	-1	5	5044	5045	5063	5062	6044	6045	6063	6062	11
5045	muscle	2	-1	5	5045	5046	5064	5063	6045	6046	6064	6063	11
5046	muscle	3	-1	5	5046	5047	5065	5064	6046	6047	6065	6064	11
5047	muscle	4	-1	5	5047	5048	5066	5065	6047	6048	6066	6065	11
5048	muscle	5	-1	5	5048	5049	5067	5066	6048	6049	6067	6066	11
5049	muscle	6	-1	5	5049	5050	5068	5067	6049	6050	6068	6067	11
5050	air	7	-1	5	5050	5051	5069	5068	6050	6051	6069	6068	3
5051	air	8	-1	5	5051	5052	5070	5069	6051	6052	6070	6069	3
5052	air	9	-1	5	5052	5053	5071	5070	6052	6053	6071	6070	3
5053	air	10	-1	5	5053	5054	5072	5071	6053	6054	6072	6071	3
5055	air	-6	0	5	5055	5056	5074	5073	6055	6056	6074	6073	3
5056	fat	-5	0	5	5056	5057	5075	5074	6056	6057	6075	6074	8
5057	fat	-4	0	5	5057	5058	5076	5075	6057	6058	6076	6075	8
5058	bone	-3	0	5	5058	5059	5077	5076	6058	6059	6077	6076	15
5059	bone	-2	0	5	5059	5060	5078	5077	6059	6060	6078	6077	15
5060	bone	-1	0	5	5060	5061	5079	5078	6060	6061	6079	6078	15
5061	bone	0	0	5	5061	5062	5080	5079	6061	6062	6080	6079	15
5062	muscle	1	0	5	5062	5063	5081	5080	6062	6063	6081	6080	11
5063	muscle	2	0	5	5063	5064	5082	5081	6063	6064	6082	6081	11
5064	muscle	3	0	5	5064	5065	5083	5082	6064	6065	6083	6082	11
5065	muscle	4	0	5	5065	5066	5084	5083	6065	6066	6084	6083	11
5066	muscle	5	0	5	5066	5067	5085	5084	6066	6067	6085	6084	11
5067	muscle	6	0	5	5067	5068	5086	5085	6067	6068	6086	6085	11
5068	muscle	7	0	5	5068	5069	5087	5086	6068	6069	6087	6086	11
5069	air	8	0	5	5069	5070	5088	5087	6069	6070	6088	6087	3
5070	air	9	0	5	5070	5071	5089	5088	6070	6071	6089	6088	3
5071	air	10	0	5	5071	5072	5090	5089	6071	6072	6090	6089	3
5073	air	-6	1	5	5073	5074	5092	5091	6073	6074	6092	6091	3
5074	fat	-5	1	5	5074	5075	5093	5092	6074	6075	6093	6092	8
5075	fat	-4	1	5	5075	5076	5094	5093	6075	6076	6094	6093	8
5076	fat	-3	1	5	5076	5077	5095	5094	6076	6077	6095	6094	8
5077	bone	-2	1	5	5077	5078	5096	5095	6077	6078	6096	6095	15
5078	muscle	-1	1	5	5078	5079	5097	5096	6078	6079	6097	6096	11
5079	muscle	0	1	5	5079	5080	5098	5097	6079	6080	6098	6097	11

Element Number	Tissue type	Location			Nodes on this slice				Nodes on slice above				Mesh Color
		X	Y	Z	LL	LR	UR	UL	LL	LR	UR	UL	
5080	muscle	1	1	5	5080	5081	5099	5098	6080	6081	6099	6098	11
5081	fat	2	1	5	5081	5082	5100	5099	6081	6082	6100	6099	8
5082	muscle	3	1	5	5082	5083	5101	5100	6082	6083	6101	6100	11
5083	muscle	4	1	5	5083	5084	5102	5101	6083	6084	6102	6101	11
5084	muscle	5	1	5	5084	5085	5103	5102	6084	6085	6103	6102	11
5085	muscle	6	1	5	5085	5086	5104	5103	6085	6086	6104	6103	11
5086	muscle	7	1	5	5086	5087	5105	5104	6086	6087	6105	6104	11
5087	muscle	8	1	5	5087	5088	5106	5105	6087	6088	6106	6105	11
5088	air	9	1	5	5088	5089	5107	5106	6088	6089	6107	6106	3
5089	air	10	1	5	5089	5090	5108	5107	6089	6090	6108	6107	3
5091	air	-6	2	5	5091	5092	5110	5109	6091	6092	6110	6109	3
5092	air	-5	2	5	5092	5093	5111	5110	6092	6093	6111	6110	3
5093	fat	-4	2	5	5093	5094	5112	5111	6093	6094	6112	6111	8
5094	muscle	-3	2	5	5094	5095	5113	5112	6094	6095	6113	6112	11
5095	muscle	-2	2	5	5095	5096	5114	5113	6095	6096	6114	6113	11
5096	muscle	-1	2	5	5096	5097	5115	5114	6096	6097	6115	6114	11
5097	muscle	0	2	5	5097	5098	5116	5115	6097	6098	6116	6115	11
5098	fat	1	2	5	5098	5099	5117	5116	6098	6099	6117	6116	8
5099	fat	2	2	5	5099	5100	5118	5117	6099	6100	6118	6117	8
5100	muscle	3	2	5	5100	5101	5119	5118	6100	6101	6119	6118	11
5101	muscle	4	2	5	5101	5102	5120	5119	6101	6102	6120	6119	11
5102	muscle	5	2	5	5102	5103	5121	5120	6102	6103	6121	6120	11
5103	muscle	6	2	5	5103	5104	5122	5121	6103	6104	6122	6121	11
5104	muscle	7	2	5	5104	5105	5123	5122	6104	6105	6123	6122	11
5105	fat	8	2	5	5105	5106	5124	5123	6105	6106	6124	6123	8
5106	air	9	2	5	5106	5107	5125	5124	6106	6107	6125	6124	3
5107	air	10	2	5	5107	5108	5126	5125	6107	6108	6126	6125	3
5109	air	-6	3	5	5109	5110	5128	5127	6109	6110	6128	6127	3
5110	air	-5	3	5	5110	5111	5129	5128	6110	6111	6129	6128	3
5111	muscle	-4	3	5	5111	5112	5130	5129	6111	6112	6130	6129	11
5112	muscle	-3	3	5	5112	5113	5131	5130	6112	6113	6131	6130	11
5113	muscle	-2	3	5	5113	5114	5132	5131	6113	6114	6132	6131	11
5114	muscle	-1	3	5	5114	5115	5133	5132	6114	6115	6133	6132	11
5115	muscle	0	3	5	5115	5116	5134	5133	6115	6116	6134	6133	11
5116	fat	1	3	5	5116	5117	5135	5134	6116	6117	6135	6134	8
5117	fat	2	3	5	5117	5118	5136	5135	6117	6118	6136	6135	8
5118	muscle	3	3	5	5118	5119	5137	5136	6118	6119	6137	6136	11
5119	muscle	4	3	5	5119	5120	5138	5137	6119	6120	6138	6137	11

Element Number	Tissue type	Location			Nodes on this slice				Nodes on slice above				Mesh Color
		X	Y	Z	LL	LR	UR	UL	LL	LR	UR	UL	
5120	muscle	5	3	5	5120	5121	5139	5138	6120	6121	6139	6138	11
5121	muscle	6	3	5	5121	5122	5140	5139	6121	6122	6140	6139	11
5122	fat	7	3	5	5122	5123	5141	5140	6122	6123	6141	6140	8
5123	fat	8	3	5	5123	5124	5142	5141	6123	6124	6142	6141	8
5124	air	9	3	5	5124	5125	5143	5142	6124	6125	6143	6142	3
5125	air	10	3	5	5125	5126	5144	5143	6125	6126	6144	6143	3
5127	air	-6	4	5	5127	5128	5146	5145	6127	6128	6146	6145	3
5128	air	-5	4	5	5128	5129	5147	5146	6128	6129	6147	6146	3
5129	air	-4	4	5	5129	5130	5148	5147	6129	6130	6148	6147	3
5130	muscle	-3	4	5	5130	5131	5149	5148	6130	6131	6149	6148	11
5131	muscle	-2	4	5	5131	5132	5150	5149	6131	6132	6150	6149	11
5132	muscle	-1	4	5	5132	5133	5151	5150	6132	6133	6151	6150	11
5133	muscle	0	4	5	5133	5134	5152	5151	6133	6134	6152	6151	11
5134	muscle	1	4	5	5134	5135	5153	5152	6134	6135	6153	6152	11
5135	muscle	2	4	5	5135	5136	5154	5153	6135	6136	6154	6153	11
5136	muscle	3	4	5	5136	5137	5155	5154	6136	6137	6155	6154	11
5137	muscle	4	4	5	5137	5138	5156	5155	6137	6138	6156	6155	11
5138	muscle	5	4	5	5138	5139	5157	5156	6138	6139	6157	6156	11
5139	muscle	6	4	5	5139	5140	5158	5157	6139	6140	6158	6157	11
5140	fat	7	4	5	5140	5141	5159	5158	6140	6141	6159	6158	8
5141	air	8	4	5	5141	5142	5160	5159	6141	6142	6160	6159	3
5142	air	9	4	5	5142	5143	5161	5160	6142	6143	6161	6160	3
5143	air	10	4	5	5143	5144	5162	5161	6143	6144	6162	6161	3
5145	air	-6	5	5	5145	5146	5164	5163	6145	6146	6164	6163	3
5146	air	-5	5	5	5146	5147	5165	5164	6146	6147	6165	6164	3
5147	air	-4	5	5	5147	5148	5166	5165	6147	6148	6166	6165	3
5148	air	-3	5	5	5148	5149	5167	5166	6148	6149	6167	6166	3
5149	muscle	-2	5	5	5149	5150	5168	5167	6149	6150	6168	6167	11
5150	muscle	-1	5	5	5150	5151	5169	5168	6150	6151	6169	6168	11
5151	muscle	0	5	5	5151	5152	5170	5169	6151	6152	6170	6169	11
5152	muscle	1	5	5	5152	5153	5171	5170	6152	6153	6171	6170	11
5153	muscle	2	5	5	5153	5154	5172	5171	6153	6154	6172	6171	11
5154	muscle	3	5	5	5154	5155	5173	5172	6154	6155	6173	6172	11
5155	fat	4	5	5	5155	5156	5174	5173	6155	6156	6174	6173	8
5156	fat	5	5	5	5156	5157	5175	5174	6156	6157	6175	6174	8
5157	air	6	5	5	5157	5158	5176	5175	6157	6158	6176	6175	3
5158	air	7	5	5	5158	5159	5177	5176	6158	6159	6177	6176	3
5159	air	8	5	5	5159	5160	5178	5177	6159	6160	6178	6177	3

Element Number	Tissue type	Location			Nodes on this slice				Nodes on slice above				Mesh Color
		X	Y	Z	LL	LR	UR	UL	LL	LR	UR	UL	
5160	air	9	5	5	5160	5161	5179	5178	6160	6161	6179	6178	3
5161	air	10	5	5	5161	5162	5180	5179	6161	6162	6180	6179	3
5163	air	-6	6	5	5163	5164	5182	5181	6163	6164	6182	6181	3
5164	air	-5	6	5	5164	5165	5183	5182	6164	6165	6183	6182	3
5165	air	-4	6	5	5165	5166	5184	5183	6165	6166	6184	6183	3
5166	air	-3	6	5	5166	5167	5185	5184	6166	6167	6185	6184	3
5167	air	-2	6	5	5167	5168	5186	5185	6167	6168	6186	6185	3
5168	muscle	-1	6	5	5168	5169	5187	5186	6168	6169	6187	6186	11
5169	fat	0	6	5	5169	5170	5188	5187	6169	6170	6188	6187	8
5170	fat	1	6	5	5170	5171	5189	5188	6170	6171	6189	6188	8
5171	muscle	2	6	5	5171	5172	5190	5189	6171	6172	6190	6189	11
5172	air	3	6	5	5172	5173	5191	5190	6172	6173	6191	6190	3
5173	air	4	6	5	5173	5174	5192	5191	6173	6174	6192	6191	3
5174	air	5	6	5	5174	5175	5193	5192	6174	6175	6193	6192	3
5175	air	6	6	5	5175	5176	5194	5193	6175	6176	6194	6193	3
5176	air	7	6	5	5176	5177	5195	5194	6176	6177	6195	6194	3
5177	air	8	6	5	5177	5178	5196	5195	6177	6178	6196	6195	3
5178	air	9	6	5	5178	5179	5197	5196	6178	6179	6197	6196	3
5179	air	10	6	5	5179	5180	5198	5197	6179	6180	6198	6197	3
5181	air	-6	7	5	5181	5182	5200	5199	6181	6182	6200	6199	3
5182	air	-5	7	5	5182	5183	5201	5200	6182	6183	6201	6200	3
5183	air	-4	7	5	5183	5184	5202	5201	6183	6184	6202	6201	3
5184	air	-3	7	5	5184	5185	5203	5202	6184	6185	6203	6202	3
5185	air	-2	7	5	5185	5186	5204	5203	6185	6186	6204	6203	3
5186	air	-1	7	5	5186	5187	5205	5204	6186	6187	6205	6204	3
5187	air	0	7	5	5187	5188	5206	5205	6187	6188	6206	6205	3
5188	air	1	7	5	5188	5189	5207	5206	6188	6189	6207	6206	3
5189	air	2	7	5	5189	5190	5208	5207	6189	6190	6208	6207	3
5190	air	3	7	5	5190	5191	5209	5208	6190	6191	6209	6208	3
5191	air	4	7	5	5191	5192	5210	5209	6191	6192	6210	6209	3
5192	air	5	7	5	5192	5193	5211	5210	6192	6193	6211	6210	3
5193	air	6	7	5	5193	5194	5212	5211	6193	6194	6212	6211	3
5194	air	7	7	5	5194	5195	5213	5212	6194	6195	6213	6212	3
5195	air	8	7	5	5195	5196	5214	5213	6195	6196	6214	6213	3
5196	air	9	7	5	5196	5197	5215	5214	6196	6197	6215	6214	3
5197	air	10	7	5	5197	5198	5216	5215	6197	6198	6216	6215	3
5199	air	-6	8	5	5199	5200	5218	5217	6199	6200	6218	6217	3
5200	air	-5	8	5	5200	5201	5219	5218	6200	6201	6219	6218	3

Element Number	Tissue type	Location			Nodes on this slice				Nodes on slice above				Mesh Color
		X	Y	Z	LL	LR	UR	UL	LL	LR	UR	UL	
5201	air	-4	8	5	5201	5202	5220	5219	6201	6202	6220	6219	3
5202	air	-3	8	5	5202	5203	5221	5220	6202	6203	6221	6220	3
5203	air	-2	8	5	5203	5204	5222	5221	6203	6204	6222	6221	3
5204	air	-1	8	5	5204	5205	5223	5222	6204	6205	6223	6222	3
5205	air	0	8	5	5205	5206	5224	5223	6205	6206	6224	6223	3
5206	air	1	8	5	5206	5207	5225	5224	6206	6207	6225	6224	3
5207	air	2	8	5	5207	5208	5226	5225	6207	6208	6226	6225	3
5208	air	3	8	5	5208	5209	5227	5226	6208	6209	6227	6226	3
5209	air	4	8	5	5209	5210	5228	5227	6209	6210	6228	6227	3
5210	air	5	8	5	5210	5211	5229	5228	6210	6211	6229	6228	3
5211	air	6	8	5	5211	5212	5230	5229	6211	6212	6230	6229	3
5212	air	7	8	5	5212	5213	5231	5230	6212	6213	6231	6230	3
5213	air	8	8	5	5213	5214	5232	5231	6213	6214	6232	6231	3
5214	air	9	8	5	5214	5215	5233	5232	6214	6215	6233	6232	3
5215	air	10	8	5	5215	5216	5234	5233	6215	6216	6234	6233	3
5217	air	-6	9	5	5217	5218	5236	5235	6217	6218	6236	6235	3
5218	air	-5	9	5	5218	5219	5237	5236	6218	6219	6237	6236	3
5219	air	-4	9	5	5219	5220	5238	5237	6219	6220	6238	6237	3
5220	air	-3	9	5	5220	5221	5239	5238	6220	6221	6239	6238	3
5221	air	-2	9	5	5221	5222	5240	5239	6221	6222	6240	6239	3
5222	air	-1	9	5	5222	5223	5241	5240	6222	6223	6241	6240	3
5223	air	0	9	5	5223	5224	5242	5241	6223	6224	6242	6241	3
5224	air	1	9	5	5224	5225	5243	5242	6224	6225	6243	6242	3
5225	air	2	9	5	5225	5226	5244	5243	6225	6226	6244	6243	3
5226	air	3	9	5	5226	5227	5245	5244	6226	6227	6245	6244	3
5227	air	4	9	5	5227	5228	5246	5245	6227	6228	6246	6245	3
5228	air	5	9	5	5228	5229	5247	5246	6228	6229	6247	6246	3
5229	air	6	9	5	5229	5230	5248	5247	6229	6230	6248	6247	3
5230	air	7	9	5	5230	5231	5249	5248	6230	6231	6249	6248	3
5231	air	8	9	5	5231	5232	5250	5249	6231	6232	6250	6249	3
5232	air	9	9	5	5232	5233	5251	5250	6232	6233	6251	6250	3
5233	air	10	9	5	5233	5234	5252	5251	6233	6234	6252	6251	3

**Table 11 - FEM Conversion Table for Leg of Lamb at Z = 6 cm**

Element Number	Tissue type	Location			Nodes on this slice				Nodes on slice above				Mesh Color
		X	Y	Z	LL	LR	UR	UL	LL	LR	UR	UL	
6001	air	-6	-3	6	6001	6002	6020	6019	7001	7002	7020	7019	3
6002	air	-5	-3	6	6002	6003	6021	6020	7002	7003	7021	7020	3
6003	air	-4	-3	6	6003	6004	6022	6021	7003	7004	7022	7021	3
6004	air	-3	-3	6	6004	6005	6023	6022	7004	7005	7023	7022	3
6005	air	-2	-3	6	6005	6006	6024	6023	7005	7006	7024	7023	3
6006	air	-1	-3	6	6006	6007	6025	6024	7006	7007	7025	7024	3
6007	air	0	-3	6	6007	6008	6026	6025	7007	7008	7026	7025	3
6008	air	1	-3	6	6008	6009	6027	6026	7008	7009	7027	7026	3
6009	air	2	-3	6	6009	6010	6028	6027	7009	7010	7028	7027	3
6010	air	3	-3	6	6010	6011	6029	6028	7010	7011	7029	7028	3
6011	air	4	-3	6	6011	6012	6030	6029	7011	7012	7030	7029	3
6012	air	5	-3	6	6012	6013	6031	6030	7012	7013	7031	7030	3
6013	air	6	-3	6	6013	6014	6032	6031	7013	7014	7032	7031	3
6014	air	7	-3	6	6014	6015	6033	6032	7014	7015	7033	7032	3
6015	air	8	-3	6	6015	6016	6034	6033	7015	7016	7034	7033	3
6016	air	9	-3	6	6016	6017	6035	6034	7016	7017	7035	7034	3
6017	air	10	-3	6	6017	6018	6036	6035	7017	7018	7036	7035	3
6019	air	-6	-2	6	6019	6020	6038	6037	7019	7020	7038	7037	3
6020	bone	-5	-2	6	6020	6021	6039	6038	7020	7021	7039	7038	15
6021	fat	-4	-2	6	6021	6022	6040	6039	7021	7022	7040	7039	8
6022	air	-3	-2	6	6022	6023	6041	6040	7022	7023	7041	7040	3
6023	air	-2	-2	6	6023	6024	6042	6041	7023	7024	7042	7041	3
6024	air	-1	-2	6	6024	6025	6043	6042	7024	7025	7043	7042	3
6025	air	0	-2	6	6025	6026	6044	6043	7025	7026	7044	7043	3
6026	air	1	-2	6	6026	6027	6045	6044	7026	7027	7045	7044	3
6027	air	2	-2	6	6027	6028	6046	6045	7027	7028	7046	7045	3
6028	air	3	-2	6	6028	6029	6047	6046	7028	7029	7047	7046	3
6029	air	4	-2	6	6029	6030	6048	6047	7029	7030	7048	7047	3
6030	air	5	-2	6	6030	6031	6049	6048	7030	7031	7049	7048	3
6031	air	6	-2	6	6031	6032	6050	6049	7031	7032	7050	7049	3
6032	air	7	-2	6	6032	6033	6051	6050	7032	7033	7051	7050	3
6033	air	8	-2	6	6033	6034	6052	6051	7033	7034	7052	7051	3
6034	air	9	-2	6	6034	6035	6053	6052	7034	7035	7053	7052	3
6035	air	10	-2	6	6035	6036	6054	6053	7035	7036	7054	7053	3
6037	fat	-6	-1	6	6037	6038	6056	6055	7037	7038	7056	7055	8
6038	bone	-5	-1	6	6038	6039	6057	6056	7038	7039	7057	7056	15
6039	bone	-4	-1	6	6039	6040	6058	6057	7039	7040	7058	7057	15

Element Number	Tissue type	Location			Nodes on this slice				Nodes on slice above				Mesh Color
		X	Y	Z	LL	LR	UR	UL	LL	LR	UR	UL	
6040	bone	-3	-1	6	6040	6041	6059	6058	7040	7041	7059	7058	15
6041	bone	-2	-1	6	6041	6042	6060	6059	7041	7042	7060	7059	15
6042	bone	-1	-1	6	6042	6043	6061	6060	7042	7043	7061	7060	15
6043	bone	0	-1	6	6043	6044	6062	6061	7043	7044	7062	7061	15
6044	muscle	1	-1	6	6044	6045	6063	6062	7044	7045	7063	7062	11
6045	muscle	2	-1	6	6045	6046	6064	6063	7045	7046	7064	7063	11
6046	muscle	3	-1	6	6046	6047	6065	6064	7046	7047	7065	7064	11
6047	muscle	4	-1	6	6047	6048	6066	6065	7047	7048	7066	7065	11
6048	air	5	-1	6	6048	6049	6067	6066	7048	7049	7067	7066	3
6049	air	6	-1	6	6049	6050	6068	6067	7049	7050	7068	7067	3
6050	air	7	-1	6	6050	6051	6069	6068	7050	7051	7069	7068	3
6051	air	8	-1	6	6051	6052	6070	6069	7051	7052	7070	7069	3
6052	air	9	-1	6	6052	6053	6071	6070	7052	7053	7071	7070	3
6053	air	10	-1	6	6053	6054	6072	6071	7053	7054	7072	7071	3
6055	fat	-6	0	6	6055	6056	6074	6073	7055	7056	7074	7073	8
6056	fat	-5	0	6	6056	6057	6075	6074	7056	7057	7075	7074	8
6057	fat	-4	0	6	6057	6058	6076	6075	7057	7058	7076	7075	8
6058	bone	-3	0	6	6058	6059	6077	6076	7058	7059	7077	7076	15
6059	bone	-2	0	6	6059	6060	6078	6077	7059	7060	7078	7077	15
6060	bone	-1	0	6	6060	6061	6079	6078	7060	7061	7079	7078	15
6061	bone	0	0	6	6061	6062	6080	6079	7061	7062	7080	7079	15
6062	muscle	1	0	6	6062	6063	6081	6080	7062	7063	7081	7080	11
6063	muscle	2	0	6	6063	6064	6082	6081	7063	7064	7082	7081	11
6064	muscle	3	0	6	6064	6065	6083	6082	7064	7065	7083	7082	11
6065	muscle	4	0	6	6065	6066	6084	6083	7065	7066	7084	7083	11
6066	muscle	5	0	6	6066	6067	6085	6084	7066	7067	7085	7084	11
6067	muscle	6	0	6	6067	6068	6086	6085	7067	7068	7086	7085	11
6068	muscle	7	0	6	6068	6069	6087	6086	7068	7069	7087	7086	11
6069	muscle	8	0	6	6069	6070	6088	6087	7069	7070	7088	7087	11
6070	muscle	9	0	6	6070	6071	6089	6088	7070	7071	7089	7088	11
6071	air	10	0	6	6071	6072	6090	6089	7071	7072	7090	7089	3
6073	air	-6	1	6	6073	6074	6092	6091	7073	7074	7092	7091	3
6074	fat	-5	1	6	6074	6075	6093	6092	7074	7075	7093	7092	8
6075	fat	-4	1	6	6075	6076	6094	6093	7075	7076	7094	7093	8
6076	fat	-3	1	6	6076	6077	6095	6094	7076	7077	7095	7094	8
6077	bone	-2	1	6	6077	6078	6096	6095	7077	7078	7096	7095	15
6078	bone	-1	1	6	6078	6079	6097	6096	7078	7079	7097	7096	15
6079	muscle	0	1	6	6079	6080	6098	6097	7079	7080	7098	7097	11



Element Number	Tissue type	Location			Nodes on this slice				Nodes on slice above				Mesh Color
		X	Y	Z	LL	LR	UR	UL	LL	LR	UR	UL	
6080	fat	1	1	6	6080	6081	6099	6098	7080	7081	7099	7098	8
6081	muscle	2	1	6	6081	6082	6100	6099	7081	7082	7100	7099	11
6082	muscle	3	1	6	6082	6083	6101	6100	7082	7083	7101	7100	11
6083	muscle	4	1	6	6083	6084	6102	6101	7083	7084	7102	7101	11
6084	muscle	5	1	6	6084	6085	6103	6102	7084	7085	7103	7102	11
6085	muscle	6	1	6	6085	6086	6104	6103	7085	7086	7104	7103	11
6086	muscle	7	1	6	6086	6087	6105	6104	7086	7087	7105	7104	11
6087	muscle	8	1	6	6087	6088	6106	6105	7087	7088	7106	7105	11
6088	muscle	9	1	6	6088	6089	6107	6106	7088	7089	7107	7106	11
6089	air	10	1	6	6089	6090	6108	6107	7089	7090	7108	7107	3
6091	air	-6	2	6	6091	6092	6110	6109	7091	7092	7110	7109	3
6092	fat	-5	2	6	6092	6093	6111	6110	7092	7093	7111	7110	8
6093	muscle	-4	2	6	6093	6094	6112	6111	7093	7094	7112	7111	11
6094	muscle	-3	2	6	6094	6095	6113	6112	7094	7095	7113	7112	11
6095	fat	-2	2	6	6095	6096	6114	6113	7095	7096	7114	7113	8
6096	muscle	-1	2	6	6096	6097	6115	6114	7096	7097	7115	7114	11
6097	muscle	0	2	6	6097	6098	6116	6115	7097	7098	7116	7115	11
6098	fat	1	2	6	6098	6099	6117	6116	7098	7099	7117	7116	8
6099	fat	2	2	6	6099	6100	6118	6117	7099	7100	7118	7117	8
6100	muscle	3	2	6	6100	6101	6119	6118	7100	7101	7119	7118	11
6101	muscle	4	2	6	6101	6102	6120	6119	7101	7102	7120	7119	11
6102	muscle	5	2	6	6102	6103	6121	6120	7102	7103	7121	7120	11
6103	muscle	6	2	6	6103	6104	6122	6121	7103	7104	7122	7121	11
6104	muscle	7	2	6	6104	6105	6123	6122	7104	7105	7123	7122	11
6105	muscle	8	2	6	6105	6106	6124	6123	7105	7106	7124	7123	11
6106	fat	9	2	6	6106	6107	6125	6124	7106	7107	7125	7124	8
6107	air	10	2	6	6107	6108	6126	6125	7107	7108	7126	7125	3
6109	air	-6	3	6	6109	6110	6128	6127	7109	7110	7128	7127	3
6110	air	-5	3	6	6110	6111	6129	6128	7110	7111	7129	7128	3
6111	muscle	-4	3	6	6111	6112	6130	6129	7111	7112	7130	7129	11
6112	muscle	-3	3	6	6112	6113	6131	6130	7112	7113	7131	7130	11
6113	muscle	-2	3	6	6113	6114	6132	6131	7113	7114	7132	7131	11
6114	muscle	-1	3	6	6114	6115	6133	6132	7114	7115	7133	7132	11
6115	muscle	0	3	6	6115	6116	6134	6133	7115	7116	7134	7133	11
6116	fat	1	3	6	6116	6117	6135	6134	7116	7117	7135	7134	8
6117	fat	2	3	6	6117	6118	6136	6135	7117	7118	7136	7135	8
6118	fat	3	3	6	6118	6119	6137	6136	7118	7119	7137	7136	8
6119	muscle	4	3	6	6119	6120	6138	6137	7119	7120	7138	7137	11

Element Number	Tissue type	Location			Nodes on this slice				Nodes on slice above				Mesh Color
		X	Y	Z	LL	LR	UR	UL	LL	LR	UR	UL	
6120	muscle	5	3	6	6120	6121	6139	6138	7120	7121	7139	7138	11
6121	muscle	6	3	6	6121	6122	6140	6139	7121	7122	7140	7139	11
6122	muscle	7	3	6	6122	6123	6141	6140	7122	7123	7141	7140	11
6123	muscle	8	3	6	6123	6124	6142	6141	7123	7124	7142	7141	11
6124	fat	9	3	6	6124	6125	6143	6142	7124	7125	7143	7142	8
6125	air	10	3	6	6125	6126	6144	6143	7125	7126	7144	7143	3
6127	air	-6	4	6	6127	6128	6146	6145	7127	7128	7146	7145	3
6128	air	-5	4	6	6128	6129	6147	6146	7128	7129	7147	7146	3
6129	air	-4	4	6	6129	6130	6148	6147	7129	7130	7148	7147	3
6130	muscle	-3	4	6	6130	6131	6149	6148	7130	7131	7149	7148	11
6131	muscle	-2	4	6	6131	6132	6150	6149	7131	7132	7150	7149	11
6132	muscle	-1	4	6	6132	6133	6151	6150	7132	7133	7151	7150	11
6133	muscle	0	4	6	6133	6134	6152	6151	7133	7134	7152	7151	11
6134	muscle	1	4	6	6134	6135	6153	6152	7134	7135	7153	7152	11
6135	fat	2	4	6	6135	6136	6154	6153	7135	7136	7154	7153	8
6136	fat	3	4	6	6136	6137	6155	6154	7136	7137	7155	7154	8
6137	muscle	4	4	6	6137	6138	6156	6155	7137	7138	7156	7155	11
6138	muscle	5	4	6	6138	6139	6157	6156	7138	7139	7157	7156	11
6139	muscle	6	4	6	6139	6140	6158	6157	7139	7140	7158	7157	11
6140	muscle	7	4	6	6140	6141	6159	6158	7140	7141	7159	7158	11
6141	fat	8	4	6	6141	6142	6160	6159	7141	7142	7160	7159	8
6142	fat	9	4	6	6142	6143	6161	6160	7142	7143	7161	7160	8
6143	air	10	4	6	6143	6144	6162	6161	7143	7144	7162	7161	3
6145	air	-6	5	6	6145	6146	6164	6163	7145	7146	7164	7163	3
6146	air	-5	5	6	6146	6147	6165	6164	7146	7147	7165	7164	3
6147	air	-4	5	6	6147	6148	6166	6165	7147	7148	7166	7165	3
6148	air	-3	5	6	6148	6149	6167	6166	7148	7149	7167	7166	3
6149	muscle	-2	5	6	6149	6150	6168	6167	7149	7150	7168	7167	11
6150	muscle	-1	5	6	6150	6151	6169	6168	7150	7151	7169	7168	11
6151	muscle	0	5	6	6151	6152	6170	6169	7151	7152	7170	7169	11
6152	muscle	1	5	6	6152	6153	6171	6170	7152	7153	7171	7170	11
6153	muscle	2	5	6	6153	6154	6172	6171	7153	7154	7172	7171	11
6154	muscle	3	5	6	6154	6155	6173	6172	7154	7155	7173	7172	11
6155	muscle	4	5	6	6155	6156	6174	6173	7155	7156	7174	7173	11
6156	muscle	5	5	6	6156	6157	6175	6174	7156	7157	7175	7174	11
6157	muscle	6	5	6	6157	6158	6176	6175	7157	7158	7176	7175	11
6158	fat	7	5	6	6158	6159	6177	6176	7158	7159	7177	7176	8
6159	fat	8	5	6	6159	6160	6178	6177	7159	7160	7178	7177	8

Element Number	Tissue type	Location			Nodes on this slice				Nodes on slice above				Mesh Color
		X	Y	Z	LL	LR	UR	UL	LL	LR	UR	UL	
6160	air	9	5	6	6160	6161	6179	6178	7160	7161	7179	7178	3
6161	air	10	5	6	6161	6162	6180	6179	7161	7162	7180	7179	3
6163	air	-6	6	6	6163	6164	6182	6181	7163	7164	7182	7181	3
6164	air	-5	6	6	6164	6165	6183	6182	7164	7165	7183	7182	3
6165	air	-4	6	6	6165	6166	6184	6183	7165	7166	7184	7183	3
6166	air	-3	6	6	6166	6167	6185	6184	7166	7167	7185	7184	3
6167	fat	-2	6	6	6167	6168	6186	6185	7167	7168	7186	7185	8
6168	muscle	-1	6	6	6168	6169	6187	6186	7168	7169	7187	7186	11
6169	muscle	0	6	6	6169	6170	6188	6187	7169	7170	7188	7187	11
6170	fat	1	6	6	6170	6171	6189	6188	7170	7171	7189	7188	8
6171	muscle	2	6	6	6171	6172	6190	6189	7171	7172	7190	7189	11
6172	muscle	3	6	6	6172	6173	6191	6190	7172	7173	7191	7190	11
6173	fat	4	6	6	6173	6174	6192	6191	7173	7174	7192	7191	8
6174	fat	5	6	6	6174	6175	6193	6192	7174	7175	7193	7192	8
6175	fat	6	6	6	6175	6176	6194	6193	7175	7176	7194	7193	8
6176	air	7	6	6	6176	6177	6195	6194	7176	7177	7195	7194	3
6177	air	8	6	6	6177	6178	6196	6195	7177	7178	7196	7195	3
6178	air	9	6	6	6178	6179	6197	6196	7178	7179	7197	7196	3
6179	air	10	6	6	6179	6180	6198	6197	7179	7180	7198	7197	3
6181	air	-6	7	6	6181	6182	6200	6199	7181	7182	7200	7199	3
6182	air	-5	7	6	6182	6183	6201	6200	7182	7183	7201	7200	3
6183	air	-4	7	6	6183	6184	6202	6201	7183	7184	7202	7201	3
6184	air	-3	7	6	6184	6185	6203	6202	7184	7185	7203	7202	3
6185	air	-2	7	6	6185	6186	6204	6203	7185	7186	7204	7203	3
6186	air	-1	7	6	6186	6187	6205	6204	7186	7187	7205	7204	3
6187	air	0	7	6	6187	6188	6206	6205	7187	7188	7206	7205	3
6188	air	1	7	6	6188	6189	6207	6206	7188	7189	7207	7206	3
6189	air	2	7	6	6189	6190	6208	6207	7189	7190	7208	7207	3
6190	air	3	7	6	6190	6191	6209	6208	7190	7191	7209	7208	3
6191	air	4	7	6	6191	6192	6210	6209	7191	7192	7210	7209	3
6192	air	5	7	6	6192	6193	6211	6210	7192	7193	7211	7210	3
6193	air	6	7	6	6193	6194	6212	6211	7193	7194	7212	7211	3
6194	air	7	7	6	6194	6195	6213	6212	7194	7195	7213	7212	3
6195	air	8	7	6	6195	6196	6214	6213	7195	7196	7214	7213	3
6196	air	9	7	6	6196	6197	6215	6214	7196	7197	7215	7214	3
6197	air	10	7	6	6197	6198	6216	6215	7197	7198	7216	7215	3
6199	air	-6	8	6	6199	6200	6218	6217	7199	7200	7218	7217	3
6200	air	-5	8	6	6200	6201	6219	6218	7200	7201	7219	7218	3

Element Number	Tissue type	Location			Nodes on this slice				Nodes on slice above				Mesh Color
		X	Y	Z	LL	LR	UR	UL	LL	LR	UR	UL	
6201	air	-4	8	6	6201	6202	6220	6219	7201	7202	7220	7219	3
6202	air	-3	8	6	6202	6203	6221	6220	7202	7203	7221	7220	3
6203	air	-2	8	6	6203	6204	6222	6221	7203	7204	7222	7221	3
6204	air	-1	8	6	6204	6205	6223	6222	7204	7205	7223	7222	3
6205	air	0	8	6	6205	6206	6224	6223	7205	7206	7224	7223	3
6206	air	1	8	6	6206	6207	6225	6224	7206	7207	7225	7224	3
6207	air	2	8	6	6207	6208	6226	6225	7207	7208	7226	7225	3
6208	air	3	8	6	6208	6209	6227	6226	7208	7209	7227	7226	3
6209	air	4	8	6	6209	6210	6228	6227	7209	7210	7228	7227	3
6210	air	5	8	6	6210	6211	6229	6228	7210	7211	7229	7228	3
6211	air	6	8	6	6211	6212	6230	6229	7211	7212	7230	7229	3
6212	air	7	8	6	6212	6213	6231	6230	7212	7213	7231	7230	3
6213	air	8	8	6	6213	6214	6232	6231	7213	7214	7232	7231	3
6214	air	9	8	6	6214	6215	6233	6232	7214	7215	7233	7232	3
6215	air	10	8	6	6215	6216	6234	6233	7215	7216	7234	7233	3
6217	air	-6	9	6	6217	6218	6236	6235	7217	7218	7236	7235	3
6218	air	-5	9	6	6218	6219	6237	6236	7218	7219	7237	7236	3
6219	air	-4	9	6	6219	6220	6238	6237	7219	7220	7238	7237	3
6220	air	-3	9	6	6220	6221	6239	6238	7220	7221	7239	7238	3
6221	air	-2	9	6	6221	6222	6240	6239	7221	7222	7240	7239	3
6222	air	-1	9	6	6222	6223	6241	6240	7222	7223	7241	7240	3
6223	air	0	9	6	6223	6224	6242	6241	7223	7224	7242	7241	3
6224	air	1	9	6	6224	6225	6243	6242	7224	7225	7243	7242	3
6225	air	2	9	6	6225	6226	6244	6243	7225	7226	7244	7243	3
6226	air	3	9	6	6226	6227	6245	6244	7226	7227	7245	7244	3
6227	air	4	9	6	6227	6228	6246	6245	7227	7228	7246	7245	3
6228	air	5	9	6	6228	6229	6247	6246	7228	7229	7247	7246	3
6229	air	6	9	6	6229	6230	6248	6247	7229	7230	7248	7247	3
6230	air	7	9	6	6230	6231	6249	6248	7230	7231	7249	7248	3
6231	air	8	9	6	6231	6232	6250	6249	7231	7232	7250	7249	3
6232	air	9	9	6	6232	6233	6251	6250	7232	7233	7251	7250	3
6233	air	10	9	6	6233	6234	6252	6251	7233	7234	7252	7251	3

**Table 12 - FEM Conversion Table for Leg of Lamb at Z = 7 cm**

Element Number	Tissue Type	Location			Nodes on this slice				Nodes on slice above				Mesh Color
		X	Y	Z	LL	LR	UR	UL	LL	LR	UR	UL	
7001	air	-6	-3	7	7001	7002	7020	7019	8001	8002	8020	8019	3
7002	air	-5	-3	7	7002	7003	7021	7020	8002	8003	8021	8020	3
7003	fat	-4	-3	7	7003	7004	7022	7021	8003	8004	8022	8021	8
7004	air	-3	-3	7	7004	7005	7023	7022	8004	8005	8023	8022	3
7005	air	-2	-3	7	7005	7006	7024	7023	8005	8006	8024	8023	3
7006	air	-1	-3	7	7006	7007	7025	7024	8006	8007	8025	8024	3
7007	air	0	-3	7	7007	7008	7026	7025	8007	8008	8026	8025	3
7008	air	1	-3	7	7008	7009	7027	7026	8008	8009	8027	8026	3
7009	air	2	-3	7	7009	7010	7028	7027	8009	8010	8028	8027	3
7010	air	3	-3	7	7010	7011	7029	7028	8010	8011	8029	8028	3
7011	air	4	-3	7	7011	7012	7030	7029	8011	8012	8030	8029	3
7012	air	5	-3	7	7012	7013	7031	7030	8012	8013	8031	8030	3
7013	air	6	-3	7	7013	7014	7032	7031	8013	8014	8032	8031	3
7014	air	7	-3	7	7014	7015	7033	7032	8014	8015	8033	8032	3
7015	air	8	-3	7	7015	7016	7034	7033	8015	8016	8034	8033	3
7016	air	9	-3	7	7016	7017	7035	7034	8016	8017	8035	8034	3
7017	air	10	-3	7	7017	7018	7036	7035	8017	8018	8036	8035	3
7019	air	-6	-2	7	7019	7020	7038	7037	8019	8020	8038	8037	3
7020	fat	-5	-2	7	7020	7021	7039	7038	8020	8021	8039	8038	8
7021	fat	-4	-2	7	7021	7022	7040	7039	8021	8022	8040	8039	8
7022	muscle	-3	-2	7	7022	7023	7041	7040	8022	8023	8041	8040	11
7023	air	-2	-2	7	7023	7024	7042	7041	8023	8024	8042	8041	3
7024	air	-1	-2	7	7024	7025	7043	7042	8024	8025	8043	8042	3
7025	air	0	-2	7	7025	7026	7044	7043	8025	8026	8044	8043	3
7026	air	1	-2	7	7026	7027	7045	7044	8026	8027	8045	8044	3
7027	air	2	-2	7	7027	7028	7046	7045	8027	8028	8046	8045	3
7028	air	3	-2	7	7028	7029	7047	7046	8028	8029	8047	8046	3
7029	muscle	4	-2	7	7029	7030	7048	7047	8029	8030	8048	8047	11
7030	muscle	5	-2	7	7030	7031	7049	7048	8030	8031	8049	8048	11
7031	air	6	-2	7	7031	7032	7050	7049	8031	8032	8050	8049	3
7032	air	7	-2	7	7032	7033	7051	7050	8032	8033	8051	8050	3
7033	air	8	-2	7	7033	7034	7052	7051	8033	8034	8052	8051	3
7034	air	9	-2	7	7034	7035	7053	7052	8034	8035	8053	8052	3
7035	air	10	-2	7	7035	7036	7054	7053	8035	8036	8054	8053	3
7037	fat	-6	-1	7	7037	7038	7056	7055	8037	8038	8056	8055	8
7038	fat	-5	-1	7	7038	7039	7057	7056	8038	8039	8057	8056	8
7039	fat	-4	-1	7	7039	7040	7058	7057	8039	8040	8058	8057	8

Element Number	Tissue Type	Location			Nodes on this slice				Nodes on slice above				Mesh Color
		X	Y	Z	LL	LR	UR	UL	LL	LR	UR	UL	
7040	fat	-3	-1	7	7040	7041	7059	7058	8040	8041	8059	8058	8
7041	bone	-2	-1	7	7041	7042	7060	7059	8041	8042	8060	8059	15
7042	bone	-1	-1	7	7042	7043	7061	7060	8042	8043	8061	8060	15
7043	bone	0	-1	7	7043	7044	7062	7061	8043	8044	8062	8061	15
7044	muscle	1	-1	7	7044	7045	7063	7062	8044	8045	8063	8062	11
7045	muscle	2	-1	7	7045	7046	7064	7063	8045	8046	8064	8063	11
7046	muscle	3	-1	7	7046	7047	7065	7064	8046	8047	8065	8064	11
7047	muscle	4	-1	7	7047	7048	7066	7065	8047	8048	8066	8065	11
7048	muscle	5	-1	7	7048	7049	7067	7066	8048	8049	8067	8066	11
7049	muscle	6	-1	7	7049	7050	7068	7067	8049	8050	8068	8067	11
7050	muscle	7	-1	7	7050	7051	7069	7068	8050	8051	8069	8068	11
7051	muscle	8	-1	7	7051	7052	7070	7069	8051	8052	8070	8069	11
7052	air	9	-1	7	7052	7053	7071	7070	8052	8053	8071	8070	3
7053	air	10	-1	7	7053	7054	7072	7071	8053	8054	8072	8071	3
7055	fat	-6	0	7	7055	7056	7074	7073	8055	8056	8074	8073	8
7056	fat	-5	0	7	7056	7057	7075	7074	8056	8057	8075	8074	8
7057	muscle	-4	0	7	7057	7058	7076	7075	8057	8058	8076	8075	11
7058	bone	-3	0	7	7058	7059	7077	7076	8058	8059	8077	8076	15
7059	bone	-2	0	7	7059	7060	7078	7077	8059	8060	8078	8077	15
7060	bone	-1	0	7	7060	7061	7079	7078	8060	8061	8079	8078	15
7061	bone	0	0	7	7061	7062	7080	7079	8061	8062	8080	8079	15
7062	muscle	1	0	7	7062	7063	7081	7080	8062	8063	8081	8080	11
7063	muscle	2	0	7	7063	7064	7082	7081	8063	8064	8082	8081	11
7064	muscle	3	0	7	7064	7065	7083	7082	8064	8065	8083	8082	11
7065	muscle	4	0	7	7065	7066	7084	7083	8065	8066	8084	8083	11
7066	muscle	5	0	7	7066	7067	7085	7084	8066	8067	8085	8084	11
7067	muscle	6	0	7	7067	7068	7086	7085	8067	8068	8086	8085	11
7068	muscle	7	0	7	7068	7069	7087	7086	8068	8069	8087	8086	11
7069	muscle	8	0	7	7069	7070	7088	7087	8069	8070	8088	8087	11
7070	muscle	9	0	7	7070	7071	7089	7088	8070	8071	8089	8088	11
7071	air	10	0	7	7071	7072	7090	7089	8071	8072	8090	8089	3
7073	fat	-6	1	7	7073	7074	7092	7091	8073	8074	8092	8091	8
7074	muscle	-5	1	7	7074	7075	7093	7092	8074	8075	8093	8092	11
7075	muscle	-4	1	7	7075	7076	7094	7093	8075	8076	8094	8093	11
7076	muscle	-3	1	7	7076	7077	7095	7094	8076	8077	8095	8094	11
7077	bone	-2	1	7	7077	7078	7096	7095	8077	8078	8096	8095	15
7078	fat	-1	1	7	7078	7079	7097	7096	8078	8079	8097	8096	8
7079	fat	0	1	7	7079	7080	7098	7097	8079	8080	8098	8097	8

Element Number	Tissue Type	Location			Nodes on this slice				Nodes on slice above				Mesh Color
		X	Y	Z	LL	LR	UR	UL	LL	LR	UR	UL	
7080	fat	1	1	7	7080	7081	7099	7098	8080	8081	8099	8098	8
7081	fat	2	1	7	7081	7082	7100	7099	8081	8082	8100	8099	8
7082	muscle	3	1	7	7082	7083	7101	7100	8082	8083	8101	8100	11
7083	muscle	4	1	7	7083	7084	7102	7101	8083	8084	8102	8101	11
7084	muscle	5	1	7	7084	7085	7103	7102	8084	8085	8103	8102	11
7085	muscle	6	1	7	7085	7086	7104	7103	8085	8086	8104	8103	11
7086	muscle	7	1	7	7086	7087	7105	7104	8086	8087	8105	8104	11
7087	muscle	8	1	7	7087	7088	7106	7105	8087	8088	8106	8105	11
7088	muscle	9	1	7	7088	7089	7107	7106	8088	8089	8107	8106	11
7089	fat	10	1	7	7089	7090	7108	7107	8089	8090	8108	8107	8
7091	air	-6	2	7	7091	7092	7110	7109	8091	8092	8110	8109	3
7092	fat	-5	2	7	7092	7093	7111	7110	8092	8093	8111	8110	8
7093	muscle	-4	2	7	7093	7094	7112	7111	8093	8094	8112	8111	11
7094	muscle	-3	2	7	7094	7095	7113	7112	8094	8095	8113	8112	11
7095	fat	-2	2	7	7095	7096	7114	7113	8095	8096	8114	8113	8
7096	fat	-1	2	7	7096	7097	7115	7114	8096	8097	8115	8114	8
7097	fat	0	2	7	7097	7098	7116	7115	8097	8098	8116	8115	8
7098	fat	1	2	7	7098	7099	7117	7116	8098	8099	8117	8116	8
7099	fat	2	2	7	7099	7100	7118	7117	8099	8100	8118	8117	8
7100	fat	3	2	7	7100	7101	7119	7118	8100	8101	8119	8118	8
7101	muscle	4	2	7	7101	7102	7120	7119	8101	8102	8120	8119	11
7102	muscle	5	2	7	7102	7103	7121	7120	8102	8103	8121	8120	11
7103	muscle	6	2	7	7103	7104	7122	7121	8103	8104	8122	8121	11
7104	muscle	7	2	7	7104	7105	7123	7122	8104	8105	8123	8122	11
7105	muscle	8	2	7	7105	7106	7124	7123	8105	8106	8124	8123	11
7106	muscle	9	2	7	7106	7107	7125	7124	8106	8107	8125	8124	11
7107	fat	10	2	7	7107	7108	7126	7125	8107	8108	8126	8125	8
7109	air	-6	3	7	7109	7110	7128	7127	8109	8110	8128	8127	3
7110	fat	-5	3	7	7110	7111	7129	7128	8110	8111	8129	8128	8
7111	muscle	-4	3	7	7111	7112	7130	7129	8111	8112	8130	8129	11
7112	muscle	-3	3	7	7112	7113	7131	7130	8112	8113	8131	8130	11
7113	muscle	-2	3	7	7113	7114	7132	7131	8113	8114	8132	8131	11
7114	muscle	-1	3	7	7114	7115	7133	7132	8114	8115	8133	8132	11
7115	fat	0	3	7	7115	7116	7134	7133	8115	8116	8134	8133	8
7116	fat	1	3	7	7116	7117	7135	7134	8116	8117	8135	8134	8
7117	fat	2	3	7	7117	7118	7136	7135	8117	8118	8136	8135	8
7118	fat	3	3	7	7118	7119	7137	7136	8118	8119	8137	8136	8
7119	muscle	4	3	7	7119	7120	7138	7137	8119	8120	8138	8137	11

Element Number	Tissue Type	Location			Nodes on this slice				Nodes on slice above				Mesh Color
		X	Y	Z	LL	LR	UR	UL	LL	LR	UR	UL	
7120	muscle	5	3	7	7120	7121	7139	7138	8120	8121	8139	8138	11
7121	muscle	6	3	7	7121	7122	7140	7139	8121	8122	8140	8139	11
7122	muscle	7	3	7	7122	7123	7141	7140	8122	8123	8141	8140	11
7123	fat	8	3	7	7123	7124	7142	7141	8123	8124	8142	8141	8
7124	fat	9	3	7	7124	7125	7143	7142	8124	8125	8143	8142	8
7125	fat	10	3	7	7125	7126	7144	7143	8125	8126	8144	8143	8
7127	air	-6	4	7	7127	7128	7146	7145	8127	8128	8146	8145	3
7128	air	-5	4	7	7128	7129	7147	7146	8128	8129	8147	8146	3
7129	muscle	-4	4	7	7129	7130	7148	7147	8129	8130	8148	8147	11
7130	muscle	-3	4	7	7130	7131	7149	7148	8130	8131	8149	8148	11
7131	muscle	-2	4	7	7131	7132	7150	7149	8131	8132	8150	8149	11
7132	muscle	-1	4	7	7132	7133	7151	7150	8132	8133	8151	8150	11
7133	muscle	0	4	7	7133	7134	7152	7151	8133	8134	8152	8151	11
7134	muscle	1	4	7	7134	7135	7153	7152	8134	8135	8153	8152	11
7135	muscle	2	4	7	7135	7136	7154	7153	8135	8136	8154	8153	11
7136	muscle	3	4	7	7136	7137	7155	7154	8136	8137	8155	8154	11
7137	muscle	4	4	7	7137	7138	7156	7155	8137	8138	8156	8155	11
7138	muscle	5	4	7	7138	7139	7157	7156	8138	8139	8157	8156	11
7139	muscle	6	4	7	7139	7140	7158	7157	8139	8140	8158	8157	11
7140	muscle	7	4	7	7140	7141	7159	7158	8140	8141	8159	8158	11
7141	fat	8	4	7	7141	7142	7160	7159	8141	8142	8160	8159	8
7142	fat	9	4	7	7142	7143	7161	7160	8142	8143	8161	8160	8
7143	air	10	4	7	7143	7144	7162	7161	8143	8144	8162	8161	3
7145	air	-6	5	7	7145	7146	7164	7163	8145	8146	8164	8163	3
7146	air	-5	5	7	7146	7147	7165	7164	8146	8147	8165	8164	3
7147	air	-4	5	7	7147	7148	7166	7165	8147	8148	8166	8165	3
7148	muscle	-3	5	7	7148	7149	7167	7166	8148	8149	8167	8166	11
7149	muscle	-2	5	7	7149	7150	7168	7167	8149	8150	8168	8167	11
7150	muscle	-1	5	7	7150	7151	7169	7168	8150	8151	8169	8168	11
7151	muscle	0	5	7	7151	7152	7170	7169	8151	8152	8170	8169	11
7152	muscle	1	5	7	7152	7153	7171	7170	8152	8153	8171	8170	11
7153	muscle	2	5	7	7153	7154	7172	7171	8153	8154	8172	8171	11
7154	muscle	3	5	7	7154	7155	7173	7172	8154	8155	8173	8172	11
7155	muscle	4	5	7	7155	7156	7174	7173	8155	8156	8174	8173	11
7156	muscle	5	5	7	7156	7157	7175	7174	8156	8157	8175	8174	11
7157	fat	6	5	7	7157	7158	7176	7175	8157	8158	8176	8175	8
7158	fat	7	5	7	7158	7159	7177	7176	8158	8159	8177	8176	8
7159	air	8	5	7	7159	7160	7178	7177	8159	8160	8178	8177	3



Element Number	Tissue Type	Location			Nodes on this slice				Nodes on slice above				Mesh Color
		X	Y	Z	LL	LR	UR	UL	LL	LR	UR	UL	
7160	air	9	5	7	7160	7161	7179	7178	8160	8161	8179	8178	3
7161	air	10	5	7	7161	7162	7180	7179	8161	8162	8180	8179	3
7163	air	-6	6	7	7163	7164	7182	7181	8163	8164	8182	8181	3
7164	air	-5	6	7	7164	7165	7183	7182	8164	8165	8183	8182	3
7165	air	-4	6	7	7165	7166	7184	7183	8165	8166	8184	8183	3
7166	fat	-3	6	7	7166	7167	7185	7184	8166	8167	8185	8184	8
7167	muscle	-2	6	7	7167	7168	7186	7185	8167	8168	8186	8185	11
7168	muscle	-1	6	7	7168	7169	7187	7186	8168	8169	8187	8186	11
7169	muscle	0	6	7	7169	7170	7188	7187	8169	8170	8188	8187	11
7170	muscle	1	6	7	7170	7171	7189	7188	8170	8171	8189	8188	11
7171	fat	2	6	7	7171	7172	7190	7189	8171	8172	8190	8189	8
7172	muscle	3	6	7	7172	7173	7191	7190	8172	8173	8191	8190	11
7173	fat	4	6	7	7173	7174	7192	7191	8173	8174	8192	8191	8
7174	air	5	6	7	7174	7175	7193	7192	8174	8175	8193	8192	3
7175	air	6	6	7	7175	7176	7194	7193	8175	8176	8194	8193	3
7176	air	7	6	7	7176	7177	7195	7194	8176	8177	8195	8194	3
7177	air	8	6	7	7177	7178	7196	7195	8177	8178	8196	8195	3
7178	air	9	6	7	7178	7179	7197	7196	8178	8179	8197	8196	3
7179	air	10	6	7	7179	7180	7198	7197	8179	8180	8198	8197	3
7181	air	-6	7	7	7181	7182	7200	7199	8181	8182	8200	8199	3
7182	air	-5	7	7	7182	7183	7201	7200	8182	8183	8201	8200	3
7183	air	-4	7	7	7183	7184	7202	7201	8183	8184	8202	8201	3
7184	air	-3	7	7	7184	7185	7203	7202	8184	8185	8203	8202	3
7185	air	-2	7	7	7185	7186	7204	7203	8185	8186	8204	8203	3
7186	fat	-1	7	7	7186	7187	7205	7204	8186	8187	8205	8204	8
7187	fat	0	7	7	7187	7188	7206	7205	8187	8188	8206	8205	8
7188	fat	1	7	7	7188	7189	7207	7206	8188	8189	8207	8206	8
7189	fat	2	7	7	7189	7190	7208	7207	8189	8190	8208	8207	8
7190	air	3	7	7	7190	7191	7209	7208	8190	8191	8209	8208	3
7191	air	4	7	7	7191	7192	7210	7209	8191	8192	8210	8209	3
7192	air	5	7	7	7192	7193	7211	7210	8192	8193	8211	8210	3
7193	air	6	7	7	7193	7194	7212	7211	8193	8194	8212	8211	3
7194	air	7	7	7	7194	7195	7213	7212	8194	8195	8213	8212	3
7195	air	8	7	7	7195	7196	7214	7213	8195	8196	8214	8213	3
7196	air	9	7	7	7196	7197	7215	7214	8196	8197	8215	8214	3
7197	air	10	7	7	7197	7198	7216	7215	8197	8198	8216	8215	3
7199	air	-6	8	7	7199	7200	7218	7217	8199	8200	8218	8217	3
7200	air	-5	8	7	7200	7201	7219	7218	8200	8201	8219	8218	3

Element Number	Tissue Type	Location			Nodes on this slice				Nodes on slice above				Mesh Color
		X	Y	Z	LL	LR	UR	UL	LL	LR	UR	UL	
7201	air	-4	8	7	7201	7202	7220	7219	8201	8202	8220	8219	3
7202	air	-3	8	7	7202	7203	7221	7220	8202	8203	8221	8220	3
7203	air	-2	8	7	7203	7204	7222	7221	8203	8204	8222	8221	3
7204	air	-1	8	7	7204	7205	7223	7222	8204	8205	8223	8222	3
7205	air	0	8	7	7205	7206	7224	7223	8205	8206	8224	8223	3
7206	air	1	8	7	7206	7207	7225	7224	8206	8207	8225	8224	3
7207	air	2	8	7	7207	7208	7226	7225	8207	8208	8226	8225	3
7208	air	3	8	7	7208	7209	7227	7226	8208	8209	8227	8226	3
7209	air	4	8	7	7209	7210	7228	7227	8209	8210	8228	8227	3
7210	air	5	8	7	7210	7211	7229	7228	8210	8211	8229	8228	3
7211	air	6	8	7	7211	7212	7230	7229	8211	8212	8230	8229	3
7212	air	7	8	7	7212	7213	7231	7230	8212	8213	8231	8230	3
7213	air	8	8	7	7213	7214	7232	7231	8213	8214	8232	8231	3
7214	air	9	8	7	7214	7215	7233	7232	8214	8215	8233	8232	3
7215	air	10	8	7	7215	7216	7234	7233	8215	8216	8234	8233	3
7217	air	-6	9	7	7217	7218	7236	7235	8217	8218	8236	8235	3
7218	air	-5	9	7	7218	7219	7237	7236	8218	8219	8237	8236	3
7219	air	-4	9	7	7219	7220	7238	7237	8219	8220	8238	8237	3
7220	air	-3	9	7	7220	7221	7239	7238	8220	8221	8239	8238	3
7221	air	-2	9	7	7221	7222	7240	7239	8221	8222	8240	8239	3
7222	air	-1	9	7	7222	7223	7241	7240	8222	8223	8241	8240	3
7223	air	0	9	7	7223	7224	7242	7241	8223	8224	8242	8241	3
7224	air	1	9	7	7224	7225	7243	7242	8224	8225	8243	8242	3
7225	air	2	9	7	7225	7226	7244	7243	8225	8226	8244	8243	3
7226	air	3	9	7	7226	7227	7245	7244	8226	8227	8245	8244	3
7227	air	4	9	7	7227	7228	7246	7245	8227	8228	8246	8245	3
7228	air	5	9	7	7228	7229	7247	7246	8228	8229	8247	8246	3
7229	air	6	9	7	7229	7230	7248	7247	8229	8230	8248	8247	3
7230	air	7	9	7	7230	7231	7249	7248	8230	8231	8249	8248	3
7231	air	8	9	7	7231	7232	7250	7249	8231	8232	8250	8249	3
7232	air	9	9	7	7232	7233	7251	7250	8232	8233	8251	8250	3
7233	air	10	9	7	7233	7234	7252	7251	8233	8234	8252	8251	3

**Table 13 - FEM Conversion Table for Leg of Lamb at Z = 8 cm**

Element Number	Tissue Type	Location			Nodes on this slice				Nodes on slice above				Mesh Color
		X	Y	Z	LL	LR	UR	UL	LL	LR	UR	UL	
8001	air	-6	-3	8	8001	8002	8020	8019	9001	9002	9020	9019	3
8002	muscle	-5	-3	8	8002	8003	8021	8020	9002	9003	9021	9020	11
8003	muscle	-4	-3	8	8003	8004	8022	8021	9003	9004	9022	9021	11
8004	muscle	-3	-3	8	8004	8005	8023	8022	9004	9005	9023	9022	11
8005	air	-2	-3	8	8005	8006	8024	8023	9005	9006	9024	9023	3
8006	air	-1	-3	8	8006	8007	8025	8024	9006	9007	9025	9024	3
8007	air	0	-3	8	8007	8008	8026	8025	9007	9008	9026	9025	3
8008	air	1	-3	8	8008	8009	8027	8026	9008	9009	9027	9026	3
8009	air	2	-3	8	8009	8010	8028	8027	9009	9010	9028	9027	3
8010	air	3	-3	8	8010	8011	8029	8028	9010	9011	9029	9028	3
8011	air	4	-3	8	8011	8012	8030	8029	9011	9012	9030	9029	3
8012	air	5	-3	8	8012	8013	8031	8030	9012	9013	9031	9030	3
8013	air	6	-3	8	8013	8014	8032	8031	9013	9014	9032	9031	3
8014	air	7	-3	8	8014	8015	8033	8032	9014	9015	9033	9032	3
8015	air	8	-3	8	8015	8016	8034	8033	9015	9016	9034	9033	3
8016	air	9	-3	8	8016	8017	8035	8034	9016	9017	9035	9034	3
8017	air	10	-3	8	8017	8018	8036	8035	9017	9018	9036	9035	3
8019	fat	-6	-2	8	8019	8020	8038	8037	9019	9020	9038	9037	8
8020	muscle	-5	-2	8	8020	8021	8039	8038	9020	9021	9039	9038	11
8021	muscle	-4	-2	8	8021	8022	8040	8039	9021	9022	9040	9039	11
8022	muscle	-3	-2	8	8022	8023	8041	8040	9022	9023	9041	9040	11
8023	air	-2	-2	8	8023	8024	8042	8041	9023	9024	9042	9041	3
8024	air	-1	-2	8	8024	8025	8043	8042	9024	9025	9043	9042	3
8025	air	0	-2	8	8025	8026	8044	8043	9025	9026	9044	9043	3
8026	air	1	-2	8	8026	8027	8045	8044	9026	9027	9045	9044	3
8027	air	2	-2	8	8027	8028	8046	8045	9027	9028	9046	9045	3
8028	air	3	-2	8	8028	8029	8047	8046	9028	9029	9047	9046	3
8029	air	4	-2	8	8029	8030	8048	8047	9029	9030	9048	9047	3
8030	air	5	-2	8	8030	8031	8049	8048	9030	9031	9049	9048	3
8031	air	6	-2	8	8031	8032	8050	8049	9031	9032	9050	9049	3
8032	air	7	-2	8	8032	8033	8051	8050	9032	9033	9051	9050	3
8033	air	8	-2	8	8033	8034	8052	8051	9033	9034	9052	9051	3
8034	air	9	-2	8	8034	8035	8053	8052	9034	9035	9053	9052	3
8035	air	10	-2	8	8035	8036	8054	8053	9035	9036	9054	9053	3
8037	fat	-6	-1	8	8037	8038	8056	8055	9037	9038	9056	9055	8
8038	muscle	-5	-1	8	8038	8039	8057	8056	9038	9039	9057	9056	11
8039	muscle	-4	-1	8	8039	8040	8058	8057	9039	9040	9058	9057	11

Element Number	Tissue Type	Location			Nodes on this slice				Nodes on slice above				Mesh Color
		X	Y	Z	LL	LR	UR	UL	LL	LR	UR	UL	
8040	muscle	-3	-1	8	8040	8041	8059	8058	9040	9041	9059	9058	11
8041	bone	-2	-1	8	8041	8042	8060	8059	9041	9042	9060	9059	15
8042	bone	-1	-1	8	8042	8043	8061	8060	9042	9043	9061	9060	15
8043	bone	0	-1	8	8043	8044	8062	8061	9043	9044	9062	9061	15
8044	air	1	-1	8	8044	8045	8063	8062	9044	9045	9063	9062	3
8045	air	2	-1	8	8045	8046	8064	8063	9045	9046	9064	9063	3
8046	muscle	3	-1	8	8046	8047	8065	8064	9046	9047	9065	9064	11
8047	muscle	4	-1	8	8047	8048	8066	8065	9047	9048	9066	9065	11
8048	muscle	5	-1	8	8048	8049	8067	8066	9048	9049	9067	9066	11
8049	muscle	6	-1	8	8049	8050	8068	8067	9049	9050	9068	9067	11
8050	muscle	7	-1	8	8050	8051	8069	8068	9050	9051	9069	9068	11
8051	muscle	8	-1	8	8051	8052	8070	8069	9051	9052	9070	9069	11
8052	air	9	-1	8	8052	8053	8071	8070	9052	9053	9071	9070	3
8053	air	10	-1	8	8053	8054	8072	8071	9053	9054	9072	9071	3
8055	fat	-6	0	8	8055	8056	8074	8073	9055	9056	9074	9073	8
8056	muscle	-5	0	8	8056	8057	8075	8074	9056	9057	9075	9074	11
8057	muscle	-4	0	8	8057	8058	8076	8075	9057	9058	9076	9075	11
8058	bone	-3	0	8	8058	8059	8077	8076	9058	9059	9077	9076	15
8059	bone	-2	0	8	8059	8060	8078	8077	9059	9060	9078	9077	15
8060	bone	-1	0	8	8060	8061	8079	8078	9060	9061	9079	9078	15
8061	bone	0	0	8	8061	8062	8080	8079	9061	9062	9080	9079	15
8062	muscle	1	0	8	8062	8063	8081	8080	9062	9063	9081	9080	11
8063	muscle	2	0	8	8063	8064	8082	8081	9063	9064	9082	9081	11
8064	muscle	3	0	8	8064	8065	8083	8082	9064	9065	9083	9082	11
8065	muscle	4	0	8	8065	8066	8084	8083	9065	9066	9084	9083	11
8066	muscle	5	0	8	8066	8067	8085	8084	9066	9067	9085	9084	11
8067	muscle	6	0	8	8067	8068	8086	8085	9067	9068	9086	9085	11
8068	muscle	7	0	8	8068	8069	8087	8086	9068	9069	9087	9086	11
8069	muscle	8	0	8	8069	8070	8088	8087	9069	9070	9088	9087	11
8070	muscle	9	0	8	8070	8071	8089	8088	9070	9071	9089	9088	11
8071	air	10	0	8	8071	8072	8090	8089	9071	9072	9090	9089	3
8073	fat	-6	1	8	8073	8074	8092	8091	9073	9074	9092	9091	8
8074	muscle	-5	1	8	8074	8075	8093	8092	9074	9075	9093	9092	11
8075	muscle	-4	1	8	8075	8076	8094	8093	9075	9076	9094	9093	11
8076	muscle	-3	1	8	8076	8077	8095	8094	9076	9077	9095	9094	11
8077	bone	-2	1	8	8077	8078	8096	8095	9077	9078	9096	9095	15
8078	muscle	-1	1	8	8078	8079	8097	8096	9078	9079	9097	9096	11
8079	muscle	0	1	8	8079	8080	8098	8097	9079	9080	9098	9097	11

Element Number	Tissue Type	Location			Nodes on this slice				Nodes on slice above				Mesh Color
		X	Y	Z	LL	LR	UR	UL	LL	LR	UR	UL	
8080	muscle	1	1	8	8080	8081	8099	8098	9080	9081	9099	9098	11
8081	muscle	2	1	8	8081	8082	8100	8099	9081	9082	9100	9099	11
8082	muscle	3	1	8	8082	8083	8101	8100	9082	9083	9101	9100	11
8083	muscle	4	1	8	8083	8084	8102	8101	9083	9084	9102	9101	11
8084	muscle	5	1	8	8084	8085	8103	8102	9084	9085	9103	9102	11
8085	muscle	6	1	8	8085	8086	8104	8103	9085	9086	9104	9103	11
8086	muscle	7	1	8	8086	8087	8105	8104	9086	9087	9105	9104	11
8087	muscle	8	1	8	8087	8088	8106	8105	9087	9088	9106	9105	11
8088	muscle	9	1	8	8088	8089	8107	8106	9088	9089	9107	9106	11
8089	fat	10	1	8	8089	8090	8108	8107	9089	9090	9108	9107	8
8091	fat	-6	2	8	8091	8092	8110	8109	9091	9092	9110	9109	8
8092	muscle	-5	2	8	8092	8093	8111	8110	9092	9093	9111	9110	11
8093	muscle	-4	2	8	8093	8094	8112	8111	9093	9094	9112	9111	11
8094	muscle	-3	2	8	8094	8095	8113	8112	9094	9095	9113	9112	11
8095	muscle	-2	2	8	8095	8096	8114	8113	9095	9096	9114	9113	11
8096	fat	-1	2	8	8096	8097	8115	8114	9096	9097	9115	9114	8
8097	fat	0	2	8	8097	8098	8116	8115	9097	9098	9116	9115	8
8098	fat	1	2	8	8098	8099	8117	8116	9098	9099	9117	9116	8
8099	muscle	2	2	8	8099	8100	8118	8117	9099	9100	9118	9117	11
8100	muscle	3	2	8	8100	8101	8119	8118	9100	9101	9119	9118	11
8101	muscle	4	2	8	8101	8102	8120	8119	9101	9102	9120	9119	11
8102	muscle	5	2	8	8102	8103	8121	8120	9102	9103	9121	9120	11
8103	muscle	6	2	8	8103	8104	8122	8121	9103	9104	9122	9121	11
8104	muscle	7	2	8	8104	8105	8123	8122	9104	9105	9123	9122	11
8105	muscle	8	2	8	8105	8106	8124	8123	9105	9106	9124	9123	11
8106	muscle	9	2	8	8106	8107	8125	8124	9106	9107	9125	9124	11
8107	fat	10	2	8	8107	8108	8126	8125	9107	9108	9126	9125	8
8109	air	-6	3	8	8109	8110	8128	8127	9109	9110	9128	9127	3
8110	fat	-5	3	8	8110	8111	8129	8128	9110	9111	9129	9128	8
8111	muscle	-4	3	8	8111	8112	8130	8129	9111	9112	9130	9129	11
8112	muscle	-3	3	8	8112	8113	8131	8130	9112	9113	9131	9130	11
8113	muscle	-2	3	8	8113	8114	8132	8131	9113	9114	9132	9131	11
8114	muscle	-1	3	8	8114	8115	8133	8132	9114	9115	9133	9132	11
8115	fat	0	3	8	8115	8116	8134	8133	9115	9116	9134	9133	8
8116	fat	1	3	8	8116	8117	8135	8134	9116	9117	9135	9134	8
8117	fat	2	3	8	8117	8118	8136	8135	9117	9118	9136	9135	8
8118	fat	3	3	8	8118	8119	8137	8136	9118	9119	9137	9136	8
8119	muscle	4	3	8	8119	8120	8138	8137	9119	9120	9138	9137	11

Element Number	Tissue Type	Location			Nodes on this slice				Nodes on slice above				Mesh Color
		X	Y	Z	LL	LR	UR	UL	LL	LR	UR	UL	
8120	muscle	5	3	8	8120	8121	8139	8138	9120	9121	9139	9138	11
8121	muscle	6	3	8	8121	8122	8140	8139	9121	9122	9140	9139	11
8122	muscle	7	3	8	8122	8123	8141	8140	9122	9123	9141	9140	11
8123	fat	8	3	8	8123	8124	8142	8141	9123	9124	9142	9141	8
8124	fat	9	3	8	8124	8125	8143	8142	9124	9125	9143	9142	8
8125	fat	10	3	8	8125	8126	8144	8143	9125	9126	9144	9143	8
8127	air	-6	4	8	8127	8128	8146	8145	9127	9128	9146	9145	3
8128	air	-5	4	8	8128	8129	8147	8146	9128	9129	9147	9146	3
8129	muscle	-4	4	8	8129	8130	8148	8147	9129	9130	9148	9147	11
8130	muscle	-3	4	8	8130	8131	8149	8148	9130	9131	9149	9148	11
8131	muscle	-2	4	8	8131	8132	8150	8149	9131	9132	9150	9149	11
8132	muscle	-1	4	8	8132	8133	8151	8150	9132	9133	9151	9150	11
8133	muscle	0	4	8	8133	8134	8152	8151	9133	9134	9152	9151	11
8134	muscle	1	4	8	8134	8135	8153	8152	9134	9135	9153	9152	11
8135	fat	2	4	8	8135	8136	8154	8153	9135	9136	9154	9153	8
8136	muscle	3	4	8	8136	8137	8155	8154	9136	9137	9155	9154	11
8137	muscle	4	4	8	8137	8138	8156	8155	9137	9138	9156	9155	11
8138	muscle	5	4	8	8138	8139	8157	8156	9138	9139	9157	9156	11
8139	muscle	6	4	8	8139	8140	8158	8157	9139	9140	9158	9157	11
8140	muscle	7	4	8	8140	8141	8159	8158	9140	9141	9159	9158	11
8141	fat	8	4	8	8141	8142	8160	8159	9141	9142	9160	9159	8
8142	fat	9	4	8	8142	8143	8161	8160	9142	9143	9161	9160	8
8143	air	10	4	8	8143	8144	8162	8161	9143	9144	9162	9161	3
8145	air	-6	5	8	8145	8146	8164	8163	9145	9146	9164	9163	3
8146	air	-5	5	8	8146	8147	8165	8164	9146	9147	9165	9164	3
8147	fat	-4	5	8	8147	8148	8166	8165	9147	9148	9166	9165	8
8148	muscle	-3	5	8	8148	8149	8167	8166	9148	9149	9167	9166	11
8149	muscle	-2	5	8	8149	8150	8168	8167	9149	9150	9168	9167	11
8150	muscle	-1	5	8	8150	8151	8169	8168	9150	9151	9169	9168	11
8151	muscle	0	5	8	8151	8152	8170	8169	9151	9152	9170	9169	11
8152	muscle	1	5	8	8152	8153	8171	8170	9152	9153	9171	9170	11
8153	muscle	2	5	8	8153	8154	8172	8171	9153	9154	9172	9171	11
8154	muscle	3	5	8	8154	8155	8173	8172	9154	9155	9173	9172	11
8155	muscle	4	5	8	8155	8156	8174	8173	9155	9156	9174	9173	11
8156	muscle	5	5	8	8156	8157	8175	8174	9156	9157	9175	9174	11
8157	muscle	6	5	8	8157	8158	8176	8175	9157	9158	9176	9175	11
8158	fat	7	5	8	8158	8159	8177	8176	9158	9159	9177	9176	8
8159	fat	8	5	8	8159	8160	8178	8177	9159	9160	9178	9177	8

Element Number	Tissue Type	Location			Nodes on this slice				Nodes on slice above				Mesh Color
		X	Y	Z	LL	LR	UR	UL	LL	LR	UR	UL	
8160	air	9	5	8	8160	8161	8179	8178	9160	9161	9179	9178	3
8161	air	10	5	8	8161	8162	8180	8179	9161	9162	9180	9179	3
8163	air	-6	6	8	8163	8164	8182	8181	9163	9164	9182	9181	3
8164	air	-5	6	8	8164	8165	8183	8182	9164	9165	9183	9182	3
8165	air	-4	6	8	8165	8166	8184	8183	9165	9166	9184	9183	3
8166	air	-3	6	8	8166	8167	8185	8184	9166	9167	9185	9184	3
8167	fat	-2	6	8	8167	8168	8186	8185	9167	9168	9186	9185	8
8168	muscle	-1	6	8	8168	8169	8187	8186	9168	9169	9187	9186	11
8169	muscle	0	6	8	8169	8170	8188	8187	9169	9170	9188	9187	11
8170	fat	1	6	8	8170	8171	8189	8188	9170	9171	9189	9188	8
8171	muscle	2	6	8	8171	8172	8190	8189	9171	9172	9190	9189	11
8172	muscle	3	6	8	8172	8173	8191	8190	9172	9173	9191	9190	11
8173	fat	4	6	8	8173	8174	8192	8191	9173	9174	9192	9191	8
8174	fat	5	6	8	8174	8175	8193	8192	9174	9175	9193	9192	8
8175	fat	6	6	8	8175	8176	8194	8193	9175	9176	9194	9193	8
8176	air	7	6	8	8176	8177	8195	8194	9176	9177	9195	9194	3
8177	air	8	6	8	8177	8178	8196	8195	9177	9178	9196	9195	3
8178	air	9	6	8	8178	8179	8197	8196	9178	9179	9197	9196	3
8179	air	10	6	8	8179	8180	8198	8197	9179	9180	9198	9197	3
8181	air	-6	7	8	8181	8182	8200	8199	9181	9182	9200	9199	3
8182	air	-5	7	8	8182	8183	8201	8200	9182	9183	9201	9200	3
8183	air	-4	7	8	8183	8184	8202	8201	9183	9184	9202	9201	3
8184	air	-3	7	8	8184	8185	8203	8202	9184	9185	9203	9202	3
8185	air	-2	7	8	8185	8186	8204	8203	9185	9186	9204	9203	3
8186	air	-1	7	8	8186	8187	8205	8204	9186	9187	9205	9204	3
8187	air	0	7	8	8187	8188	8206	8205	9187	9188	9206	9205	3
8188	fat	1	7	8	8188	8189	8207	8206	9188	9189	9207	9206	8
8189	fat	2	7	8	8189	8190	8208	8207	9189	9190	9208	9207	8
8190	fat	3	7	8	8190	8191	8209	8208	9190	9191	9209	9208	8
8191	air	4	7	8	8191	8192	8210	8209	9191	9192	9210	9209	3
8192	air	5	7	8	8192	8193	8211	8210	9192	9193	9211	9210	3
8193	air	6	7	8	8193	8194	8212	8211	9193	9194	9212	9211	3
8194	air	7	7	8	8194	8195	8213	8212	9194	9195	9213	9212	3
8195	air	8	7	8	8195	8196	8214	8213	9195	9196	9214	9213	3
8196	air	9	7	8	8196	8197	8215	8214	9196	9197	9215	9214	3
8197	air	10	7	8	8197	8198	8216	8215	9197	9198	9216	9215	3
8199	air	-6	8	8	8199	8200	8218	8217	9199	9200	9218	9217	3
8200	air	-5	8	8	8200	8201	8219	8218	9200	9201	9219	9218	3

Element Number	Tissue Type	Location			Nodes on this slice				Nodes on slice above				Mesh Color
		X	Y	Z	LL	LR	UR	UL	LL	LR	UR	UL	
8201	air	-4	8	8	8201	8202	8220	8219	9201	9202	9220	9219	3
8202	air	-3	8	8	8202	8203	8221	8220	9202	9203	9221	9220	3
8203	air	-2	8	8	8203	8204	8222	8221	9203	9204	9222	9221	3
8204	air	-1	8	8	8204	8205	8223	8222	9204	9205	9223	9222	3
8205	air	0	8	8	8205	8206	8224	8223	9205	9206	9224	9223	3
8206	air	1	8	8	8206	8207	8225	8224	9206	9207	9225	9224	3
8207	air	2	8	8	8207	8208	8226	8225	9207	9208	9226	9225	3
8208	air	3	8	8	8208	8209	8227	8226	9208	9209	9227	9226	3
8209	air	4	8	8	8209	8210	8228	8227	9209	9210	9228	9227	3
8210	air	5	8	8	8210	8211	8229	8228	9210	9211	9229	9228	3
8211	air	6	8	8	8211	8212	8230	8229	9211	9212	9230	9229	3
8212	air	7	8	8	8212	8213	8231	8230	9212	9213	9231	9230	3
8213	air	8	8	8	8213	8214	8232	8231	9213	9214	9232	9231	3
8214	air	9	8	8	8214	8215	8233	8232	9214	9215	9233	9232	3
8215	air	10	8	8	8215	8216	8234	8233	9215	9216	9234	9233	3
8217	air	-6	9	8	8217	8218	8236	8235	9217	9218	9236	9235	3
8218	air	-5	9	8	8218	8219	8237	8236	9218	9219	9237	9236	3
8219	air	-4	9	8	8219	8220	8238	8237	9219	9220	9238	9237	3
8220	air	-3	9	8	8220	8221	8239	8238	9220	9221	9239	9238	3
8221	air	-2	9	8	8221	8222	8240	8239	9221	9222	9240	9239	3
8222	air	-1	9	8	8222	8223	8241	8240	9222	9223	9241	9240	3
8223	air	0	9	8	8223	8224	8242	8241	9223	9224	9242	9241	3
8224	air	1	9	8	8224	8225	8243	8242	9224	9225	9243	9242	3
8225	air	2	9	8	8225	8226	8244	8243	9225	9226	9244	9243	3
8226	air	3	9	8	8226	8227	8245	8244	9226	9227	9245	9244	3
8227	air	4	9	8	8227	8228	8246	8245	9227	9228	9246	9245	3
8228	air	5	9	8	8228	8229	8247	8246	9228	9229	9247	9246	3
8229	air	6	9	8	8229	8230	8248	8247	9229	9230	9248	9247	3
8230	air	7	9	8	8230	8231	8249	8248	9230	9231	9249	9248	3
8231	air	8	9	8	8231	8232	8250	8249	9231	9232	9250	9249	3
8232	air	9	9	8	8232	8233	8251	8250	9232	9233	9251	9250	3
8233	air	10	9	8	8233	8234	8252	8251	9233	9234	9252	9251	3



**Table 14 - FEM Conversion Table for Leg of Lamb at Z = 9 cm**

Element Number	Tissue Type	Location X Y Z	Nodes on this slice				Nodes on slice above			
			LL	LR	UR	UL	LL	LR	UR	UL
9001	air	-6 -3 9	9001	9002	9020	9019	10001	10002	10020	10019
9002	air	-5 -3 9	9002	9003	9021	9020	10002	10003	10021	10020
9003	air	-4 -3 9	9003	9004	9022	9021	10003	10004	10022	10021
9004	air	-3 -3 9	9004	9005	9023	9022	10004	10005	10023	10022
9005	air	-2 -3 9	9005	9006	9024	9023	10005	10006	10024	10023
9006	air	-1 -3 9	9006	9007	9025	9024	10006	10007	10025	10024
9007	air	0 -3 9	9007	9008	9026	9025	10007	10008	10026	10025
9008	air	1 -3 9	9008	9009	9027	9026	10008	10009	10027	10026
9009	air	2 -3 9	9009	9010	9028	9027	10009	10010	10028	10027
9010	air	3 -3 9	9010	9011	9029	9028	10010	10011	10029	10028
9011	air	4 -3 9	9011	9012	9030	9029	10011	10012	10030	10029
9012	air	5 -3 9	9012	9013	9031	9030	10012	10013	10031	10030
9013	air	6 -3 9	9013	9014	9032	9031	10013	10014	10032	10031
9014	air	7 -3 9	9014	9015	9033	9032	10014	10015	10033	10032
9015	air	8 -3 9	9015	9016	9034	9033	10015	10016	10034	10033
9016	air	9 -3 9	9016	9017	9035	9034	10016	10017	10035	10034
9017	air	10 -3 9	9017	9018	9036	9035	10017	10018	10036	10035
9019	fat	-6 -2 9	9019	9020	9038	9037	10019	10020	10038	10037
9020	muscle	-5 -2 9	9020	9021	9039	9038	10020	10021	10039	10038
9021	muscle	-4 -2 9	9021	9022	9040	9039	10021	10022	10040	10039
9022	muscle	-3 -2 9	9022	9023	9041	9040	10022	10023	10041	10040
9023	muscle	-2 -2 9	9023	9024	9042	9041	10023	10024	10042	10041
9024	air	-1 -2 9	9024	9025	9043	9042	10024	10025	10043	10042
9025	air	0 -2 9	9025	9026	9044	9043	10025	10026	10044	10043
9026	air	1 -2 9	9026	9027	9045	9044	10026	10027	10045	10044
9027	air	2 -2 9	9027	9028	9046	9045	10027	10028	10046	10045
9028	air	3 -2 9	9028	9029	9047	9046	10028	10029	10047	10046
9029	air	4 -2 9	9029	9030	9048	9047	10029	10030	10048	10047
9030	air	5 -2 9	9030	9031	9049	9048	10030	10031	10049	10048
9031	air	6 -2 9	9031	9032	9050	9049	10031	10032	10050	10049
9032	air	7 -2 9	9032	9033	9051	9050	10032	10033	10051	10050
9033	air	8 -2 9	9033	9034	9052	9051	10033	10034	10052	10051
9034	air	9 -2 9	9034	9035	9053	9052	10034	10035	10053	10052
9035	air	10 -2 9	9035	9036	9054	9053	10035	10036	10054	10053
9037	fat	-6 -1 9	9037	9038	9056	9055	10037	10038	10056	10055
9038	muscle	-5 -1 9	9038	9039	9057	9056	10038	10039	10057	10056
9039	muscle	-4 -1 9	9039	9040	9058	9057	10039	10040	10058	10057

Element Number	Tissue Type	Location			Nodes on this slice				Nodes on slice above			
		X	Y	Z	LL	LR	UR	UL	LL	LR	UR	UL
9040	muscle	-3	-1	9	9040	9041	9059	9058	10040	10041	10059	10058
9041	bone	-2	-1	9	9041	9042	9060	9059	10041	10042	10060	10059
9042	bone	-1	-1	9	9042	9043	9061	9060	10042	10043	10061	10060
9043	bone	0	-1	9	9043	9044	9062	9061	10043	10044	10062	10061
9044	muscle	1	-1	9	9044	9045	9063	9062	10044	10045	10063	10062
9045	muscle	2	-1	9	9045	9046	9064	9063	10045	10046	10064	10063
9046	air	3	-1	9	9046	9047	9065	9064	10046	10047	10065	10064
9047	muscle	4	-1	9	9047	9048	9066	9065	10047	10048	10066	10065
9048	muscle	5	-1	9	9048	9049	9067	9066	10048	10049	10067	10066
9049	air	6	-1	9	9049	9050	9068	9067	10049	10050	10068	10067
9050	air	7	-1	9	9050	9051	9069	9068	10050	10051	10069	10068
9051	air	8	-1	9	9051	9052	9070	9069	10051	10052	10070	10069
9052	air	9	-1	9	9052	9053	9071	9070	10052	10053	10071	10070
9053	air	10	-1	9	9053	9054	9072	9071	10053	10054	10072	10071
9055	muscle	-6	0	9	9055	9056	9074	9073	10055	10056	10074	10073
9056	muscle	-5	0	9	9056	9057	9075	9074	10056	10057	10075	10074
9057	muscle	-4	0	9	9057	9058	9076	9075	10057	10058	10076	10075
9058	muscle	-3	0	9	9058	9059	9077	9076	10058	10059	10077	10076
9059	bone	-2	0	9	9059	9060	9078	9077	10059	10060	10078	10077
9060	bone	-1	0	9	9060	9061	9079	9078	10060	10061	10079	10078
9061	bone	0	0	9	9061	9062	9080	9079	10061	10062	10080	10079
9062	muscle	1	0	9	9062	9063	9081	9080	10062	10063	10081	10080
9063	muscle	2	0	9	9063	9064	9082	9081	10063	10064	10082	10081
9064	muscle	3	0	9	9064	9065	9083	9082	10064	10065	10083	10082
9065	muscle	4	0	9	9065	9066	9084	9083	10065	10066	10084	10083
9066	muscle	5	0	9	9066	9067	9085	9084	10066	10067	10085	10084
9067	muscle	6	0	9	9067	9068	9086	9085	10067	10068	10086	10085
9068	muscle	7	0	9	9068	9069	9087	9086	10068	10069	10087	10086
9069	air	8	0	9	9069	9070	9088	9087	10069	10070	10088	10087
9070	air	9	0	9	9070	9071	9089	9088	10070	10071	10089	10088
9071	air	10	0	9	9071	9072	9090	9089	10071	10072	10090	10089
9073	fat	-6	1	9	9073	9074	9092	9091	10073	10074	10092	10091
9074	muscle	-5	1	9	9074	9075	9093	9092	10074	10075	10093	10092
9075	muscle	-4	1	9	9075	9076	9094	9093	10075	10076	10094	10093
9076	muscle	-3	1	9	9076	9077	9095	9094	10076	10077	10095	10094
9077	bone	-2	1	9	9077	9078	9096	9095	10077	10078	10096	10095
9078	bone	-1	1	9	9078	9079	9097	9096	10078	10079	10097	10096
9079	muscle	0	1	9	9079	9080	9098	9097	10079	10080	10098	10097

Element Number	Tissue Type	Location			Nodes on this slice				Nodes on slice above			
		X	Y	Z	LL	LR	UR	UL	LL	LR	UR	UL
9080	muscle	1	1	9	9080	9081	9099	9098	10080	10081	10099	10098
9081	muscle	2	1	9	9081	9082	9100	9099	10081	10082	10100	10099
9082	fat	3	1	9	9082	9083	9101	9100	10082	10083	10101	10100
9083	muscle	4	1	9	9083	9084	9102	9101	10083	10084	10102	10101
9084	muscle	5	1	9	9084	9085	9103	9102	10084	10085	10103	10102
9085	muscle	6	1	9	9085	9086	9104	9103	10085	10086	10104	10103
9086	muscle	7	1	9	9086	9087	9105	9104	10086	10087	10105	10104
9087	muscle	8	1	9	9087	9088	9106	9105	10087	10088	10106	10105
9088	air	9	1	9	9088	9089	9107	9106	10088	10089	10107	10106
9089	air	10	1	9	9089	9090	9108	9107	10089	10090	10108	10107
9091	fat	-6	2	9	9091	9092	9110	9109	10091	10092	10110	10109
9092	muscle	-5	2	9	9092	9093	9111	9110	10092	10093	10111	10110
9093	muscle	-4	2	9	9093	9094	9112	9111	10093	10094	10112	10111
9094	muscle	-3	2	9	9094	9095	9113	9112	10094	10095	10113	10112
9095	muscle	-2	2	9	9095	9096	9114	9113	10095	10096	10114	10113
9096	fat	-1	2	9	9096	9097	9115	9114	10096	10097	10115	10114
9097	fat	0	2	9	9097	9098	9116	9115	10097	10098	10116	10115
9098	fat	1	2	9	9098	9099	9117	9116	10098	10099	10117	10116
9099	fat	2	2	9	9099	9100	9118	9117	10099	10100	10118	10117
9100	muscle	3	2	9	9100	9101	9119	9118	10100	10101	10119	10118
9101	muscle	4	2	9	9101	9102	9120	9119	10101	10102	10120	10119
9102	muscle	5	2	9	9102	9103	9121	9120	10102	10103	10121	10120
9103	muscle	6	2	9	9103	9104	9122	9121	10103	10104	10122	10121
9104	muscle	7	2	9	9104	9105	9123	9122	10104	10105	10123	10122
9105	muscle	8	2	9	9105	9106	9124	9123	10105	10106	10124	10123
9106	air	9	2	9	9106	9107	9125	9124	10106	10107	10125	10124
9107	air	10	2	9	9107	9108	9126	9125	10107	10108	10126	10125
9109	fat	-6	3	9	9109	9110	9128	9127	10109	10110	10128	10127
9110	fat	-5	3	9	9110	9111	9129	9128	10110	10111	10129	10128
9111	muscle	-4	3	9	9111	9112	9130	9129	10111	10112	10130	10129
9112	muscle	-3	3	9	9112	9113	9131	9130	10112	10113	10131	10130
9113	muscle	-2	3	9	9113	9114	9132	9131	10113	10114	10132	10131
9114	muscle	-1	3	9	9114	9115	9133	9132	10114	10115	10133	10132
9115	muscle	0	3	9	9115	9116	9134	9133	10115	10116	10134	10133
9116	muscle	1	3	9	9116	9117	9135	9134	10116	10117	10135	10134
9117	fat	2	3	9	9117	9118	9136	9135	10117	10118	10136	10135
9118	fat	3	3	9	9118	9119	9137	9136	10118	10119	10137	10136
9119	muscle	4	3	9	9119	9120	9138	9137	10119	10120	10138	10137

Element Number	Tissue Type	Location			Nodes on this slice				Nodes on slice above			
		X	Y	Z	LL	LR	UR	UL	LL	LR	UR	UL
9120	muscle	5	3	9	9120	9121	9139	9138	10120	10121	10139	10138
9121	muscle	6	3	9	9121	9122	9140	9139	10121	10122	10140	10139
9122	muscle	7	3	9	9122	9123	9141	9140	10122	10123	10141	10140
9123	muscle	8	3	9	9123	9124	9142	9141	10123	10124	10142	10141
9124	air	9	3	9	9124	9125	9143	9142	10124	10125	10143	10142
9125	air	10	3	9	9125	9126	9144	9143	10125	10126	10144	10143
9127	air	-6	4	9	9127	9128	9146	9145	10127	10128	10146	10145
9128	fat	-5	4	9	9128	9129	9147	9146	10128	10129	10147	10146
9129	muscle	-4	4	9	9129	9130	9148	9147	10129	10130	10148	10147
9130	muscle	-3	4	9	9130	9131	9149	9148	10130	10131	10149	10148
9131	muscle	-2	4	9	9131	9132	9150	9149	10131	10132	10150	10149
9132	muscle	-1	4	9	9132	9133	9151	9150	10132	10133	10151	10150
9133	muscle	0	4	9	9133	9134	9152	9151	10133	10134	10152	10151
9134	muscle	1	4	9	9134	9135	9153	9152	10134	10135	10153	10152
9135	muscle	2	4	9	9135	9136	9154	9153	10135	10136	10154	10153
9136	muscle	3	4	9	9136	9137	9155	9154	10136	10137	10155	10154
9137	muscle	4	4	9	9137	9138	9156	9155	10137	10138	10156	10155
9138	muscle	5	4	9	9138	9139	9157	9156	10138	10139	10157	10156
9139	muscle	6	4	9	9139	9140	9158	9157	10139	10140	10158	10157
9140	muscle	7	4	9	9140	9141	9159	9158	10140	10141	10159	10158
9141	fat	8	4	9	9141	9142	9160	9159	10141	10142	10160	10159
9142	air	9	4	9	9142	9143	9161	9160	10142	10143	10161	10160
9143	air	10	4	9	9143	9144	9162	9161	10143	10144	10162	10161
9145	air	-6	5	9	9145	9146	9164	9163	10145	10146	10164	10163
9146	air	-5	5	9	9146	9147	9165	9164	10146	10147	10165	10164
9147	muscle	-4	5	9	9147	9148	9166	9165	10147	10148	10166	10165
9148	muscle	-3	5	9	9148	9149	9167	9166	10148	10149	10167	10166
9149	muscle	-2	5	9	9149	9150	9168	9167	10149	10150	10168	10167
9150	muscle	-1	5	9	9150	9151	9169	9168	10150	10151	10169	10168
9151	muscle	0	5	9	9151	9152	9170	9169	10151	10152	10170	10169
9152	muscle	1	5	9	9152	9153	9171	9170	10152	10153	10171	10170
9153	muscle	2	5	9	9153	9154	9172	9171	10153	10154	10172	10171
9154	muscle	3	5	9	9154	9155	9173	9172	10154	10155	10173	10172
9155	muscle	4	5	9	9155	9156	9174	9173	10155	10156	10174	10173
9156	muscle	5	5	9	9156	9157	9175	9174	10156	10157	10175	10174
9157	muscle	6	5	9	9157	9158	9176	9175	10157	10158	10176	10175
9158	muscle	7	5	9	9158	9159	9177	9176	10158	10159	10177	10176
9159	fat	8	5	9	9159	9160	9178	9177	10159	10160	10178	10177

Element Number	Tissue Type	Location			Nodes on this slice				Nodes on slice above			
		X	Y	Z	LL	LR	UR	UL	LL	LR	UR	UL
9160	air	9	5	9	9160	9161	9179	9178	10160	10161	10179	10178
9161	air	10	5	9	9161	9162	9180	9179	10161	10162	10180	10179
9163	air	-6	6	9	9163	9164	9182	9181	10163	10164	10182	10181
9164	air	-5	6	9	9164	9165	9183	9182	10164	10165	10183	10182
9165	air	-4	6	9	9165	9166	9184	9183	10165	10166	10184	10183
9166	fat	-3	6	9	9166	9167	9185	9184	10166	10167	10185	10184
9167	muscle	-2	6	9	9167	9168	9186	9185	10167	10168	10186	10185
9168	muscle	-1	6	9	9168	9169	9187	9186	10168	10169	10187	10186
9169	muscle	0	6	9	9169	9170	9188	9187	10169	10170	10188	10187
9170	fat	1	6	9	9170	9171	9189	9188	10170	10171	10189	10188
9171	muscle	2	6	9	9171	9172	9190	9189	10171	10172	10190	10189
9172	muscle	3	6	9	9172	9173	9191	9190	10172	10173	10191	10190
9173	muscle	4	6	9	9173	9174	9192	9191	10173	10174	10192	10191
9174	muscle	5	6	9	9174	9175	9193	9192	10174	10175	10193	10192
9175	muscle	6	6	9	9175	9176	9194	9193	10175	10176	10194	10193
9176	fat	7	6	9	9176	9177	9195	9194	10176	10177	10195	10194
9177	fat	8	6	9	9177	9178	9196	9195	10177	10178	10196	10195
9178	air	9	6	9	9178	9179	9197	9196	10178	10179	10197	10196
9179	air	10	6	9	9179	9180	9198	9197	10179	10180	10198	10197
9181	air	-6	7	9	9181	9182	9200	9199	10181	10182	10200	10199
9182	air	-5	7	9	9182	9183	9201	9200	10182	10183	10201	10200
9183	air	-4	7	9	9183	9184	9202	9201	10183	10184	10202	10201
9184	air	-3	7	9	9184	9185	9203	9202	10184	10185	10203	10202
9185	fat	-2	7	9	9185	9186	9204	9203	10185	10186	10204	10203
9186	fat	-1	7	9	9186	9187	9205	9204	10186	10187	10205	10204
9187	fat	0	7	9	9187	9188	9206	9205	10187	10188	10206	10205
9188	fat	1	7	9	9188	9189	9207	9206	10188	10189	10207	10206
9189	muscle	2	7	9	9189	9190	9208	9207	10189	10190	10208	10207
9190	fat	3	7	9	9190	9191	9209	9208	10190	10191	10209	10208
9191	muscle	4	7	9	9191	9192	9210	9209	10191	10192	10210	10209
9192	muscle	5	7	9	9192	9193	9211	9210	10192	10193	10211	10210
9193	fat	6	7	9	9193	9194	9212	9211	10193	10194	10212	10211
9194	fat	7	7	9	9194	9195	9213	9212	10194	10195	10213	10212
9195	air	8	7	9	9195	9196	9214	9213	10195	10196	10214	10213
9196	air	9	7	9	9196	9197	9215	9214	10196	10197	10215	10214
9197	air	10	7	9	9197	9198	9216	9215	10197	10198	10216	10215
9199	air	-6	8	9	9199	9200	9218	9217	10199	10200	10218	10217
9200	air	-5	8	9	9200	9201	9219	9218	10200	10201	10219	10218

Element Number	Tissue Type	Location			Nodes on this slice				Nodes on slice above			
		X	Y	Z	LL	LR	UR	UL	LL	LR	UR	UL
9201	air	-4	8	9	9201	9202	9220	9219	10201	10202	10220	10219
9202	air	-3	8	9	9202	9203	9221	9220	10202	10203	10221	10220
9203	air	-2	8	9	9203	9204	9222	9221	10203	10204	10222	10221
9204	air	-1	8	9	9204	9205	9223	9222	10204	10205	10223	10222
9205	air	0	8	9	9205	9206	9224	9223	10205	10206	10224	10223
9206	air	1	8	9	9206	9207	9225	9224	10206	10207	10225	10224
9207	air	2	8	9	9207	9208	9226	9225	10207	10208	10226	10225
9208	air	3	8	9	9208	9209	9227	9226	10208	10209	10227	10226
9209	air	4	8	9	9209	9210	9228	9227	10209	10210	10228	10227
9210	air	5	8	9	9210	9211	9229	9228	10210	10211	10229	10228
9211	air	6	8	9	9211	9212	9230	9229	10211	10212	10230	10229
9212	air	7	8	9	9212	9213	9231	9230	10212	10213	10231	10230
9213	air	8	8	9	9213	9214	9232	9231	10213	10214	10232	10231
9214	air	9	8	9	9214	9215	9233	9232	10214	10215	10233	10232
9215	air	10	8	9	9215	9216	9234	9233	10215	10216	10234	10233
9217	air	-6	9	9	9217	9218	9236	9235	10217	10218	10236	10235
9218	air	-5	9	9	9218	9219	9237	9236	10218	10219	10237	10236
9219	air	-4	9	9	9219	9220	9238	9237	10219	10220	10238	10237
9220	air	-3	9	9	9220	9221	9239	9238	10220	10221	10239	10238
9221	air	-2	9	9	9221	9222	9240	9239	10221	10222	10240	10239
9222	air	-1	9	9	9222	9223	9241	9240	10222	10223	10241	10240
9223	air	0	9	9	9223	9224	9242	9241	10223	10224	10242	10241
9224	air	1	9	9	9224	9225	9243	9242	10224	10225	10243	10242
9225	air	2	9	9	9225	9226	9244	9243	10225	10226	10244	10243
9226	air	3	9	9	9226	9227	9245	9244	10226	10227	10245	10244
9227	air	4	9	9	9227	9228	9246	9245	10227	10228	10246	10245
9228	air	5	9	9	9228	9229	9247	9246	10228	10229	10247	10246
9229	air	6	9	9	9229	9230	9248	9247	10229	10230	10248	10247
9230	air	7	9	9	9230	9231	9249	9248	10230	10231	10249	10248
9231	air	8	9	9	9231	9232	9250	9249	10231	10232	10250	10249
9232	air	9	9	9	9232	9233	9251	9250	10232	10233	10251	10250
9233	air	10	9	9	9233	9234	9252	9251	10233	10234	10252	10251

**Table 15 - FEM Conversion Table for Leg of Lamb at Z = 10 cm**

Element Number	Tissue Type	Location			Nodes on this slice				Nodes on slice above			
		X	Y	Z	LL	LR	UR	UL	LL	LR	UR	UL
10001	air	-6	-3	10	10001	10002	10020	10019	11001	11002	11020	11019
10002	air	-5	-3	10	10002	10003	10021	10020	11002	11003	11021	11020
10003	air	-4	-3	10	10003	10004	10022	10021	11003	11004	11022	11021
10004	air	-3	-3	10	10004	10005	10023	10022	11004	11005	11023	11022
10005	air	-2	-3	10	10005	10006	10024	10023	11005	11006	11024	11023
10006	air	-1	-3	10	10006	10007	10025	10024	11006	11007	11025	11024
10007	air	0	-3	10	10007	10008	10026	10025	11007	11008	11026	11025
10008	air	1	-3	10	10008	10009	10027	10026	11008	11009	11027	11026
10009	air	2	-3	10	10009	10010	10028	10027	11009	11010	11028	11027
10010	air	3	-3	10	10010	10011	10029	10028	11010	11011	11029	11028
10011	air	4	-3	10	10011	10012	10030	10029	11011	11012	11030	11029
10012	air	5	-3	10	10012	10013	10031	10030	11012	11013	11031	11030
10013	air	6	-3	10	10013	10014	10032	10031	11013	11014	11032	11031
10014	air	7	-3	10	10014	10015	10033	10032	11014	11015	11033	11032
10015	air	8	-3	10	10015	10016	10034	10033	11015	11016	11034	11033
10016	air	9	-3	10	10016	10017	10035	10034	11016	11017	11035	11034
10017	air	10	-3	10	10017	10018	10036	10035	11017	11018	11036	11035
10019	fat	-6	-2	10	10019	10020	10038	10037	11019	11020	11038	11037
10020	muscle	-5	-2	10	10020	10021	10039	10038	11020	11021	11039	11038
10021	muscle	-4	-2	10	10021	10022	10040	10039	11021	11022	11040	11039
10022	muscle	-3	-2	10	10022	10023	10041	10040	11022	11023	11041	11040
10023	muscle	-2	-2	10	10023	10024	10042	10041	11023	11024	11042	11041
10024	air	-1	-2	10	10024	10025	10043	10042	11024	11025	11043	11042
10025	air	0	-2	10	10025	10026	10044	10043	11025	11026	11044	11043
10026	air	1	-2	10	10026	10027	10045	10044	11026	11027	11045	11044
10027	air	2	-2	10	10027	10028	10046	10045	11027	11028	11046	11045
10028	air	3	-2	10	10028	10029	10047	10046	11028	11029	11047	11046
10029	air	4	-2	10	10029	10030	10048	10047	11029	11030	11048	11047
10030	air	5	-2	10	10030	10031	10049	10048	11030	11031	11049	11048
10031	air	6	-2	10	10031	10032	10050	10049	11031	11032	11050	11049
10032	air	7	-2	10	10032	10033	10051	10050	11032	11033	11051	11050
10033	air	8	-2	10	10033	10034	10052	10051	11033	11034	11052	11051
10034	air	9	-2	10	10034	10035	10053	10052	11034	11035	11053	11052
10035	air	10	-2	10	10035	10036	10054	10053	11035	11036	11054	11053
10037	muscle	-6	-1	10	10037	10038	10056	10055	11037	11038	11056	11055
10038	muscle	-5	-1	10	10038	10039	10057	10056	11038	11039	11057	11056
10039	muscle	-4	-1	10	10039	10040	10058	10057	11039	11040	11058	11057

Element Number	Tissue Type	Location			Nodes on this slice				Nodes on slice above			
		X	Y	Z	LL	LR	UR	UL	LL	LR	UR	UL
10040	muscle	-3	-1	10	10040	10041	10059	10058	11040	11041	11059	11058
10041	muscle	-2	-1	10	10041	10042	10060	10059	11041	11042	11060	11059
10042	bone	-1	-1	10	10042	10043	10061	10060	11042	11043	11061	11060
10043	bone	0	-1	10	10043	10044	10062	10061	11043	11044	11062	11061
10044	air	1	-1	10	10044	10045	10063	10062	11044	11045	11063	11062
10045	air	2	-1	10	10045	10046	10064	10063	11045	11046	11064	11063
10046	muscle	3	-1	10	10046	10047	10065	10064	11046	11047	11065	11064
10047	muscle	4	-1	10	10047	10048	10066	10065	11047	11048	11066	11065
10048	air	5	-1	10	10048	10049	10067	10066	11048	11049	11067	11066
10049	air	6	-1	10	10049	10050	10068	10067	11049	11050	11068	11067
10050	air	7	-1	10	10050	10051	10069	10068	11050	11051	11069	11068
10051	air	8	-1	10	10051	10052	10070	10069	11051	11052	11070	11069
10052	air	9	-1	10	10052	10053	10071	10070	11052	11053	11071	11070
10053	air	10	-1	10	10053	10054	10072	10071	11053	11054	11072	11071
10055	muscle	-6	0	10	10055	10056	10074	10073	11055	11056	11074	11073
10056	muscle	-5	0	10	10056	10057	10075	10074	11056	11057	11075	11074
10057	muscle	-4	0	10	10057	10058	10076	10075	11057	11058	11076	11075
10058	muscle	-3	0	10	10058	10059	10077	10076	11058	11059	11077	11076
10059	bone	-2	0	10	10059	10060	10078	10077	11059	11060	11078	11077
10060	bone	-1	0	10	10060	10061	10079	10078	11060	11061	11079	11078
10061	bone	0	0	10	10061	10062	10080	10079	11061	11062	11080	11079
10062	muscle	1	0	10	10062	10063	10081	10080	11062	11063	11081	11080
10063	muscle	2	0	10	10063	10064	10082	10081	11063	11064	11082	11081
10064	muscle	3	0	10	10064	10065	10083	10082	11064	11065	11083	11082
10065	muscle	4	0	10	10065	10066	10084	10083	11065	11066	11084	11083
10066	muscle	5	0	10	10066	10067	10085	10084	11066	11067	11085	11084
10067	muscle	6	0	10	10067	10068	10086	10085	11067	11068	11086	11085
10068	muscle	7	0	10	10068	10069	10087	10086	11068	11069	11087	11086
10069	air	8	0	10	10069	10070	10088	10087	11069	11070	11088	11087
10070	air	9	0	10	10070	10071	10089	10088	11070	11071	11089	11088
10071	air	10	0	10	10071	10072	10090	10089	11071	11072	11090	11089
10073	fat	-6	1	10	10073	10074	10092	10091	11073	11074	11092	11091
10074	muscle	-5	1	10	10074	10075	10093	10092	11074	11075	11093	11092
10075	muscle	-4	1	10	10075	10076	10094	10093	11075	11076	11094	11093
10076	muscle	-3	1	10	10076	10077	10095	10094	11076	11077	11095	11094
10077	bone	-2	1	10	10077	10078	10096	10095	11077	11078	11096	11095
10078	bone	-1	1	10	10078	10079	10097	10096	11078	11079	11097	11096
10079	muscle	0	1	10	10079	10080	10098	10097	11079	11080	11098	11097



Element Number	Tissue Type	Location			Nodes on this slice				Nodes on slice above			
		X	Y	Z	LL	LR	UR	UL	LL	LR	UR	UL
10080	muscle	1	1	10	10080	10081	10099	10098	11080	11081	11099	11098
10081	muscle	2	1	10	10081	10082	10100	10099	11081	11082	11100	11099
10082	muscle	3	1	10	10082	10083	10101	10100	11082	11083	11101	11100
10083	muscle	4	1	10	10083	10084	10102	10101	11083	11084	11102	11101
10084	muscle	5	1	10	10084	10085	10103	10102	11084	11085	11103	11102
10085	muscle	6	1	10	10085	10086	10104	10103	11085	11086	11104	11103
10086	muscle	7	1	10	10086	10087	10105	10104	11086	11087	11105	11104
10087	fat	8	1	10	10087	10088	10106	10105	11087	11088	11106	11105
10088	air	9	1	10	10088	10089	10107	10106	11088	11089	11107	11106
10089	air	10	1	10	10089	10090	10108	10107	11089	11090	11108	11107
10091	fat	-6	2	10	10091	10092	10110	10109	11091	11092	11110	11109
10092	muscle	-5	2	10	10092	10093	10111	10110	11092	11093	11111	11110
10093	muscle	-4	2	10	10093	10094	10112	10111	11093	11094	11112	11111
10094	muscle	-3	2	10	10094	10095	10113	10112	11094	11095	11113	11112
10095	muscle	-2	2	10	10095	10096	10114	10113	11095	11096	11114	11113
10096	muscle	-1	2	10	10096	10097	10115	10114	11096	11097	11115	11114
10097	muscle	0	2	10	10097	10098	10116	10115	11097	11098	11116	11115
10098	muscle	1	2	10	10098	10099	10117	10116	11098	11099	11117	11116
10099	muscle	2	2	10	10099	10100	10118	10117	11099	11100	11118	11117
10100	muscle	3	2	10	10100	10101	10119	10118	11100	11101	11119	11118
10101	muscle	4	2	10	10101	10102	10120	10119	11101	11102	11120	11119
10102	muscle	5	2	10	10102	10103	10121	10120	11102	11103	11121	11120
10103	muscle	6	2	10	10103	10104	10122	10121	11103	11104	11122	11121
10104	muscle	7	2	10	10104	10105	10123	10122	11104	11105	11123	11122
10105	fat	8	2	10	10105	10106	10124	10123	11105	11106	11124	11123
10106	air	9	2	10	10106	10107	10125	10124	11106	11107	11125	11124
10107	air	10	2	10	10107	10108	10126	10125	11107	11108	11126	11125
10109	fat	-6	3	10	10109	10110	10128	10127	11109	11110	11128	11127
10110	fat	-5	3	10	10110	10111	10129	10128	11110	11111	11129	11128
10111	muscle	-4	3	10	10111	10112	10130	10129	11111	11112	11130	11129
10112	muscle	-3	3	10	10112	10113	10131	10130	11112	11113	11131	11130
10113	muscle	-2	3	10	10113	10114	10132	10131	11113	11114	11132	11131
10114	muscle	-1	3	10	10114	10115	10133	10132	11114	11115	11133	11132
10115	muscle	0	3	10	10115	10116	10134	10133	11115	11116	11134	11133
10116	muscle	1	3	10	10116	10117	10135	10134	11116	11117	11135	11134
10117	fat	2	3	10	10117	10118	10136	10135	11117	11118	11136	11135
10118	fat	3	3	10	10118	10119	10137	10136	11118	11119	11137	11136
10119	muscle	4	3	10	10119	10120	10138	10137	11119	11120	11138	11137

Element Number	Tissue Type	Location			Nodes on this slice				Nodes on slice above			
		X	Y	Z	LL	LR	UR	UL	LL	LR	UR	UL
10120	muscle	5	3	10	10120	10121	10139	10138	11120	11121	11139	11138
10121	muscle	6	3	10	10121	10122	10140	10139	11121	11122	11140	11139
10122	fat	7	3	10	10122	10123	10141	10140	11122	11123	11141	11140
10123	fat	8	3	10	10123	10124	10142	10141	11123	11124	11142	11141
10124	air	9	3	10	10124	10125	10143	10142	11124	11125	11143	11142
10125	air	10	3	10	10125	10126	10144	10143	11125	11126	11144	11143
10127	air	-6	4	10	10127	10128	10146	10145	11127	11128	11146	11145
10128	fat	-5	4	10	10128	10129	10147	10146	11128	11129	11147	11146
10129	muscle	-4	4	10	10129	10130	10148	10147	11129	11130	11148	11147
10130	muscle	-3	4	10	10130	10131	10149	10148	11130	11131	11149	11148
10131	muscle	-2	4	10	10131	10132	10150	10149	11131	11132	11150	11149
10132	muscle	-1	4	10	10132	10133	10151	10150	11132	11133	11151	11150
10133	muscle	0	4	10	10133	10134	10152	10151	11133	11134	11152	11151
10134	muscle	1	4	10	10134	10135	10153	10152	11134	11135	11153	11152
10135	muscle	2	4	10	10135	10136	10154	10153	11135	11136	11154	11153
10136	fat	3	4	10	10136	10137	10155	10154	11136	11137	11155	11154
10137	muscle	4	4	10	10137	10138	10156	10155	11137	11138	11156	11155
10138	muscle	5	4	10	10138	10139	10157	10156	11138	11139	11157	11156
10139	muscle	6	4	10	10139	10140	10158	10157	11139	11140	11158	11157
10140	fat	7	4	10	10140	10141	10159	10158	11140	11141	11159	11158
10141	fat	8	4	10	10141	10142	10160	10159	11141	11142	11160	11159
10142	air	9	4	10	10142	10143	10161	10160	11142	11143	11161	11160
10143	air	10	4	10	10143	10144	10162	10161	11143	11144	11162	11161
10145	air	-6	5	10	10145	10146	10164	10163	11145	11146	11164	11163
10146	air	-5	5	10	10146	10147	10165	10164	11146	11147	11165	11164
10147	muscle	-4	5	10	10147	10148	10166	10165	11147	11148	11166	11165
10148	muscle	-3	5	10	10148	10149	10167	10166	11148	11149	11167	11166
10149	muscle	-2	5	10	10149	10150	10168	10167	11149	11150	11168	11167
10150	muscle	-1	5	10	10150	10151	10169	10168	11150	11151	11169	11168
10151	muscle	0	5	10	10151	10152	10170	10169	11151	11152	11170	11169
10152	muscle	1	5	10	10152	10153	10171	10170	11152	11153	11171	11170
10153	fat	2	5	10	10153	10154	10172	10171	11153	11154	11172	11171
10154	muscle	3	5	10	10154	10155	10173	10172	11154	11155	11173	11172
10155	muscle	4	5	10	10155	10156	10174	10173	11155	11156	11174	11173
10156	muscle	5	5	10	10156	10157	10175	10174	11156	11157	11175	11174
10157	fat	6	5	10	10157	10158	10176	10175	11157	11158	11176	11175
10158	fat	7	5	10	10158	10159	10177	10176	11158	11159	11177	11176
10159	air	8	5	10	10159	10160	10178	10177	11159	11160	11178	11177

Element Number	Tissue Type	Location			Nodes on this slice				Nodes on slice above			
		X	Y	Z	LL	LR	UR	UL	LL	LR	UR	UL
10160	air	9	5	10	10160	10161	10179	10178	11160	11161	11179	11178
10161	air	10	5	10	10161	10162	10180	10179	11161	11162	11180	11179
10163	air	-6	6	10	10163	10164	10182	10181	11163	11164	11182	11181
10164	air	-5	6	10	10164	10165	10183	10182	11164	11165	11183	11182
10165	air	-4	6	10	10165	10166	10184	10183	11165	11166	11184	11183
10166	fat	-3	6	10	10166	10167	10185	10184	11166	11167	11185	11184
10167	muscle	-2	6	10	10167	10168	10186	10185	11167	11168	11186	11185
10168	muscle	-1	6	10	10168	10169	10187	10186	11168	11169	11187	11186
10169	muscle	0	6	10	10169	10170	10188	10187	11169	11170	11188	11187
10170	fat	1	6	10	10170	10171	10189	10188	11170	11171	11189	11188
10171	muscle	2	6	10	10171	10172	10190	10189	11171	11172	11190	11189
10172	muscle	3	6	10	10172	10173	10191	10190	11172	11173	11191	11190
10173	muscle	4	6	10	10173	10174	10192	10191	11173	11174	11192	11191
10174	muscle	5	6	10	10174	10175	10193	10192	11174	11175	11193	11192
10175	fat	6	6	10	10175	10176	10194	10193	11175	11176	11194	11193
10176	fat	7	6	10	10176	10177	10195	10194	11176	11177	11195	11194
10177	air	8	6	10	10177	10178	10196	10195	11177	11178	11196	11195
10178	air	9	6	10	10178	10179	10197	10196	11178	11179	11197	11196
10179	air	10	6	10	10179	10180	10198	10197	11179	11180	11198	11197
10181	air	-6	7	10	10181	10182	10200	10199	11181	11182	11200	11199
10182	air	-5	7	10	10182	10183	10201	10200	11182	11183	11201	11200
10183	air	-4	7	10	10183	10184	10202	10201	11183	11184	11202	11201
10184	air	-3	7	10	10184	10185	10203	10202	11184	11185	11203	11202
10185	air	-2	7	10	10185	10186	10204	10203	11185	11186	11204	11203
10186	fat	-1	7	10	10186	10187	10205	10204	11186	11187	11205	11204
10187	fat	0	7	10	10187	10188	10206	10205	11187	11188	11206	11205
10188	fat	1	7	10	10188	10189	10207	10206	11188	11189	11207	11206
10189	muscle	2	7	10	10189	10190	10208	10207	11189	11190	11208	11207
10190	muscle	3	7	10	10190	10191	10209	10208	11190	11191	11209	11208
10191	muscle	4	7	10	10191	10192	10210	10209	11191	11192	11210	11209
10192	fat	5	7	10	10192	10193	10211	10210	11192	11193	11211	11210
10193	fat	6	7	10	10193	10194	10212	10211	11193	11194	11212	11211
10194	air	7	7	10	10194	10195	10213	10212	11194	11195	11213	11212
10195	air	8	7	10	10195	10196	10214	10213	11195	11196	11214	11213
10196	air	9	7	10	10196	10197	10215	10214	11196	11197	11215	11214
10197	air	10	7	10	10197	10198	10216	10215	11197	11198	11216	11215
10199	air	-6	8	10	10199	10200	10218	10217	11199	11200	11218	11217
10200	air	-5	8	10	10200	10201	10219	10218	11200	11201	11219	11218

Element Number	Tissue Type	Location			Nodes on this slice				Nodes on slice above			
		X	Y	Z	LL	LR	UR	UL	LL	LR	UR	UL
10201	air	-4	8	10	10201	10202	10220	10219	11201	11202	11220	11219
10202	air	-3	8	10	10202	10203	10221	10220	11202	11203	11221	11220
10203	air	-2	8	10	10203	10204	10222	10221	11203	11204	11222	11221
10204	air	-1	8	10	10204	10205	10223	10222	11204	11205	11223	11222
10205	air	0	8	10	10205	10206	10224	10223	11205	11206	11224	11223
10206	air	1	8	10	10206	10207	10225	10224	11206	11207	11225	11224
10207	air	2	8	10	10207	10208	10226	10225	11207	11208	11226	11225
10208	air	3	8	10	10208	10209	10227	10226	11208	11209	11227	11226
10209	air	4	8	10	10209	10210	10228	10227	11209	11210	11228	11227
10210	air	5	8	10	10210	10211	10229	10228	11210	11211	11229	11228
10211	air	6	8	10	10211	10212	10230	10229	11211	11212	11230	11229
10212	air	7	8	10	10212	10213	10231	10230	11212	11213	11231	11230
10213	air	8	8	10	10213	10214	10232	10231	11213	11214	11232	11231
10214	air	9	8	10	10214	10215	10233	10232	11214	11215	11233	11232
10215	air	10	8	10	10215	10216	10234	10233	11215	11216	11234	11233
10217	air	-6	9	10	10217	10218	10236	10235	11217	11218	11236	11235
10218	air	-5	9	10	10218	10219	10237	10236	11218	11219	11237	11236
10219	air	-4	9	10	10219	10220	10238	10237	11219	11220	11238	11237
10220	air	-3	9	10	10220	10221	10239	10238	11220	11221	11239	11238
10221	air	-2	9	10	10221	10222	10240	10239	11221	11222	11240	11239
10222	air	-1	9	10	10222	10223	10241	10240	11222	11223	11241	11240
10223	air	0	9	10	10223	10224	10242	10241	11223	11224	11242	11241
10224	air	1	9	10	10224	10225	10243	10242	11224	11225	11243	11242
10225	air	2	9	10	10225	10226	10244	10243	11225	11226	11244	11243
10226	air	3	9	10	10226	10227	10245	10244	11226	11227	11245	11244
10227	air	4	9	10	10227	10228	10246	10245	11227	11228	11246	11245
10228	air	5	9	10	10228	10229	10247	10246	11228	11229	11247	11246
10229	air	6	9	10	10229	10230	10248	10247	11229	11230	11248	11247
10230	air	7	9	10	10230	10231	10249	10248	11230	11231	11249	11248
10231	air	8	9	10	10231	10232	10250	10249	11231	11232	11250	11249
10232	air	9	9	10	10232	10233	10251	10250	11232	11233	11251	11250
10233	air	10	9	10	10233	10234	10252	10251	11233	11234	11252	11251

**Table 16 - FEM Conversion Table for Leg of Lamb at Z = 11 cm**

Element Number	Tissue Type	Location X Y Z	Nodes on this slice				Nodes on slice above			
			LL	LR	UR	UL	LL	LR	UR	UL
11001	air	-6 -3 11	11001	11002	11020	11019	12001	12002	12020	12019
11002	air	-5 -3 11	11002	11003	11021	11020	12002	12003	12021	12020
11003	muscle	-4 -3 11	11003	11004	11022	11021	12003	12004	12022	12021
11004	muscle	-3 -3 11	11004	11005	11023	11022	12004	12005	12023	12022
11005	muscle	-2 -3 11	11005	11006	11024	11023	12005	12006	12024	12023
11006	air	-1 -3 11	11006	11007	11025	11024	12006	12007	12025	12024
11007	air	0 -3 11	11007	11008	11026	11025	12007	12008	12026	12025
11008	air	1 -3 11	11008	11009	11027	11026	12008	12009	12027	12026
11009	air	2 -3 11	11009	11010	11028	11027	12009	12010	12028	12027
11010	air	3 -3 11	11010	11011	11029	11028	12010	12011	12029	12028
11011	air	4 -3 11	11011	11012	11030	11029	12011	12012	12030	12029
11012	air	5 -3 11	11012	11013	11031	11030	12012	12013	12031	12030
11013	air	6 -3 11	11013	11014	11032	11031	12013	12014	12032	12031
11014	air	7 -3 11	11014	11015	11033	11032	12014	12015	12033	12032
11015	air	8 -3 11	11015	11016	11034	11033	12015	12016	12034	12033
11016	air	9 -3 11	11016	11017	11035	11034	12016	12017	12035	12034
11017	air	10 -3 11	11017	11018	11036	11035	12017	12018	12036	12035
11019	air	-6 -2 11	11019	11020	11038	11037	12019	12020	12038	12037
11020	muscle	-5 -2 11	11020	11021	11039	11038	12020	12021	12039	12038
11021	muscle	-4 -2 11	11021	11022	11040	11039	12021	12022	12040	12039
11022	muscle	-3 -2 11	11022	11023	11041	11040	12022	12023	12041	12040
11023	muscle	-2 -2 11	11023	11024	11042	11041	12023	12024	12042	12041
11024	muscle	-1 -2 11	11024	11025	11043	11042	12024	12025	12043	12042
11025	air	0 -2 11	11025	11026	11044	11043	12025	12026	12044	12043
11026	air	1 -2 11	11026	11027	11045	11044	12026	12027	12045	12044
11027	air	2 -2 11	11027	11028	11046	11045	12027	12028	12046	12045
11028	air	3 -2 11	11028	11029	11047	11046	12028	12029	12047	12046
11029	air	4 -2 11	11029	11030	11048	11047	12029	12030	12048	12047
11030	air	5 -2 11	11030	11031	11049	11048	12030	12031	12049	12048
11031	air	6 -2 11	11031	11032	11050	11049	12031	12032	12050	12049
11032	air	7 -2 11	11032	11033	11051	11050	12032	12033	12051	12050
11033	air	8 -2 11	11033	11034	11052	11051	12033	12034	12052	12051
11034	air	9 -2 11	11034	11035	11053	11052	12034	12035	12053	12052
11035	air	10 -2 11	11035	11036	11054	11053	12035	12036	12054	12053
11037	muscle	-6 -1 11	11037	11038	11056	11055	12037	12038	12056	12055
11038	muscle	-5 -1 11	11038	11039	11057	11056	12038	12039	12057	12056
11039	muscle	-4 -1 11	11039	11040	11058	11057	12039	12040	12058	12057
11040	muscle	-3 -1 11	11040	11041	11059	11058	12040	12041	12059	12058
11041	muscle	-2 -1 11	11041	11042	11060	11059	12041	12042	12060	12059

Element Number	Tissue Type	Location			Nodes on this slice				Nodes on slice above			
		X	Y	Z	LL	LR	UR	UL	LL	LR	UR	UL
11042	bone	-1	-1	11	11042	11043	11061	11060	12042	12043	12061	12060
11043	bone	0	-1	11	11043	11044	11062	11061	12043	12044	12062	12061
11044	air	1	-1	11	11044	11045	11063	11062	12044	12045	12063	12062
11045	air	2	-1	11	11045	11046	11064	11063	12045	12046	12064	12063
11046	air	3	-1	11	11046	11047	11065	11064	12046	12047	12065	12064
11047	air	4	-1	11	11047	11048	11066	11065	12047	12048	12066	12065
11048	air	5	-1	11	11048	11049	11067	11066	12048	12049	12067	12066
11049	air	6	-1	11	11049	11050	11068	11067	12049	12050	12068	12067
11050	air	7	-1	11	11050	11051	11069	11068	12050	12051	12069	12068
11051	air	8	-1	11	11051	11052	11070	11069	12051	12052	12070	12069
11052	air	9	-1	11	11052	11053	11071	11070	12052	12053	12071	12070
11053	air	10	-1	11	11053	11054	11072	11071	12053	12054	12072	12071
11055	muscle	-6	0	11	11055	11056	11074	11073	12055	12056	12074	12073
11056	muscle	-5	0	11	11056	11057	11075	11074	12056	12057	12075	12074
11057	muscle	-4	0	11	11057	11058	11076	11075	12057	12058	12076	12075
11058	muscle	-3	0	11	11058	11059	11077	11076	12058	12059	12077	12076
11059	bone	-2	0	11	11059	11060	11078	11077	12059	12060	12078	12077
11060	bone	-1	0	11	11060	11061	11079	11078	12060	12061	12079	12078
11061	bone	0	0	11	11061	11062	11080	11079	12061	12062	12080	12079
11062	muscle	1	0	11	11062	11063	11081	11080	12062	12063	12081	12080
11063	muscle	2	0	11	11063	11064	11082	11081	12063	12064	12082	12081
11064	muscle	3	0	11	11064	11065	11083	11082	12064	12065	12083	12082
11065	muscle	4	0	11	11065	11066	11084	11083	12065	12066	12084	12083
11066	muscle	5	0	11	11066	11067	11085	11084	12066	12067	12085	12084
11067	muscle	6	0	11	11067	11068	11086	11085	12067	12068	12086	12085
11068	muscle	7	0	11	11068	11069	11087	11086	12068	12069	12087	12086
11069	air	8	0	11	11069	11070	11088	11087	12069	12070	12088	12087
11070	air	9	0	11	11070	11071	11089	11088	12070	12071	12089	12088
11071	air	10	0	11	11071	11072	11090	11089	12071	12072	12090	12089
11073	fat	-6	1	11	11073	11074	11092	11091	12073	12074	12092	12091
11074	muscle	-5	1	11	11074	11075	11093	11092	12074	12075	12093	12092
11075	muscle	-4	1	11	11075	11076	11094	11093	12075	12076	12094	12093
11076	muscle	-3	1	11	11076	11077	11095	11094	12076	12077	12095	12094
11077	bone	-2	1	11	11077	11078	11096	11095	12077	12078	12096	12095
11078	bone	-1	1	11	11078	11079	11097	11096	12078	12079	12097	12096
11079	muscle	0	1	11	11079	11080	11098	11097	12079	12080	12098	12097
11080	muscle	1	1	11	11080	11081	11099	11098	12080	12081	12099	12098
11081	muscle	2	1	11	11081	11082	11100	11099	12081	12082	12100	12099
11082	muscle	3	1	11	11082	11083	11101	11100	12082	12083	12101	12100
11083	muscle	4	1	11	11083	11084	11102	11101	12083	12084	12102	12101
11084	muscle	5	1	11	11084	11085	11103	11102	12084	12085	12103	12102

Element Number	Tissue Type	Location			Nodes on this slice				Nodes on slice above			
		X	Y	Z	LL	LR	UR	UL	LL	LR	UR	UL
11085	muscle	6	1	11	11085	11086	11104	11103	12085	12086	12104	12103
11086	bone	7	1	11	11086	11087	11105	11104	12086	12087	12105	12104
11087	bone	8	1	11	11087	11088	11106	11105	12087	12088	12106	12105
11088	air	9	1	11	11088	11089	11107	11106	12088	12089	12107	12106
11089	air	10	1	11	11089	11090	11108	11107	12089	12090	12108	12107
11091	fat	-6	2	11	11091	11092	11110	11109	12091	12092	12110	12109
11092	muscle	-5	2	11	11092	11093	11111	11110	12092	12093	12111	12110
11093	muscle	-4	2	11	11093	11094	11112	11111	12093	12094	12112	12111
11094	muscle	-3	2	11	11094	11095	11113	11112	12094	12095	12113	12112
11095	muscle	-2	2	11	11095	11096	11114	11113	12095	12096	12114	12113
11096	muscle	-1	2	11	11096	11097	11115	11114	12096	12097	12115	12114
11097	muscle	0	2	11	11097	11098	11116	11115	12097	12098	12116	12115
11098	muscle	1	2	11	11098	11099	11117	11116	12098	12099	12117	12116
11099	muscle	2	2	11	11099	11100	11118	11117	12099	12100	12118	12117
11100	muscle	3	2	11	11100	11101	11119	11118	12100	12101	12119	12118
11101	muscle	4	2	11	11101	11102	11120	11119	12101	12102	12120	12119
11102	muscle	5	2	11	11102	11103	11121	11120	12102	12103	12121	12120
11103	muscle	6	2	11	11103	11104	11122	11121	12103	12104	12122	12121
11104	bone	7	2	11	11104	11105	11123	11122	12104	12105	12123	12122
11105	bone	8	2	11	11105	11106	11124	11123	12105	12106	12124	12123
11106	air	9	2	11	11106	11107	11125	11124	12106	12107	12125	12124
11107	air	10	2	11	11107	11108	11126	11125	12107	12108	12126	12125
11109	air	-6	3	11	11109	11110	11128	11127	12109	12110	12128	12127
11110	fat	-5	3	11	11110	11111	11129	11128	12110	12111	12129	12128
11111	muscle	-4	3	11	11111	11112	11130	11129	12111	12112	12130	12129
11112	muscle	-3	3	11	11112	11113	11131	11130	12112	12113	12131	12130
11113	muscle	-2	3	11	11113	11114	11132	11131	12113	12114	12132	12131
11114	muscle	-1	3	11	11114	11115	11133	11132	12114	12115	12133	12132
11115	muscle	0	3	11	11115	11116	11134	11133	12115	12116	12134	12133
11116	muscle	1	3	11	11116	11117	11135	11134	12116	12117	12135	12134
11117	fat	2	3	11	11117	11118	11136	11135	12117	12118	12136	12135
11118	muscle	3	3	11	11118	11119	11137	11136	12118	12119	12137	12136
11119	muscle	4	3	11	11119	11120	11138	11137	12119	12120	12138	12137
11120	muscle	5	3	11	11120	11121	11139	11138	12120	12121	12139	12138
11121	muscle	6	3	11	11121	11122	11140	11139	12121	12122	12140	12139
11122	bone	7	3	11	11122	11123	11141	11140	12122	12123	12141	12140
11123	bone	8	3	11	11123	11124	11142	11141	12123	12124	12142	12141
11124	air	9	3	11	11124	11125	11143	11142	12124	12125	12143	12142
11125	air	10	3	11	11125	11126	11144	11143	12125	12126	12144	12143
11127	air	-6	4	11	11127	11128	11146	11145	12127	12128	12146	12145
11128	fat	-5	4	11	11128	11129	11147	11146	12128	12129	12147	12146

Element Number	Tissue Type	Location			Nodes on this slice				Nodes on slice above			
		X	Y	Z	LL	LR	UR	UL	LL	LR	UR	UL
11129	muscle	-4	4	11	11129	11130	11148	11147	12129	12130	12148	12147
11130	muscle	-3	4	11	11130	11131	11149	11148	12130	12131	12149	12148
11131	muscle	-2	4	11	11131	11132	11150	11149	12131	12132	12150	12149
11132	muscle	-1	4	11	11132	11133	11151	11150	12132	12133	12151	12150
11133	muscle	0	4	11	11133	11134	11152	11151	12133	12134	12152	12151
11134	muscle	1	4	11	11134	11135	11153	11152	12134	12135	12153	12152
11135	muscle	2	4	11	11135	11136	11154	11153	12135	12136	12154	12153
11136	muscle	3	4	11	11136	11137	11155	11154	12136	12137	12155	12154
11137	muscle	4	4	11	11137	11138	11156	11155	12137	12138	12156	12155
11138	muscle	5	4	11	11138	11139	11157	11156	12138	12139	12157	12156
11139	bone	6	4	11	11139	11140	11158	11157	12139	12140	12158	12157
11140	bone	7	4	11	11140	11141	11159	11158	12140	12141	12159	12158
11141	air	8	4	11	11141	11142	11160	11159	12141	12142	12160	12159
11142	air	9	4	11	11142	11143	11161	11160	12142	12143	12161	12160
11143	air	10	4	11	11143	11144	11162	11161	12143	12144	12162	12161
11145	air	-6	5	11	11145	11146	11164	11163	12145	12146	12164	12163
11146	air	-5	5	11	11146	11147	11165	11164	12146	12147	12165	12164
11147	muscle	-4	5	11	11147	11148	11166	11165	12147	12148	12166	12165
11148	muscle	-3	5	11	11148	11149	11167	11166	12148	12149	12167	12166
11149	muscle	-2	5	11	11149	11150	11168	11167	12149	12150	12168	12167
11150	muscle	-1	5	11	11150	11151	11169	11168	12150	12151	12169	12168
11151	muscle	0	5	11	11151	11152	11170	11169	12151	12152	12170	12169
11152	muscle	1	5	11	11152	11153	11171	11170	12152	12153	12171	12170
11153	muscle	2	5	11	11153	11154	11172	11171	12153	12154	12172	12171
11154	muscle	3	5	11	11154	11155	11173	11172	12154	12155	12173	12172
11155	fat	4	5	11	11155	11156	11174	11173	12155	12156	12174	12173
11156	fat	5	5	11	11156	11157	11175	11174	12156	12157	12175	12174
11157	fat	6	5	11	11157	11158	11176	11175	12157	12158	12176	12175
11158	fat	7	5	11	11158	11159	11177	11176	12158	12159	12177	12176
11159	air	8	5	11	11159	11160	11178	11177	12159	12160	12178	12177
11160	air	9	5	11	11160	11161	11179	11178	12160	12161	12179	12178
11161	air	10	5	11	11161	11162	11180	11179	12161	12162	12180	12179
11163	air	-6	6	11	11163	11164	11182	11181	12163	12164	12182	12181
11164	air	-5	6	11	11164	11165	11183	11182	12164	12165	12183	12182
11165	air	-4	6	11	11165	11166	11184	11183	12165	12166	12184	12183
11166	muscle	-3	6	11	11166	11167	11185	11184	12166	12167	12185	12184
11167	muscle	-2	6	11	11167	11168	11186	11185	12167	12168	12186	12185
11168	muscle	-1	6	11	11168	11169	11187	11186	12168	12169	12187	12186
11169	muscle	0	6	11	11169	11170	11188	11187	12169	12170	12188	12187
11170	muscle	1	6	11	11170	11171	11189	11188	12170	12171	12189	12188
11171	muscle	2	6	11	11171	11172	11190	11189	12171	12172	12190	12189



Element Number	Tissue Type	Location			Nodes on this slice				Nodes on slice above			
		X	Y	Z	LL	LR	UR	UL	LL	LR	UR	UL
11172	muscle	3	6	11	11172	11173	11191	11190	12172	12173	12191	12190
11173	muscle	4	6	11	11173	11174	11192	11191	12173	12174	12192	12191
11174	fat	5	6	11	11174	11175	11193	11192	12174	12175	12193	12192
11175	fat	6	6	11	11175	11176	11194	11193	12175	12176	12194	12193
11176	fat	7	6	11	11176	11177	11195	11194	12176	12177	12195	12194
11177	air	8	6	11	11177	11178	11196	11195	12177	12178	12196	12195
11178	air	9	6	11	11178	11179	11197	11196	12178	12179	12197	12196
11179	air	10	6	11	11179	11180	11198	11197	12179	12180	12198	12197
11181	air	-6	7	11	11181	11182	11200	11199	12181	12182	12200	12199
11182	air	-5	7	11	11182	11183	11201	11200	12182	12183	12201	12200
11183	air	-4	7	11	11183	11184	11202	11201	12183	12184	12202	12201
11184	air	-3	7	11	11184	11185	11203	11202	12184	12185	12203	12202
11185	muscle	-2	7	11	11185	11186	11204	11203	12185	12186	12204	12203
11186	muscle	-1	7	11	11186	11187	11205	11204	12186	12187	12205	12204
11187	muscle	0	7	11	11187	11188	11206	11205	12187	12188	12206	12205
11188	fat	1	7	11	11188	11189	11207	11206	12188	12189	12207	12206
11189	muscle	2	7	11	11189	11190	11208	11207	12189	12190	12208	12207
11190	muscle	3	7	11	11190	11191	11209	11208	12190	12191	12209	12208
11191	fat	4	7	11	11191	11192	11210	11209	12191	12192	12210	12209
11192	fat	5	7	11	11192	11193	11211	11210	12192	12193	12211	12210
11193	fat	6	7	11	11193	11194	11212	11211	12193	12194	12212	12211
11194	air	7	7	11	11194	11195	11213	11212	12194	12195	12213	12212
11195	air	8	7	11	11195	11196	11214	11213	12195	12196	12214	12213
11196	air	9	7	11	11196	11197	11215	11214	12196	12197	12215	12214
11197	air	10	7	11	11197	11198	11216	11215	12197	12198	12216	12215
11199	air	-6	8	11	11199	11200	11218	11217	12199	12200	12218	12217
11200	air	-5	8	11	11200	11201	11219	11218	12200	12201	12219	12218
11201	air	-4	8	11	11201	11202	11220	11219	12201	12202	12220	12219
11202	air	-3	8	11	11202	11203	11221	11220	12202	12203	12221	12220
11203	air	-2	8	11	11203	11204	11222	11221	12203	12204	12222	12221
11204	air	-1	8	11	11204	11205	11223	11222	12204	12205	12223	12222
11205	air	0	8	11	11205	11206	11224	11223	12205	12206	12224	12223
11206	air	1	8	11	11206	11207	11225	11224	12206	12207	12225	12224
11207	fat	2	8	11	11207	11208	11226	11225	12207	12208	12226	12225
11208	fat	3	8	11	11208	11209	11227	11226	12208	12209	12227	12226
11209	fat	4	8	11	11209	11210	11228	11227	12209	12210	12228	12227
11210	fat	5	8	11	11210	11211	11229	11228	12210	12211	12229	12228
11211	air	6	8	11	11211	11212	11230	11229	12211	12212	12230	12229
11212	air	7	8	11	11212	11213	11231	11230	12212	12213	12231	12230
11213	air	8	8	11	11213	11214	11232	11231	12213	12214	12232	12231
11214	air	9	8	11	11214	11215	11233	11232	12214	12215	12233	12232

Element Number	Tissue Type	Location			Nodes on this slice				Nodes on slice above			
		X	Y	Z	LL	LR	UR	UL	LL	LR	UR	UL
11215	air	10	8	11	11215	11216	11234	11233	12215	12216	12234	12233
11217	air	-6	9	11	11217	11218	11236	11235	12217	12218	12236	12235
11218	air	-5	9	11	11218	11219	11237	11236	12218	12219	12237	12236
11219	air	-4	9	11	11219	11220	11238	11237	12219	12220	12238	12237
11220	air	-3	9	11	11220	11221	11239	11238	12220	12221	12239	12238
11221	air	-2	9	11	11221	11222	11240	11239	12221	12222	12240	12239
11222	air	-1	9	11	11222	11223	11241	11240	12222	12223	12241	12240
11223	air	0	9	11	11223	11224	11242	11241	12223	12224	12242	12241
11224	air	1	9	11	11224	11225	11243	11242	12224	12225	12243	12242
11225	air	2	9	11	11225	11226	11244	11243	12225	12226	12244	12243
11226	air	3	9	11	11226	11227	11245	11244	12226	12227	12245	12244
11227	air	4	9	11	11227	11228	11246	11245	12227	12228	12246	12245
11228	air	5	9	11	11228	11229	11247	11246	12228	12229	12247	12246
11229	air	6	9	11	11229	11230	11248	11247	12229	12230	12248	12247
11230	air	7	9	11	11230	11231	11249	11248	12230	12231	12249	12248
11231	air	8	9	11	11231	11232	11250	11249	12231	12232	12250	12249
11232	air	9	9	11	11232	11233	11251	11250	12232	12233	12251	12250
11233	air	10	9	11	11233	11234	11252	11251	12233	12234	12252	12251

**Table 17 - FEM Conversion Table for Leg of Lamb at Z = 12 cm**

Element Number	Tissue Type	Location X Y Z	Nodes on this slice				Nodes on slice above			
			LL	LR	UR	UL	LL	LR	UR	UL
12001	air	-6 -3 12	12001	12002	12020	12019	13001	13002	13020	13019
12002	air	-5 -3 12	12002	12003	12021	12020	13002	13003	13021	13020
12003	muscle	-4 -3 12	12003	12004	12022	12021	13003	13004	13022	13021
12004	muscle	-3 -3 12	12004	12005	12023	12022	13004	13005	13023	13022
12005	air	-2 -3 12	12005	12006	12024	12023	13005	13006	13024	13023
12006	air	-1 -3 12	12006	12007	12025	12024	13006	13007	13025	13024
12007	air	0 -3 12	12007	12008	12026	12025	13007	13008	13026	13025
12008	air	1 -3 12	12008	12009	12027	12026	13008	13009	13027	13026
12009	air	2 -3 12	12009	12010	12028	12027	13009	13010	13028	13027
12010	air	3 -3 12	12010	12011	12029	12028	13010	13011	13029	13028
12011	air	4 -3 12	12011	12012	12030	12029	13011	13012	13030	13029
12012	air	5 -3 12	12012	12013	12031	12030	13012	13013	13031	13030
12013	air	6 -3 12	12013	12014	12032	12031	13013	13014	13032	13031
12014	air	7 -3 12	12014	12015	12033	12032	13014	13015	13033	13032
12015	air	8 -3 12	12015	12016	12034	12033	13015	13016	13034	13033
12016	air	9 -3 12	12016	12017	12035	12034	13016	13017	13035	13034
12017	air	10 -3 12	12017	12018	12036	12035	13017	13018	13036	13035
12019	muscle	-6 -2 12	12019	12020	12038	12037	13019	13020	13038	13037
12020	muscle	-5 -2 12	12020	12021	12039	12038	13020	13021	13039	13038
12021	muscle	-4 -2 12	12021	12022	12040	12039	13021	13022	13040	13039
12022	muscle	-3 -2 12	12022	12023	12041	12040	13022	13023	13041	13040
12023	muscle	-2 -2 12	12023	12024	12042	12041	13023	13024	13042	13041
12024	air	-1 -2 12	12024	12025	12043	12042	13024	13025	13043	13042
12025	air	0 -2 12	12025	12026	12044	12043	13025	13026	13044	13043
12026	air	1 -2 12	12026	12027	12045	12044	13026	13027	13045	13044
12027	air	2 -2 12	12027	12028	12046	12045	13027	13028	13046	13045
12028	air	3 -2 12	12028	12029	12047	12046	13028	13029	13047	13046
12029	air	4 -2 12	12029	12030	12048	12047	13029	13030	13048	13047
12030	air	5 -2 12	12030	12031	12049	12048	13030	13031	13049	13048
12031	air	6 -2 12	12031	12032	12050	12049	13031	13032	13050	13049
12032	air	7 -2 12	12032	12033	12051	12050	13032	13033	13051	13050
12033	air	8 -2 12	12033	12034	12052	12051	13033	13034	13052	13051
12034	air	9 -2 12	12034	12035	12053	12052	13034	13035	13053	13052
12035	air	10 -2 12	12035	12036	12054	12053	13035	13036	13054	13053
12037	muscle	-6 -1 12	12037	12038	12056	12055	13037	13038	13056	13055
12038	muscle	-5 -1 12	12038	12039	12057	12056	13038	13039	13057	13056
12039	muscle	-4 -1 12	12039	12040	12058	12057	13039	13040	13058	13057
12040	muscle	-3 -1 12	12040	12041	12059	12058	13040	13041	13059	13058
12041	muscle	-2 -1 12	12041	12042	12060	12059	13041	13042	13060	13059

Element Number	Tissue Type	Location			Nodes on this slice				Nodes on slice above			
		X	Y	Z	LL	LR	UR	UL	LL	LR	UR	UL
12042	bone	-1	-1	12	12042	12043	12061	12060	13042	13043	13061	13060
12043	bone	0	-1	12	12043	12044	12062	12061	13043	13044	13062	13061
12044	air	1	-1	12	12044	12045	12063	12062	13044	13045	13063	13062
12045	air	2	-1	12	12045	12046	12064	12063	13045	13046	13064	13063
12046	air	3	-1	12	12046	12047	12065	12064	13046	13047	13065	13064
12047	air	4	-1	12	12047	12048	12066	12065	13047	13048	13066	13065
12048	air	5	-1	12	12048	12049	12067	12066	13048	13049	13067	13066
12049	air	6	-1	12	12049	12050	12068	12067	13049	13050	13068	13067
12050	air	7	-1	12	12050	12051	12069	12068	13050	13051	13069	13068
12051	air	8	-1	12	12051	12052	12070	12069	13051	13052	13070	13069
12052	air	9	-1	12	12052	12053	12071	12070	13052	13053	13071	13070
12053	air	10	-1	12	12053	12054	12072	12071	13053	13054	13072	13071
12055	muscle	-6	0	12	12055	12056	12074	12073	13055	13056	13074	13073
12056	muscle	-5	0	12	12056	12057	12075	12074	13056	13057	13075	13074
12057	muscle	-4	0	12	12057	12058	12076	12075	13057	13058	13076	13075
12058	muscle	-3	0	12	12058	12059	12077	12076	13058	13059	13077	13076
12059	muscle	-2	0	12	12059	12060	12078	12077	13059	13060	13078	13077
12060	bone	-1	0	12	12060	12061	12079	12078	13060	13061	13079	13078
12061	bone	0	0	12	12061	12062	12080	12079	13061	13062	13080	13079
12062	muscle	1	0	12	12062	12063	12081	12080	13062	13063	13081	13080
12063	muscle	2	0	12	12063	12064	12082	12081	13063	13064	13082	13081
12064	muscle	3	0	12	12064	12065	12083	12082	13064	13065	13083	13082
12065	muscle	4	0	12	12065	12066	12084	12083	13065	13066	13084	13083
12066	muscle	5	0	12	12066	12067	12085	12084	13066	13067	13085	13084
12067	air	6	0	12	12067	12068	12086	12085	13067	13068	13086	13085
12068	air	7	0	12	12068	12069	12087	12086	13068	13069	13087	13086
12069	air	8	0	12	12069	12070	12088	12087	13069	13070	13088	13087
12070	air	9	0	12	12070	12071	12089	12088	13070	13071	13089	13088
12071	air	10	0	12	12071	12072	12090	12089	13071	13072	13090	13089
12073	muscle	-6	1	12	12073	12074	12092	12091	13073	13074	13092	13091
12074	muscle	-5	1	12	12074	12075	12093	12092	13074	13075	13093	13092
12075	muscle	-4	1	12	12075	12076	12094	12093	13075	13076	13094	13093
12076	muscle	-3	1	12	12076	12077	12095	12094	13076	13077	13095	13094
12077	bone	-2	1	12	12077	12078	12096	12095	13077	13078	13096	13095
12078	bone	-1	1	12	12078	12079	12097	12096	13078	13079	13097	13096
12079	muscle	0	1	12	12079	12080	12098	12097	13079	13080	13098	13097
12080	muscle	1	1	12	12080	12081	12099	12098	13080	13081	13099	13098
12081	muscle	2	1	12	12081	12082	12100	12099	13081	13082	13100	13099
12082	muscle	3	1	12	12082	12083	12101	12100	13082	13083	13101	13100
12083	muscle	4	1	12	12083	12084	12102	12101	13083	13084	13102	13101
12084	muscle	5	1	12	12084	12085	12103	12102	13084	13085	13103	13102

Element Number	Tissue Type	Location			Nodes on this slice				Nodes on slice above			
		X	Y	Z	LL	LR	UR	UL	LL	LR	UR	UL
12085	muscle	6	1	12	12085	12086	12104	12103	13085	13086	13104	13103
12086	bone	7	1	12	12086	12087	12105	12104	13086	13087	13105	13104
12087	air	8	1	12	12087	12088	12106	12105	13087	13088	13106	13105
12088	air	9	1	12	12088	12089	12107	12106	13088	13089	13107	13106
12089	air	10	1	12	12089	12090	12108	12107	13089	13090	13108	13107
12091	muscle	-6	2	12	12091	12092	12110	12109	13091	13092	13110	13109
12092	muscle	-5	2	12	12092	12093	12111	12110	13092	13093	13111	13110
12093	muscle	-4	2	12	12093	12094	12112	12111	13093	13094	13112	13111
12094	muscle	-3	2	12	12094	12095	12113	12112	13094	13095	13113	13112
12095	muscle	-2	2	12	12095	12096	12114	12113	13095	13096	13114	13113
12096	bone	-1	2	12	12096	12097	12115	12114	13096	13097	13115	13114
12097	fat	0	2	12	12097	12098	12116	12115	13097	13098	13116	13115
12098	muscle	1	2	12	12098	12099	12117	12116	13098	13099	13117	13116
12099	muscle	2	2	12	12099	12100	12118	12117	13099	13100	13118	13117
12100	muscle	3	2	12	12100	12101	12119	12118	13100	13101	13119	13118
12101	muscle	4	2	12	12101	12102	12120	12119	13101	13102	13120	13119
12102	muscle	5	2	12	12102	12103	12121	12120	13102	13103	13121	13120
12103	bone	6	2	12	12103	12104	12122	12121	13103	13104	13122	13121
12104	air	7	2	12	12104	12105	12123	12122	13104	13105	13123	13122
12105	air	8	2	12	12105	12106	12124	12123	13105	13106	13124	13123
12106	air	9	2	12	12106	12107	12125	12124	13106	13107	13125	13124
12107	air	10	2	12	12107	12108	12126	12125	13107	13108	13126	13125
12109	fat	-6	3	12	12109	12110	12128	12127	13109	13110	13128	13127
12110	muscle	-5	3	12	12110	12111	12129	12128	13110	13111	13129	13128
12111	muscle	-4	3	12	12111	12112	12130	12129	13111	13112	13130	13129
12112	muscle	-3	3	12	12112	12113	12131	12130	13112	13113	13131	13130
12113	muscle	-2	3	12	12113	12114	12132	12131	13113	13114	13132	13131
12114	muscle	-1	3	12	12114	12115	12133	12132	13114	13115	13133	13132
12115	muscle	0	3	12	12115	12116	12134	12133	13115	13116	13134	13133
12116	muscle	1	3	12	12116	12117	12135	12134	13116	13117	13135	13134
12117	muscle	2	3	12	12117	12118	12136	12135	13117	13118	13136	13135
12118	muscle	3	3	12	12118	12119	12137	12136	13118	13119	13137	13136
12119	muscle	4	3	12	12119	12120	12138	12137	13119	13120	13138	13137
12120	muscle	5	3	12	12120	12121	12139	12138	13120	13121	13139	13138
12121	bone	6	3	12	12121	12122	12140	12139	13121	13122	13140	13139
12122	bone	7	3	12	12122	12123	12141	12140	13122	13123	13141	13140
12123	air	8	3	12	12123	12124	12142	12141	13123	13124	13142	13141
12124	air	9	3	12	12124	12125	12143	12142	13124	13125	13143	13142
12125	air	10	3	12	12125	12126	12144	12143	13125	13126	13144	13143
12127	air	-6	4	12	12127	12128	12146	12145	13127	13128	13146	13145
12128	fat	-5	4	12	12128	12129	12147	12146	13128	13129	13147	13146

Element Number	Tissue Type	Location			Nodes on this slice				Nodes on slice above			
		X	Y	Z	LL	LR	UR	UL	LL	LR	UR	UL
12129	fat	-4	4	12	12129	12130	12148	12147	13129	13130	13148	13147
12130	muscle	-3	4	12	12130	12131	12149	12148	13130	13131	13149	13148
12131	muscle	-2	4	12	12131	12132	12150	12149	13131	13132	13150	13149
12132	muscle	-1	4	12	12132	12133	12151	12150	13132	13133	13151	13150
12133	muscle	0	4	12	12133	12134	12152	12151	13133	13134	13152	13151
12134	muscle	1	4	12	12134	12135	12153	12152	13134	13135	13153	13152
12135	muscle	2	4	12	12135	12136	12154	12153	13135	13136	13154	13153
12136	muscle	3	4	12	12136	12137	12155	12154	13136	13137	13155	13154
12137	fat	4	4	12	12137	12138	12156	12155	13137	13138	13156	13155
12138	bone	5	4	12	12138	12139	12157	12156	13138	13139	13157	13156
12139	bone	6	4	12	12139	12140	12158	12157	13139	13140	13158	13157
12140	air	7	4	12	12140	12141	12159	12158	13140	13141	13159	13158
12141	air	8	4	12	12141	12142	12160	12159	13141	13142	13160	13159
12142	air	9	4	12	12142	12143	12161	12160	13142	13143	13161	13160
12143	air	10	4	12	12143	12144	12162	12161	13143	13144	13162	13161
12145	air	-6	5	12	12145	12146	12164	12163	13145	13146	13164	13163
12146	fat	-5	5	12	12146	12147	12165	12164	13146	13147	13165	13164
12147	fat	-4	5	12	12147	12148	12166	12165	13147	13148	13166	13165
12148	muscle	-3	5	12	12148	12149	12167	12166	13148	13149	13167	13166
12149	muscle	-2	5	12	12149	12150	12168	12167	13149	13150	13168	13167
12150	muscle	-1	5	12	12150	12151	12169	12168	13150	13151	13169	13168
12151	muscle	0	5	12	12151	12152	12170	12169	13151	13152	13170	13169
12152	muscle	1	5	12	12152	12153	12171	12170	13152	13153	13171	13170
12153	muscle	2	5	12	12153	12154	12172	12171	13153	13154	13172	13171
12154	muscle	3	5	12	12154	12155	12173	12172	13154	13155	13173	13172
12155	muscle	4	5	12	12155	12156	12174	12173	13155	13156	13174	13173
12156	bone	5	5	12	12156	12157	12175	12174	13156	13157	13175	13174
12157	bone	6	5	12	12157	12158	12176	12175	13157	13158	13176	13175
12158	air	7	5	12	12158	12159	12177	12176	13158	13159	13177	13176
12159	air	8	5	12	12159	12160	12178	12177	13159	13160	13178	13177
12160	air	9	5	12	12160	12161	12179	12178	13160	13161	13179	13178
12161	air	10	5	12	12161	12162	12180	12179	13161	13162	13180	13179
12163	air	-6	6	12	12163	12164	12182	12181	13163	13164	13182	13181
12164	air	-5	6	12	12164	12165	12183	12182	13164	13165	13183	13182
12165	air	-4	6	12	12165	12166	12184	12183	13165	13166	13184	13183
12166	muscle	-3	6	12	12166	12167	12185	12184	13166	13167	13185	13184
12167	muscle	-2	6	12	12167	12168	12186	12185	13167	13168	13186	13185
12168	muscle	-1	6	12	12168	12169	12187	12186	13168	13169	13187	13186
12169	muscle	0	6	12	12169	12170	12188	12187	13169	13170	13188	13187
12170	muscle	1	6	12	12170	12171	12189	12188	13170	13171	13189	13188
12171	muscle	2	6	12	12171	12172	12190	12189	13171	13172	13190	13189

Element Number	Tissue Type	Location			Nodes on this slice				Nodes on slice above			
		X	Y	Z	LL	LR	UR	UL	LL	LR	UR	UL
12172	fat	3	6	12	12172	12173	12191	12190	13172	13173	13191	13190
12173	bone	4	6	12	12173	12174	12192	12191	13173	13174	13192	13191
12174	bone	5	6	12	12174	12175	12193	12192	13174	13175	13193	13192
12175	bone	6	6	12	12175	12176	12194	12193	13175	13176	13194	13193
12176	air	7	6	12	12176	12177	12195	12194	13176	13177	13195	13194
12177	air	8	6	12	12177	12178	12196	12195	13177	13178	13196	13195
12178	air	9	6	12	12178	12179	12197	12196	13178	13179	13197	13196
12179	air	10	6	12	12179	12180	12198	12197	13179	13180	13198	13197
12181	air	-6	7	12	12181	12182	12200	12199	13181	13182	13200	13199
12182	air	-5	7	12	12182	12183	12201	12200	13182	13183	13201	13200
12183	air	-4	7	12	12183	12184	12202	12201	13183	13184	13202	13201
12184	air	-3	7	12	12184	12185	12203	12202	13184	13185	13203	13202
12185	muscle	-2	7	12	12185	12186	12204	12203	13185	13186	13204	13203
12186	muscle	-1	7	12	12186	12187	12205	12204	13186	13187	13205	13204
12187	muscle	0	7	12	12187	12188	12206	12205	13187	13188	13206	13205
12188	muscle	1	7	12	12188	12189	12207	12206	13188	13189	13207	13206
12189	muscle	2	7	12	12189	12190	12208	12207	13189	13190	13208	13207
12190	fat	3	7	12	12190	12191	12209	12208	13190	13191	13209	13208
12191	fat	4	7	12	12191	12192	12210	12209	13191	13192	13210	13209
12192	fat	5	7	12	12192	12193	12211	12210	13192	13193	13211	13210
12193	fat	6	7	12	12193	12194	12212	12211	13193	13194	13212	13211
12194	air	7	7	12	12194	12195	12213	12212	13194	13195	13213	13212
12195	air	8	7	12	12195	12196	12214	12213	13195	13196	13214	13213
12196	air	9	7	12	12196	12197	12215	12214	13196	13197	13215	13214
12197	air	10	7	12	12197	12198	12216	12215	13197	13198	13216	13215
12199	air	-6	8	12	12199	12200	12218	12217	13199	13200	13218	13217
12200	air	-5	8	12	12200	12201	12219	12218	13200	13201	13219	13218
12201	air	-4	8	12	12201	12202	12220	12219	13201	13202	13220	13219
12202	air	-3	8	12	12202	12203	12221	12220	13202	13203	13221	13220
12203	air	-2	8	12	12203	12204	12222	12221	13203	13204	13222	13221
12204	air	-1	8	12	12204	12205	12223	12222	13204	13205	13223	13222
12205	air	0	8	12	12205	12206	12224	12223	13205	13206	13224	13223
12206	air	1	8	12	12206	12207	12225	12224	13206	13207	13225	13224
12207	fat	2	8	12	12207	12208	12226	12225	13207	13208	13226	13225
12208	fat	3	8	12	12208	12209	12227	12226	13208	13209	13227	13226
12209	fat	4	8	12	12209	12210	12228	12227	13209	13210	13228	13227
12210	fat	5	8	12	12210	12211	12229	12228	13210	13211	13229	13228
12211	air	6	8	12	12211	12212	12230	12229	13211	13212	13230	13229
12212	air	7	8	12	12212	12213	12231	12230	13212	13213	13231	13230
12213	air	8	8	12	12213	12214	12232	12231	13213	13214	13232	13231
12214	air	9	8	12	12214	12215	12233	12232	13214	13215	13233	13232

Element Number	Tissue Type	Location X Y Z	Nodes on this slice				Nodes on slice above			
			LL	LR	UR	UL	LL	LR	UR	UL
12215	air	10 8 12	12215	12216	12234	12233	13215	13216	13234	13233
12217	air	-6 9 12	12217	12218	12236	12235	13217	13218	13236	13235
12218	air	-5 9 12	12218	12219	12237	12236	13218	13219	13237	13236
12219	air	-4 9 12	12219	12220	12238	12237	13219	13220	13238	13237
12220	air	-3 9 12	12220	12221	12239	12238	13220	13221	13239	13238
12221	air	-2 9 12	12221	12222	12240	12239	13221	13222	13240	13239
12222	air	-1 9 12	12222	12223	12241	12240	13222	13223	13241	13240
12223	air	0 9 12	12223	12224	12242	12241	13223	13224	13242	13241
12224	air	1 9 12	12224	12225	12243	12242	13224	13225	13243	13242
12225	air	2 9 12	12225	12226	12244	12243	13225	13226	13244	13243
12226	fat	3 9 12	12226	12227	12245	12244	13226	13227	13245	13244
12227	fat	4 9 12	12227	12228	12246	12245	13227	13228	13246	13245
12228	air	5 9 12	12228	12229	12247	12246	13228	13229	13247	13246
12229	air	6 9 12	12229	12230	12248	12247	13229	13230	13248	13247
12230	air	7 9 12	12230	12231	12249	12248	13230	13231	13249	13248
12231	air	8 9 12	12231	12232	12250	12249	13231	13232	13250	13249
12232	air	9 9 12	12232	12233	12251	12250	13232	13233	13251	13250
12233	air	10 9 12	12233	12234	12252	12251	13233	13234	13252	13251



## APPENDIX F - ATROPHY LAMB FEM MODEL TARGET MUSCLE ELEMENT

Table 18 - Leg of Lamb FEM Model Target Muscle Elements

1115	1116	1117	1131	1132	1133	1134
1135	1152	<b>1153</b>	2115	2116	2117	2131
2132	<b>2133</b>	2134	2135	2150	2151	2152
2153	2154	3113	3114	3115	3116	3117
3131	3132	3133	<b>3134</b>	3135	3150	3151
3152	<b>3153</b>	3154	4112	4113	4114	4115
<b>4116</b>	41331	4132	<b>4133</b>	4134	4135	4136
4150	4151	5112	<b>5113</b>	5114	5115	5130
5131	5132	5133	<b>5134</b>	5135	5149	5150
5151	5152	5153	5154	6111	<b>6112</b>	6113
6114	6115	6130	6131	6132	6133	6149
6150	6151	<b>6152</b>	6168	6169	7111	7112
7113	7114	7130	7131	7132	7133	7134
7148	7149	7150	7151	<b>7152</b>	7168	7169
7170	8111	8112	8113	8114	8129	8130

Elements converted to adipose tissue are in **bold**

8131	8132	<b>8133</b>	8134	8148	8149	<b>8150</b>
8151	8152	8168	<b>8169</b>	9111	9112	9113
9114	9115	9129	9130	9131	9132	9133
9134	9135	9148	9149	9150	<b>9151</b>	9152
9167	9168	<b>9169</b>	10113	10114	10115	10129
10130	10131	<b>10132</b>	10133	10134	10135	10148
10149	<b>10150</b>	10151	10152	10167	10168	10169
11114	11115	<b>11129</b>	11130	<b>11131</b>	11132	11133
11134	11135	11136	11148	11149	11150	11151
<b>11152</b>	11153	11166	11167	11168	11169	11170
11187	12133	12134	12135	12136	12148	12149
12150	12151	12152	12153	12154	<b>12155</b>	12166
12167	12168	12169	12170	<b>12171</b>	12186	12187
12188	12189	Elements converted to adipose tissue are in <b>bold</b>				

## APPENDIX G - MATLAB CODE USED TO CREATE LABORATORY MEASUREMENT RESULTS GRAPHS

```
% This is the data file for the Lamb measurements
% For the slice at z=2. The first column is the X
% Location, Second column is the Y location and
% Third is the Voltage/cm corrected for gain
```

```
slice2=[0.0  6.0  0.022;
0.0  5.0  0.02;
0.0  4.0  0.013;
0.0  3.0  0.011;
0.0  2.0  0.011;
2.6  6.3  0.011;
2.3  5.5  0.0104;
1.8  4.5  0.00945;
1.5  3.6  0.0085;
-1.9  4.6  0.012;
-1.5  3.6  0.01;
-3.2  3.3  0.0097;
-2.5  2.5  0.01];
```

```
outline2=[-1, 6;      %outline of the FEM slice
6, 6;      %to superimpose over the
6, 5;      %top view measurement plot
7, 5;
7, 2;
6, 2;
6, 1;
5, 1;
5, 0;
4, 0;
4, -1;
1, -1;
1, -2;
-2, -2;
-2, -1;
-4, -1;
-4, 2;
-3, 2;
-3, 4;
-2, 4;
-2, 5;
-1, 5;
```

```

-1, 6];

ox=outline2(:,1);
oy=outline2(:,2);

xmin=min(outline2(:,1));
xmax=max(outline2(:,1));
ymin=min(outline2(:,2));
ymax=max(outline2(:,2));
zmin=min(slice2(:,3)*1000);
zmax=max(slice2(:,3)*1000);

x=slice2(:,1);
y=slice2(:,2);
z=slice2(:,3)*1000;
N=length(x);
c=round(z*.25);
for a=1:N;
    if c(a) == 6                % Creates false color scale for markers
        cv(a)='m';
    elseif c(a) == 5
        cv(a)='r';
    elseif c(a) == 4
        cv(a)='y';
    elseif c(a) == 3
        cv(a)='g';
    elseif c(a) == 2
        cv(a)='c';
    else
        cv(a)='b';
    end;
end;

for a=1:N;
    subplot(2,1,1);
    stem3(x(a),y(a),z(a),cv(a),'filled');
    hold on;
    xlabel('x axis'), ylabel('y axis'), zlabel('mVz/cm');
    title('3-dimensional view');
end;

subplot(2,1,2);                % Outlines the slice
plot(ox,oy);
grid on;
hold on;

```

```

        axis([xmin xmax ymin ymax]);
        xlabel('x axis'), ylabel('y axis');
        title('top view');

for a=1:N;
    subplot(2,1,2);
    hold on;
    scatter(x(a),y(a),cv(a),'filled');
end;

figure(2)
for a=1:N;
    stem3(x(a),y(a),z(a),cv(a),'filled');
    hold on;
end;
    xlabel('x axis'), ylabel('y axis'), zlabel('mVz/cm');
    title('3-dimensional view');

figure(3)
    plot(ox,oy);
    grid on;
    hold on;
    axis([xmin xmax ymin ymax]);
    xlabel('x axis'), ylabel('y axis');
    title('top view');

for a=1:N;
    scatter(x(a),y(a),cv(a),'filled');
    hold on;
end;

```